Advances in supramolecular polymer chemistry : well-defined terpyridine-functionalized materials

Advances in Supramolecular Polymer Chemistry:

Well-defined Terpyridine-functionalized Materials

PROEFSCHRIFT

ter verkrijging van de graad van doctor aan de
Technische Universiteit Eindhoven, op gezag van de
Rector Magnificus, prof.dr.ir. C.J. van Duijn, voor een
commissie aangewezen door het College voor
Promoties in het openbaar te verdedigen
op maandag 15 december 2008 om 14.00 uur

door

Christina Ott

geboren te Gera, Duitsland

Dit proefschrift is goedgekeurd door de promotoren:

prof.dr. U.S. Schubert
en
prof.dr. J.-F. Gohy

Copromotor:
dr.ir. R. Hoogenboom

This research has been financially supported by the Dutch Organization for Scientific Research (NWO).

Cover design: Christina Ott

Printed by: PrintPartners Ipskamp, Enschede, The Netherlands

Advances in Supramolecular Polymer Chemistry: Well-defined Terpyridine-functionalized Materials by Christina Ott.
Eindhoven: Technische Universiteit Eindhoven, 2008.

A catalogue record is available from the Eindhoven University of Technology Library

ISBN: 978-90-386-1478-6

Advances in Supramolecular Polymer Chemistry:

Well-defined Terpyridine-functionalized Materials

Kerncommissie: prof. dr. U.S. Schubert (Eindhoven University of Technology)
dr. R. Hoogenboom (Eindhoven University of Technology)
prof. dr. J.-F. Gohy (Université Catholique de Louvain)
prof. dr. A.M. van Herk (Eindhoven University of Technology)
prof. dr. G.N. Tew (University of Massachusetts Amherst)
dr. R.K. O'Reilly (University of Cambridge)

Für meine Eltern

Table of contents

Chapter 1

Chapter 2

Chapter 3

Chapter 4

Chapter 5

CHAPTER 1

Supramolecular polymers: Design principles, functionalization, and applications

Abstract

Over the past two decades, the field of supramolecular polymer chemistry has enormously developed into a sophisticated area of polymer science. The introduction of directional supramolecular motifs into synthetic polymers was found to represent a promising approach towards 'smart' materials which combine the (reversible) binding behavior of supramolecular interactions and the processing advantages of polymers. This new methodology provides access to highly complex materials that are extremely difficult or even impossible to synthesize with current covalent techniques. Since supramolecular chemistry is often inspired by large biological systems, special attention is paid to well-defined polymeric assemblies. Therefore, this chapter is devoted to the fundamental concepts of self-assembly, the design principles as well as functionalization strategies employed in the field of supramolecular polymer chemistry by highlighting the recent developments in the area of "living" and controlled polymerization techniques in connection with non-covalent interactions.

Parts of this chapter have been published: C. Ott, B.G.G. Lohmeijer, D. Wouters, U.S. Schubert, *Macromol. Chem. Phys.* **2006**, *207*, 1439-1449; C. Ott, D. Wouters, H.M.L. Thijs, U.S. Schubert, *J. Inorg. Organometal. Polym. Mater.* **2007**, *17*, 241-249; C. Ott, R. Hoogenboom, U.S. Schubert, *Chem. Commun.* **2008**, 3516-3518.

1.1 Supramolecular chemistry

Supramolecular chemistry, *i.e.* chemistry beyond the molecule,[1,2] focuses on non-covalent interactions of molecules which are usually associated with reversible and self-assembly processes. While traditional chemistry involves covalent bonds, supramolecular chemistry deals with generally weaker interactions, including hydrogen bonding, metal coordination, van der Waals forces, π-π interactions and electrostatic effects.[1,2] Nowadays, supramolecular interactions are believed to be key factors for the understanding of important biological and chemical processes as well as the development of functional and 'smart' materials. Enormous advances have been made in the last thirty years, as well as in the exploration of the non-covalent bond for the design of complex architectures.[1,3-7] Moreover, traditional covalent-based strategies have become increasingly difficult to employ when macromolecular structures with a high degree of complexity and function are desired. Therefore, covalent-based synthetic strategies are being replaced more and more by self-assembly processes in order to overcome a variety of synthetic difficulties.[3,5,7-9] Even though "self-assembly" is a common expression in today's scientific research repertoire, the definition of this term has increasingly become an issue of discussion due to the large number of scientific disciplines which fully or partially embody the original concepts of supramolecular science.[4] One of the most frequently cited definitions originates from Lehn, who describes self-assembly[1] as "…*the spontaneous association of either a few or many components, resulting in the generation of either discrete oligomolecular supermolecules or of extended polymolecular assemblies."* This definition clearly emphasizes the process of the formation of complexes via the association of components, on the other hand the nature of the "higher ordered" structures is less emphasized. In this thesis, self-assembly is discussed based on the metal-ligand coordination, even though it might not necessarily result in the formation of highly ordered supramolecular structures.

Non-covalent interactions can be considered as tools to construct complex architectures. While in general they are classified by the nature of interactions, special attention has to be paid to the bond strength or bond energy when selecting an interaction for use in a self-assembled system. Figure 1.1 outlines a variety of non-covalent interactions and their respective bond strengths in comparison to the covalent C-C bond. According to the bond strength, van der Waals forces[1,4] and hydrogen bonding[1,10-12] are considered to be weaker interactions, whereas stronger interactions are found in ionic[1,13] and metal coordination[1,14] systems. The strength of most non-covalent interactions is highly dependant on external influences such as temperature, solvent or pressure. Furthermore, the strength of interaction can be tuned by the right choice of interacting system. In the following part, some general aspects of metal-coordination and hydrogen bonding are discussed. These highly directional interactions are the most popular non-covalent interactions used in supramolecular chemistry.

In the case of metal coordination complexes, the interaction is strongly dependent on the ligand system and the metal ion. As a consequence, extremely stable (also referred to as inert complexes) as well as labile metal complexes can be obtained simply by changing the metal ion, which is largely affected by the crystal field theory.[15] The most important factors responsible for the coordination strength are the degree of orbital overlap between the metal ion and the ligand as well as the location of the ligand along the spectrochemical series. Nowadays, the supramolecular toolbox offers a variety of coordination systems to choose from; each possessing different interaction strengths and of course various physical properties. An appropriate selection of a suitable metal ligand system is therefore dependent on the desired application. For electro-optical applications a strong and stable non-covalent bond is required whereas systems designed for drug delivery prefer weaker non-covalent bonds in order to allow an easy drug release.

The strength of a single hydrogen bond is generally weak and highly dependent upon the electronic nature of the donor and acceptor.[10-12] Nevertheless, an increase of the strength and

stability can be achieved by the combination of multiple hydrogen bonds. Moreover, the arrangement of the donor and acceptor sites plays a significant role, as recognized by Jørgenson and coworkers.[16,17] They showed that these differences in stability can be largely attributed to attractive and repulsive secondary interactions. Stabilization arises from electrostatic attraction between positively and negatively polarized atoms in adjacent hydrogen bonds, whereas destabilization is likewise the result of electrostatic repulsions between two positively or negatively polarized atoms. It was found that a molecule consisting of only donors and the complementary partners only of acceptors, *i.e.* the secondary interactions are favorable, results in a much stronger hydrogen bonded complex (attractive secondary interactions) compared to alternating donor and acceptor units.

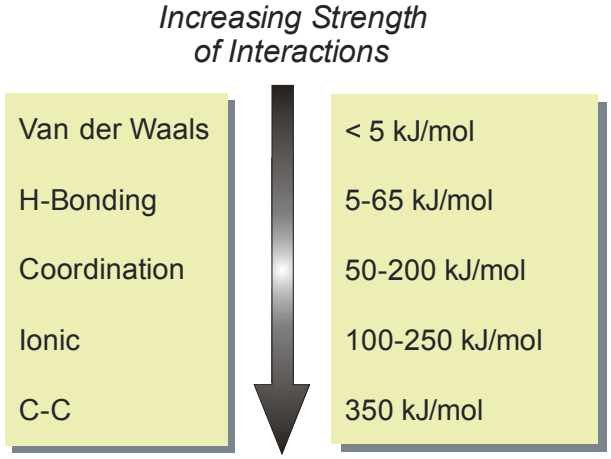

Figure 1.1 *Non-covalent interactions ordered according to their bond strength.*[18]

1.2 Basic design principles for supramolecular polymers

Significant progress in the field of polymer science has been achieved as a consequence of combining self-assembly, supramolecular science and polymer chemistry. The attachment of highly directional and sufficiently strong non-covalent recognition units, either in the main chain or in the side chain of a polymer (Figure 1.2), leads to self-assembly and provides unique and highly functional polymeric structures.[3,5,8,9,14] These new materials feature interesting properties such as reversibility, self-healing character, and susceptibility to external stimuli while in the most cases retaining the strength and physical properties of covalently bonded polymers. Main chain supramolecular polymers can be described as polymeric systems that are held together by directional non-covalent interactions in the polymer backbone. While functionalization at only one polymer chain end can be used to link two macromolecules, functionalization on both chain ends leads to the formation of chain extended supramolecular polymers. In contrast, side chain supramolecular polymers are based on a covalent polymer backbone that contains molecular recognition units in the side chain able to form graft-like structures as shown in Figure 1.2. Both main chain and side chain supramolecular polymers can be subcategorized as self-complementary or complementary according to the nature of the recognition unit incorporated.[5] In self-complementary assembly, the recognition units possess a high tendency to dimerize.

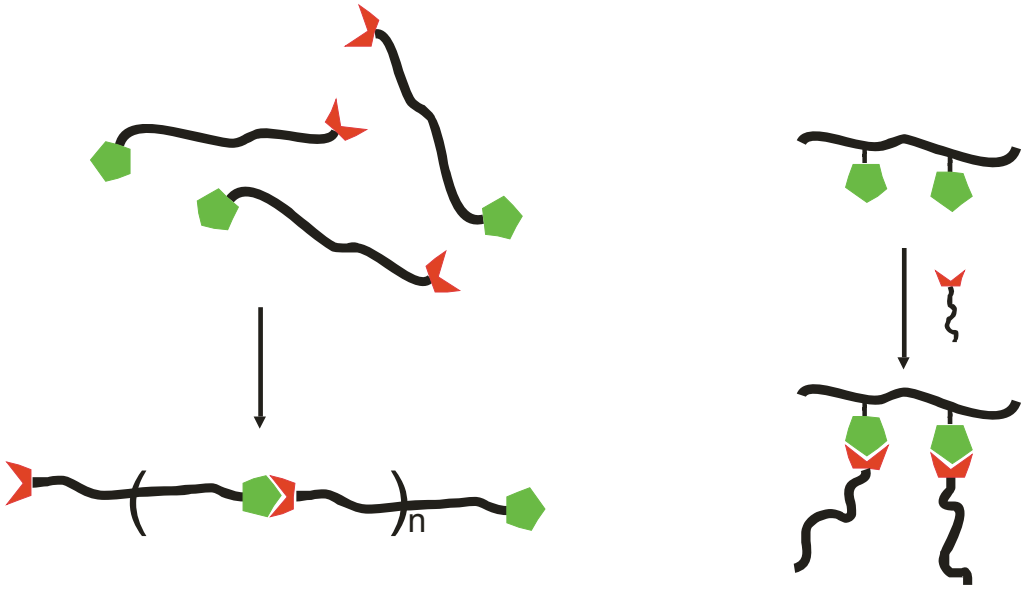

Figure 1.2 *Schematic representation of main chain self-assembled (chain extended) polymers (left) and side-chain self-assembled polymers (right).*

On the other hand, polymers based on complementary recognition units have strong association constants and possess a low tendency to dimerize. Meijer and coworkers have reported one example of strong self-complementary main chain self-assembly by incorporating two ureidopyrimidinone units at the ends of an alkyl chain resulting in the formation of a linear chain extended polymer.[19,20] In comparison, thermally reversible cross-linked polymers are accessible from self-assembled polymers consisting of self-complementary recognition units in the side chain.[21] In principle, main chain self-assembled polymers can be also obtained using heteronuclear recognition units. For this purpose, two symmetrically *bis*-functionalized monomers (of complementary recognition moieties) are reacted to obtain the respective $(AABB)_n$ self-assembled alternating copolymer.[22,23] Multifunctional polymers have been widely investigated since such polymers are potential materials for a variety of applications ranging from electronic devices to biological materials.[7,24-26] If polymers consist of multiple self-complementary recognition units in the side-chain of a polymer backbone, intramolecular folding[27] is likely to occur. However, this is also dependent on the number and location (distribution) of the complementary pairs along the side chain. In contrast, side-chain functionalized polymers bearing non-self-complementary recognition units allow modular or intermolecular functionalization. [28,29] Both processes can be found in biological systems. An example for self-functionalization is the formation of hierarchical peptide architectures, *e.g.* α-helices and ß-sheets, while DNA replication is based on the modular functionalization strategy.[30,31] Furthermore, cyclic products can be formed which is highly depending on the spacer-group used. For instance rigid angular spacer groups preferably lead to the formation of rings whereas rigid linear spacers favor the formation of linear products. On the other hand, flexible spacer groups usually afford a mixture of various ring structures as well as chain-extended polymers. The respective ring-chain-equilibrium is strongly dependent on the concentration of the reactants which allows a change of the obtained macromolecular architecture.[32,33]

The following section discusses selected examples of recent developments in the field of well-defined supramolecular polymers based on the two most important supramolecular binding motifs hydrogen bonding and metal coordination in combination with living and controlled polymerization techniques, respectively. In order to obtain well-defined supramolecular polymers by employing established polymerization techniques, several synthetic approaches are imaginable (Figure 1.3).

First, the functional group is incorporated after performing the polymerization or by end-group modification reactions. The second synthetic strategy involves the use of post-modification reactions for the incorporation of the supramolecular moiety into the side chain of the polymer. The third method requires the synthesis of functionalized macromonomers which are either copolymerized or homopolymerized. Furthermore, the use of functionalized initiators is another elegant procedure to obtain tailor-made polymeric architectures.

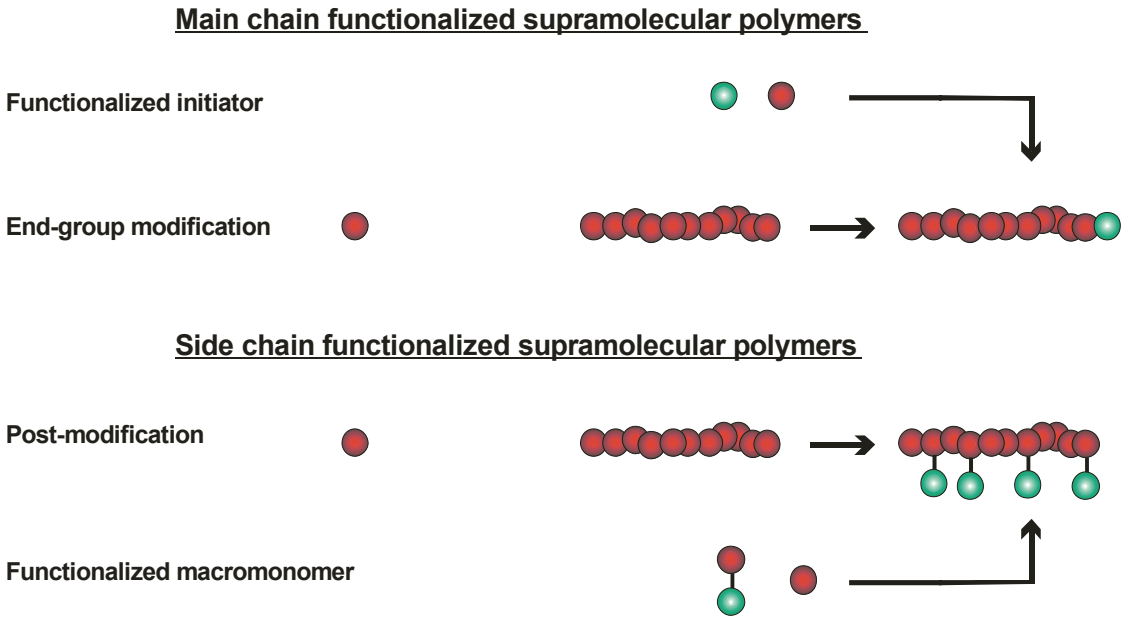

Figure 1.3 *Schematic illustration for the functionalization of polymers using various synthetic strategies.*

1.2.1 Main chain functionalized polymers by end-group modification

Main chain functionalized polymers can be synthesized *via* end-group-functionalization methods as it is schematically depicted in Figure 1.3. In particular, mono- and telechelic hydroxyl-functionalized polymers derived by anionic polymerization are versatile precursor compounds since modification of the hydroxy end-group can easily be established by etherification reactions,[34,35] urethane-formation[34] or the formation of imidazolides[36] which show a high reactivity towards amines. This strategy has been applied for the incorporation of chelating ligands, *i.e.* bipyridine or terpyridine that were subsequently used for the construction of larger macromolecular structures *via* metal coordination. Rowan and coworkers reported the functionalization of *bis*-hydroxy functionalized polytetrahydrofurane (PTHF), which can easily be prepared by cationic-opening polymerization, with 4-hydroxy-2,6-*bis*(1'-methylbenzimidazolyl)-pyridine.[37] The end-group modification reaction was performed using diethylazodicarboxylate (DEAD) and triphenylphosphine (PPh_3) resulting in the desired *bis*-functionalized polymer. The terdentate ligand 2,6-*bis*(benzimidazolyl)-4-oxypyridine forms stable *bis*-complexes with transition metal ions. Accordingly, chain-extended supramolecular polymers with zinc, cadmium, cobalt and iron ions were prepared leading to the formation of thermoplastic elastomeric films in which phase separation occurred between the ionic blocks and the soft PTHF segments. Similarly, as it was described before, Hadjichristidis and coworkers reported the synthesis of well-defined hydroxyl-functionalized poly(styrene-*block*-isoprene) block copolymers which were reacted subsequently

with an isocyanate-functionalized ureidopyrimidinone resulting in the incorporation of the quadruple hydrogen bonding moiety.[38] The respective functionalized block copolymers combined two reversible phenomena in one material: micellization of block copolymers and interactions through the formation of hydrogen bonds in a non-polar solvent. This resulted in the development of a dynamic system responsive to its chemical environment and the temperature. In the group of Schubert, an *in situ* functionalization for the anionic polymerization of styrene was achieved by reacting the polystyryl-lithium species with 1,1-diphenylethylene (DPE) which was found to be a necessary step in order to promote an efficient chain-end functionalization and to avoid undesired side reactions.[39] Afterwards, the terpyridine ligand was introduced which was exploited for self-assembly processes. Diethylene glycol was applied as an initiator for the controlled ring-opening polymerization of *ε*-caprolactone by Sijbesma and coworkers[40] followed by post-modification of the terminal hydroxyl-groups (Scheme 1.1). The telechelic polycaprolactones with ureidopyrimidinone end-groups connected *via* urethane linkages revealed to be strong and elastic materials compared to the unfunctionalized materials. This feature is attributed to supramolecular chain extension by hydrogen bonding.[20]

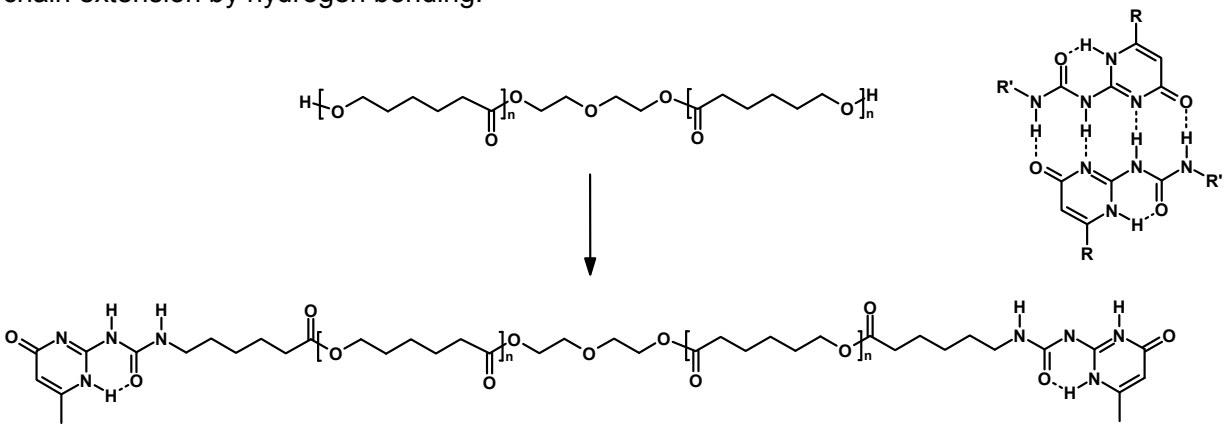

Scheme 1.1 *Schematic representation of the end-group modification with ureidopyrimidinone and the dimer formation of the self-complementary quadruple hydrogen bonding unit (right).*

1.2.2 Functional initiators

Substantial progress in the field of polymer chemistry was mainly achieved by the development of the controlled ('living') radical polymerization techniques,[41-45] including nitroxide-mediated polymerization (NMP), atom transfer radical polymerization (ATRP) and reversible addition-fragmentation chain transfer polymerization (RAFT). These techniques allow the synthesis of well-defined macromolecules with accurate control over architecture and functionality. The combination of controlled radical polymerization techniques with supramolecular chemistry brings scientists one step closer to their goal of perfectly copying natural systems. ATRP is the most widely explored polymerization method among the three different techniques. Fraser and coworkers have demonstrated in their pioneering work the feasibility of combining ATRP with functionalized bipyridines.[46,47] The most recent results in this direction include the synthesis of unsymmetrical, difunctional bipyridine initiators that were used to perform ATRP of MMA and styrene using *α*-bromoester initiating groups, while maintaining a functional hydroxyl-group for subsequent ring-opening polymerizations of *ε*-caprolactone.[48] In a different report, the preparation of symmetrical polymeric macroligands is described where first a ring-opening polymerization of lactide and *ε*-caprolactone was performed followed by the controlled polymerization of MMA and

*t*BA by ATRP. Furthermore, the obtained bipyridine-containing block copolymers were utilized for self-assembly with iron ions resulting in the formation of metallo-supramolecular star block copolymer architectures.[49] A similar architecture was reported by Haddleton and Le Bozec who applied *tris*(dialkylaminostyryl-bipyridine) iron(II) and zinc(II) complexes equipped with 6 *α*-bromoester functional groups for the polymerization of MMA by ATRP.[50] The excellent film formation of the synthesized metallo-supramolecular star polymer and its respective photo-physical features prove the creation of the novel material due to the combined properties of the polymer and the metal complex.

The controlled ring-opening polymerization of lactide was successfully performed using an hydroxy-functionalized iron(III) *tris*(dibenzoylmethane) complex (dbm) by Fraser *et al.*[51] Those researchers have developed a method where the metal chelation acts as a dbm protecting group and catalyst at the same time, resulting in the formation of well-defined metallo-supramolecular polylactide stars up to high monomer conversion. The same group recently reported the synthesis of star-shaped ruthenium-centered poly(2-ethyl-2-oxazoline) performed by cationic ring-opening polymerization.[52] Acid hydrolysis of these materials gave rise to the transformation of poly(2-ethyl-2-oxazoline) to poly(ethyleneimine) which is able to electrostatically bind and protect DNA, and is therefore commonly used in gene delivery.[53,54] The group of Scherman performed the ROP of *ε*-caprolactone using an ureidopyrimidinone-functionalized initiator.[55] The authors describe successful polymerization in toluene where the precursor molecule generates a dimer due to the high association constant of the ureidopyrimidinone (UPy) units. Thus, the presented synthetic approach prevents the interference of the UPy units with the $Sn(Oct)_2$ catalyst which does not allow the alkoxide formation of the alcohol initiator. Likewise, poly(caprolactone) was synthesized by ROP using a terpyridine-functionalized initiator (Scheme 1.2).[56] Subsequently, the terminal hydroxyl group of the macroligand was coupled to an ureidopyrimidinone unit *via* isocyanate coupling, resulting in polymers bearing metal-coordination ligands as well as hydrogen bonding units as chain ends.

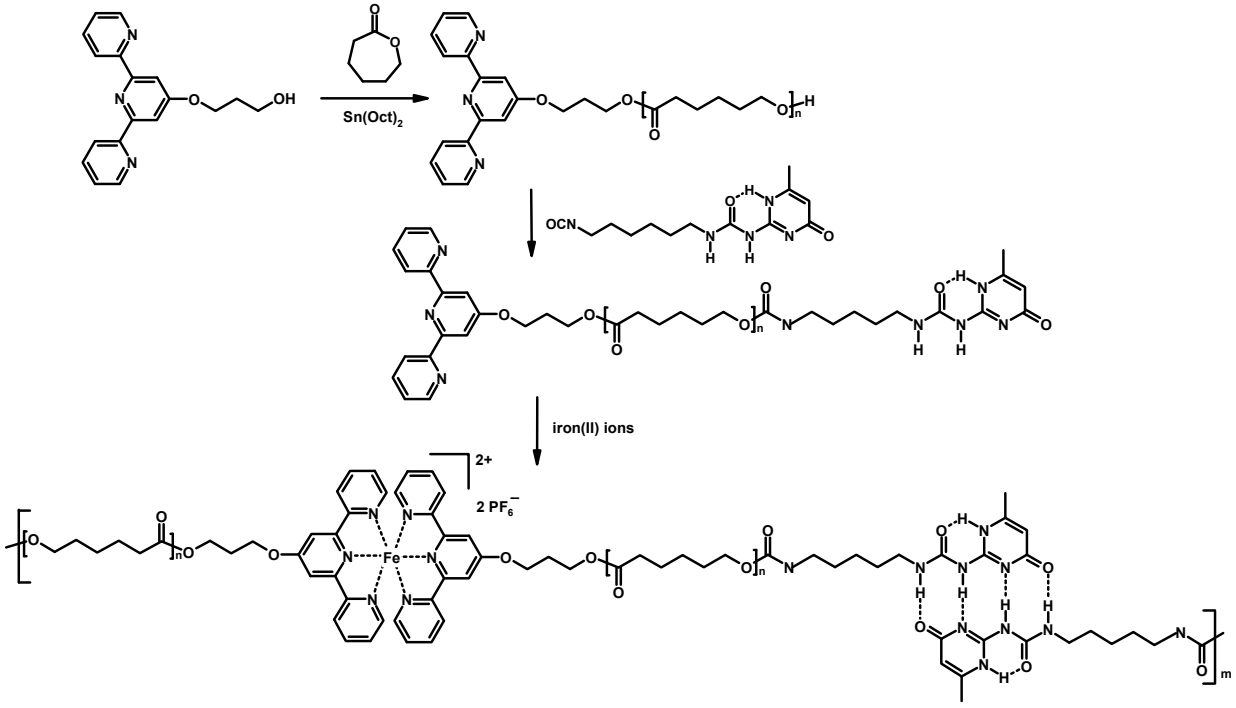

Scheme 1.2 *Schematic representation of the synthesis of a chain-extended metallo-supramolecular polymer using two different non-covalent interactions: terpyridine coordination and quadruple hydrogen bonding, respectively.*

The addition of iron(II) ions to this polymer resulted in the formation of high molar mass supramolecular polymers as demonstrated by viscometry and rheometry measurements. In addition, the viscosity of obtained polymer is strongly dependent on temperature due to the decreased hydrogen bonding interactions at elevated temperatures.

The previous part of this section has dealt with the metal-catalyzed polymerizations ATRP and ROP. In the following two paragraphs the metal-free polymerizations RAFT and NMP will be discussed. These techniques seem to be very promising candidates in particular when chelating ligands such as terpyridines are involved; however more effort has to be made to synthesize the highly complex RAFT agents and NMP initiators. In 2003, the first attempts towards supramolecular RAFT agents were reported by Ghiggino who demonstrated the controlled polymerization of styrene.[57] Only one year later, Zhou and Harruna reported the synthesis of a bipyridine-functionalized dithioester which was applied as RAFT agent for the polymerization of styrene[58] and *N*-isopropylacrylamide.[59] In both cases, the supramolecular polymers were reacted with $Ru(bpy)_2$ to obtain the corresponding metallo-supramolecular polymers. A similar synthetic approach was applied by Zhou and Harruna for the synthesis of a terpyridine-connected RAFT agent.[60] It was demonstrated that this initiator could be successfully applied for the controlled polymerization of styrene and *N*-isopropylacrylamide which were subsequently used to form the homoleptic complexes as well as the heteroleptic complex with ruthenium(II) ions. The most recent metallo-supramolecular RAFT agent was synthesized by Chen and coworkers.[61] The telechelic *bis*-terpyridine functionalized trithiocarbonate RAFT agent was applied for the polymerization of styrene and *n*-butyl acrylate leading to well-defined *bis*-terpyridine functionalized PS homopolymers and PS-PnBA-PS triblock copolymers. Figure 1.4 summarizes the RAFT agents discussed in this section.

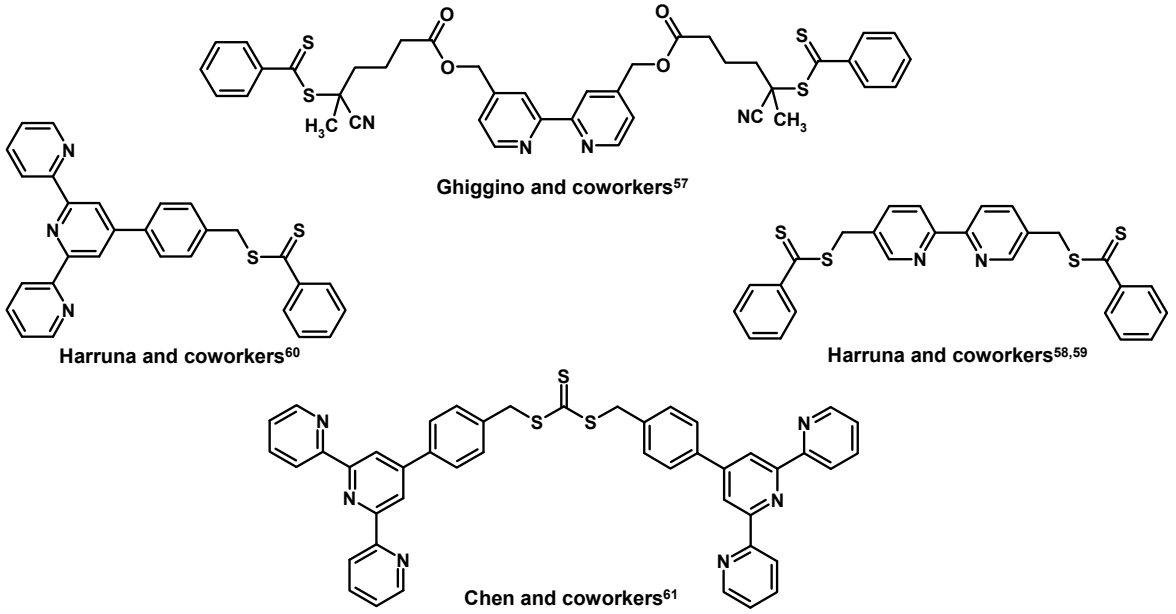

Figure 1.4 *RAFT agents possessing bipyridine or terpyridine chelating ligands for the synthesis of well-defined metallo-polymers.*

A terpyridine-functionalized initiator for NMP was reported by Schubert and coworkers.[62-66] For this purpose, a preformed benzyl chloride initiator was coupled to 2,6-di(2-pyridyl)-4-pyridone. It was demonstrated that this initiator successfully polymerizes a variety of monomers while maintaining the coordination moiety at the chain end for further modifications. Moreover, it was demonstrated that after the polymerization the nitroxide end-group could be replaced by a

terpyridine-functionalized maleimide resulting in the formation of telechelic polymers. The incorporation of terpyridine ligands into polymers represents an attractive alternative towards the design of complex structures. The tridentate ligand possesses excellent complexation abilities with a large variety of transition metal as well as lanthanide ions, and each of them having a preferred coordination geometry. The strength and lifetime of the non-covalent interaction can be controlled simply by the choice of the metal ion. In contrast to hydrogen bonding systems, the formation of metal-ligand interactions is not limited to solvents of low polarity but also to polar solvents, such as water, which certainly broadens their range of applications. Amphiphilic metallo-supramolecular block copolymers were prepared in a simple two-step synthesis by the coordination of two well-defined macroligands. This straightforward approach allowed for the preparation of a 4 × 4 library of PS_x-[Ru]-PEG_y block copolymers. The morphology of thin films obtained from these copolymers was investigated by scanning force microscopy (SFM) revealing that a wide variety of morphologies with tunable domain size can be obtained from a rather limited number of terpyridine-functionalized blocks.[67] This combinatorial approach is certainly an advantage of metallo-supramolecular block copolymers compared to classical covalent block copolymers. The micellization behavior in water of such non-covalently bonded block copolymers was extensively studied by Gohy and coworkers.[68] Investigations by AFM and TEM revealed that this core size did not scale linearly with the degree of polymerization (DP) of the PS block as expected from the theory of classical covalent copolymers. Only two core sizes were observed in these studies: 10 nm for a DP of 70 and below; and one around 20 nm for a DP of 200 and above. Moreover, two populations were observed when the DP was between 70 and 200. The unusual behavior has been attributed to electrostatic repulsions between the charged *bis*-terpyridine ruthenium complexes which strongly affect the self-assembly behavior. The repulsions could be screened out by the addition of salt to the micellar aggregates leading to linear core diameter scaling with $DP^{3/5}$. The characteristic feature of non-covalent interactions is their reversibility which could be explored for the creation of nanoporous structures.[69] In this respect, cylindrical microdomains oriented normally to the substrate were easily obtained by spin coating of a solution of PS_{375}-[Ru]-PEG_{225} in a non-selective solvent. Subsequently, the metal-ligand complexes were opened by oxidizing the Ru(II) to Ru(III) ions using Ce(IV) as oxidizing agent at pH 1. Using this approach the PEG block was released which was evidenced by AFM, X-ray photoelectron spectroscopy as well as X-ray reflectivity. Excellent work in this direction using the same initiator was recently published by O'Reilly and coworkers who prepared hollow responsive functional nanocages.[70] Therein, the synthesis of well-defined terpyridine-functionalized polystyrene and poly(*t*-butyl acrylate) is described using the unimolecular terpyridine initiator developed by Schubert *et al*. After deprotecting the *t*-butyl group with trifluoroacetic acid, the two polymer blocks were linked together *via* metal ligand complexation to yield the respective ruthenium-containing poly(acrylic acid-*b*-styrene) block copolymer. The amphiphilic material was self-assembled into spherical micelles which were treated with 2,2'-(ethylenedioxy)-*bis*(ethylamine) in the presence of 1-[3'-(dimethylamino)propyl]-3-ethylcarbodiimide methiodide to afford well-defined outer shell cross-linked nanoparticles. Subsequently, the non-covalent metal-ligand bond was effectively cleaved by the addition of the competitive ligand *N*-hydroxyethylethylenediamine triacetic acid (HEEDTA) resulting in the formation of hydrophilic, pH-responsive nanocages. In addition to that, the authors reported a similar approach towards hollow polymeric nanocages by applying a different synthetic strategy. Herein the authors report the synthesis of a SCS "pincer"-based NMP initiator and a pyridine-functionalized NMP initiator which were employed for the polymerization of styrene and *t*-butyl acrylate, respectively.[71] After the deprotection of the *t*-butyl group, the two polymers were connected to form the amphiphilic block copolymer using the relatively weak pyridine-palladium(II) interactions as well as strong interactions of the palladium(II) metal center to the SCS pincer ligand. Polymeric shell-stabilized nanoparticles were formed which were readily treated with dialysis at low pH. As a result, the

hydrophobic core domain was removed and hollow nanocages with well-defined interior functionality were obtained (Figure 1.5).

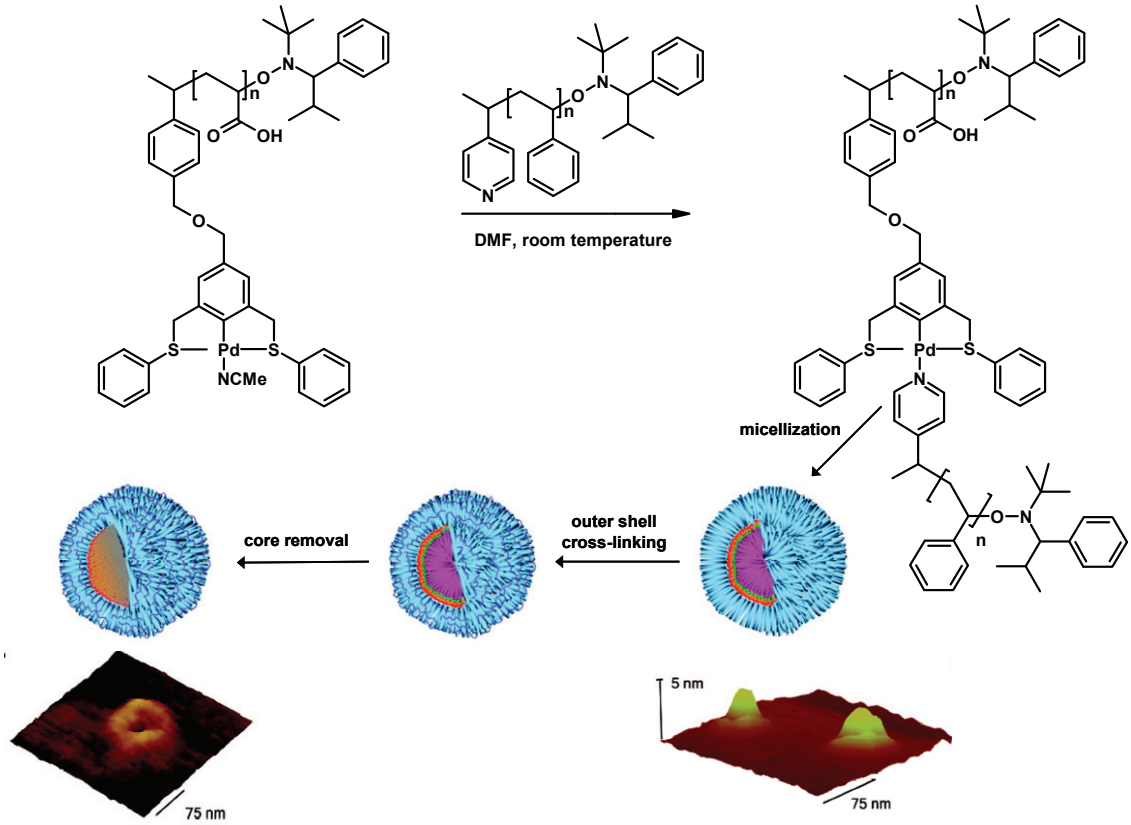

Figure 1.5 *Schematic representation of the synthesis of the amphiphilic metallo-supramolecular block copolymer based on palladium SCS "pincer" coordination (top) which was used for the preparation of hollow nanocages. Bottom row shows the AFM images of the non-covalently connected micelles (right) and the nanocages (left) after core removal and dialysis (reprinted from ref. 69).*

1.2.3 Side chain functionalized polymers by post-modification reactions

In the last decade, the use of self-assembly processes towards the synthesis of side-chain functionalized polymers have been extensively investigated due to a variety of potential applications ranging from electro-optical materials to drug delivery systems. In this section, selected recent synthetic approaches are described which lead to the incorporation of supramolecular moieties in the side-chains of polymers.

The copolymerization of maleic anhydride and a styrylic macromonomer carrying Fréchet-type polyether dendrons was performed in the group of Chen. Terpyridine groups were introduced along the polymer backbone through amidolysis of the anhydride groups.[72] The incorporation of terpyridine-functionalized polyethylene glycol chains *via* metal-ligand coordination resulted in the formation of dendronized polymer brushes with amphiphilic properties. Another universal approach for the facile access of side chain functionalized materials is the utilization of activated succinimide esters which was introduced by Tew. This synthetic strategy was explored by employing the controlled radical polymerization techniques RAFT[73] and ATRP.[74] It has been demonstrated that the respective *N*-methacryloxysuccinimide and *para*-vinylbenzyl-*N*-succinimide

units readily react in a substitution reaction with amino-functionalized materials (Scheme 1.3). In this way, the incorporation of terpyridines in the side chain of polymers was explored.

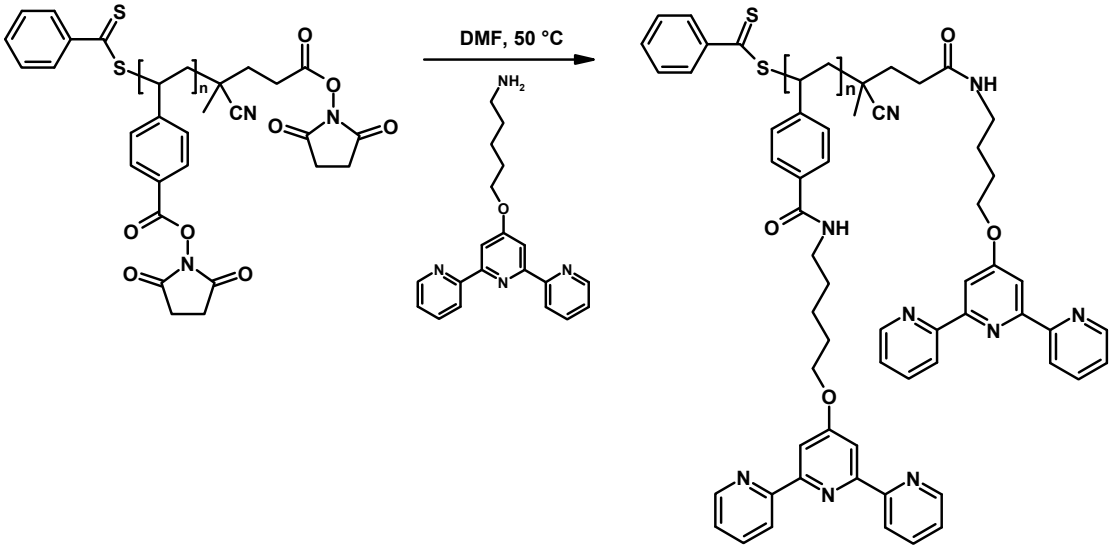

Scheme 1.3 *Schematic representation of the side-chain modification of poly(N-succinimide para-vinyl benzoate) as reported by Tew et al.*[73]

Moreover, the authors reported the complexation with different lanthanide ions which leads to emissive materials with blue, green, red or purple emission depending on the metal ion used. Tew and coworkers have also reported the synthesis of well-defined poly(*t*-butyl acrylate) by ATRP. After the cleavage of the *t*-butyl group using trifluoroacetic acid, amino-functionalized *bis*-terpyridine ruthenium(II) complexes were grafted onto the homopolymer backbone.[75] The obtained materials revealed lyotropic liquid crystalline behavior which is attributed to the inserted charged complex containing a long C_{16} alkyl chain. A very different synthetic approach to introduce functional groups has been recently reported by Schubert and coworkers. This group has demonstrated a versatile post-modification approach of pentafluorostyrene building blocks by taking advantage of the selective replacement of the *para*-fluorine groups.[76] The incorporation of terpyridines in the side-chain of the polymer resulted in the formation of a cross-linked system upon addition of iron(II) ions (see Chapter 3).

The post-modification reactions mentioned in this section represent efficient strategies for the functionalization of macromolecules. Furthermore, they allow the introduction of multiple functionalization motifs as well as the fine-tuning of selected polymer properties which opens avenues towards tailor-made functional materials.

1.2.4 Side chain functionalized polymers: polymerization of macromonomers

A common synthetic strategy to obtain side chain functionalized polymers is the modification of a monomer before it is applied for polymerization (Figure 1.3). The development of well-defined olefin-metathesis initiators based on ruthenium was a major break-through because these complexes are considerably active and exhibit favorable functional group tolerance.[77] The most recent initiator, $[(H_2IMes)(py)_2Cl_2Ru(benzylidene)]$, even possesses fast initiation characteristics and is therefore the initiator of choice when living polymerizations have to be performed. Ring-opening metathesis polymerization (ROMP) has emerged as a powerful tool for the synthesis of

well-defined polymers bearing supramolecular binding motifs in the side chain. Weck[78] and Sleiman[79] were the first groups who reported the polymerization of monomers containing 2,2'-bipyridine based metal complexes by ruthenium-catalyzed ROMP. Moreover, Weck and coworkers described the synthesis of well-defined copolymers consisting of pendant phosphorescent iridium complexes as well as 2,7-di(carbazol-9-yl)fluorene-type host moieties using the ROMP copolymerization method.[80] The copolymers feature interesting photo- and electrophysical properties which can be attributed to the iridium complex. Furthermore, the copolymer was tested in an organic light emitting device revealing sufficient performance for display and lighting applications. Thermoreversible polymer networks with tuneable rheological properties could be obtained by combining ROMP with the incorporation of hydrogen bonding motifs (Scheme 1.4).[81] Thereby, different types of complementary hydrogen bonding units were chosen which resulted in the formation of highly viscous fluids or viscoelastic gels depending on the supramolecular cross-linking agent used. Furthermore, one example is reported in literature where three different recognition motifs were incorporated in one polymer backbone. For this purpose, ring-opening metathesis polymerization was performed with differently functionalized norbonene macromonomers which led to the formation of random terpolymers containing SCS palladated pincer complexes, dibenzo[24]crown-8 rings and diaminopyridine moieties.[82] Functionalization of the terpolymers was achieved by self-assembling pyridines to the palladium pincer complexes, dibenzylammonium ions to the crown ether rings and thymines to the hydrogen bonding receptors.

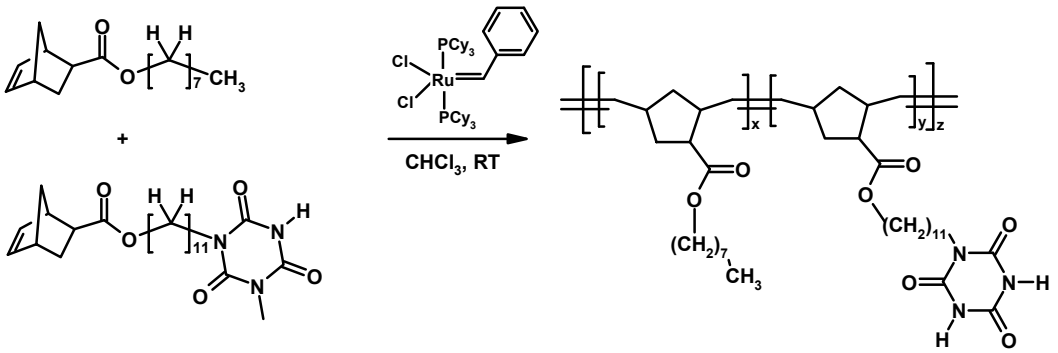

Scheme 1.4 *Schematic representation of the synthesis of side-chain functionalized poly(norbonenes) via ROMP using Grubbs' first generation initiator.*

In addition, the controlled radical polymerization techniques, *i.e*. NMP, RAFT and ATRP, are suitable candidates to polymerize functionalized macromonomers. For example, Kallitsis described the homopolymerization of a terpyridine-functionalized macroinitiator by ATRP.[83] Afterwards, the polymers were connected to a telechelic di(styryl)-anthracene derivative and the free terpyridines ligands in the side-chain of the polymer were complexed with a *bis*(dodecyloxy)-functionalized terpyridine moiety using ruthenium ions. Tew and coworkers reported the synthesis of a terpyridine-functionalized styrene-based macromonomer which was obtained by performing a dicyclohexylcarbodiimide (DCC) / *N*-hydroxybenzotriazole (HOBT) coupling. Subsequently the monomer was applied for NMP[84] and RAFT[84,85] to yield well-defined random and block copolymers. The application of terpyridine-modified macromonomers for the preparation of side-chain functionalized polymers has been also explored by O'Reilly and coworkers.[86] To afford the functionalized macromonomer, 4-vinyl benzylchloride was reacted with 2,6-*bis*(pyrid-2-yl)-4-pyridone. The copolymerization of this monomer was performed by employing a nitroxide-mediated polymerization procedure. The synthetic goal of this research was the preparation of an amphiphilic block copolymer which was obtained by polymerizing the macroinitiator with *t*-butyl acrylate and the subsequent deprotection with trifluoroacetic acid (TFA). Core reactive spherical

micelles were prepared from this material which consists of selectively located terpyridine moieties in the hydrophobic core. Their modification by metal complexation (Fe, Ru, Cu) afforded novel functionalized polymer nanostructures. An efficient difunctional alkoxyamine initiator ($DEPN_2$) was synthesized and exploited for the preparation of triblock copolymers by Long and coworkers.[87] Complementary hydrogen bonding triblock copolymers containing adenine (A) and thymine (T) nucleobase-functionalized outer blocks were synthesized (Scheme 1.5). Thermoplastic elastomeric block copolymers were prepared where a poly(*n*-butyl acrylate) rubber block served as midsegment. The morphology of this triblock copolymer was investigated by SAXS and AFM revealing intermediate interdomain spacing and surface textures for the blends compared to the individual precursors.

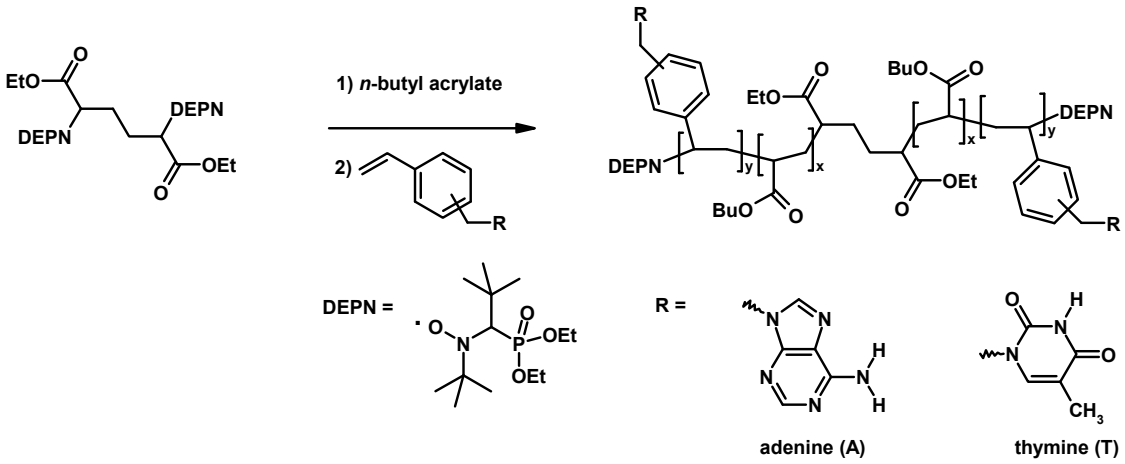

Scheme 1.5 *Schematic representation of the synthesis of adenine and thmine-functionalized triblock copolymers.*

The design and preparation of new materials that combine reversible properties provided by supramolecular binding motifs and the processability and mechanical properties of polymers are thriving fields in polymer science. This section contained the most recent synthetic approaches which are applied to introduce supramolecular functional group(s) into the polymer backbone. The combination of supramolecular functionalities and controlled/"living" polymerization techniques provide well-defined materials with control over architecture and composition, respectively.

1.3 Applications

Even though tremendous progress has been made in the field of commodity thermoplastics and elastomers in the last couple of decades, the focus in modern polymer science has shifted more and more to specialty or 'value-added' materials with advanced properties. Researchers in this field achieve the desired function of a material by choosing the appropriate supramolecular connectors, spacer groups and polymer backbones. The examples presented in this part are not necessarily based on well-defined supramolecular polymers.

The reversible nature of non-covalent interactions offers in particular promising application as self-healing materials. The structural framework of self-healing materials is based on reversible, or dynamic, chemical bonds, such as either metal-ligand coordination interactions, hydrogen or directed electrostatic interactions. Recently, a room-temperature self-healing rubber[88] on the basis of hydrogen bonds was developed (Figure 1.6).

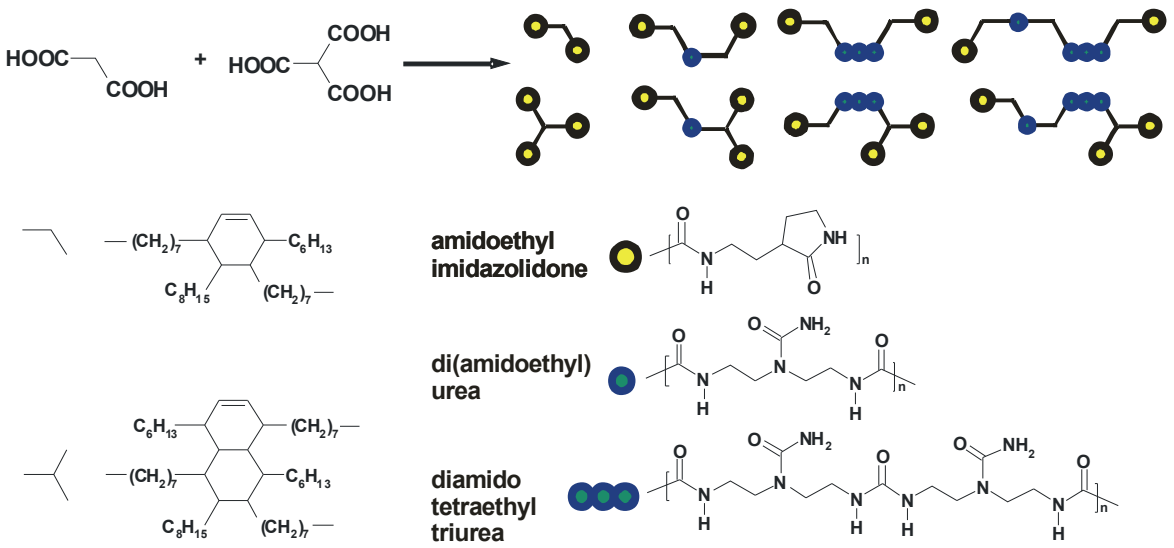

Figure 1.6 *Schematic representation of the synthesis of oligomers equipped with complementary hydrogen bonding groups for self-healing applications as reported by Leibler et al.*[88]

The basic concept of these materials is that they can exist in either polymeric or monomeric status, depending on their environment. Consequently, the material can switch between good mechanical properties attributed to the polymer and good dynamic properties (monomer) if material has to be transported to damaged areas. Also metal-ligand coordination is a suitable tool for these kinds of applications. A promising system was presented by Rowan and coworkers.[89,90] A bifunctional tridentate pyridine-based ligand, namely 2,6-*bis*(1'-methylbenzimidazolyl)-4-hydroxypyridine, is able to coordinate various dicationic (Zn^{2+}, Fe^{2+}, Co^{2+}) and tricationic (La^{3+}, Eu^{3+}) metals. Whereas the divalent metal ions are responsible for the formation of linear coordination polymers, the trivalent metal ions are able to accommodate up to three ligands which results in the formation of cross-linked gel-forming materials (Figure 1.7). When heat or mechanical stress is applied to the system, the cross-links break and the material starts to flow. Upon the removal of the stimulus, the material regains its original mechanical properties due to the beginning self-assembly process. Photoluminescent metal-containing polymers as reported by Rowan and coworkers[91] exhibit appreciable mechanical strength and are easier to process compared to high molar mass organic analogues.

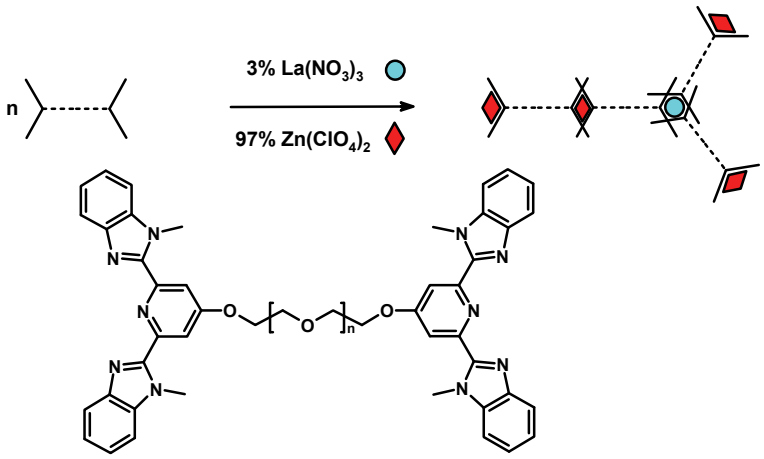

Figure 1.7 *Schematic representation of the formation of a metallo-supramolecular gel using the combination of lanthanoid and transition metal ion.*[89,90]

Metal-ligand coordination polymers represent an important class of materials due to their high non-covalent bond strength as well as the unique physical properties of transition metal complexes. The careful selection of a suitable chelating ligand and the respective metal ion are responsible for the particular bond strength and the photophysical and electrochemical properties. For example, the choice of a different ligand may influence the luminescence: $Ru(bpy)_3$ complexes possess luminescent properties, whereas $Ru(tpy)_2$ complexes only show luminescence at low temperature. On the other hand, highly luminescent materials can be easily obtained by using lanthanide ions. The valence electron structure of lanthanide ions is well-suited for strong luminescence. The excitation of the coordinated ligands and the subsequent energy transfer to the metal ion are the reason for their characteristic luminescence properties ("antenna effect"). Since the non-covalent interaction between lanthanide ion and chelating ligand is relatively weak, these materials find potential applications as optical chemical sensors.[92,93] A polymeric memory device has also been prepared using a redox-active copolymer with carbazole electron donors and europium-complexes as electron acceptors both located in the side chain of the polymer (Figure 1.8).[94] Polymeric systems with highly efficient phosphorescent emitters are interesting candidates for light-emitting applications, such as organic light emitting diodes (OLED's). In particular, iridium(III) complexes are rather attractive due to their ability to tune the wavelength of emission by making use of different chelating ligands.[95] These polymer-based materials feature an improved processability due to the advantageous film forming properties as well as suppressed phase separation.

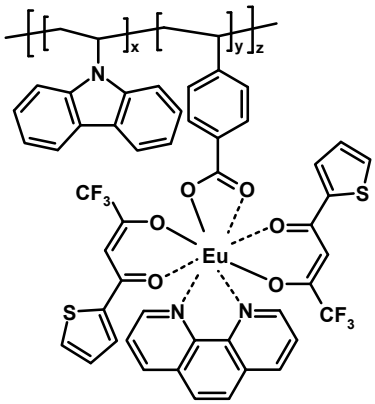

Figure 1.8 *Schematic representation of a redox-active copolymer containing europium-complexes as electron acceptors.*[92]

The basic principles of supramolecular chemistry were rapidly applied in the field of polymer science. Nowadays, two different polymer chains can be connected with each other via non-covalent interactions. Of course, this is an advantageous and easy strategy for the preparation of amphiphilic materials. Polymeric micelles and vesicles resulting from self-assembly processes of these materials in selective solvents may potentially be used as drug delivery agents.[96,97] Moreover, the reversibility and switchability provided by the non-covalent binding motif might be utilized for nanocatalysis or as scaffold for dynamic libraries.[98] Thin films of block copolymers with well-defined phase behavior and highly ordered morphology can give rise to patterned functional materials by breaking the non-covalent bond and washing out one of the blocks using selective solvents. Another approach is the modification of supramolecular-functionalized block copolymer micelles. Recently, an interesting method was reported for tuning block copolymer micelles by metal-ligand interactions.[99] Terpyridine ligands located in the corona of the micelle are available for complexation with metal ions. The authors report an approach to tune the size, conformation

and functionality of coronal chains in block copolymer micelles by adding various metal ions to the system which resulted in intramicellar complexation.

The examples described in this section clearly demonstrate that supramolecular polymer chemistry offers exciting future opportunities. In addition, more applications may come within reach upon further developments in supramolecular chemistry.

1.4 Aim and scope of the thesis

Supramolecular chemistry is a new emerging interdisciplinary field combining concepts and systems from chemistry, biochemistry, physics and material science. During the last decades, researchers from different fields of science have been developing new strategies dealing with the design and formation of complex molecular structures which are expected to display targeted properties and functions. In particular, metallo-supramolecular polymers offer the attractive combination of metal ion induced functionality, mechanical properties and processability of polymers as well as the self-assembly characteristics and dynamic nature of supramolecular chemistry. Nowadays, many promising nanotechnology devices are based on this so-called "bottom-up" approach. This thesis focuses on the preparation of new well-defined polymeric materials using different polymerization techniques. Terpyridine ligands incorporated at the polymer chain end act as the supramolecular motifs which are able to form switchable metal-ligand interactions. By making use of homoleptic and heteroleptic *bis*-terpyridine complexes, a wide range of different macromolecular architectures can be prepared in a straightforward fashion.

Chapter 2 of this thesis reports different synthetic pathways for the coordination of functionalized terpyridine ligands with transition metal ions. The first part deals with the synthesis and characterization of homoleptic and heteroleptic ruthenium(II) complexes. The synthesis of mixed-ligand iridium(III) complexes using orthometallated dimeric iridium precursors is discussed in the second part of this chapter.

Chapter 3 introduces a series of well-defined homopolymers and block copolymers which were obtained by employing nitroxide-mediated radical polymerization methods using a terpyridine-modified alkoxyamine initiator. Furthermore, a versatile post-modification of pentafluorostyrene building blocks is presented which allows the easy insertion of functional groups which were exploited by applying different controlled polymerization techniques resulting in the formation of graft-architectures.

Chapter 4 describes the synthesis and characterization of new amphiphilic block copolymers which were obtained by connecting different polymer chains together via non-covalent coordination chemistry using ruthenium(II) ions. The self-assembly of the obtained block copolymers was investigated in solution. Moreover, this chapter contains the synthesis and characterization of light-emitting iridium(III) polymers which reveal a different emission behavior upon changing the ligand.

Chapter 5 introduces the preparation of well-defined terpyridine-functionalized alternating copolymers which were obtained by living anionic polymerization. Special focus in this chapter is given to terpyridine chain-end functionalization. Well-defined metallo-supramolecular block copolymers were formed upon complexation with ruthenium(II) ions. Analytical ultracentrifugation and depth sensing indentation were used as characterization techniques to investigate in detail the properties of the prepared block copolymer library. This section also includes the preparation of well-defined block copolymers by sequential monomer addition.

1.5 References

1 J.-M. Lehn, *Supramolecular Chemistry: Concepts and Perspectives*, VCH, Weinheim, **1995**.
2 J.-M. Lehn, *Science* **1993**, *260*, 1762.
3 A. Ciferri, *Supramolecular Polymers*, Dekker, New York, NY, **2000**.
4 J.W. Steed, J.L. Atwood, *Supramolecular Chemistry*, John Wiley & Sons Ltd, Chichester, West Sussex, **2000**.
5 L. Brunsfeld, B.J.B. Folmer, E.W. Meijer, R.P. Sijbesma, *Chem. Rev.* **2001**, *101*, 4071.
6 D.N. Reinhoudt, M. Crego-Calama, *Science* **2002**, *295*, 2403.
7 O. Ikkala, G. ten Brinke, *Science* **2002**, *295*, 2407.
8 A. Ciferri, *Macromol. Rapid Commun.* **2002**, *23*, 511.
9 J.-M. Lehn, *Polym. Int.* **2002**, *51*, 825.
10 L.J. Prins, D.N. Reinhoudt, P. Timmerman, *Angew. Chem. Int. Ed.* **2001**, *40*, 2382.
11 G.A. Jeffery, *An Introduction to Hydrogen Bonding,* Oxford University Press, Oxford, **1997**.
12 G. Cooke, V.M. Rotello, *Chem. Soc. Rev.* **2002**, *31*, 274.
13 M. Alamgir Hossain, H.-J. Schneider, *Chem. Eur. J.* **1999**, *5*, 1284.
14 T. Kaliyappan, P. Kannan, *Prog. Polym. Sci.* **2000**, *25*, 343.
15 F.A. Cotton, G. Wilkinson, C.A. Murillo, M. Bochmann, *Advanced Inorganic Chemistry*, 6th edt., John Wiley Sons, Inc., New York, NY, **1999**.
16 W.L. Jørgenson, J. Pranata, *J. Am. Chem. Soc*. **1990**, *112*, 2008.
17 J. Pranata, S.G. Wierschke, W.L. Jørgenson, *J. Am. Chem. Soc*. **1991**, *113*, 2810.
18 A.J. Goshe, I.M. Steele, C. Ceccarelli, A.L. Rheingold, B. Bosnich, *Proc. Natl. Acad. Sci.* **2002**, *99*, 4823.
19 B.J.B. Folmer, E. Cavini, R.P. Sijbesma, E.W. Meijer, *Chem. Commun*. **1998**, 1847.
20 B.J.B. Folmer, R.P. Sijbesma, R.M. Versteegen, J.A.J. van der Rijt, E.W. Meijer, *Adv. Mater.* **2000**, *12*, 874.
21 L.R. Rieth, R.F. Eaton, G.W. Coates, *Angew. Chem. Int. Ed*. **2001**, *40*, 2153.
22 C. Fouquey, J.-M. Lehn, A.M. Levelut, *Adv. Mater.* **1990**, *2*, 254.
23 M. Kotera, J.-M. Lehn, J.P. Vigneron, *J. Chem. Soc. Chem. Commun.* **1994**, 197.
24 R.J. Christie, D.W. Grainger, *Adv. Drug Deliv. Rev*. **2003**, *55*, 421.
25 K. Ramanathan, M.A. Bangar, M. Yun, W. Chen, N.V. Myung, A. Mulchandani, *J. Am. Chem. Soc.* **2005**, *127*, 496.
26 R. Haag, F. Kratz, *Angew. Chem. Int. Ed*. **2006**, *45*, 1198.
27 H.S. Bazzi, J. Bouffard, H.F. Sleiman, *Macromolecules* **2003**, *36*, 7899.
28 T. Kato, O. Ihata, S. Ujiie, M. Tokita, J. Watanabe, *Macromolecules* **1998**, *31*, 3551.
29 A.K. Boal, F. Ilhan, J.E. DeRouchey, T. Thurn-Albrecht, T.P. Russell, V.M. Rotello, *Nature* **2000**, *404*, 746.
30 J.S. Lindsey, *New J. Chem.* **1991**, *15*, 153.
31 D. Philp, J.F. Stoddart, *Angew. Chem. Int. Ed*. **1996**, *35*, 1154.
32 C.B. Smith, E.C. Constable, C.E. Housecroft, B.M. Kariuki, *Chem. Commun.* **2002**, 2068.
33 G.U. Priimov, P. Moore, P.K. Maritim, P.K. Butalanyi, N.W. Alcock, *J. Chem. Soc., Dalton Trans.* **2000**, 445.
34 B.G.G. Lohmeijer, U.S. Schubert, *J. Polym. Sci., Part A: Polym. Chem.* **2003**, *41*, 1413.
35 B.G.G. Lohmeijer, U.S. Schubert, *Angew. Chem. Int. Ed.* **2002**, *41*, 3825.
36 V. Marin, E. Holder, M.A.R. Meier, R. Hoogenboom, U.S. Schubert, *Macromol. Rapid Commun.* **2004**, *25*, 793.
37 J.B. Beck, J.M. Ineman, S.J. Rowan, *Macromolecules* **2005**, *38*, 5060.
38 A. Karatzas, M. Talelli, M. Pitsikalis, N. Hadjichristidis, *Macromolecules* **2006**, *39*, 8456.
39 C. Guerrero-Sanchez, B.G.G. Lohmeijer, M.A.R. Meier, U.S. Schubert, *Macromolecules* **2005**, *38*, 10388.
40 D.J.M. van Beek, A.J.H. Spiering, G.W.M. Peters, K. te Nijenhuis, R.P. Sijbesma, *Macromolecules* **2007**, *40*, 8464.
41 K. Matyjaszewski, J. Xia, *Chem. Rev.* **2001**, *101*, 2921.
42 M. Kamigaito, T. Ando, M. Sawamoto, *Chem. Rev.* **2001**, *101*, 3689.

43 C.J. Hawker, A.W. Bosman, E. Harth, *Chem. Rev.* **2001**, *101*, 3661.
44 H. Fischer, *Chem. Rev.* **2001**, *101*, 3581.
45 G. Moad, E. Rizzardo, S.H. Thang, *Polymer* **2008**, *49*, 1079.
46 J.E. Collins, C.L. Fraser, *Macromolecules* **1998**, *31*, 6715.
47 R.M. Johnson, P.S. Corbin, C. Ng, C.L. Fraser, *Macromolecules* **2000**, *33*, 7404.
48 A.P. Smith, C.L. Fraser, *Macromolecules* **2003**, *36*, 2654.
49 R.M. Johnson, C.L. Fraser, *Macromolecules* **2004**, *37*, 2718.
50 L. Viau, M. Even, O. Maury, D.M. Haddleton, H. Le Bozec, *Macromol. Rapid Commun.* **2003**, *24*, 630.
51 J.L. Gorczynski, J. Chen, C.L. Fraser, *J. Am. Chem. Soc.* **2005**, *127*, 14956.
52 G.L. Fiore, J.M. Edwards, S.J. Payne, J.L. Klinkenberg, D.G. Gioeli, J.N. Demas, C.L. Fraser, *Biomacromolecules* **2007**, *8*, 2829.
53 R. Kircheis, L. Wightman, E. Wagner, *Adv. Drug Deliv. Rev.* **2001**, *53*, 341.
54 T. Merdan, J. Kopecek, T. Kissel, *Adv. Drug Deliv. Rev.* **2002**, *54*, 715.
55 A.D. Celiz, O.A. Scherman, *Macromolecules* **2008**, *41*, 4115.
56 H. Hofmeier, R. Hoogenboom, M.E.L. Wouters, U.S. Schubert, *J. Am. Chem. Soc.* **2005**, *127*, 2913.
57 M. Chen, K.P. Ghiggino, A. Launikonis, A.W.H. Mau, E. Rizzardo, W.H.F. Sasse, S.H. Thang, G.J. Wilson, *J. Mater. Chem.* **2003**, *13*, 2696.
58 G. Zhou, I.I. Harruna, *Macromolecules* **2004**, *37*, 7132.
59 G. Zhou, I.I. Harruna, C.W. Ingram, *Polymer* **2005**, *46*, 10672.
60 G. Zhou, I.I. Harruna, *Macromolecules* **2005**, *38*, 4114.
61 L. Zhang, Y, Zhang, Y. Chen, *Eur. Polym. J.* **2006**, *42*, 2398.
62 B.G.G. Lohmeijer, U.S. Schubert, *J. Polym. Sci., Part A: Polym. Chem.* **2003**, *41*, 1413.
63 B.G.G. Lohmeijer, U.S. Schubert, *J. Polym. Sci., Part A: Polym. Chem.* **2004**, *42*, 4016.
64 B.G.G. Lohmeijer, U.S. Schubert, *J. Polym. Sci., Part A: Polym. Chem.* **2005**, *43*, 6331.
65 C. Ott, B.G.G. Lohmeijer, U.S. Schubert, *Macromol. Chem. Phys.* **2006**, *207*, 1439.
66 C. Ott, D. Wouters, H.M.L. Thijs, U.S. Schubert, *J. Inorg. Organometal. Polym. Mater.* **2007**, *17*, 241.
67 B.G.G. Lohmeijer, D. Wouters, Z. Yin, U.S. Schubert, *Chem. Commun.* **2004**, 2886.
68 P. Guillet, C.-A. Fustin, B.G.G. Lohmeijer, U.S. Schubert, J.F. Gohy, *Macromolecules* **2006**, *39*, 5484.
69 C.-A. Fustin, B.G.G. Lohmeijer, A.S. Duwez, A.M. Jonas, U.S. Schubert, J.-F. Gohy, *Adv. Mater.* **2005**, *17*, 1162.
70 A.D. Ievins, A.O. Moughton, R.K. O'Reilly, *Macromolecules* **2008**, *41*, 3571.
71 A.O. Moughton, R.K. O'Reilly, *J. Am. Chem. Soc.* **2008**, *130*, 8714.
72 Y. Zhang, Z. Xu, X. Li, Y. Chen, *J. Polym. Sci., Part A: Polym. Chem.* **2007**, *45*, 3303.
73 K.A. Aamer, G.N. Tew, *J. Polym. Sci., Part A: Polym. Chem.* **2007**, *45*, 5618.
74 R. Shunmugam, G.N. Tew, *J. Polym. Sci., Part A: Polym. Chem.* **2005**, *43*, 5831.
75 K.A. Aamer, G.N. Tew, *Macromolecules* **2007**, *40*, 2737.
76 C. Ott, R. Hoogenboom, U.S. Schubert, *Chem. Commun.* **2008**, 3516.
77 T.M. Trnka, R.H. Grubbs, *Acc. Chem. Res.* **2001**, *34*, 18.
78 J.R. Carlise, M. Weck, *J. Polym. Sci., Part A: Polym. Chem.* **2004**, *42*, 2973.
79 B. Chen, H.F. Sleiman, *Macromolecules* **2004**, *37*, 5866.
80 A. Kimyonok, B. Domercq, A. Haldi, J.-Y. Cho, J.R. Carlise, X.-Y. Wang, L.E. Hayden, S.C. Jones, S. Barlow, S.R. Marder, B. Kippelen, M. Weck, *Chem. Mater.* **2007**, *19*, 5602.
81 K.P. Nair, V. Breedveld, M. Weck, *Macromolecules* **2008**, *41*, 3429.
82 C.R. South, K.C.-F. Leung, D. Lanari, J.F. Stoddart, M. Weck, *Macromolecules* **2006**, *39*, 3738.
83 N.P. Tzanetos, A.K. Andreopoulou, J.K. Kallitsis, *J. Polym. Sci., Part A: Polym. Chem.* **2005**, *43*, 4838.
84 K.A. Aamer, G.N. Tew, *Macromolecules* **2004**, *37*, 1990.
85 K.A. Aamer, R. Shunmugam, G.N. Tew, *Polymer* **2005**, *46*, 8440.
86 A.D. Ievins, X. Wang, A.O. Moughton, J. Skey, R.K. O'Reilly, *Macromolecules* **2008**, *41*, 2998.
87 B.D. Mather, M.B. Baker, F.L. Beyer, M.A.G. Berg, M.D. Green, T.E. Long, *Macromolecules* **2007**, *40*, 6834.

88 P. Cordier, F. Tournilhac, C. Soulié-Ziakovic, L. Leibler, *Nature* **2008**, *451*, 977.
89 J.B. Beck, S.J. Rowan, *J. Am. Chem. Soc.* **2003**, *125*, 13922.
90 Y. Zhao, J.B. Beck, S.J. Rowan, A.M. Jamieson, *Macromolecules* **2004**, *37*, 3529.
91 D. Knapton, S.J. Rowan, C. Weder, *Macromolecules* **2006**, *39*, 651.
92 D. Knapton, M. Burnworth, S.J. Rowan, C. Weder, *Angew. Chem. Int. Ed.* **2006**, *45*, 5825.
93 R. Shunmugam, G.N. Tew, *Chem. Eur. J.* **2008**, *14*, 5409.
94 Q. Ling, Y. Song, S.J. Ding, C. Zhu, D.S.H. Chan, D.-L. Kwong, E.-T. Kang, K.-G. Neoh, *Adv. Mater.* **2005**, *17*, 455.
95 V. Marin, E. Holder, R. Hoogenboom, U.S. Schubert, *Chem. Soc. Rev.* **2007**, *36*, 618.
96 G. Cevc, *Adv. Drug Deliv. Rev.* **2004**, *56*, 675.
97 U. Boas, P.H.M. Heegaard, *Chem. Soc. Rev.* **2004**, *33*, 43.
98 J.-F. Gohy, B.G.G. Lohmeijer, U.S. Schubert, *Chem. Eur. J.* **2003**, *9*, 3472.
99 P. Guillet, C.-A. Fustin, C. Mugemana, C. Ott, U.S. Schubert, J.-F. Gohy, *Soft Matter* **2008**, *4*, 2278.

CHAPTER 2

4'-Functionalized 2,2':6',2''-terpyridine complexes based on ruthenium(II) and iridium(III) ions

Abstract

Differently substituted terpyridine complexes have been prepared by making use of the chelating properties of 2,2':6',2"-terpyridine and 2,2'-bipyridine towards ruthenium(II) and iridium(III) metal ions. The first part of the chapter describes different synthetic approaches to synthesize several homoleptic as well as heteroleptic bis-terpyridine ruthenium(II) complexes. The second part involves the synthesis of mixed-ligand iridium(III) complexes obtained using orthometallated dimeric iridium-precursors. Characterization techniques for the prepared model complexes include ^{1}H NMR spectroscopy, gel permeation chromatography (GPC), absorption and emission spectroscopy, elemental analysis, MALDI-TOF mass spectrometry and X-ray analysis. The terpyridine-ligands with different functional groups in the 4'-position allow further chemical modification of the complexes. The synthetic approach to prepare model complexes is the same as for polymeric complexes which are of great interest in materials research since interesting photophysical and electrochemical properties can be incorporated into the materials. Incorporating metal complexes into polymers can be achieved by two synthetic methods: (1) substitution reactions on the functional group or (2) by using the functional group to initiate "living" or controlled polymerization processes (e.g. atom transfer radical polymerization (ATRP), cationic ring-opening polymerization (CROP), nitroxide-mediated polymerization (NMRP), etc.).

2.1 Introduction

In the last couple of decades, the field of supramolecular chemistry has attracted special interest and represents an important area of today's material research. Non-covalent interactions, including hydrogen bonding, metal coordination, van der Waals forces, electrostatic effects and hydrophilic-hydrophobic interactions, can be used to self assemble molecules into supramolecular materials. As a consequence, the materials are expected to reveal new properties with respect to film formation, surface activity, and reversibility of the complexation, which can result in "switchable" systems under certain conditions.[1,2]

Metallo-supramolecular chemistry is the assembly of supramolecular structures through the interaction of metal ions with metal-binding sites (ligands). The characteristic interactions are defined by the preferred coordination number, geometry and donor-type of the metal-ion, and the number, type and spatial arrangement of the donor atoms of the metal-binding domain. Commonly used nitrogen-based metal-binding entities are presented in Scheme 2.1.

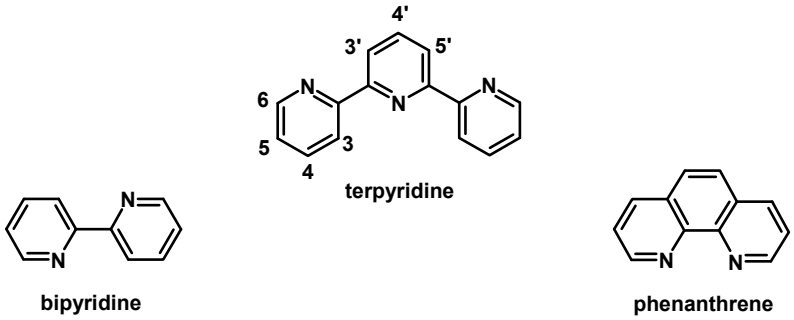

Scheme 2.1 *Schematic representation of the structures of the most commonly encountered oligopyridine ligands. The terpyridine ligand is depicted in the trans, trans-conformation. The ring atom numbering scheme is shown for substituents in terpyridine derivatives.*

The first isolation of 2,2':6',2"-terpyridine was reported in 1932 by Morgan and Burstall.[3] The reaction involved an oxidative condensation of pyridine with iron(III) chloride in an autoclave. Terpyridine was isolated as one of 20 products of this reaction. Nowadays, a variety of synthetic routes exist for the preparation of the chelating ligand. They are generally based on two different methods, ring closure and ring coupling. Ring closure procedures introduced by Kröhnke[4] and Potts[5] afford the nucleophilic 4'-hydroxy terpyridine and the electrophilic 4'-chloro terpyridine, key intermediates for further functionalization in the 4' position.[6] From these two intermediates, a great variety of functionalized species is available (section 2.2). The substituted terpyridine ligands are valuable building blocks in metallo-supramolecular chemistry since these ligands readily coordinate to a wide variety of transition metal ions.[7] 2,2':6',2"-Terpyridine commonly acts as a tridentate N_3 donor, although a few examples of the ligand acting as bidentate or monodentate donor have been reported.[7] Terpyridine forms stable 2:1 octahedral complexes (ideally D_{2d} symmetry) with a large variety of transition metal ions in low oxidation states, such as Ru(II), Fe(II), Zn(II), Co(II) and Cu(II), due to strong metal to ligand $d\pi$-$p\pi^*$ back donation. The tridentate binding mode is used for these metal ions which requires a change in conformation from *trans, trans* of the free ligand to *cis, cis* conformation; this has consequences for the kinetics of coordination. When the symmetrical 4'-substituted terpyridine ligand is coordinated to a metal ion, it affords the formation of one product without isomers. This is a significant advantage over bipyridine (bpy) and phenanthrene (phen) which, if *mono*-substituted, are asymmetrical. Upon complexation of bpy or phen, a statistical mixture of diastereomers (*fac* and *mer*) with different spatial arrangements is produced.

The metal center plays a crucial role for chemical and photophysical properties of the supramolecule as well as for the control of the kinetics of the assembly. Kinetically inert metal ions such as ruthenium(II) are used as preformed complex building blocks while labile metal ions are usually encountered in spontaneous self-assembly reactions, during which a new *bis*-terpyridine metal complex is generated. The metallo-supramolecular complexes described in section 2.3 are coordinated to ruthenium(II) ions, thus forming inert metal complexes which reveal interesting optical and photophysical properties.[8-10] Ruthenium(II) ions allow the direct synthesis of homoleptic and heteroleptic complexes which can be conducted in a simple two-step sequence using either ruthenium(III) or ruthenium(II) intermediates. Section 2.4 exemplifies the terpyridine ligand as nitrogen bidentate donor forming stable/inert mixed-ligand iridium(III) complexes in a bridge-splitting reaction with dimeric iridium-precursors. The complex formation studies of this chapter were performed to optimize the complexation reaction which is later applied for the preparation of block copolymers.

2.2 Synthesis of supramolecular terpyridine ligands

4'-Terpyridinoxy derivatives are conveniently accessible via (1) nucleophilic aromatic substitution of 4'-chloroterpyridine by any primary alcohol (and analogs)[11-16] or (2) via S_N2-type nucleophilic substitution of the alcoholates of 4'-hydroxy-terpyridine by, *e.g.*, alkylhalides and tosylates. The introduction of different functionalities into the 4'-position of 2,2':6',2"-terpyridine was carried out utilizing the base supported nucleophilic substitution of the chloro-functionality with various alcoholates formed *in situ* under strong basic conditions with potassium hydroxide in aprotic solvents such as dimethyl sulfoxide (DMSO) (Scheme 2.2). Using the synthetic pathway (1), the nucleophilic aromatic substitution was performed effectively to yield compounds **II-1**, **II-2** and **II-3**, respectively.

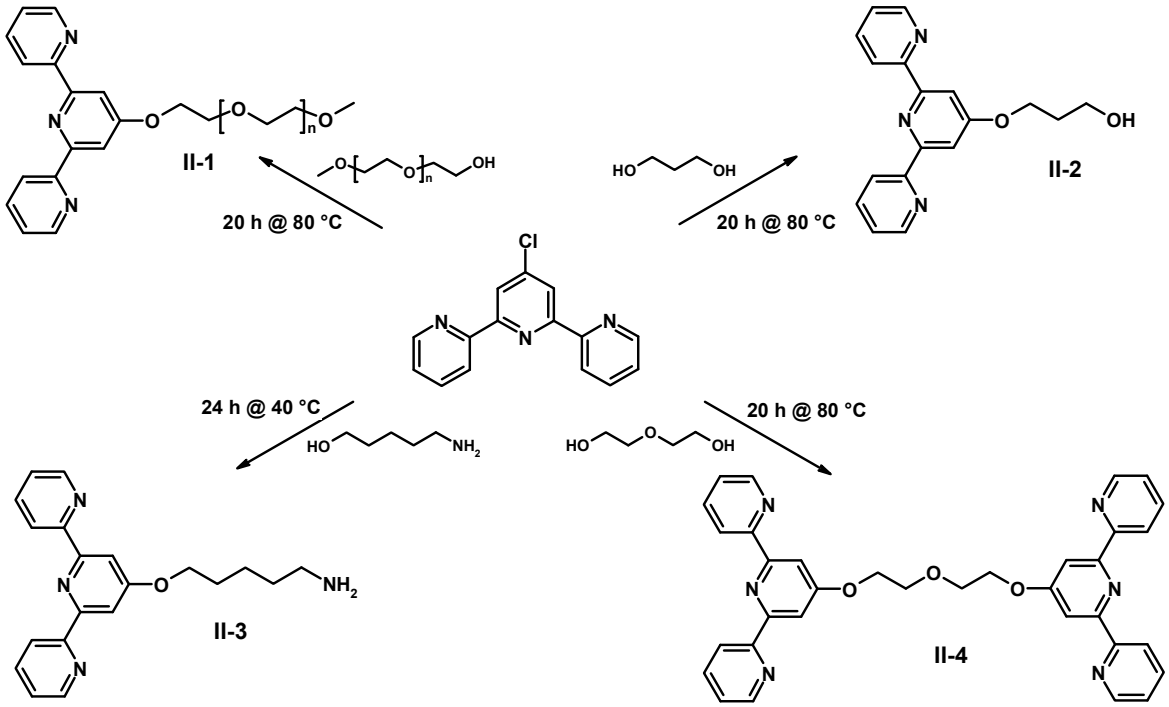

Scheme 2.2 *Schematic representation of the synthesis of several 4'-terpyridinoxy derivatives performed in DMSO using KOH to create the corresponding alcoholate.*

In the case of diols as starting materials *mono*- and *bis*-functionalization was performed successfully by controlling the stoichiometry. In order to obtain *mono*-functionalized product, a 10 fold excess of diol was used to prevent the formation of telechelics. On the other hand, a 1.2 excess of 4'-chloroterpyridine is sufficient to obtain the desired telechelic compound **II-4**. Purification of the terpyridine-functionalized compounds was carried out by double precipitation from chloroform into methanol or ice-cold water. Yields of 74% and higher were obtained for the substitution reactions depicted in Scheme 2.2. Figure 2.1 shows the ^{1}H NMR spectra of the compounds **II-2** and **II-4** demonstrating the successful incorporation of the terpyridine ligand. The spectra clearly reveal that in case of the desired telechelic compound the excess of 4'-chloroterpyridine was removed in the purification step. Moreover, the spectral evidence indicates a degree of functionalization of 100% which can be determined by integration over the signals belonging to the terpyridine end-group with respect to the signals belonging to the backbone.

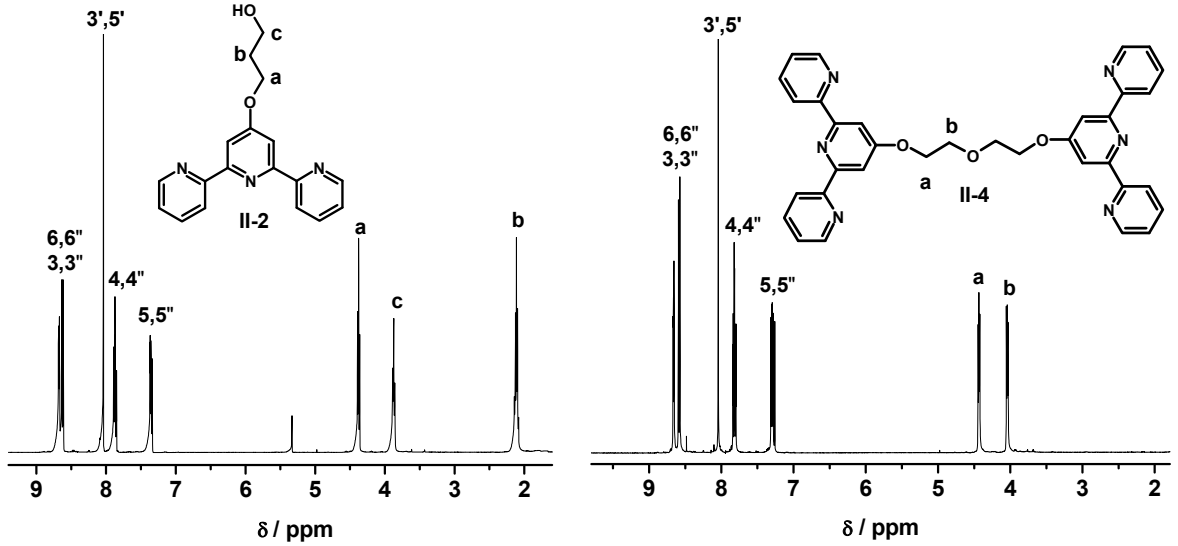

Figure 2.1 *^{1}H NMR spectra of the obtained compounds **II-2** (in CD_2Cl_2) and **II-4** (in $CHCl_3$) after the substitution reaction with 4'-chloro-terpyridine.*

The hydroxy-functionality of compound **II-2** is available for further chemical modification. The hydroxy end-group was converted into a chloro-functionality simply by refluxing compound **II-2** in $SOCl_2$ to yield the corresponding chloro-propoxy-terpyridine **II-5** (Scheme 2.3). Compound **II-5** was characterized by ^{1}H NMR spectroscopy revealing the disappearance of the signal attributed to the hydroxy-group as well as a downfield shift of the signal adjacent to the chloro-functionality from 3.59 to 3.83 ppm. Elemental analysis was chosen as an additional characterization technique which proved the purity of the synthesized ligand.

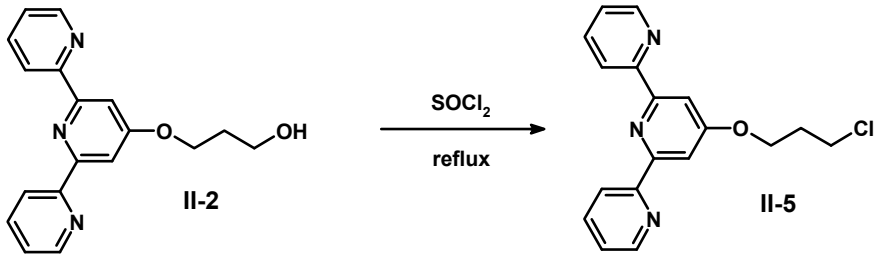

Scheme 2.3 *Schematic representation of the synthesis of chloro-propoxy-terpyridine from the respective hydroxyl-terpyridine.*

4'-Arylterpyridines can be easily prepared by reacting 2-acetylpyridine with benzaldehyde and sodium hydride (NaH) according to a modified Kröhnke reaction.[17,18] This synthetic approach allows the direct introduction of several functional groups into the 4'-position. Since most of the applied methodologies suffer from limitations and drawbacks, *e.g.* low yields, the use of toxic solvents and reagents as well as extensive purification due to a number of side products, the 4'-substituted arylterpyridines were prepared using a slightly changed protocol.[19] The synthesis was performed in a one-pot reaction and involved the use of environmentally friendly PEG and aqueous ammonia as solvent. This procedure features a one-pot two-step synthetic route, short reaction times, easy purification, and remarkably higher yields in comparison to conventional methods. As shown in Scheme 2.4, the formation of 4'-substituted arylterpyridines was carried out in a straightforward one-pot reaction. The addition of 2-acetylpyridine to a suspension of sodium hydroxide in PEG300 at 0 °C resulted in the *in situ* formation of the enolate anion. After ten minutes the aromatic aldehyde was added and the reaction mixture was stirred for two hours at this temperature. Upon formation of the 1,5-dione, the color changed from yellow to a reddish brown. Cyclization of the 1,5-dione intermediate occurred (without prior isolation) by adding concentrated aqueous ammonia instead of ammonium acetate.[20] Thus, the excess of inorganic salts was reduced significantly using this synthetic approach. Upon heating to 100 °C for two hours the product precipitated in the form of a microcrystalline solid. Further purification was achieved by recrystallization from ethanol. The modified Kröhnke reaction was applied for the preparation of two 4'-arylterpyridines where R represents CH_3 (**II-6**) and O-$(CH_2)_2$-OH (**II-7**), respectively. The synthesized ligands **II-6** and **II-7** were analyzed by ^{1}H NMR spectroscopy and elemental analysis, both giving evidence for the purity of the compounds. The ligands described in this section were used for the preparation of homoleptic and heteroleptic *bis*-terpyridine ruthenium(II) complexes which will be discussed in detail in section 2.3. In general, 4'-sustituted aryl terpyridines are fluorescent in the UV region of the spectrum compared to terpyridines without an adjacent phenylring. These materials reveal fluorescence lifetimes in solution in the range of 1 to 5 ns.[21]

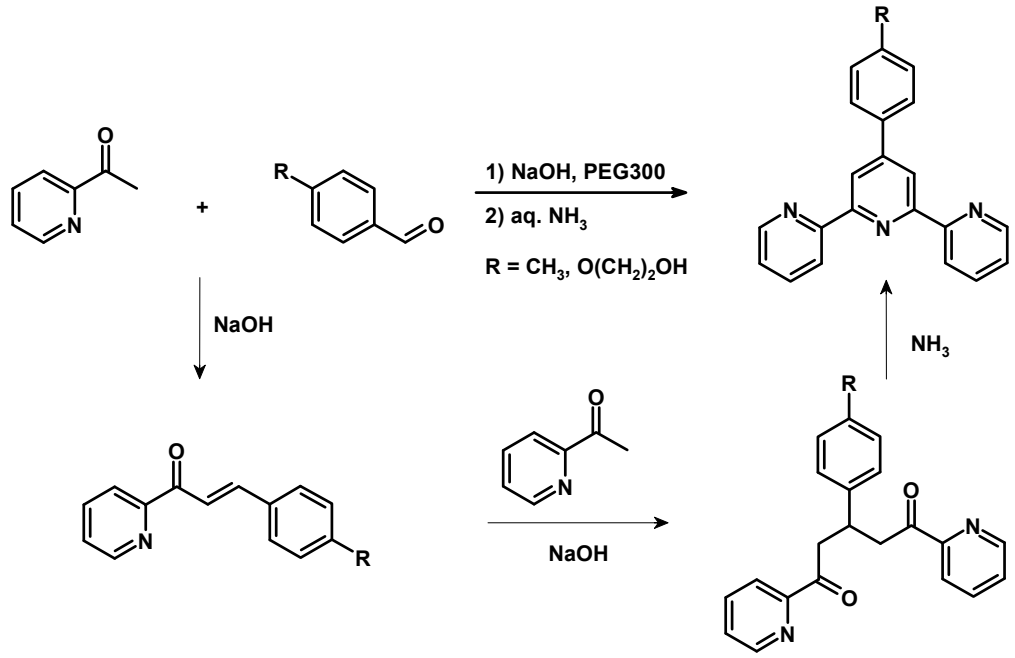

Scheme 2.4 *Schematic representation of the general reaction mechanism for the synthesis of 4'-substituted arylterpyridines.*

2.3 Synthesis of *bis*-terpyridine ruthenium(II) complexes

Although there are several possible metals which can coordinate with terpyridine ligands, the focus of this section is on ruthenium(II) ions. Ruthenium(II) ions have the electron configuration d^6 and the resulting complexes are diamagnetic in a low spin electron configuration (due to a strong crystal field splitting).[22,23] Inert *bis*-terpyridine metal complexes allow the connection of two differently substituted terpyridine ligands, thus the formation of heteroleptic complexes. Inert complexes with terpyridines are also formed with chromium(III), cobalt(III), osmium(II) and iridium(III) ions. These complexes can be regarded as dormant switch within the supramolecular molecule due to the high complex stability. Nevertheless, the non-covalent interaction can be cleaved under harsh reaction conditions, *i.e.* either by the addition of large amounts of a competitive ligand such as *N*-hydroxyethylethylenediamine triacetic acid sodium salt (HEEDTA)[24,25] or by the addition of an aqueous $Ce(SO_4)_2$ solution which can oxidize Ru(II) to Ru(III) due to the reduction potential of 1.43 V *vs*. saturated calomel electrode (SCE) (the oxidation potential of the $Ru(tpy)_2$ complex is 1.19 *vs.* SCE).[26] The ruthenium(II)-based *bis*-terpyridine heteroleptic complexes can be either prepared via a ruthenium(III) or a ruthenium(II) *mono*-complex. Examples for both synthetic routes are shown and discussed in the following part.

2.3.1 Bis-terpyridine complexes via Ru(III) *mono*-complexes

In order to obtain heteroleptic $[Ru(tpy)_2]^{2+}$ complexes, a directed strategy has to be applied where the two ligands are introduced in a two-step process. In the first step, the terpyridine ligand is added to an excess of $RuCl_3$ in an appropriate solvent, resulting in the formation of the respective *mono*-complex which can be isolated and characterized. In a second step, the Ru(III) *mono*-complex is reduced *in situ* to Ru(II) in the presence of *N*-ethylmorpholine[27] and methanol. The reduced species reacts with a second equivalent of a differently substituted terpyridine to afford the desired asymmetric complex.[28,29] This synthetic route was utilized for the preparation of two polymeric model complexes. In the first step, the Ru(III) *mono*-complex had to be formed. For this purpose, terpyridine-functionalized poly(ethylene glycol) (PEG) was treated with $RuCl_3$ in dry *N,N*-dimethyacetamide (DMA). The *mono*-complex was isolated by extraction and subsequent precipitation (for experimental details see Chapter 4). Afterwards, the compound was analyzed by ^{1}H NMR spectroscopy where no terpyridine signals were observed due to the paramagnetic nature of the complex, by UV-vis spectroscopy the characteristic MLCT-band at around 400 nm was evident, and by GPC which clearly showed a single polymer distribution indicating the successful complex formation. In a following step, the heteroleptic complex can be formed. To a solution of the *mono*-complex and the uncoordinated second ligand, a few drops of *N*-ethylmorpholine is added: Ru(III) is reduced to Ru(II) and the second ligand displaces the remaining chlorides (Scheme 2.5). The complexes **II-8** and **II-9** were purified in a simple two-step procedure: (1) exchange of the counterions by addition of NH_4PF_6 in methanol and (2) precipitation into ice-cold diethyl ether. The ^{1}H NMR spectra of both compounds revealed the characteristic shifts from the protons in the 3',5' and 6,6"-position of the terpyridine ligand. The signal belonging to the 6,6"-protons shifted from 8.7 upfield to 7.3 ppm and the signal belonging to the 3',5'-protons shifted downfield from 8.0 to 8.3 ppm, respectively. After complexation, a splitting of the signal related to the 3',5'-protons is observed which is due to the different 4'-substitution of the two connected terpyridines, thus indicating the formation of the heteroleptic complex.

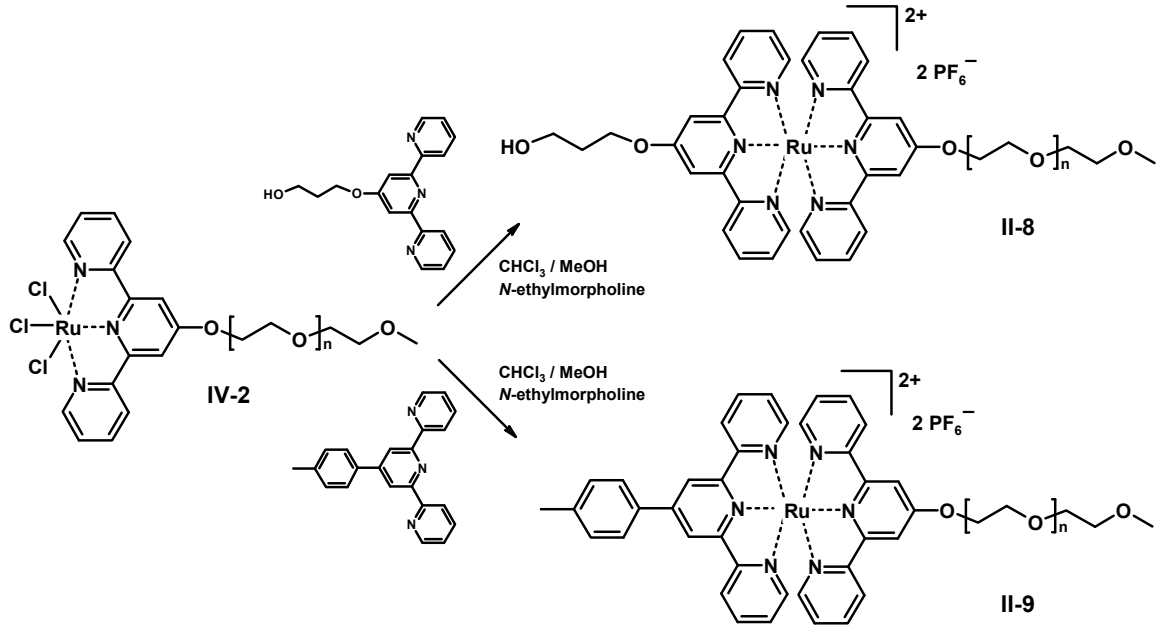

Scheme 2.5 *Schematic representation of the synthesis of the polymeric model complexes **II-8** and **II-9** using Ru(III) / Ru(II) chemistry.*

In the UV-vis spectra of the compounds **II-8** and **II-9** the characteristic metal-to-ligand charge transfer band at around 490 nm can be observed (λ_{max} = 493 nm (**II-8**) and λ_{max} = 487 nm (**II-9**), respectively), which are shown together with a three-dimensional GPC chromatogram of **II-8** in Figure 2.2. Moreover, a new π-band appears around 307 nm for both compounds,[29] and the characteristic MLCT-band for the *mono*-complex at 400 nm disappeared. The GPC chromatogram proves the purity and the successful formation of the *bis*-terpyridine ruthenium(II) complex since it reveals only a narrow molar mass distribution which clearly shows the MLCT band at 490 nm.

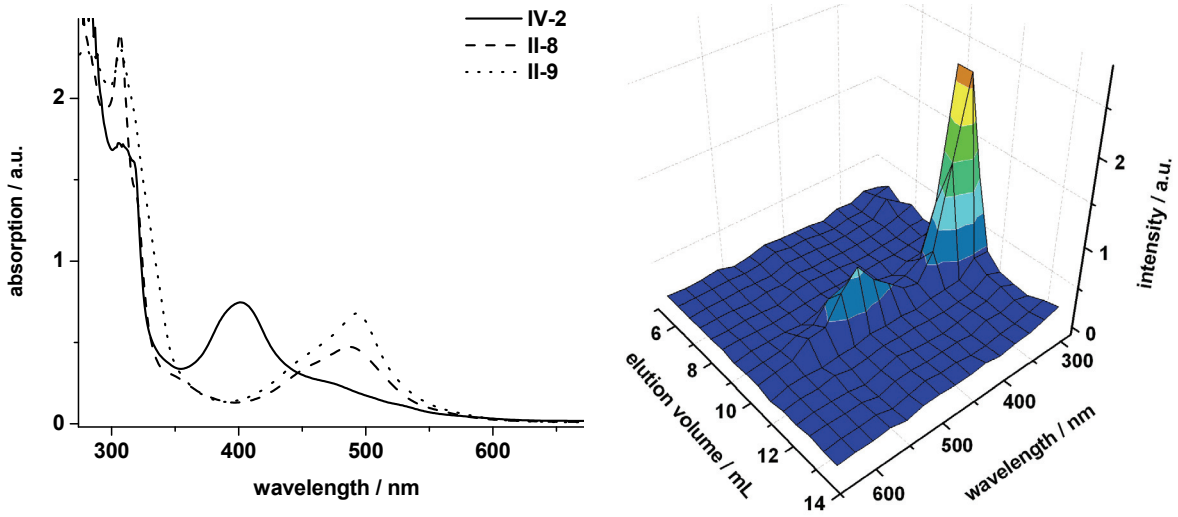

Figure 2.2 *UV-vis spectra of the complexes **II-8** and **II-9** (left) in $CHCl_3$ and GPC chromatogram (with PDA-detector) of **II-8** demonstrating both the MLCT at 490 nm which is characteristic for bis-terpyridine ruthenium(II) complexes (right).*

2.3.1 Bis-terpyridine complexes via $Ru^{II}(DMSO)_4Cl_2$

One of the mildest procedures for the preparation of *bis*-terpyridine ruthenium(II) complexes utilizes dichloro-*tetrakis*(dimethyl sulphoxide)-ruthenium(II) [$Ru(DMSO)_4Cl_2$] as precursor.[30] This synthetic approach is particularly suitable when terpyridines substituted with sensitive groups are involved since the classical method using $RuCl_3$ as precursor requires stringent reaction conditions to perform the *in situ* reduction of Ru(III) to Ru(II).[31] The $Ru(DMSO)_4Cl_2$ precursor was prepared by refluxing $RuCl_3$ in DMSO according to literature procedures.[32] After removing some of the solvent (DMSO), the product was precipitated into acetone. The dried complex was subsequently characterized by elemental analysis proving the formation of the desired complex (see Experimental Part). The precursor readily reacts with terpyridines to form *mono*-terpyridine ruthenium(II) complexes[33] bearing labile ligands. This reaction was performed for 7 hours at 85 °C in degassed methylene chloride or chloroform yielding a mixture of two poorly soluble isomers as demonstrated schematically in Figure 2.3. Both, temperature and solvent, have an influence on the formation of the respective isomer. Reacting the terpyridine ligand with $Ru(DMSO)_4Cl_2$ using methylene chloride as solvent usually yields an excess of the *trans*-isomer. On the other hand, an excess of the *cis*-isomer can be obtained by performing the complexation reaction in chloroform. Figure 2.4 shows the ^1H NMR spectrum for the *mono*-complex **II-10** formed in a reaction with 4'-(2-hydroxy-ethoxy-phenyl)-terpyridine. Both isomers exhibit different NMR patterns. The signals were assigned using literature data[30] (confirmed by X-ray analysis). A deshielding of the 6,6"-protons (Δ = 0.33 ppm) and a shielding of the 5,5"-protons (Δ = 0.26 ppm) can be observed which could be probably induced by stereoelectronic effect of the DMSO and/or Cl ligand.

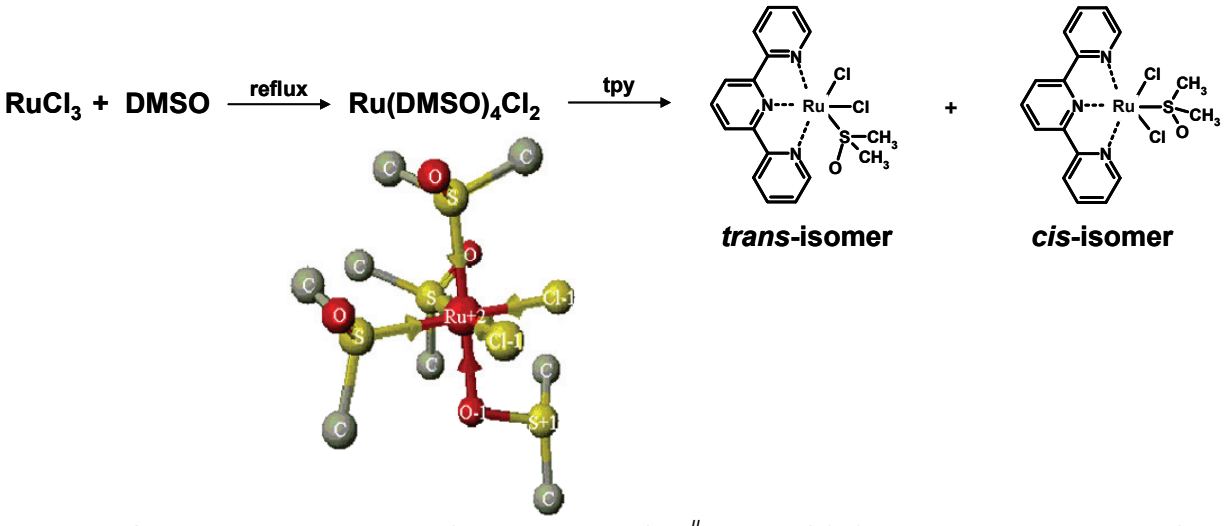

Figure 2.3 *Schematic representation of the synthesis of $Ru^{II}(tpy)(DMSO)Cl_2$ including the structure of the $Ru(DMSO)_4Cl_2$ complex[34] determined by theoretical CAChe modeling and the X-ray molecular structure of the trans-isomer (bottom right).[30]*

Figure 2.4 also illustrates the absorption spectrum of **II-10** in DMSO solution. The isomer mixture displays a strong absorption band in the UV region at approximately 320 nm, which can be assigned to the π-π* transition of the terpyridine ligand. In the low energy region of the spectrum, a weaker absorption is observed (between 420 and 600 nm, λ_{max} = 516 nm) assigned to the metal-to-ligand charge transfer (MLCT) state of the complex. It has been described in literature that all transitions are bathochromically shifted for the *trans*-complex compared to the *cis*-complex which could be related to a significant decrease of the HOMO/LUMO gap (electrochemical data). Since the assignment of the ^1H NMR clearly shows a majority of the *trans*-

isomer (65% *trans* : 35% *cis*), it can be assumed that the characteristic shifted absorption bands of the *cis*-isomer are hidden under the absorption belonging to the *trans*-isomer.

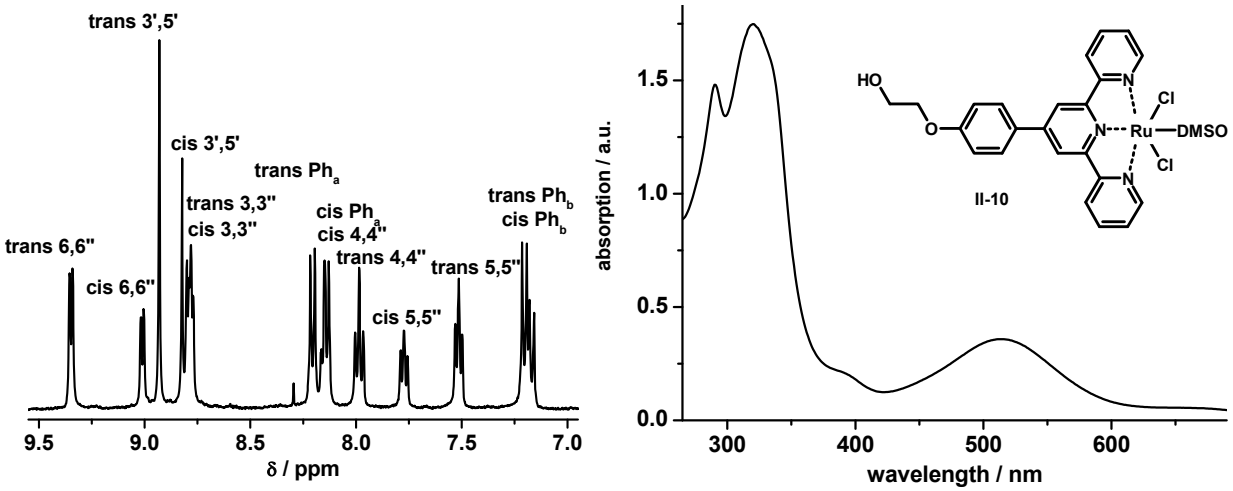

Figure 2.4 *^{1}H NMR spectrum of the aromatic region with assignment of **II-10** in d_6-DMSO revealing the presence of the two isomers (left). UV-vis spectrum of the cis and trans-isomer containing compound **II-10** (right).*

In addition to complex **II-10**, Ru(II) *mono*-complexes of 4'-chloroterpyridine (**II-11**), 4'-(3-hydroxy-propoxy)-terpyridine (**II-12**) and 4'-(3-(2-bromo-isobutyryl)-propoxy)-terpyridine (**II-13**) have been prepared and characterized by ^{1}H NMR and UV-vis spectroscopy. All *mono*-complexes form a mixture of isomers. The respective UV-vis spectrum revealed the hypsochromic shifts of the absorption bands where a λ_{max} of 493 nm (MLCT) and 314 nm (LC) could be observed. It was reported in literature that both isomers show the same reactivity towards the preparation of *bis*-terpyridine ruthenium(II) complexes.[30] For this reason, it was not necessary to separate the isomeric mixture. The above mentioned ruthenium(II) *mono*-complexes react, after silver dehalogenation using $AgBF_4$, under mild conditions (80 °C in methanol for 9 hours) with free terpyridine ligands resulting in the formation of unsymmetrical or symmetrical *bis*-complexes depending on the added terpyridine ligand. A general reaction scheme is shown in Scheme 2.6.

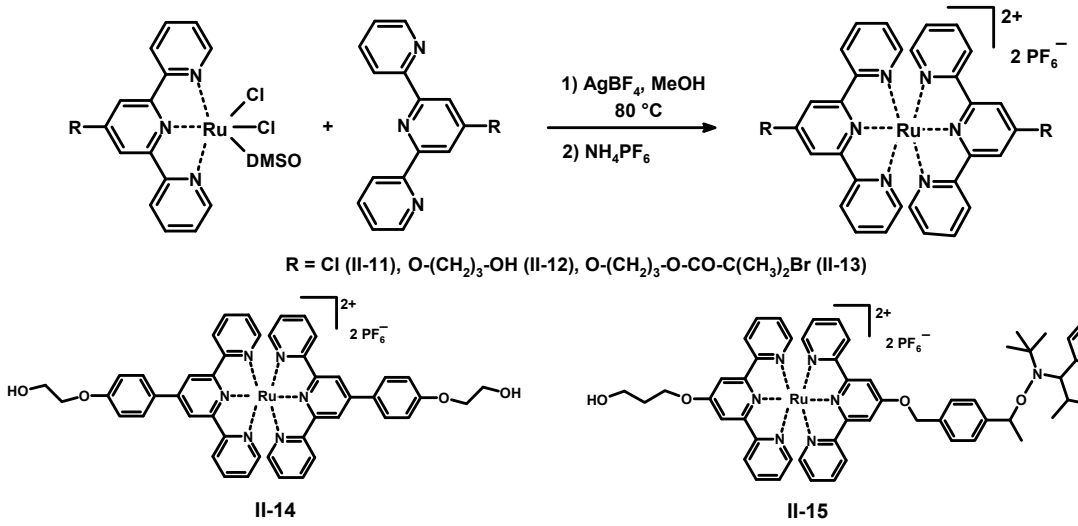

Scheme 2.6 *Schematic representation of the synthesis of bis-terpyridine ruthenium(II) complexes via Ru(II) mono-complexes (top). Synthesized homoleptic (**II-14**) and heteroleptic (**II-15**) complexes (bottom).*

A more direct synthesis of symmetrical *bis*-terpyridine complexes can be performed using a one-pot procedure according to literature procedures.[35,36] This synthetic approach requires only the $Ru(DMSO)_4Cl_2$ precursor and the respective terpyridine compound which are reacted for 3 hours in an ethylene glycol/methanol/water mixture. Two more homoleptic complexes were obtained in excellent yields (86% and 92%, respectively) by employing this procedure (Scheme 2.7).

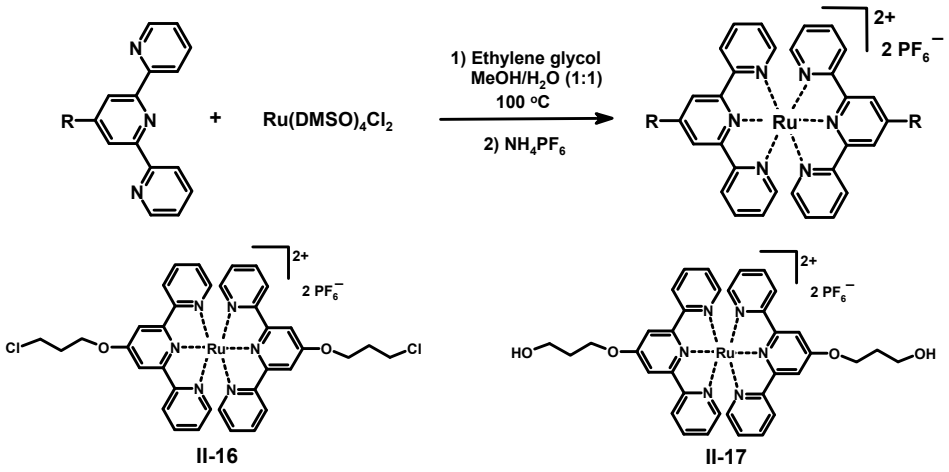

Scheme 2.7 *Schematic representation of the synthesis of homoleptic bis-terpyridine ruthenium(II) model complexes (top).*

The four complexes were analyzed using different characterization tools. The ^{1}H NMR spectra for the free ligand and the respective *bis*-terpyridine ruthenium(II) complex showed the characteristic shift for the 6,6”-proton signals due to the change in configuration upon complexation.

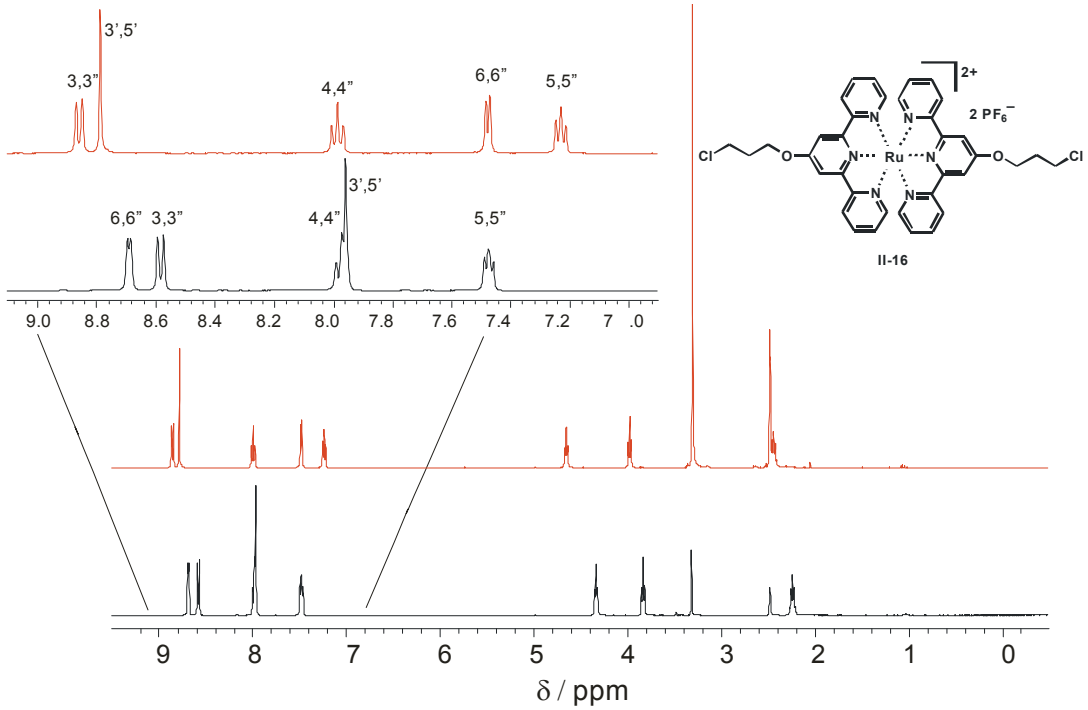

Figure 2.5 *^{1}H NMR spectra of the terpyridine ligand **II-5** (bottom) and the respective homoleptic bis-complex **II-16** (top) in d_6-DMSO. The inset shows the enlarged aromatic region with the assigned terpyridine signals.*

The 6,6"-protons in the *bis*-complex are located above the ring plane of the aromatic ring of the adjacent ligand, causing the observed upfield shift in the ^{1}H NMR spectrum. Also the 3',5'-protons experience a significant influence upon coordination with the second terpyridine ligand resulting in downfield shifted resonances. A representative example is shown for **II-16** in Figure 2.5 demonstrating the changes in the aromatic region upon complexation.

Due to the extra phenyl-ring in complex **II-14**, a two dimensional ^{1}H-^{1}H correlated NMR spectrum (COSY) was required to fully assign all proton signals in the aromatic region (Figure 2.6). Cross peaks corresponding to the coupling aromatic protons can be identified. Absorption spectroscopy revealed the characteristic metal-to-ligand charge transfer band at approximately 490 nm for the complexes **II-14**, **II-15**, **II-16** and **II-17**, respectively. Moreover, the complexes display two strong absorption bands in the UV region at approximately 280 and 320 nm, which can be assigned to the π-π* transition of the terpyridine ligand. In contrast to bipyridine complexes, *bis*-terpyridine complexes are barely emissive due to efficient deactivation of the excited triplet ^{3}MLCT state via the low-lying triplet metal-centered (^{3}MC) state of the ruthenium ion.[37] Only at low temperatures excitation leads to the ^{3}MLCT emission around 625 nm.[29,38] Therefore, no emission spectra were recorded. MALDI-TOF mass spectrometry is well-suited for the analysis of *bis*-terpyridine metal complexes.[39] Complex fragmentation can occur when higher laser energies are applied, thus allowing an estimation of the complex's binding strength. The detected species are singly, positively charged.

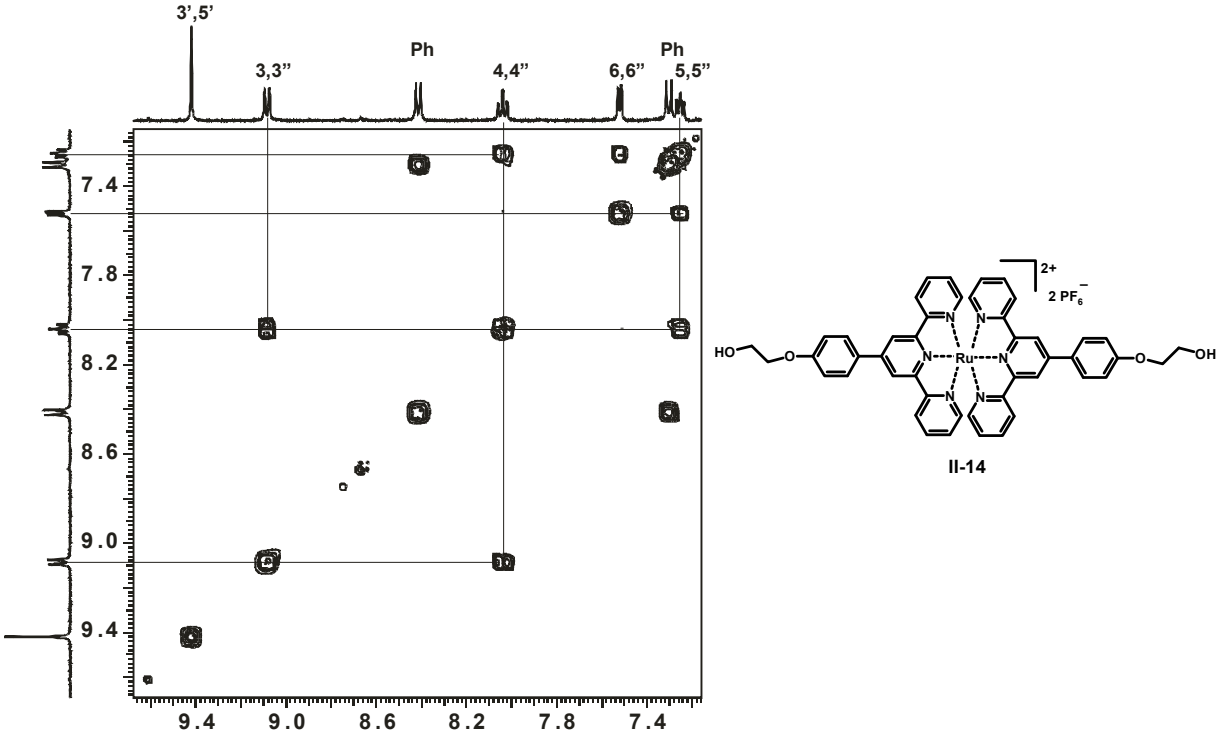

Figure 2.6 *^{1}H-^{1}H COSY spectrum of the model complex **II-14** demonstrating the cross-coupling within the terpyridine ligand and the assignment of the signals (in d_6-DMSO).*

Typically, the isotopic distribution pattern of a MALDI-TOF MS spectrum reveals an excellent correlation with that obtained by simulation. Usually complexes without counterions as well as ion pairs with one counterion and in some cases with two counterions are detected, in which the complex without counterions shows the highest intensity. The MALDI-TOF MS spectrum is shown for the complexes **II-16** and **II-17** in Figure 2.7 revealing in both cases the complex with one counterion PF_6 (860.73 and 897.29) and the complex without counterions (715.85 and 752.28)

(highest intensity). Moreover, another signal is observed at 656.81 and 674.28 respectively which can be explained by fragmentation of the ligand. The complex is still intact; however, one $(CH_2)_3$-OH side chain in the case of **II-17** and one $(CH_2)_3$-Cl side chain in the case of **II-16** were splitted off during the measurement.

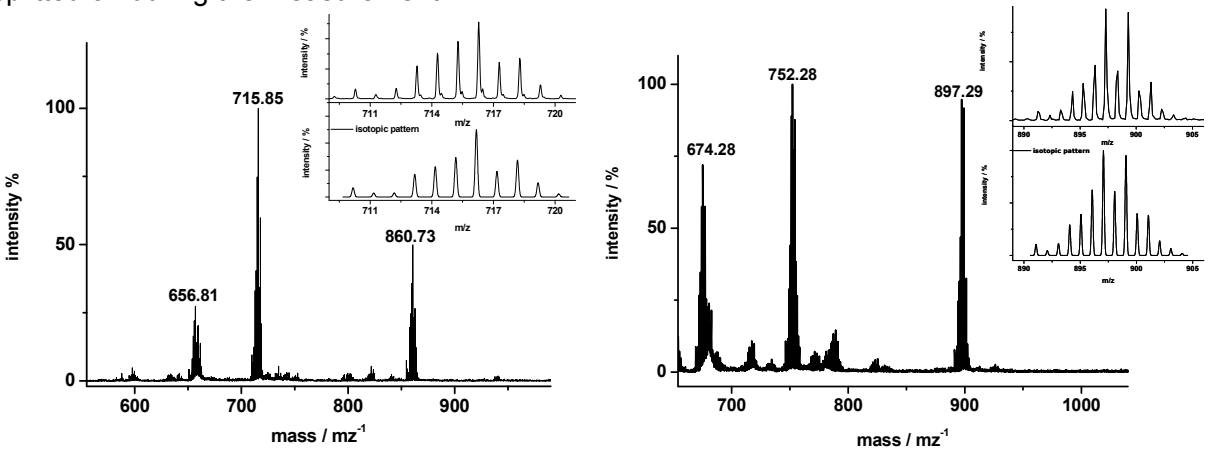

Figure 2.7 *MALDI-TOF mass spectra of the homoleptic bis-terpyridine ruthenium(II) complexes **II-16** (right) and **II-17** (left).*

Single crystals were obtained by slow diffusion of diethyl ether into an acetonitrile solution of complex **II-17**. X-ray crystallography on the metal complex demonstrates that the metal is surrounded by the ligands in an octahedral fashion. Figure 2.8 shows the crystal structure of complex **II-17** revealing a closed space packing of the molecules in the crystalline lattice.

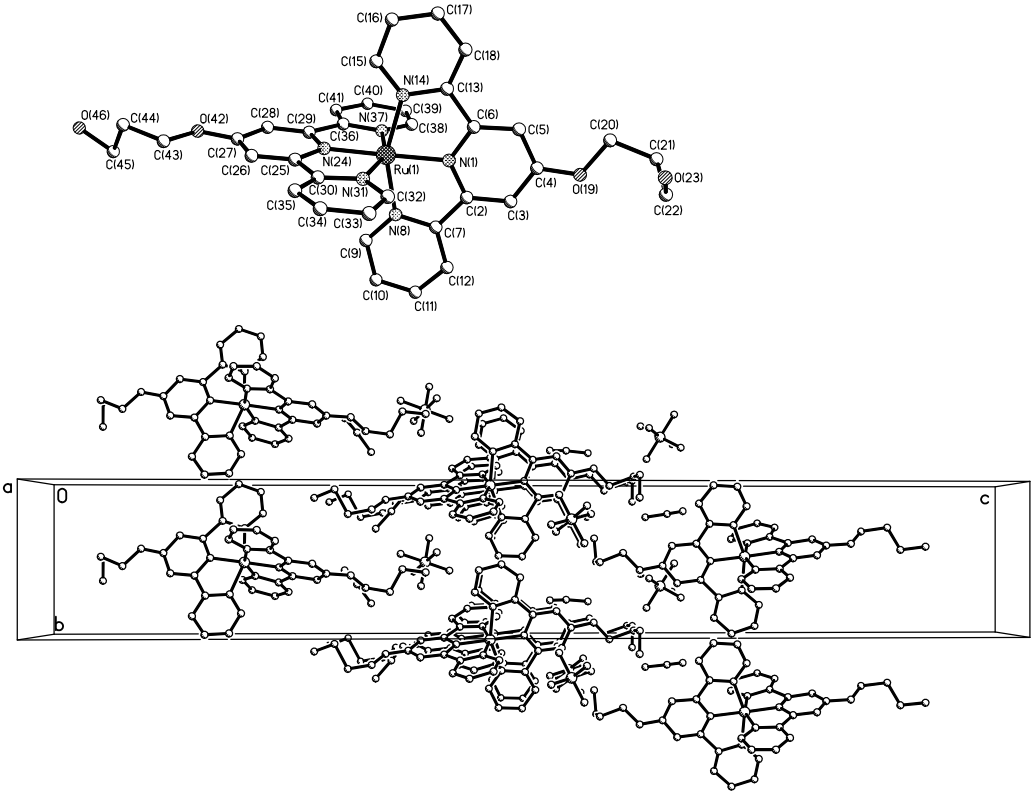

Figure 2.8 *X-ray structure of the ruthenium(II) bis-complex **II-17** with thermal ellipsoids (top) and the crystalline lattice (bottom).*

Complex **II-17** was dissolved in a small amount of acetonitrile and subsequently placed on a purified glass slide. The solvent evaporated slowly and tiny crystals formed on the glass surface, which were subsequently investigated by optical microscopy. If light is polarized in one direction and then passed through a polarizer at a different angle to the first polarizer, only the polarized light which is in the same direction as the new polarizer will be transmitted. A polarized light microscope was used having a polarizer and an analyzer fitted at 90° ("crossed polars") to each other in an illuminating system. In this arrangement extinction usually occurs, *i.e.* no light is transmitted and the image appears dark, because there is no component of the polarized light which can pass through the second polarizer. However, anisotropic materials such as the crystalline *bis*-terpyridine ruthenium(II) complex **II-17** is able to change the polarization of the light. Consequently, there is a component of the light which can pass through the second polarizer resulting in the visualization of the crystals (Figure 2.9). The anisotropic crystals may appear differently colored when crossed polarizers are used due to interference effects between the light waves emerging from the analyzer. Certain wavelengths and therefore certain colors will be extinguished due to destructive interference. The observed colors depend on the birefringence of the crystal, its thickness, and the orientation of the section relative to the optic axis.

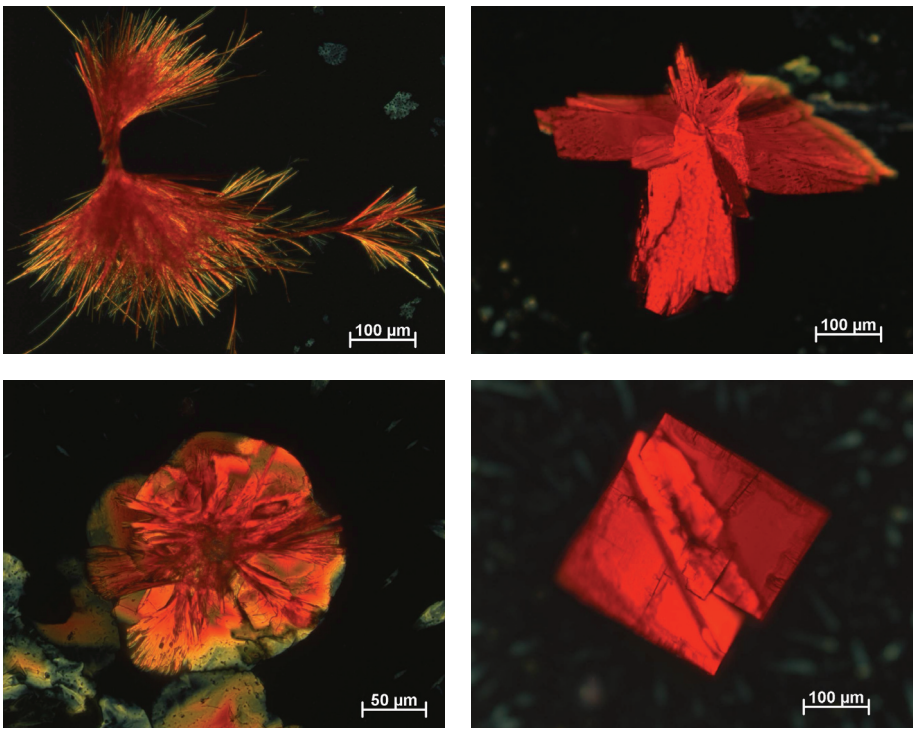

Figure 2.9 *Crystals obtained from complex **II-17** detected using a crossed polarizer microscope.*

The model complexes prepared in this section can also be analyzed by GPC due to the fact that they are complex and highly charged which results in a relatively large hydrodynamic volume. A narrow molar mass distribution was observed for all complexes (**II-14**, **II-15**, **II-16** and **II-17**) (Figure 2.10) revealing the MLCT band at approximately 490 nm which is characteristic for the *bis*-terpyridine ruthenium(II) complexes. The broadening of the GPC-traces of these monodisperse compounds is due to diffusion effects in the GPC.

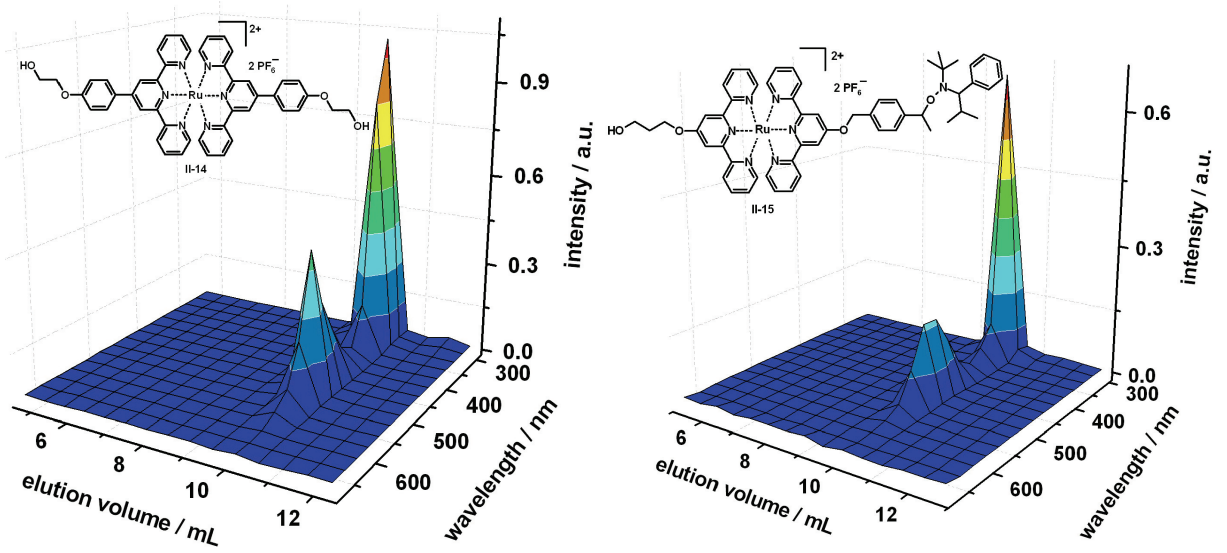

Figure 2.10 *GPC chromatograms recorded with the PDA detector of the complexes **II-14** (left) and **II-15** (right) demonstrating the formation of the desired bis-terpyridine complex. Both graphs reveal a narrow molar mass distribution as well as the characteristic MLCT band at 490 nm.*

For coordination chemistry, terpyridines are of special interest due to their ability of forming stable complexes with many transition metal ions featuring interesting photophysical, electrochemical and photochemical properties.[40] Potential applications for such complexes range from redox and photoactive systems, to catalysis and to biologically active media. The complexes presented in this section possess different functional groups; hence they can be employed for various chemical post-modification reactions. Of particular importance are polymers with incorporated metal complexes since they combine the processing properties of polymers and the outstanding properties of the metal complex within one material. Complex **II-16** would be therefore a suitable candidate to perform the Huisgen 1,3-dipolar cycloaddition reaction ("click" reaction)[41,42] after introducing a "click" functionality or ring opening polymerization of oxazolines. The hydroxy-groups of the complexes **II-14** and **II-17** could be used as precursors for ring opening polymerizations of cyclic esters. Complex **II-15** could act as a hetero-bifunctional initiator due to its hydroxyl group on the one end and the nitroxide group capable for controlled radical polymerizations on the other end. As a proof of principle, the ring opening polymerization of *L*-lactide was performed on complex **II-17** as initiator. A recently reported method was applied to obtain well-defined polymers by organometallic catalytic ring opening polymerization.[43] For this purpose, complex **II-17** was reacted at room temperature with *L*-lactide and a catalytic amount of 1,8-diazabicyclo[5.4.0]undec-7-ene (DBU) for one hour in a chloroform/acetonitrile mixture. Acetonitrile was added to ensure the solubility of the complex in the reaction mixture; however, this decreases the rate of reaction since the DBU hydrogen bonding strength is decreased with increasing polarity. Consequently, no polymer could be obtained using these conditions. Therefore, the mixture was heated for 2 days in a closed reaction vial at 90 °C. Under these reaction conditions the polymerization was successful; however no high degree of polymerization could be reached. The resulting polymer **II-18** was characterized by ^{1}H-NMR and UV-vis spectroscopy as well as GPC. The GPC chromatogram revealed a clearly visible shift to higher molar mass (Figure 2.11). The combination of GPC with the PDA detector proves that the model complex acted as the precursor for the polymerization since the molar mass distribution of the polymer exhibits the characteristic metal-to-ligand charge transfer band at 490 nm.

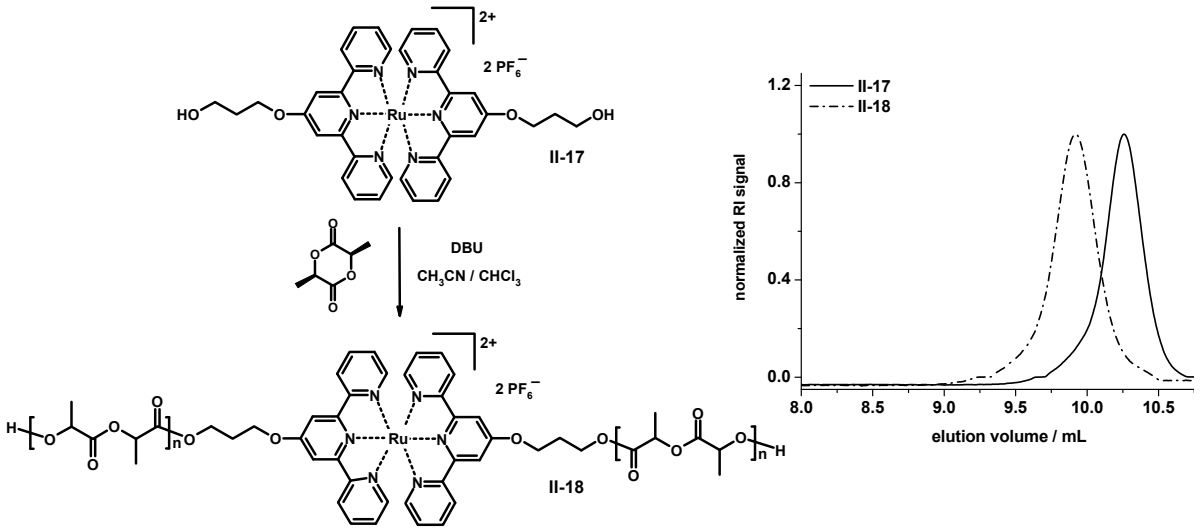

Figure 2.11 *Schematic representation of the ring opening polymerization of L-lactide using complex **II-17** as precursor (left) and corresponding GPC-traces of the precursor complex **II-17** (solid line) and the polymer complex **II-18** (dash-dotted line)(right). DBU = 1,8-diazabicyclo[5.4.0]undec-7-ene.*

2.4 Synthesis of mixed-ligand iridium(III) complexes

Iridium complexes exhibit favorable electro-optical properties, such as high quantum yields,[44] a reversible redox-behavior[45-47] and the ability to tune the phosphorescent emission color by insertion of different ligands,[44,48-51] which are of special importance for potential applications in light-emitting cells (LECs). Iridium(III) forms photo- and electro-active complexes in the presence of suitable chelating ligands, *e.g.* with terpyridines and bipyridines. From a structural point of view, the terpyridine ligand is superior to the bidentate one. However, along with this structural advantage, terpyridine complexes have the serious drawback of a relatively short-lived ^{3}MLCT with weak emission. For the design of Ir(III) terpyridine complexes with intense emission, we aimed to obtain *mono*-terpyridine complexes by performing bridge-splitting reactions with *N,C*-cyclometallating ligands.[52] The incorporation of the *ortho*metallated Ir(ppy)$_2$-fragment into a mononuclear or multinuclear species can be simply achieved by reacting the desired chelating ligand with dimeric precursor complexes [(ppy)$_2$Ir-μ-Cl]$_2$, which was prepared according to literature procedures.[53] The reaction was performed at 80 °C in a methylene chloride / methanol mixture.[54] After performing the reaction under argon atmosphere for 5 hours the counterions were exchanged by the addition of NH_4PF_6 into the reaction mixture. Scheme 2.8 depicts the synthesis of mixed-ligand iridium(III) complexes.

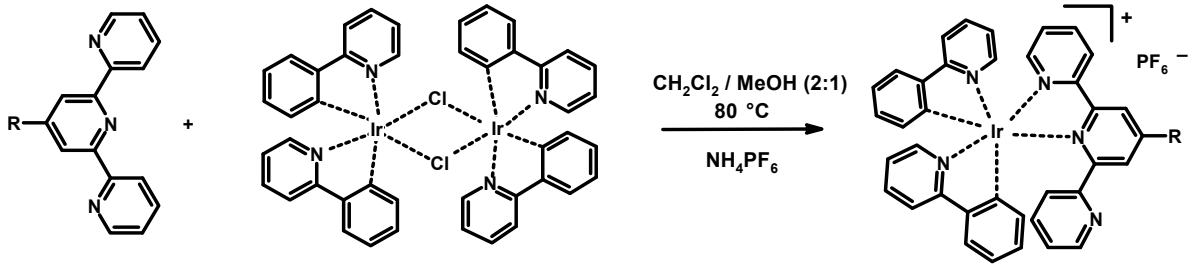

Scheme 2.8 *Schematic representation of the synthesis of mixed-ligand iridium(III) complexes.*

Five complexes were prepared using two different precursor complexes. Ligands **II-2**, **II-4** and **II-5** were reacted with $[(ppy\text{-}NO_2)_2Ir\text{-}\mu\text{-}Cl]_2$; ligand **II-3** and a dimeric π-conjugated ligand were used for the reaction with $[(ppy)_2Ir\text{-}\mu\text{-}Cl]_2$. The synthesized complexes are summarized in Figure 2.12.

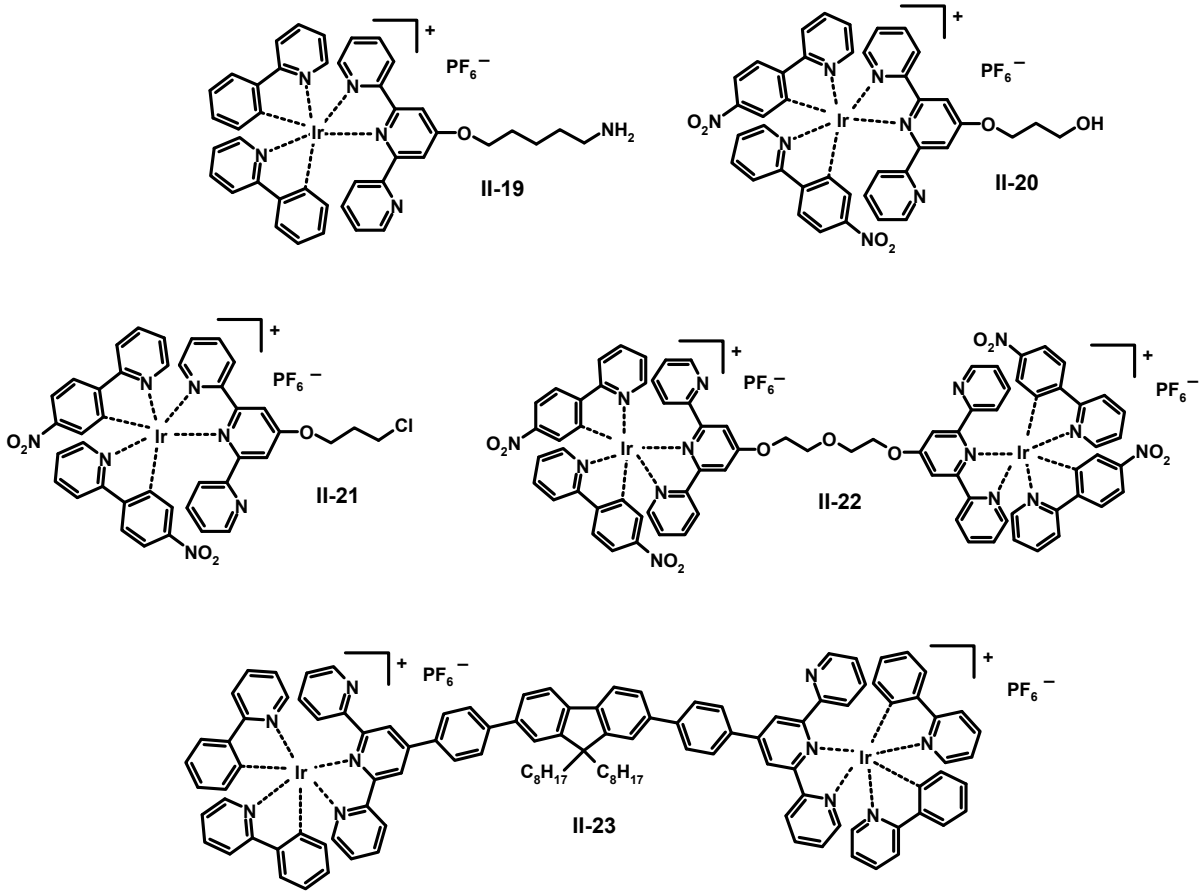

Figure 2.12 *Schematic representation of the synthesized mixed-ligand iridium(III) complexes.*

Complexes **II-19**, **II-20** and **II-21** were purified by precipitation into ice-cold diethyl ether leading to the removal of unreacted terpyridine. The complexes were subsequently analyzed by ^1H NMR spectroscopy revealing the presence of only one isomer. One pyridine ring of the terpyridine moiety does not coordinate. The assignment of the complexes was carried out using ^1H-^1H correlation spectroscopy (COSY). The selected aromatic region of the proton resonances is displayed in Figure 2.13. As an example the coupling systems of the nitro-phenyl group are highlighted.

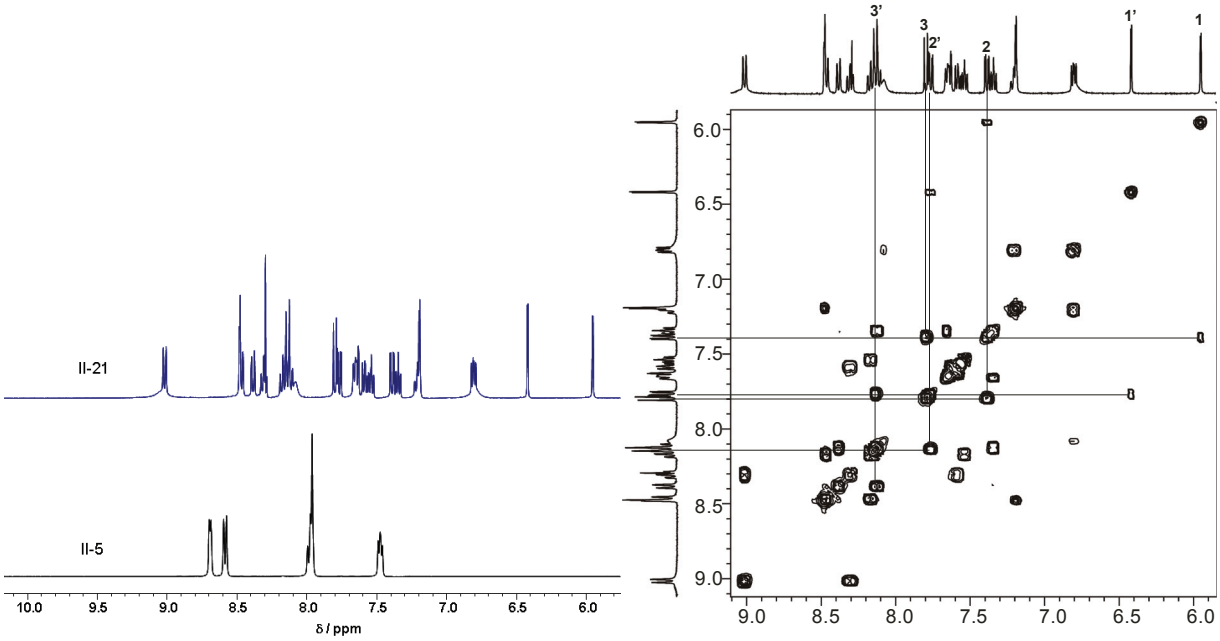

Figure 2.13 *^{1}H NMR of the free terpyridine ligand **II-5** and the corresponding mixed-ligand iridium(III) complex **II-21** in d_6-DMSO (left). Assignment of the coupling systems using ^{1}H-^{1}H COSY spectroscopy (right).*

The complexes **II-22** and **II-23** were both purified by preparative size exclusion chromatography (BioBeads SX-1, CH_2Cl_2). This technique allowed the easy separation of single-complexed and double-complexed material. Even though MALDI-TOF MS of the two binuclear complexes revealed the presence of the mononuclear complex as major signal, the final proof was obtained by ^{1}H NMR spectroscopy since the free terpyridine signals were not observed in both spectra as it is demonstrated in Figure 2.14.

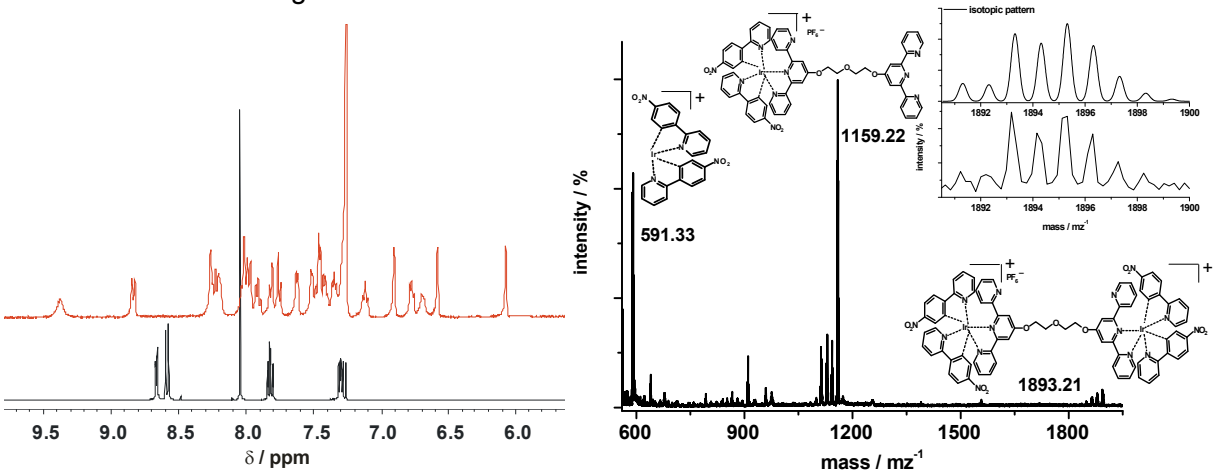

Figure 2.14 *Left: ^{1}H NMR spectra of the free ligand **II-4** (bottom) and the corresponding binuclear complex **II-22** (top) in $CDCl_3$. Right: MALDI-TOF mass spectrum of **II-22** revealing a main peak at 1159 m/z which corresponds to the mononuclear complex.*

Obviously, the ionization of the binuclear complexes requires more energy compared to the mononuclear complexes **II-19**, **II-20** and **II-21** which, in turn, results in the fragmentation of one iridium(III) complex. The detected molecule (highest intensity) contains one free terpyridine

moiety and one iridium(III) complex. The loss of the $Ir(ppy)_2$-fragment was also observed for the mononuclear complexes; however, the peak with the highest intensity corresponded to the respective complex without the counterion PF_6^-. On the other hand, the binuclear complex **II-21** shows only a very small peak at 1893 which is related to the intact complex. Complex **II-22** displays only the fragmented complex. The MALDI-TOF mass spectrometry spectra are shown for the mononuclear complexes **II-19** and **II-20** (Figure 2.15) representing an excellent fit of the isotopic distribution patterns for all cases. The MALDI-TOF MS spectrum of complex **II-20** revealed a stepwise fragmentation of the alkyl-chain which is attached to the terpyridine ligand in 4'-position. The first fragmentation at 881 corresponds to the loss of the hydroxy-group, afterwards the loss of three CH_2-groups (14 mass units) is observed.

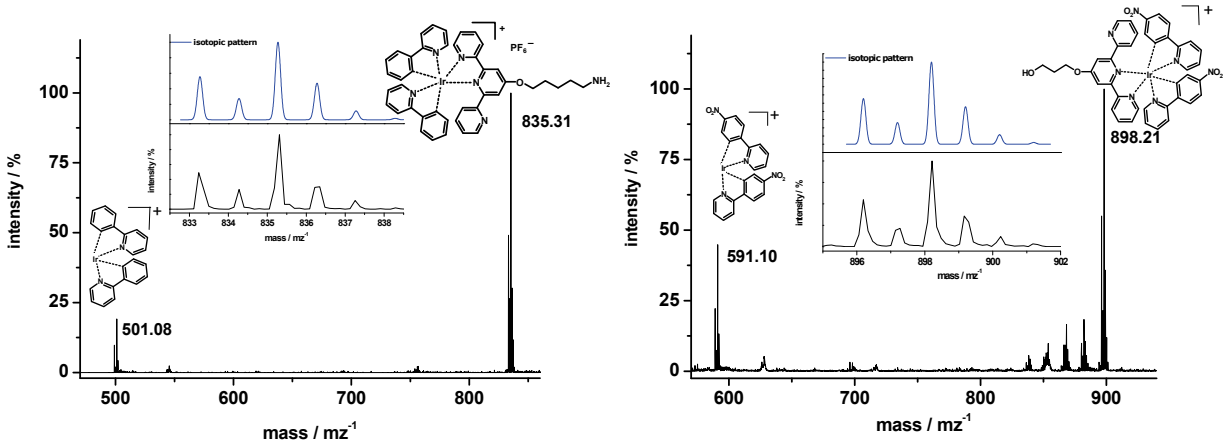

Figure 2.15 *MALDI-TOF mass spectra of the complexes **II-19** (left) and **II-20** (right).*

The five iridium(III) complexes were further investigated towards their absorption and emission properties. All complexes show a strong absorption band at about 260 nm, which is attributed to the ligand-centered π→π* transitions on the chelating ligand and on the cyclometallating 2-phenyl-pyridine (ppy) as well as the 2-(4-nitro-phenyl)-pyridine (ppy-NO_2), respectively. The broad absorption bands at lower energy (around 380 nm) are due to spin-allowed metal-to ligand charge transfer transitions (^{1}MLCT, (dπ(Ir)→π*) terpyridine and phenyl-pyridine transitions). The shoulder tailing to 440 nm was assigned to spin-forbidden ^{3}MLCT (dπ(Ir)→π*) terpyridine. Excitation of the model complexes at 370 nm (^{1}MLCT) led in all cases to an unstructured emission band revealing a broad emission (between 580 nm and 600 nm) due to ^{3}IC π→π* transitions on the cyclometallating ligand excited states.[55] Moreover, there might be some ^{3}MLCT (dπ(Ir)→π* phenyl-pyridine) excited states involved. Model complex **II-23** shows a further absorption band with a maximum at 385 nm which can be assigned to π→π* transitions of the conjugated compound in conjunction with the fluorene group. Due to the conjugated system, the absorption is shifted bathochromically. For this reason, complex **II-23** also revealed a bathochrom shifted emission band with a maximum at 600 nm. Moreover, the fluorenyl group could be considered as a weak electron-donor, the terpyridine groups on the other hand as an acceptor which could result in a weak push-pull effect. The quantum yields were measured in methylene chloride in the presence as well as in the absence of oxygen. The latter measurements revealed higher values (9% for **II-23** and 12% for **II-21**). Oxygen is known to quench the emission of iridium(III) complexes[56] since they are triplet emitters meaning that emission can be efficiently achieved from the ^{3}MLCT-state and/or ^{3}LC-state.[57,58]

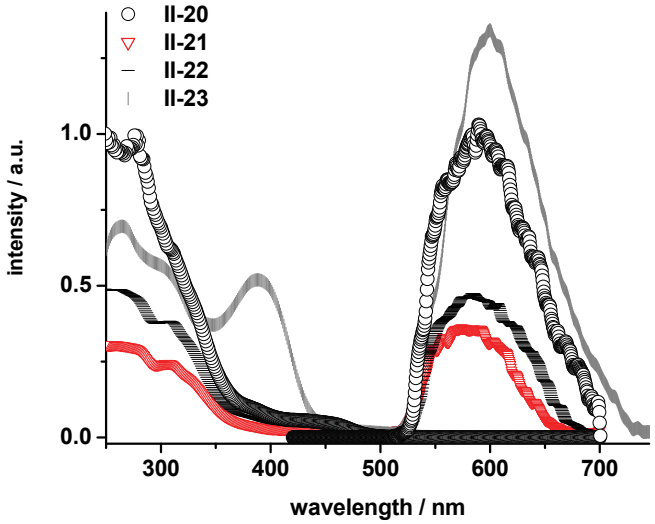

Figure 2.16 *Absorption and emission spectra of the mixed-ligand iridium(III) complexes* ***II-20****,* ***II-21****,* ***II-22*** *and* ***II-23****, respectively (in methylene chloride).*

2.5 Conclusions

This chapter was devoted to the synthesis and characterization of terpyridine ligands and their respective *bis*-terpyridine ruthenium(II) as well as mixed-ligand iridium(III) complexes. The ruthenium(II) and the iridium(III) metal ions impart valuable photophysical as well as electrochemical properties to the materials, paving the way to potential applications in energy and/or electron transfer processes. Two different synthetic approaches for the synthesis of homoleptic and heteroleptic *bis*-terpyridine ruthenium(II) complexes were discussed. For this purpose, ruthenium(III) and ruthenium (II) precursors were synthesized, isolated and subsequently analyzed using different characterization tools. $Ru(DMSO)_4Cl_2$ was found to be a suitable precursor for the synthesis of *bis*-terpyridine ruthenium(II) complexes since the formed ruthenium(II) intermediate reacts under mild conditions to form the desired *bis*-complex. The complexes were characterized by ^1H NMR (as well as ^1H-^1H correlation) spectroscopy, UV-vis spectroscopy, MALDI-TOF MS, GPC and X-ray analysis. The complexes are equipped with different functional groups, which provide the possibility to further modify the complexes, *e.g.* the incorporation of the complex into polymeric architectures either by substitution reactions or by using the synthesized complexes directly as initiators for polymerizations as demonstrated for the polymerization of *L*-lactide. The formation of heteroleptic complexes is of special importance when dealing with polymers. The terpyridine ligand can act in those cases as key compound to connect different polymer chains together in a non-covalent fashion, *i.e.* providing an easy alternative for the formation of block copolymers (see also Chapter 4). The second part of the chapter dealt with the synthesis of mixed-ligand *ortho*metallated iridium(III) complexes obtained in a bridge-splitting reaction with dimeric iridium precursor complexes. The synthesized mononuclear and binuclear complexes were characterized by means of ^1H NMR spectroscopy and MALDI-TOF MS. Furthermore, the absorption and emission properties of the materials were investigated.

2.6 Experimental

Solvents were purchased from Biosolve and all other chemicals from Aldrich, Acros or Fluka. *L*-Lactide was recrystallized from ethyl acetate. The telechelic conjugated terpyridine compound for the preparation of **23** was prepared according to literature procedures via Suzuki-coupling. For preparative size exclusion chromatography, Bio-Rad SX-1 Beads swollen in CH_2Cl_2 was used. Proton nuclear magnetic resonance spectra (^{1}H-NMR) were recorded on a Varian Gemini 400 MHz spectrometer at room temperature. Chemical shifts are given in parts per million (ppm) downfield from an internal standard tetramethylsilane (TMS). Coupling constants (*J* values) are reported in Hertz (Hz). GPC measurements were performed on a Waters system with a 1515 pump, a 2414 refractive index detector, and a Waters Styragel HT4 column utilizing a *N,N*-dimethylformamide (DMF) / 5 mM NH_4PF_6 mixture as eluent at a flow rate of 0.5 mL/min at 50 °C. MALDI-TOF-MS analysis was performed on a Voyager-DE PRO Biospectrometry workstation (Applied Biosystems) in linear operation mode. Spectra were obtained in positive ion mode; ionization was performed with a 337 nm pulsed nitrogen laser. Data were processed using the Data Explorer software package (Applied Biosystems). Elemental analysis was carried out on an Eurovector Euro EA Elemental Analyzer equipped with an EuroCAP 40-2 autosampler. UV-Vis spectra were recorded on a Perkin Elmer Lambda 45P spectrophotometer. Emission spectra were recorded on a Perkin Elmer LS50B Luminescence spectrometer. The absolute quantum yields of bulk materials were determined using a multi-channel analyzer Hamamatsu of the type C10027 equipped with a BT-CCD linear image sensor, a Czerny-Turner spectrograph and a xenon/mercury-xenon lamp as excitation light source. All reactions were carried out under argon atmosphere unless stated otherwise.

Terpyridine-functionalized poly(ethylene glycol) (II-1)
Powdered KOH (0.56 g, 10 mmol) and *α*-methoxy-*ω*-hydroxy-poly(ethylene oxide) with M_n = 3,000 g/mol (10 g, 3.33 mmol, PDI = 1.08) were stirred under argon in dry dimethyl sulfoxide (DMSO) at 70 ºC. After 30 minutes a two times excess of 4'-chloro-2,2':6',2"-terpyridine (1.78 g, 6.7 mmol) was added. The mixture was stirred for 24 h at the given temperature, then poured into cold water and extracted with CH_2Cl_2. The combined organic layers were dried over Na_2SO_4 and the solvent was removed *in vacuo*. The polymer was purified by a double precipitation from THF into diethyl ether. Yield: 78%. ^{1}H-NMR (400 MHz, $CDCl_3$): δ (ppm) = 8.68 (dd, 2 H, ^3J = 4.8 Hz, ^4J = 1.6 Hz; $H_{6,6''}$), 8.61 (dd, 2 H, ^3J = 7.6 Hz , ^4J = 1.2 Hz ; $H_{3,3''}$), 8.04 (s, 2 H, $H_{3',5'}$), 7.85 (td, 2 H, ^3J = 8 Hz, ^4J = 2 Hz; $H_{4,4''}$), 7.34 (dd, 2 H, ^3J = 4.8 Hz, ^4J = 0.8 Hz; $H_{5,5''}$), 4.40 (m, 2 H; tpyO*CH*$_2$), 3.93 (m, 2 H; tpyOCH$_2$*CH*$_2$), 3.82-3.45 (m, 280 H; PEO backbone), 3.38 (s, 3 H, O*CH*$_3$). UV-vis (H_2O): λ_{max} *(ε)* = 278 (13,200), 234 (17,000) nm (L·mol^{-1}·cm^{-1}). GPC (eluent DMF with NH_4PF_6 (0.8 g/L)): M_n = 6,960 g/mol, PDI = 1.07.

3-(2,2'-6',2"-Terpyridin-4'-yloxy)propan-1-ol (II-2)
To a stirred suspension of powdered KOH (3.14 g, 56 mmol) in dry DMSO (25 mL) under nitrogen atmosphere, 1,3-propanediol (4.26 g, 56 mmol) was added. After 30 minutes 4'-chloro-2,2':6',2"-terpyridine (3.0 g, 11.2 mmol) was added and the mixture was stirred for 20 h at 80 °C and then poured into ice-water (20 mL). The white precipitate formed was collected by filtration and the crude product was recrystallized from methanol yielding **2** as a white solid. Yield: 85%. ^{1}H-NMR (400 MHz, d_6-DMSO): δ (ppm) = 8.69 (d, 2 H; ^3J = 4.8 Hz, $H_{6,6''}$), 8.59 (d, 2 H; ^3J = 7.6 Hz, $H_{3,3''}$), 7.98 (m, 4 H; $H_{3',5'}$, $H_{4,4''}$), 7.47 (dd, 2 H; ^3J = 4.8 Hz, ^4J = 0.8 Hz, $H_{5,5''}$), 4.61 (t, 1 H; ^3J = 6.0 Hz, OH), 4.29 (t, 2 H; ^3J = 5.7 Hz, O-*CH*$_2$CH$_2$CH$_2$-OH), 3.59 (q, 2 H; ^3J = 7.2 Hz, O-CH$_2$CH$_2$*CH*$_2$-OH), 1.94 (m, 2 H; CH$_2$*CH*$_2$CH$_2$). MALDI-TOF MS (matrix: dithranol) m/z = 307.85 (MH^+). Elemental analysis: $C_{21}H_{23}N_3O_2$ (307.35) calc. C 70.34%, H 5.58%, N 13.67%; found C 70.08%, H 5.49%, N 13.45%.

5-(2,2'-6',2"-Terpyridin-4'-yloxy)pentan-1-amine (II-3)
To a stirred suspension of powdered KOH (1.4 g, 25 mmol) in dry DMSO (25 mL) under nitrogen atmosphere, 5-aminopropanol (4.5 g, 44 mmol) was added. After 30 minutes 4'-chloro-2,2':6',2"-terpyridine (2.3 g, 11 mmol) was added and the mixture was stirred for 24 h at 40 °C and then poured into ice-water (20 mL). The white precipitate formed was collected by filtration and the crude product was recrystallized from methanol yielding **3** as a light yellow solid. Yield: 89%. ^{1}H-NMR (400 MHz, $CDCl_3$): δ (ppm) = 8.69 (d, 2 H; ^3J = 4.6 Hz, $H_{6,6''}$), 8.60 (d, 2 H; ^3J = 7.2 Hz, $H_{3,3''}$), 8.03 (s, 2 H; $H_{3',5'}$), 7.83 (dd, 2 H; ^3J = 7.2 Hz, ^3J = 4.9 Hz, $H_{4,4''}$), 7.32 (dd, 2 H; ^3J = 4.6 Hz, ^3J = 7.2 Hz $H_{5,5''}$), 4.23 (t, 2 H; ^3J = 6.1 Hz, O-*CH*$_2$CH$_2$CH$_2$-CH$_2$CH$_2$-NH$_2$), 2.73 (t, 2 H; ^3J = 6.1 Hz, O-CH$_2$CH$_2$CH$_2$-CH$_2$*CH*$_2$-NH$_2$), 1.87 (tt, 2 H; ^3J = 5.9 Hz, ^3J = 6.1 Hz, O-CH$_2$*CH*$_2$CH$_2$-CH$_2$CH$_2$-NH$_2$), 1.52-1.57 (m, 4 H; O-CH$_2$CH$_2$*CH*$_2$-*CH*$_2$CH$_2$-NH$_2$), 1.19 (s, 2 H; -NH$_2$). MALDI-TOF MS (matrix: dithranol) m/z = 335 (MH^+). Elemental analysis: $C_{20}H_{22}N_4O$ (334.42) calc. C 71.83%, H 6.63%, N 16.75%; found C 71.65%, H 6.27%, N 16.80%.

(*Bis*-2,2'-6',2"-terpyridin-4'-yl)diethylene glycol (II-4)
To a stirred suspension of powdered KOH (1.1 g, 20 mmol) in dry DMSO (15 mL) under nitrogen atmosphere, diethylene glycol (1.0 g, 9.4 mmol) was added. After 30 minutes 4'-chloro-2,2':6',2"-terpyridine (5.3 g, 19.8 mmol) was added and the mixture was stirred for 20 h at 80 °C and then poured into ice-water (20 mL). The white precipitate formed was collected by filtration and the crude product was recrystallized from methanol yielding 4 as a white solid. Yield: 76%. ^{1}H-NMR (400 MHz, $CDCl_3$): δ (ppm) = 8.66 (d, 4 H; ^3J = 4.6 Hz, $H_{6,6''}$), 8.57 (d, 4 H; ^3J =

7.2 Hz, $H_{3,3''}$), 8.04 (s, 4 H; $H_{3',5'}$), 7.82 (dd, 4 H; ^3J = 7.2 Hz, ^3J = 4.8 Hz, $H_{4,4''}$), 7.30 (dd, 4 H; ^3J = 4.6 Hz, ^3J = 7.2 Hz, $H_{5,5''}$), 4.44 (t, 4 H; ^3J = 6.1 Hz, tpyO-CH_2CH$_2$), 4.03 (t, 4 H; ^3J = 6.1 Hz, tpyO-CH$_2$$CH_2$). Elemental analysis: $C_{34}H_{28}N_6O_3$ (568.63) calc. C 71.82%, H 4.96%, N 14.78%; found C 71.52%, H 4.85%, N 14.81%.

4'-(3-Chloro-propoxy)-2,2'-6',2"-terpyridine (II-5)
Hydroxy-propoxy-terpyridine **2** (1.5 g, 4.9 mmol) was carefully added to 5 mL of $SOCl_2$ and refluxed for 5 h. The remaining $SOCl_2$ was removed *in vacuo* and the residue was neutralized with saturated sodium hydrogen carbonate ($NaHCO_3$) solution. The crude product was filtered and dried *in vacuo*. Purification was carried out by recrystallization from ethanol to yield the desired product as a colorless crystalline solid. Yield: 65%. ^{1}H-NMR (400 MHz, d_6-DMSO): δ(ppm) = 8.69 (d, 2 H; ^3J = 4.8 Hz, $H_{6,6''}$), 8.58 (d, 2 H; ^3J = 2.1 Hz, $H_{3,3''}$), 7.97 (m, 4 H; $H_{3',5'}$, $H_{4,4''}$), 7.47 (d, 2 H; ^3J = 7.5 Hz, $H_{5,5''}$), 4.33 (t, 2 H; ^3J = 5.8 Hz, O-CH_2CH$_2$CH$_2$-Cl), 3.83 (t, 2 H; ^3J = 6.3 Hz, O-CH$_2$CH$_2$$CH_2$-Cl), 2.24 (m, 2 H; O-CH$_2$$CH_2CH_2$-Cl). MALDI-TOF MS (matrix: dithranol) m/z = 326 (MH^+). Elemental analysis: $C_{18}H_{16}N_3OCl$ (325.79) calc. C 66.36%, H 4.95%, N 12.90%; found C 66.02%, H 5.01%, N 13.07%.

General synthesis of 4'-aryl-terpyridines
2-Acetylpyridine (5 g, 41.2 mmol) was added to a stirred suspension of crushed NaOH (1.65 g, 41.2 mmol) in PEG-300 (30 mL) at 0 °C. After 10 min the corresponding aldehyde (20.6 mmol) was added and the reaction mixture was kept at 0 °C for 2 h. In those cases where the suspension became too viscous, manual stirring was carried out occasionally. Then a concentrated solution of aq. NH_3 (25 mL) was added and the suspension was heated to 100 °C for 2 h. During this time product formed as a yellowish precipitate. The product was isolated by vacuum filtration and washed with H_2O (50 mL) and cold ethanol (10 mL). The crude product was recrystallized from EtOH and then fully characterized.

4-Tolu-yl-4'-(2,2'-6',2"-terpyridine) (II-6)
^{1}H-NMR (400 MHz, $CDCl_3$): δ(ppm) = 8.66 (d, 2 H; ^3J = 4.6 Hz, $H_{6,6''}$), 8.57 (d, 2 H; ^3J = 2.1 Hz, $H_{3,3''}$), 8.04 (s, 2 H; $H_{3',5'}$), 7.82 (dd, 2 H; ^3J = 7.2 Hz, ^3J = 7.2 Hz, $H_{4,4''}$), 7.38-7.00 (m, 6 H; Ar, $H_{5,5''}$), 2.34 (s, 3 H; Ar-CH_3). Yield: 42%. Elemental analysis: $C_{22}H_{17}N_3$ (337.40) calc. C 78.32%, H 5.08%, N 16.61%; found C 78.51%, H 5.07%, N 16.42%.

4'-(2-Hydroxy-ethoxy-phenyl)-2,2'-6',2"-terpyridine (II-7)
^{1}H-NMR (400 MHz, $CDCl_3$): δ(ppm) = 8.77 (d, 2 H; ^3J = 5.9 Hz, $H_{6,6''}$), 8.74 (s, 2 H; $H_{3',5'}$), 8.64 (d, 2 H; ^3J = 8.2 Hz, $H_{3,3''}$), 7.92 (m, 4 H; Ar, $H_{4,4''}$), 7.41 (dd, 2 H; ^3J = 6.7 Hz, ^3J = 5.9 Hz, $H_{5,5''}$), 7.04 (d, 2H; ^3J = 7.5 Hz, Ar), 4.17 (t, 2 H; ^3J = 4.8 Hz, OCH_2CH$_2$OH), 4.06 (t, 2 H; ^3J = 4.8 Hz, OCH$_2$$CH_2$OH), 3.61 (br s, 1 H; OH). Yield: 48%. Elemental analysis: $C_{23}H_{19}N_3O_2$ (369.42) calc. C 74.78%, H 5.18%, N 11.37%; found C 74.83%, H 5.24%, N 11.31%.

General procedure for the synthesis of heteroleptic *bis*-terpyridine ruthenium(II) complexes via Ru(III) intermediates
A solution of the free terpyridine ligand and the respective terpyridine ruthenium(III) *mono*-complex (1:1) was heated to reflux in methanol. After 15 minutes a few drops of *N*-ethylmorpholine were added and the reaction mixture turned from brown to purple. Stirring was continued overnight until an intense red color appeared. Subsequently a solution of NH_4PF_6 in methanol was added to the reaction mixture. The solution was allowed to cool to room temperature. The desired complex was obtained by extraction ($CHCl_3$ / H_2O) and following precipitation into ice-cold diethyl ether.

4'-(3-Hydroxy-propoxy)-2,2'-6',2"-terpyridine-4'-poly(ethylene glycol)-2,2'-6',2"-terpyridine Ru(II) di-hexafluorophosphate (II-8)
^{1}H-NMR (400 MHz, d_6-acetone): δ(ppm) = 8.86 (d, 4 H; ^3J = 7.8 Hz, $H_{3,3''}$), 8.77 (d, 4 H; ^3J = 2.1 Hz, $H_{3',5'}$), 7.98 (t, 4 H; ^3J = 8.0 Hz, $H_{4,4''}$), 7.46 (d, 4 H; ^3J = 4.8 Hz, $H_{6,6''}$), 7.22 (t, 2 H; ^3J = 7.5 Hz, $H_{5,5''}$), 4.79 (t, 1 H; ^3J = 4.6 Hz, OH), 4.60 (t, 2 H; ^3J = 4.6 Hz, OCH_2CH$_2$CH$_2$OH), 3.80-3.20 (m, 282 H; $H_{PEG\ backbone}$, OCH$_2$CH$_2$$CH_2$OH), 2.24 (q, 2 H; ^3J = 3.2 Hz, OCH$_2$$CH_2CH_2$OH). Yield: 69%. UV-vis ($CHCl_3$): λ_{max} (ε) = 309 (87,600), 493 (23,500) nm (L·mol^{-1}·cm^{-1}). GPC (eluent DMF with NH_4PF_6 (0.8 g/L)): M_n = 8,600 g/mol, PDI = 1.07.

4'-(4-Toluyl)-2,2'-6',2"-terpyridine-4'-poly(ethylene glycol)-2,2'-6',2"-terpyridine Ru(II) dihexafluoro-phosphate (II-9)
^{1}H-NMR (400 MHz, $CDCl_3$): δ(ppm) = 8.41 (d, 4 H; ^3J = 7.8 Hz, $H_{3,3''}$), 8.31 (d, 4 H; ^3J = 2.1 Hz, $H_{3',5'}$), 7.81 (t, 4 H; ^3J = 8.0 Hz, $H_{4,4''}$), 7.40-7.00 (m, 12 H; $H_{6,6''}$, $H_{5,5''}$, Ar), 2.35 (s, 3 H; Ar-CH_3). Yield: 72%. UV-vis ($CHCl_3$): λ_{max} (ε) = 308 (89,100), 487 (23,300) nm (L·mol^{-1}·cm^{-1}). GPC (eluent DMF with NH_4PF_6 (0.8 g/L)): M_n = 8,900 g/mol, PDI = 1.06.

Dichloro*tetrakis*(dimethylsulfoxide) ruthenium(II) [Ru(DMSO)$_4$Cl$_2$][32]
Ruthenium trichloride trihydrate (1 g) was refluxed in dimethyl sulfoxide (5 mL) for *5* min. The volume was reduced to half *in vacuo.* Subsequently acetone was added (20 mL) resulting in the formation of a yellow precipitate. The yellow

precipitate was filtered off, washed with acetone and diethyl ether, and vacuum dried. On standing, the filtrate deposited more of the complex. Elemental analysis: $C_8H_{24}Cl_2O_4RuS_4$ (484.52) calc. C 19.83%, H 4.99%, S 26.47%; found C 19.99%, H 4.99%, S 26.56%.

General procedure for the synthesis of terpyridine Ru(II) *mono*-complexes [Ru^{II}(tpy)(DMSO)Cl_2]
A mixture of [$Ru(DMSO)_4Cl_2$] and 4'-substituted teryridine (1.1:1) in argon-degassed $CHCl_3$ or CH_2Cl_2 was heated at 85 °C for 10 hours. During this time the solution turned brown and a brown precipitate formed slowly. After cooling to ambient temperature, the solution was filtered and the residue was washed with diethyl ether (2 × 5 mL) affording the desired *mono*-complex as an isomeric mixture.

4'-(2-Hydroxy-ethoxy-phenyl)-2,2'-6',2"-terpyridine Ru(II) (DMSO)Cl_2 (II-10)
^{1}H-NMR (400 MHz, d_6-DMSO): δ(ppm) = 9.34 (d; ^3J = 4.8 Hz, $H_{6,6"}$ trans), 9.01 (d; ^3J = 5.0 Hz, $H_{6,6"}$ cis), 8.93 (s, $H_{3',5'}$ trans), 8.82 (s, $H_{3',5'}$ cis), 8.78 (m; $H_{3,3"}$ trans & cis), 8.20 (d; ^3J = 5.0 Hz, $H_{Ar(1)}$ trans), 8.13(m; $H_{Ar(1)}$ cis, $H_{4,4"}$ cis), 7.99 (t; ^3J = 6.5 Hz, $H_{4,4"}$ trans), 7.77 (t; ^3J = 8.0 Hz, $H_{5,5"}$ cis), 7.51 (t; ^3J = 6.5 Hz, $H_{5,5"}$ trans), 7.20 (d, ^3J = 4.8 Hz, $H_{Ar(2)}$ trans), 7.17 (d, ^3J = 4.8 Hz, $H_{Ar(2)}$ cis), 4,93 (br s, 1 H, OH), 4.13 (m, 2 H; O-$CH_2$$CH_2$OH), 3.78 (m, 2 H; O-$CH_2$$CH_2$OH). Yield: 89%. UV-vis (DMSO): λ_{max} (ε) = 276 (14,400), 330 (23,700), 386 (3,500), 517 (3,900) nm (L·mol^{-1}·cm^{-1}).

4'-Chloro-2,2'-6',2"-terpyridine Ru(II) (DMSO)Cl_2 (II-11)
^{1}H-NMR (400 MHz, d_6-DMSO): δ(ppm) = 9.35 (d; ^3J = 4.8 Hz, $H_{6,6"}$ trans), 9.01 (d; ^3J = 5.0 Hz, $H_{6,6"}$ cis), 8.91 (s, $H_{3',5'}$ trans), 8.79 (s, $H_{3',5'}$ cis), 8.63 (m; $H_{3,3"}$ trans & cis), 8.16 (d; ^3J = 7.6 Hz, $H_{4,4"}$ cis), 7.99 (t; ^3J = 6.5 Hz, $H_{4,4"}$ trans), 7.81 (t; ^3J = 8.0 Hz, $H_{5,5"}$ cis), 7.54 (t; ^3J = 6.5 Hz, $H_{5,5"}$ trans). Yield: 92%. UV-vis (DMSO): λ_{max} (ε) = 271 (15,400), 314 (24,700), 330 (13,500), 481 (5,100) nm (L·mol^{-1}·cm^{-1}).

4'-(3-Hydroxy-propoxy)-2,2'-6',2"-terpyridine Ru(II) (DMSO)Cl_2 (II-12)
^{1}H-NMR (400 MHz, d_6-DMSO): δ(ppm) = 9.34 (d; ^3J = 4.8 Hz, $H_{6,6"}$ trans), 9.01 (d; ^3J = 5.0 Hz, $H_{6,6"}$ cis), 8.92 (s, $H_{3',5'}$ trans), 8.80 (s, $H_{3',5'}$ cis), 8.62 (m; $H_{3,3"}$ trans & cis), 8.16 (d; ^3J = 7.6 Hz,$H_{4,4"}$ cis), 7.98 (t; ^3J = 6.5 Hz,$H_{4,4"}$ trans), 7.79 (t; ^3J = 8.0 Hz, $H_{5,5"}$ cis), 7.55 (t; ^3J = 6.5 Hz, $H_{5,5"}$ trans), 4,93 (br s, 1 H, OH), 4.13 (m, 2 H; O-$CH_2$$CH_2$$CH_2$OH), 3.78 (m, 2 H; O-$CH_2$$CH_2$$CH_2$OH), 1.94 (m, 2 H; O-$CH_2$$CH_2$$CH_2$OH). Yield: 92%. UV-vis (DMSO): λ_{max} (ε) = 275 (18,400), 330 (25,700), 385 (3,600), 516 (4,100) nm (L·mol^{-1}·cm^{-1}).

4'-(3-(2-Bromo-isobutyryl)-propoxy)-2,2'-6',2"-terpyridine Ru(II) (DMSO)Cl_2 (II-13)
^{1}H-NMR (400 MHz, d_6-DMSO): δ(ppm) = 9.34 (d; ^3J = 4.8 Hz,$H_{6,6"}$ trans), 8.99 (d; ^3J = 5.0 Hz, $H_{6,6"}$ cis), 8.86 (s, $H_{3,3"}$ trans), 8.59 (d, ^3J = 4.8 Hz, $H_{3,3"}$ cis), 8.39 (s, $H_{3',5'}$ trans), 8.24 (s, $H_{3',5'}$ cis), 8.11 (t; ^3J = 8.0 Hz, $H_{4,4"}$ cis), 7.96 (t; ^3J = 6.5 Hz, $H_{4,4"}$ trans), 7.74 (t; ^3J = 8.0 Hz, $H_{5,5"}$ cis), 7.49 (t; ^3J = 7.5 Hz, $H_{5,5"}$ trans), 4.40 (t, 2 H; ^3J = 5.0 Hz, tpyO-$CH_2$$CH_2$$CH_2$O-), 4.37(t, 2 H; ^3J = 4.6 Hz, tpyO-$CH_2$$CH_2$$CH_2$O-), 2.22 (m, 2 H; tpyO-$CH_2$$CH_2$$CH_2$O-), 1.90 (s, 6 H; CH_3). Yield: 95%. UV-vis (DMSO): λ_{max} (ε) = 270 (15,600), 315 (24,900), 331 (14,500), 483 (5,000) nm (L·mol^{-1}·cm^{-1}).

General procedure for the synthesis of *bis*-terpyridine ruthenium(II) complexes via Ru(II) intermediates
A mixture of the respective Ru(II) *mono*-complex and $AgBF_4$ in degassed methanol was heated at 80 °C for 8 h. After cooling of the mixture to ambient temperature, the precipitate (AgCl) was separated by filtration and the red solution was allowed to react with the uncoordinated terpyridine ligand for 20 h at 80 °C. After this period, water (2 mL) containing NH_4PF_6 was added and the organic solvent was smoothly evaporated under vacuum until a precipitate was formed. The resulting solid was collected by filtration and washed with water. The complex was purified either by chromatography on alumina using a mixture of 1/1 (toluene/acetonitrile) or by precipitation into methanol.

***Bis*-4'-(2-hydroxy-ethoxy-phenyl)-2,2'-6',2"-terpyridine Ru(II) dihexafluorophosphate (II-14)**
^{1}H-NMR (400 MHz, d_6-DMSO): δ(ppm) = 9.42 (s, 4 H; $H_{3',5"}$), 9.08 (d, 4 H; ^3J = 8.0 Hz, $H_{3,3"}$), 8.41 (d, 4 H; ^3J = 7.2 Hz, Ar), 8.04 (t, 4 H; ^3J = 8.0 Hz, $H_{4,4"}$), 7.52 (d, 4 H; ^3J = 4.8 Hz, $H_{6,6"}$), 7.30 (d, 4 H; ^3J = 7.2 Hz, Ar), 7.25 (t, 4 H; ^3J = 8.0 Hz, $H_{5,5"}$), 4.96 (br s, 2 H; OH), 4.18 (t, 4 H; ^3J = 4.8 Hz, O-$CH_2$$CH_2$OH), 3.81 (m, 4 H; O-$CH_2$$CH_2$OH). MALDI-TOF MS (matrix: dithranol) m/z = 839 (M^+), 495 (M – C_2H_5O). Yield: 35%. UV-vis ($CHCl_3$): λ_{max} (ε) = 267 (55,400), 304 (62,700), shoulder at 342 (7,500), shoulder at 451 (12,000), 485 (18,100) nm (L·mol^{-1}·cm^{-1}).

4'-(3-hydroxy-propoxy)-2,2'-6',2"-terpyridine-2,2,5-trimethyl-3-(1-(4'-(4''-terpyridinyloxy)-methyl)-phenyl-ethoxy)-4-phenyl-3-azahexane-2,2'-6',2"-terpyridine Ru(II) di-hexafluorophosphate (II-15)
^{1}H-NMR ($CDCl_3$, 400 MHz): δ(ppm) = 8.61-8.35 (m, 8 H; $H_{3',5'}$, $H_{3,3"}$), 7.85 (t, 4 H, ^3J = 8.0 Hz, $H_{4,4"}$), 7.48-7.14 (m, 17 H, aromatic & $H_{6,6"}$, $H_{5,5"}$), 5.35 (s, 2 H, tpyOCH_2, minor), 5.30 (s, 2 H, tpyOCH_2, major), 4.94 (m, 2 H, *H*C-ON, both diastereomers), 4.79 (t, 1 H; ^3J = 4.6 Hz, OH), 4.60 (t, 2 H; ^3J = 4.8 Hz, O$CH_2$$CH_2$$CH_2$OH), 3.42 (m, 4 H, ON-C*H*, major & minor, $OCH_2CH_2CH_2OH$), 2.34 (m, 1 H, CH_3CHCH_3, major), 2.24 (q, 4 H; ^3J = 6.5 Hz, $OCH_2CH_2CH_2OH$), 1.63 (d, 3 H, ^3J = 4.6 Hz, CH_3CH-ON, major), 1.55 (d, 3 H, ^3J = 4.6 Hz, CH_3CH-ON, minor), 1.39 (m, 1 H, CH_3CHCH_3, minor), 1.31 (d, 3 H, ^3J = 4.6 Hz, CH_3CHCH$_3$, major), 1.04 (s, 9 H, C(CH_3)$_3$, minor), 0.89 (d, 3 H, *J* = 6.0 Hz, CH_3CHCH_3, major), 0.77 (s, 9 H, C(CH_3)$_3$, major), 0.54 (d, 3 H, ^3J = 6.0 Hz, CH_3CHCH$_3$,

minor), 0.17 (d, 3 H, ^3J = 6.0 Hz, CH_3CHCH_3, minor). Yield: 29%. UV-vis ($CHCl_3$): λ_{max} (ε) = 270 (57,400), 304 (62,000), shoulder at 344 (6,500), shoulder at 452 (12,500), 485 (20,100) nm ($L \cdot mol^{-1} \cdot cm^{-1}$).

General procedure for the synthesis of homoleptic *bis*-terpyridine ruthenium(II) complexes using $Ru(DMSO)_4Cl_2$

The terpyridine ligand in 10 mL ethylene glycol was added to the ruthenium(II) precursor $Ru(DMSO)_4Cl_2$ in 4 mL of a 1:1 MeOH / H_2O mixture. The mixture was heated under argon atmosphere at 100 °C for 2.5 h, producing a red solution, which was then cooled to room temperature. Water containing NH_4PF_6 was added to the mixture whereupon a red precipitate formed. The precipitate was washed thoroughly with H_2O, precipitated into methanol and dried under vacuum.

***Bis*-4'-(3-chloro-propoxy)-2,2'-6',2"-terpyridine Ru(II) dihexafluorophosphate (II-16)**

^{1}H-NMR (400 MHz, d_6-DMSO): δ(ppm) = 8.86 (d, 4 H; ^3J = 8.0 Hz, $H_{3,3''}$), 8.79 (s, 4 H; $H_{3',5''}$), 7.99 (t, 4 H; ^3J = 8.0 Hz, $H_{4,4''}$), 7.47 (d, 4 H; ^3J = 4.8 Hz, $H_{6,6''}$), 7.23 (t, 4 H; ^3J = 6.5 Hz, $H_{5,5''}$), 4.65 (t, 4 H; ^3J = 4.8 Hz, O-$CH_2$$CH_2CH_2$-Cl), 3.98 (t, 2 H; ^3J = 4.8 Hz, O-$CH_2CH_2CH_2$-Cl), 2.44 (q, 2 H; ^3J = 4.6 Hz, O-$CH_2CH_2$$CH_2$-Cl). MALDI-TOF MS (matrix: dithranol) m/z = 897 ($M^+ + PF_6$), 752 (M^+), 674 ($M^+ - C_3H_6Cl$). Yield: 86%. UV-vis ($CHCl_3$): λ_{max} (ε) = 270 (53,100), 305 (60,200), shoulder at 340 (5,200), shoulder at 451 (11,500), 484 (20,100) nm ($L \cdot mol^{-1} \cdot cm^{-1}$).

***Bis*-4'-(3-hydroxy-propoxy)-2,2'-6',2"-terpyridine Ru(II) dihexafluorophosphate (II-17)**

^{1}H-NMR (400 MHz, d_6-acetone): δ(ppm) = 8.86 (d, 4 H; ^3J = 8.0 Hz, $H_{3,3''}$), 8.77 (d, 4 H; ^3J = 1.4 Hz, $H_{3',5'}$), 7.98 (t, 4 H; ^3J = 8.0 Hz, $H_{4,4''}$), 7.46 (d, 4 H; ^3J = 4.8 Hz, $H_{6,6''}$), 7.22 (t, 4 H; ^3J = 6.5 Hz, $H_{5,5''}$), 4.79 (m, 1 H; OH), 4.60 (t, 4 H; ^3J = 4.8 Hz, O$CH_2CH_2CH_2$OH), 3.80-3.20 (q, 4 H; ^3J = 4.8 Hz, $OCH_2CH_2CH_2OH$), 2.24 (q, 4 H; ^3J = 4.8 Hz, $OCH_2CH_2CH_2OH$). MALDI-TOF MS (matrix: dithranol) m/z = 860 ($M^+ + PF_6$), 716 (M^+), 656 ($M^+ - C_3H_6OH$). Yield: 92%. UV-vis ($CHCl_3$): λ_{max} (ε) = 270 (57,300), 305 (66,000), shoulder at 342 (6,100), shoulder at 453 (10,900), 483 (19,600) nm ($L \cdot mol^{-1} \cdot cm^{-1}$).

The iridium(III) precursor complexes were synthesized according to published procedures.[59]

***Tetrakis*(2-phenylpyridine-C^2,N')(*μ*-dichloro)diiridium**

^{1}H-NMR (CD_2Cl_2): δ(ppm) = 5.79 (d, 4 H; $^3J_{H,H}$ = 8.8 Hz, $H^{6'}$), 6.50-6.54 (m, 4 H; $H^{5'}$), 6.71-6.76 (m, 8 H; $H^{4'}$, H^5), 7.46-7.49 (m, 4 H; $H^{3'}$), 7.69-7.74 (m, 4 H; H^4), 7.86 (d, 4 H; $^3J_{H,H}$ = 8.00 Hz, H^3), 9.17 (d, 4 H; $^3J_{H,H}$ = 5.60 Hz, H^6).

***Tetrakis*(2-phenyl-4-nitro-pyridine-C^2,N')(*μ*-dichloro)diiridium**

^{1}H-NMR (CD_2Cl_2): δ(ppm) = 6.61 (s, 4 H; ^3J = 8.8 Hz, $H^{6'}$); 7.11 (t, 4 H, ^3J = 7.6 Hz, H^5); 7.80-6.78 (m, 8H, H^3, H^4); 8.20-8.02 (m, 8 H, $H^{3'}$, $H^{4'}$); 9.23 (d, 4 H, ^3J = 5.6 Hz, H^6).

General procedure of the complexation with iridium(III) precursor complexes

The iridium(III) precursor complex and the terpyridine-functionalized ligand are added into a vial containing a mixture of degassed CH_2Cl_2 and MeOH. Subsequently, the reaction mixture was heated to 80 °C for 6 h. After cooling the reaction mixture to room temperature an excess of NH_4PF_6 was added. The solvent was removed *in vacuo* and the reaction mixture was partitioned between 25 mL water and 25 mL methylene chloride (CH_2Cl_2). The organic layer was washed with water (3 × 25 mL), dried over Na_2SO_4 and finally removed *in vacuo*. The metallo-supramolecular complex was further purified by precipitation into ice-cold diethyl ether.

Iridium(III)(5-(2,2'-6',2"-terpyridine-4'-yloxy)-hexylamine)(ppy_2) hexafluorophosphate (II-19)

^{1}H-NMR (400 MHz, CD_2Cl_2): δ(ppm) = 8.88 (d, 1 H; ^3J = 6.6 Hz, H^6-ppy), 8.51 (d, 1 H; ^3J = 7.6 Hz, H^6-ppy), 8.19 (d, 1 H; ^3J = 4.4 Hz, H_6-tpy), 8.13 (m, 1 H; H^5-ppy), 7.97 (d, 1 H; ^3J = 2.8 Hz, $H_{6''}$-tpy),7.94-7.73 (m, 5 H; $H_{4''}$-tpy, $H_{3',5'}$-tpy, H^3-ppy, H^4-ppy), 7.61 (d, 1 H; ^3J = 7.6 Hz, $H^{3'}$-ppy), 7.44 (d, 1 H; ^3J = 6.0 Hz, $H_{3''}$-tpy), 7.36 (m, 2 H; H^4-ppy, $H^{3'}$-ppy), 7.16 (ddd, 1 H, ^3J = 1.6 Hz, ^3J = 6.0 Hz, ^3J = 7.6 Hz, H^5-ppy), 7.09 (ddd, 1 H; ^3J = 1.6 Hz, ^3J = 6.0 Hz, ^3J = 7.7 Hz, H_4-tpy), 6.99 (m, 2 H; H^3-ppy, $H^{4'}$-ppy), 6.90 (m, 2 H; $H_{5,5''}$-tpy), 6.77 (m, 1 H; $H^{5'}$-ppy), 6.64 (m, 1 H; $H^{4'}$-ppy), 6.50 (d, 1 H; ^3J = 7.6 Hz, H_3-tpy), 6.32 (m, 1 H; $H^{5'}$-ppy), 5.91 (d, 1 H; ^3J = 7.6 Hz, $H^{6'}$-ppy), 5.54 (d, 1 H; ^3J = 7.6 Hz, $H^{6'}$-ppy), 4.25 (t, 2 H; ^3J = 6.6 Hz, H^a), 2.73 (m, 2 H; H^f), 1.89 (m, 4 H; H^b, H^e), 1.54 (m, 2 H; $H^{c,d}$). MALDI-TOF MS (matrix: dithranol) M ($C_{43}H_{40}N_5OIr$) = 835; m/z = 835 g/mol (M^+), 501 (ppy_2-Ir). Yield: 84%. UV-vis (CH_2Cl_2): λ_{max} (ε) = 261 (35,100), 342 (6,300), 381 (3,400), 451 (1,800) nm ($L \cdot mol^{-1} \cdot cm^{-1}$).

Iridium(III)(3-hydroxy-propoxy)- 2,2'-6',2"-terpyridine (ppy_2-NO_2) hexa-fluorophosphate (II-20)

^{1}H-NMR (400 MHz, $CDCl_3$): δ(ppm) = 9.38 (m, 1 H; H^6-ppy), 8.85 (d, 1 H; ^3J = 6.6 Hz, H^6-ppy), 8.28-8.19 (m, 2 H; H_6-tpy, H^5-ppy), 8.08-7.71 (m, 9 H; $H_{6''}$-tpy, $H_{4''}$-tpy, $H_{3',5'}$-tpy, H^3-ppy, H^4-ppy, $H^{3'}$-ppy, $H^{4'}$-ppy), 7.62 (d, 1 H; ^3J = 7.6 Hz, $H^{4'}$-ppy), 7.58-7.30 (m, 3 H; H^5-ppy, $H^{4'}$-ppy, H_3-tpy), 7.12 (t, 1 H; ^3J = 7.5 Hz, H_4-tpy), 6.91 (m, 2 H; $H_{5,5''}$-tpy), 6.78 (m, 1 H, H^3-ppy), 6.69 (m, 1 H; H_3-tpy), 6.58 (d, 1 H; ^3J = 7.0 Hz, $H^{6'}$-ppy), 6.07 (d, 1 H; ^3J = 7.6 Hz, $H^{6'}$-ppy), 4.46 (t, 2 H; ^3J = 6.6 Hz, tpy-O$CH_2CH_2CH_2OH$), 3.78 (t, 2 H; ^3J = 6.6 Hz, tpy-$OCH_2CH_2CH_2$OH), 2.31 (q, 2 H;

^3J = 4.8 Hz, tpy-OCH$_2$*CH$_2$*CH$_2$OH). MALDI-TOF MS (matrix: dithranol) M ($C_{40}H_{31}N_7O_6Ir$) = 897.95 g/mol; m/z = 898 (M^+), 591 ((ppy-NO_2)$_2$-Ir). Yield: 86%. UV-vis (CH_2Cl_2): λ_{max} (ε) = 276 (30,100), 340 (5,300), 381 (2,900), 451 (1,300) nm (L·mol^{-1}·cm^{-1}). Quantum yield (CH_2Cl_2) = 0.11.

Iridium(III)(3-chloro-propoxy)- 2,2'-6',2"-terpyridine (ppy$_2$-NO$_2$) hexa-fluorophosphate (II-21)
^{1}H-NMR (400 MHz, $CDCl_3$): δ (ppm) = 9.37 (m, 1 H; H^6-ppy), 8.84 (d, 1 H; ^3J = 6.6 Hz, H^6-ppy), 8.26-8.19 (m, 2 H; H$_6$-tpy, H^5-ppy), 8.08-7.71 (m, 9 H; H$_{6"}$-tpy, H$_{4"}$-tpy, H$_{3',5'}$-tpy, H^3-ppy, H^4-ppy, H$^{3'}$-ppy, H$^{4'}$-ppy), 7.62 (d, 1 H; ^3J = 7.6 Hz, H$^{4'}$-ppy), 7.58-7.30 (m, 3 H; H^5-ppy, H$^{4'}$-ppy, H$_3$-tpy), 7.12 (t, 1 H; ^3J = 7.5 Hz, H$_4$-tpy), 6.91 (m, 2 H; H$_{5,5"}$-tpy), 6.78 (m, 1 H, H^3-ppy), 6.69 (m, 1 H; H$_3$-tpy), 6.58 (d, 1 H; ^3J = 7.6 Hz, H$^{6'}$-ppy), 6.07 (d, 1 H; ^3J = 7.6 Hz, H$^{6'}$-ppy), 4.44 (t, 2 H; ^3J = 6.6 Hz, tpy-O*CH$_2$*CH$_2$CH$_2$Cl), 3.78 (t, 2 H; ^3J = 6.6 Hz, tpy-OCH$_2$CH$_2$*CH$_2$*Cl), 2.34 (q, 2 H; ^3J = 4.8 Hz, tpy-OCH$_2$*CH$_2$*CH$_2$Cl). Elemental analysis: $C_{40}H_{30}N_7O_5ClIr$ calc. C 45.27%, H 2.85%, N 9.24%; found C 45.57%, H 2.93%, N 8.92%. MALDI-TOF MS (matrix: dithranol) M ($C_{40}H_{30}N_7O_5Ir$) = 916.39 g/mol; m/z = 898 (M^+), 591 ((ppy-NO_2)$_2$-Ir). Yield: 87%. UV-vis (CH_2Cl_2): λ_{max} (ε) = 255 (32,100), 306 (18,200), 340 (7,000), 381 (3,500), 451 (1,900) nm (L·mol^{-1}·cm^{-1}). Quantum yield (CH_2Cl_2) = 0.12.

Iridium(III) diethylene glycol- di-2,2'-6',2"-terpyridine (ppy$_2$-NO$_2$) hexa-fluorophosphate (II-22)
^{1}H-NMR (400 MHz, $CDCl_3$): δ (ppm) = 9.37 (m, 1 H; H^6-ppy), 8.84 (d, 1 H; ^3J = 6.6 Hz, H^6-ppy), 8.26-8.19 (m, 2 H; H$_6$-tpy, H^5-ppy), 8.08-7.71 (m, 9 H; H$_{6"}$-tpy, H$_{4"}$-tpy, H$_{3',5'}$-tpy, H^3-ppy, H^4-ppy, H$^{3'}$-ppy, H$^{4'}$-ppy), 7.62 (d, 1 H; ^3J = 7.6 Hz, H$^{4'}$-ppy), 7.58-7.30 (m, 3 H; H^5-ppy, H$^{4'}$-ppy, H$_3$-tpy), 7.12 (t, 1 H; ^3J = 7.5 Hz, H$_4$-tpy), 6.91 (m, 2 H; H$_{5,5"}$-tpy), 6.78 (m, 1 H, H^3-ppy), 6.69 (m, 1 H; H$_3$-tpy), 6.58 (d, 1 H; ^3J = 7.6 Hz, H$^{6'}$-ppy), 6.07 (d, 1 H; ^3J = 7.6 Hz, H$^{6'}$-ppy), 4.53 (br s, 2 H, tpy-O*CH$_2$*CH$_2$-O), 3.98 (br s, 2 H, tpy-OCH$_2$*CH$_2$*-O). MALDI-TOF MS (matrix: dithranol) M ($C_{78}H_{56}N_{14}O_{11}Ir_2P_2F_{12}$) = 2039.76 g/ mol; m/z = 1893 (M^+ - PF_6), 1159 (M^+ - PF_6 – (ppy-NO_2)$_2$-Ir), 591 ((ppy-NO_2)-Ir). Yield: 65%. UV-vis (CH_2Cl_2): λ_{max} (ε) = 263 (29,100), 309 (20,300), 341 (6,800), 381 (3,300), 436 (2,500) nm (L·mol^{-1}·cm^{-1}). Quantum yield (CH_2Cl_2) = 0.05.

Iridium(III) 4,4'-(4,4'-(9,9-dioctyl-9*H*-fluorene-2,7-diyl)*bis*(4,1-phenylen))di-2,2'-6',2"-terpyridine (ppy$_2$) hexa-fluorophosphate (II-23)
^{1}H-NMR (400 MHz, $CDCl_3$): δ (ppm) = 8.93-8.85 (m, 2 H; H^6-ppy), 8.25-8.19 (m, 2 H; H$_6$-tpy, H^5-ppy), 8.02 (d, 1 H; ^3J = 6.6 Hz, H$_{6"}$-tpy), 7.95-7.70 (m, 6 H; H$_{4"}$-tpy, H$_{3',5'}$-tpy, H^3-ppy, H^4-ppy, H$_{fluorene}$), 7.63 (m, 2 H; H$^{3'}$-ppy, H^4-ppy), 7.55 (m, 3 H; H$^{3'}$-ppy, H$_{Ar}$, H$_{fluorene}$), 7.32 (m, 3 H; H$_{3"}$-tpy, H$_{Ar}$, H$_{fluorene}$), 7.20-7.05 (m, 2 H, H^5-ppy, H$_4$-tpy), 6.92 (m, 2 H; H^3-ppy, H^4-ppy), 6.74 (t, 1 H; ^3J = 7.5 Hz, H^5-ppy), 6.60 (t, 1 H; ^3J = 7.5 Hz, H$^{4'}$-ppy), 6.54 (d, 1 H; ^3J = 7.6 Hz, H$_4$-tpy), 6.31 (t, 1 H; ^3J = 5.0 Hz, H$^{5'}$-ppy), 5.88 (d, 1 H; ^3J = 4.8 Hz, H$^{6'}$-ppy), 5.47 (d, 1 H; ^3J = 4.8 Hz, H$^{6'}$-ppy). MALDI-TOF MS (matrix: dithranol) M ($C_{101}H_{80}N_{10}Ir_2P_2F_{12}$) = 2108.2 g/ mol; m/z = 1506 (M^+ - PF_6 - (ppy$_2$-Ir), 501 (ppy$_2$)-Ir). Yield: 59%. UV-vis (CH_2Cl_2): λ_{max} (ε) = 264 (36,400), 303 (21,300), 389 (19,100) nm (L·mol^{-1}·cm^{-1}). Quantum yield (CH_2Cl_2) = 0.09.

2.7 References

1 B.G.G. Lohmeijer, U.S. Schubert, *Macromol. Chem. Phys.* **2003**, *204*, 1072.
2 J.-F. Gohy, B.G.G. Lohmeijer, U.S. Schubert, *Macromol. Rapid Commun.* **2002**, *23*, 555.
3 G.T. Morgan, F.S. Burstall, *J. Chem. Soc.* **1932**, 20.
4 F. Kröhnke, *Synthesis* **1976**, 1.
5 K.T. Potts, *Bull. Soc. Chim. Belg.* **1990**, *99*, 741.
6 E.C. Constable, M.D. Ward, *J. Chem. Soc., Dalton Trans.* **1990**, 1405.
7 E.C. Constable, *Adv. Inorg. Chem. Radiochem.* **1986**, 69.
8 A. Islam, N. Ikeda, K. Nozaki, Y. Okamoto, B. Gholamkhass, A. Yoshimura, T. Ohno, *Coord. Chem. Rev.* **1998**, *171*, 355.
9 M.L. Stone, G.A. Crosby, *Chem. Phys. Lett.* **1981**, *79*, 169.
10 U.S. Schubert, C. Eschbaumer, P. Andres, H. Hofmeier, C.H. Weidl, E. Herdtweck, E. Dulkeith, A. Morteani, N.E. Hecker, J. Feldmann, *Synth. Met.* **2001**, *121*, 1249.
11 U.S. Schubert, C. Eschbaumer, O. Hien, P.R. Andres, *Tetrahedron Lett.* **2001**, *42*, 4705.
12 P.R. Andres, R. Lunkwitz, G.R. Pabst, K. Boehn, D. Wouters, S. Schmatloch, U.S. Schubert, *Eur. J. Org. Chem.* **2003**, 3769.
13 U.S. Schubert, O. Hien, C. Eschbaumer, *Macromol. Rapid Commun.* **2000**, *21*, 1156.
14 U.S. Schubert, C. Eschbaumer, *Macromol. Symp.* **2001**, *163*, 177.
15 U.S. Schubert, S. Schmatloch, A.A. Precup, *Design. Monom. Polym.* **2002**, *5*, 211.

16 G.R. Newkome, F. Cardullo, E.C. Constable, C.N. Moorefield, A.M.W.C. Thompson, *Chem. Commun.* **1993**, 925.
17 E.C. Constable, J. Lewis, M.C. Liptrot, P.R. Raithby, *Inorg. Chim. Acta.* **1990**, *178*, 47.
18 E.C. Constable, A.M.W.C. Thompson, N. Armaroli, V. Balzani, M. Maestri, *Polyhedron* **1992**, *11*, 2707.
19 A. Winter, A.M.J. van den Berg, R. Hoogenboom, G. Kickelbick, U.S. Schubert, *Synthesis* **2006**, *17*, 2873.
20 C.B. Smith, C.L. Raston, A.N. Sobolev, *Green Chem.* **2005**, 650.
21 W. Goodall, K. Wild, K.J. Arm, J.A.G. Williams, *J. Chem. Soc.*, *Perkin Trans.* **2002**, *2*, 1669.
22 C.E. Housecroft, A.G. Shape, *Inorganic Chemistry 1st Ed.*, Pearson, Harlow, **2001**.
23 E.C. Constable, G. Baum, E. Bill, R. Dyson, R. van Eldik, D. Fenske, S. Kaderli, D. Morris, A. Neubrand, M. Neuburger, D.R. Smith, K. Wieghardt, M. Zehnder, A. Zuberbühler, *Chem. Eur. J.* **1999**, *5*, 497.
24 J.-F. Gohy, B.G.G. Lohmeijer, U.S. Schubert, *Chem. Eur. J.* **2003**, *9*, 3472.
25 A.D. Ievins, A.O. Moughton, R.K. O'Reilly, *Macromolecules* **2008**, *41*, 3571.
26 C.-A. Fustin, B.G.G. Lohmeijer, A.S. Duwez, A.M. Jonas, U.S. Schubert, J.-F. Gohy, *Adv. Mater.* **2005**, *17*, 1162.
27 B.A. Moyer, M.S. Thompson, *J. Am. Chem. Soc.* **1980**, *102*, 2310.
28 E.C. Constable, A.M.W.C. Thompson, *New J. Chem.* **1992**, *16*, 855.
29 M. Maestri, N. Armaroli, V. Balzani, E.C. Constable, A.M.W.C. Thompson, *Inorg. Chem.* **1995**, *35*, 2759.
30 R. Ziessel, V. Grosshenny, M. Hissler, C. Stroh, *Inorg. Chem.* **2004**, *43*, 4262.
31 K.J. Takeuchi, M.S. Thompson, D.W. Pipes, T.J. Meyer, *Inorg. Chem.* **1984**, *23*, 1845.
32 I.P. Evans, A. Spencer, G. Wilkinson, *J. Chem. Soc., Dalton Trans.* **1973**, 204.
33 V. Grosshenny, R. Ziessel, *J. Organomet. Chem.* **1993**, *453*, C19.
34 A. Mercer, J. Trotter, *J. Chem. Soc. Dalton Trans*. **1975**, 2480.
35 C.J. Bloom, M. Elliot, P.G. Schroeder, C.B. France, B.A. Parkinson, *J. Phys. Chem. B* **2003**, *107*, 2933.
36 Y. Li, C. Huffman, A.H. Flood, *Chem. Commun.* **2007**, 2692.
37 J.P. Sauvage, J.P. Collin, J.C. Chambron, S. Guillerez, C. Coudret, V. Balzani, F. Barigelletti, L. de Cola, L. Flamigni, *Chem. Rev.* **1994**, *94*, 993.
38 J.P. Collin, S. Guillerez, J.P. Sauvage, F. Barigelletti, L. Flamigni, L. de Cola, V. Balzani, *Coord. Chem. Rev.* **1991**, *111*, 291.
39 M.A.R. Meier, B.G.G. Lohmeijer, U.S. Schubert, *J. Mass. Spectrom.* **2003**, *38*, 510.
40 U.S. Schubert, C. Eschbaumer, P.R. Andres, H. Hofmeier, C.H. Weidl, E. Herdtweck, E. Dulkeith, A. Morteani, N.E. Hecker, J. Feldmann, *Synth. Met.* **2001**, *121*, 1249.
41 V.V. Rostovtsev, L.G. Green, V.V. Fokin, K.B. Sharpless, *Angew. Chem. Int. Ed.* **2002**, *41*, 2596.
42 T.R. Chan, R. Hilgraf, K.B. Sharpless, V.V. Fokin, *Org. Lett.* **2004**, *6*, 2853.
43 B.G.G. Lohmeijer, R.C. Pratt, F. Leibfarth, J.W. Logan, D.A. Long, A.P. Dove, F. Nederberg, J. Choi, C. Wade, R.M. Waymouth, J.L. Hedrick, *Macromolecules* **2006**, *39*, 8574.
44 E. Holder, B.M.W. Langeveld, U.S. Schubert, *Adv. Mater.* **2005**, *17*, 1109.
45 E. Holder, V. Marin, D. Kozodaev, M.A.R. Meier, B.G.G. Lohmeijer, U.S. Schubert, *Macromol. Chem. Phys.* **2005**, *206*, 989.
46 E. Holder. V. Marin, A. Alexeev, U.S. Schubert, *J. Polym. Sci., Part A: Polym. Chem.* **2005**, *43*, 2765.
47 V. Marin, E. Holder, R. Hoogenboom, E. Tekin, U.S. Schubert, *Dalton Trans.* **2006**, 1636.
48 X. Yang, D.C. Müller, D. Neher, K. Meerholz, *Adv. Mater.* **2006**, *18*, 948.
49 R.C. Kwong, S. Lamansky, M.E. Thompson, *Adv. Mater.* **2000**, *12*, 1134.
50 H.J. Bolink, L. Cappelli, E. Coronado, A. Parham, P. Stössel, *Chem. Mater.* **2006**, *18*, 2778.
51 N.R. Evans, L.S. Devi, C.S.K. Mak, S.E. Watkins, S.I. Pascu, A. Köhler, R.H. Friend, C.K. Williams, A.B. Holmes, *J. Am. Chem. Soc.* **2006**, *128*, 6647.
52 F. Neve, A. Crispini, *J. Inorg. Chem.* **2000**, *5*, 1039.
53 S. Sprouse, K.A. King, P.J. Spellane, R.J. Watts, *J. Am. Chem. Soc.* **1984**, *106*, 6647.
54 F. Neve, A. Crispini, S. Campagna, S. Serroni, *Inorg. Chem.* **1999**, *38*, 2250.
55 E. Holder, V. Marin, M.A.R. Meier, U.S. Schubert, *Macromol. Rapid Commun.* **2004**, *25*, 1491.

56 R. Gao, D.G. Ho, B. Hernandez, M. Selke, D. Murphy, P.I. Djurovich, M.E. Thompson, *J. Am. Chem. Soc.* **2002**, *124*, 14828.
57 S. Lamansky, P. Djurvich, D. Murphy, F. Abdel-Razzaq, H.-E. Lee, C. Adachi, P.E. Burrows, S.R. Forrest, M.E. Thompson, *J. Am. Chem. Soc.* **2001**, *123*, 4304.
58 M.C. DeRosa, P.J. Mosher, G.P.A. Yap, K.-S. Focsaneanu, R.J. Crutchley, C.E.B. Evans, *Inorg. Chem.* **2003**, *42*, 4864.
59 P. Wang, S.M. Zakeeruddin, J.E. Moser, M.K. Nazeeruddin, T. Sekiguchi, M. Grätzel, *Nature Mater*. **2003**, *2*, 498.

CHAPTER 3

Terpyridine-functionalized polymeric architectures by nitroxide-mediated radical polymerization

Abstract

Controlled radical polymerization (CRP) methodologies have proven to be extremely useful for the preparation of new polymeric materials that are unattainable through other polymerization techniques since they allow control over composition, architecture and functionality. This chapter describes the synthesis and characterization of well-defined polymeric architectures by employing the nitroxide-mediated radical polymerization (NMRP) procedure. Based on a terpyridine-modified alkoxyamine initiator, different monomers from various monomer-groups were chosen and polymerized in a controlled fashion yielding low-polydispersity homopolymers, diblock copolymers and triblock terpolymers. Furthermore, a versatile post-modification approach of a fluorinated polymer is demonstrated in order to design multifunctional graft copolymers by taking advantage of the selective replacement of a fluorine atom. This is a straightforward approach that allows the easy insertion of different additional functional groups into the polymeric chain which can be further modified for several purposes including additional controlled post-polymerizations, e.g., ring opening polymerization (ROP) and atom transfer radical polymerization (ATRP). The synthetic work presented in this chapter leads to a toolbox that allows the construction of a seemingly unlimited variety of highly functionalized metallo-supramolecular materials.

Parts of this chapter have been and will be published: C. Ott, B.G.G. Lohmeijer, D. Wouters, U.S. Schubert, *Macromol. Chem. Phys.* **2006**, *207*, 1439-1449; C. Ott, D. Wouters, H.M.L. Thijs, U.S. Schubert, *J. Inorg. Organometal. Polym. Mater.* **2007**, *17*, 241-249; C. Ott, R. Hoogenboom, U.S. Schubert, *Chem. Commun.* **2008**, 3516-3518; C. Ott, R. Hoogenboom, S. Hoeppener, D. Wouters, J.-F. Gohy, U.S. Schubert, *Soft Matter* **2009**, in press.

3.1 Introduction

The previous chapter dealt with the synthesis and characterization of various substituted *bis*-terpyridine metal complexes. In order to connect different polymer chains with each other, the terpyridine ligand has to be connected to a polymer backbone. There are several synthetic approaches which can be successfully applied to insert the supramolecular binding motif either at the chain end(s) or to the side chains of the polymer. Figure 3.1 shows possible routes towards terpyridine-functionalized polymers.

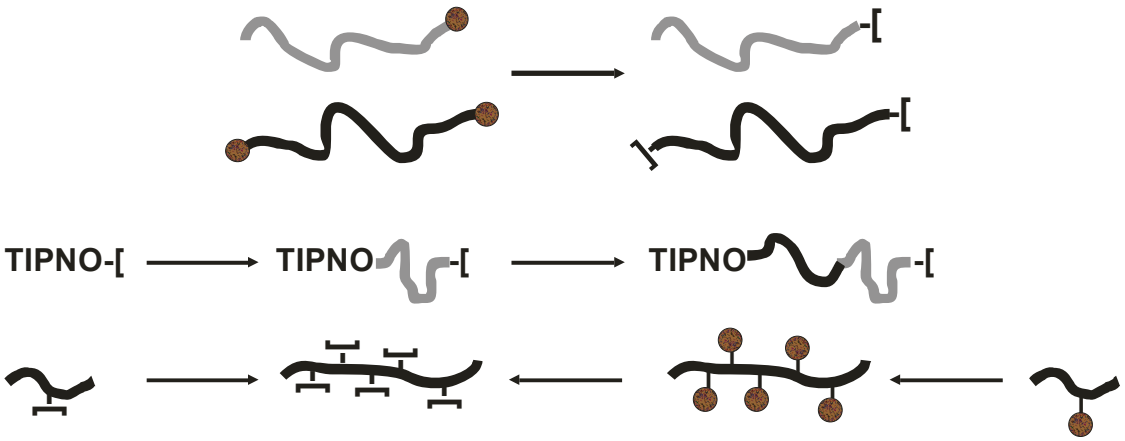

Figure 3.1 *Possible synthetic approaches towards mono- and telechelic terpyridine-functionalized polymers as well as polymers with terpyridines in the side chain. TIPNO represents a specific nitroxide radical (see Section 3.2). The functional group (circle) allows the incorporation of the terpyridine moiety (-[).*

The first approach involves the modification of existing functional polymer end groups which have been introduced by established polymerization processes. In particular mono- and telechelic hydroxy-functionalities achieved by anionic polymerization provide a basis for chemical modification, since these groups can be easily converted using etherification reactions. 4'-Chloroterpyridine and isocyanide-functionalized terpyridines are potential building blocks for this purpose.[1] The second route requires the synthesis of a terpyridine-functionalized initiator, which automatically leads to polymers containing the terpyridine moiety at the chain end upon polymerization. Therefore, a modified initiator for nitroxide-mediated polymerization was designed capable for the controlled radical polymerization of vinylic monomers such as styrenes, acrylates, acrylamides, dienes and vinylpyridines. The synthesis of terpyridine-functionalized homo-polymers[2] is described in Section 3.2.1. Section 3.2.2 demonstrates the successful synthesis of block copolymers by further utilizing the obtained homopolymers as macroinitiators.[2,3] The third route includes the preparation of polymers bearing terpyridine ligands in the side chain. This can be achieved either by (co)polymerization of a terpyridine-functionalized macromonomer[4-6] or by (co)polymerization of functionalized monomers[7] which allow the incorporation of the supramolecular binding motif using suitable substitution reactions. The last section of this chapter deals with a versatile post-modification reaction allowing the construction of multifunctional graft copolymers in a simple and efficient manner. This approach opens unprecedented possibilities for synthetic polymer chemists. The powerful strategy of combining nitroxide-mediated polymerization with the before mentioned post-modification reaction facilitates the synthesis of well-defined copolymers and provides the opportunity to accurately tune selected material properties by controlling their macromolecular structure. All polymers described in this chapter can be regarded as a macromolecular toolbox which offers the potential to engineer a wide diversity of metallo-supramolecular architectures.

3.2 Nitroxide-mediated controlled radical polymerization

In the last decade, significant advances have been made in the field of controlled ('living') radical polymerization,[8-12] including nitroxide-mediated polymerization (NMP), atom transfer radical polymerization (ATRP) and reversible addition-fragmentation chain transfer polymerization (RAFT). Their widespread acceptance and exploitation in polymer synthesis is justified by the seemingly unlimited potential to create a wide range of well-defined macromolecules with accurate control over architecture and functionality.[13] The NMP technique has attracted great interest because of its simplicity, since in most cases it requires only the addition of a suitable alkoxyamine to the polymerization system. Moreover, NMP does not require any metals and it is effective for the polymerization of a broad range of monomers. This system provides colorless and odorless polymers with no demanding purification procedures.

Rizzardo[14] and Georges[15] were the first who introduced the use of 2,2,6,6-tetramethyl-1-piperidynyloxyl nitroxide, known as TEMPO, to control radical polymerizations; however, this nitroxide is limited to polymerize styrene and its derivatives. Therefore, second-generation nitroxides have been developed to extend this technique to different monomers. The design of acyclic nitroxides, for example *N*-*tert*-butyl-*N*-(1-diethylphosphono-2,2-dimethylproxyl) nitroxide (SG1) or 2,2,5-trimethyl-4-phenyl-3-azahexane nitroxide (TIPNO), allowed the expansion of this technique to acrylate derivatives. Scheme 3.1 shows a general reaction scheme of NMP and a selection of commonly utilized nitroxides.

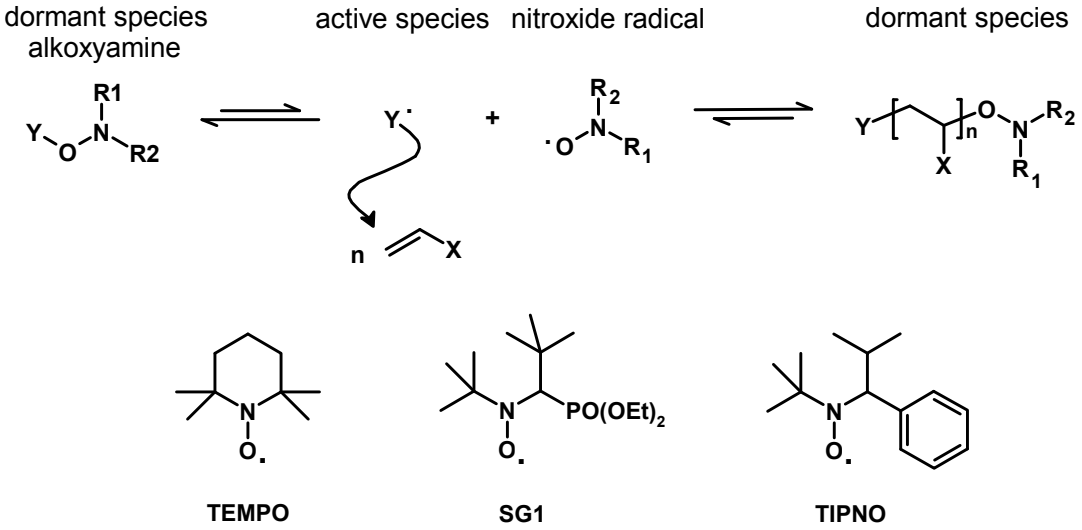

Scheme 3.1 *Schematic representation of the simplified reaction scheme for the nitroxide-mediated radical polymerization process. The polymerization is based on stable radicals (see bottom line) and involves reversible dissociation which leads to propagating carbon-centered radicals and to terminated chain ends in the reversible recombination.*

Typically, alkoxyamines are used as unimolecular initiators in the polymerization process. At elevated temperatures, homolysis of the C-O bond forms a stable nitroxide radical and an active alkyl radical. Monomer units add to this alkyl radical to form a growing polymer chain. Throughout the polymerization, the persistent nitroxide radical reversibly caps and de-caps the active radical chain end, converting it either to the dormant or active state. However, most of the polymer chains are in the dormant state which limits irreversible terminations. Hence, the majority of the propagating chains can grow, resulting in a polymer with "living" character and a narrow molar mass distribution. The obtained control and the "living" character of the polymerization are

dependent on the different alkyl moieties (secondary or tertiary stabilized radicals), which strongly influence the rate of dissociation of the initiating alkoxyamine. As a result, the design of the initiator plays a crucial role for the performance of the polymerization. In 1999, Hawker and coworkers promoted the TIPNO-based alkoxyamines as efficient controlling agents for the polymerization of styrene and acrylate monomers, with the presence of an extra amount of TIPNO nitroxide for the polymerization of acrylates as well as several other monomers.[16] A universal alkoxyamine bearing a chloro-functionality was reported in literature suitable for the controlled polymerization of various monomer groups, including styrenes, acrylates, acrylamides, dienes and vinylpyridines.[16-18] This TIPNO-based alkoxyamine provided the opportunity to specifically modify the initiator. For this purpose, the chloro-functionalized alkoxyamine was reacted with 2,6-*bis*-(2'-pyridyl)-4-pyridone yielding a unimolecular initiator bearing the supramolecular metal-coordinating terpyridine entity as end group, which can be exploited for the preparation of (reversible) supramolecular block copolymers.[1] Scheme 3.2 shows the synthesis of the desired terpyridine-functionalized initiator **III-1**.

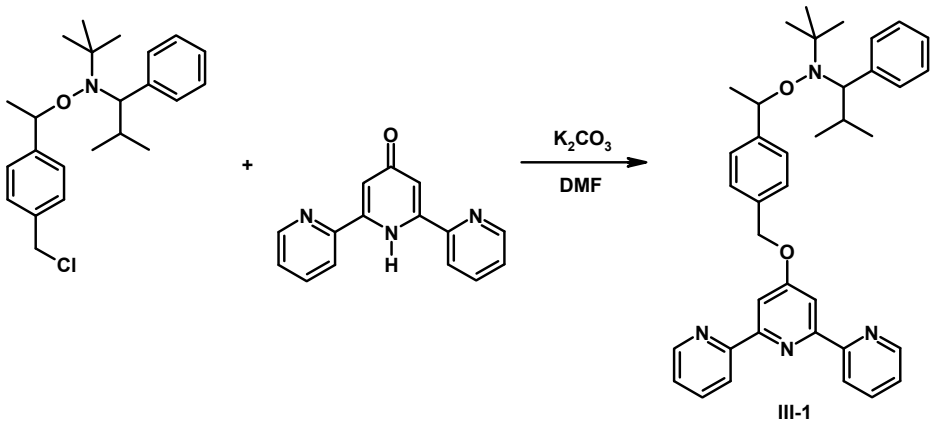

Scheme 3.2 *Schematic representation of the synthetic route for the preparation of the terpyridine-functionalized initiator **III-1** suitable for nitroxide-mediated polymerization.*

The chloromethyl-TIPNO derivative and the pyridone were synthesized as published before.[16,19,20] The mild base K_2CO_3 abstracts the acidic proton from the pyridone, effectively producing a phenolate nucleophile which is highly reactive in the DMF solution. In a S_N2-reaction this ligand displaces the chloride, which is a good leaving group. Subsequently, a facile purification can be performed using a filtration column. The first fraction was discarded since it contained a small amount of impurity. However, the second and largest fraction contained the desired unimolecular initiator bearing the supramolecular terpyridine ligand. Figure 3.2 shows the ^{1}H NMR spectrum, where the characteristic terpyridine signals are visible between 8.8 and 7.2 ppm. Moreover, the signal of the CH_2-group connecting the terpyridine to the styrene-fragment has shifted from 4.66 to 5.35 ppm with respect to the chloromethyl derivative. Due to the fact that the initiator contains two stereo-centers, four isomers can be expected. The diastereomers show different signals in the ^{1}H NMR spectrum and are present in a 45:55 ratio. The stereoisomers have not been separated from each other because no difference in initiating efficiency of the stereoisomers was reported.[21] As mentioned before, polymerizations initiated by this unimolecular initiator will automatically lead to polymers bearing the terpyridine ligand at one chain end and the nitroxide at the other. In the following sections the successful application of this initiator for controlled radical polymerizations is demonstrated. A variety of vinylic monomers were selected and (co)polymerized in a controlled fashion (Section 3.2.1 and 3.2.3). Moreover, the presence of the nitroxide group allowed the preparation of well-defined block copolymers which is shown in Section 3.2.2.

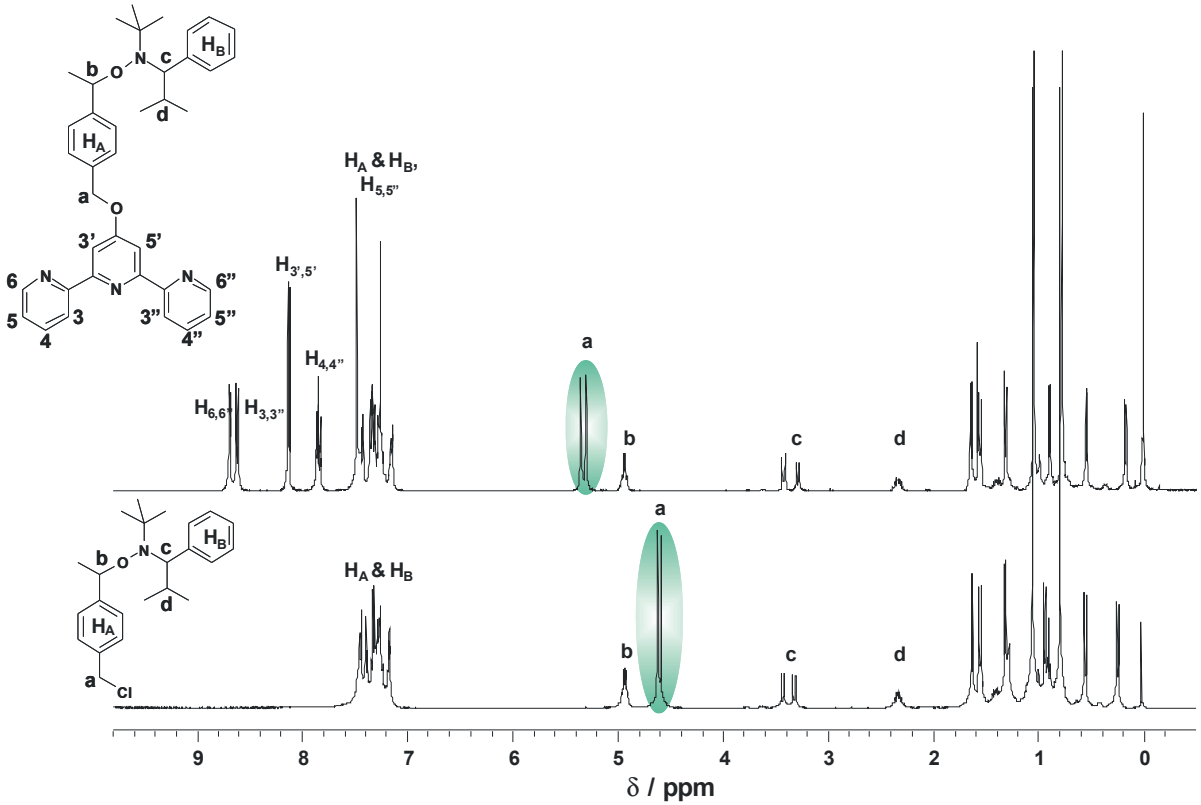

Figure 3.2 *^{1}H NMR spectra of the synthesized chloromethyl derivative and the terpyridine-functionalized initiator **III-1**. The latter clearly shows the characteristic terpyridine signals between 8.8 and 7.2 ppm as well as the signal at 5.35 belonging to the CH_2 connected to the phenyl ring.*

3.2.1 Synthesis of homopolymers

In general, control of the polymerization by NMP is provided by reversible capping and de-capping of the growing (radical) polymer chain by a nitroxide radical. As a result, the concentration of the growing radical species is decreased and the speed of the polymerization is significantly decelerated. Consequently, the polymer chains grow with a (quasi) uniform speed, and side reactions, like the bimolecular termination, are kept at a minimum. In all radical polymerizations, biradical termination reactions occur at a rate R_t, which is dependent on the concentration of the growing radicals [P*], where $R_t = k_t [P^*]^2$. Therefore, by pushing the equilibrium towards the left-hand side (deactivated, dormant chains), *i.e.* lowering the concentration of growing radicals [P*], effectively reduces termination more than propagation ($R_p = k_p [P^*] [M]$).

In the literature, it has been reported that nitroxide-mediated polymerizations (theoretically) obey the kinetic laws of the persistent radical effect (PRE). This kinetic model has been established on the assumptions that side-reactions do not occur, and that the rate constants are independent of the lengths of the growing polymer chains. Initially, the nitroxide initiator undergoes a reversible homolytical cleavage by thermal activation resulting in the formation of a nitroxide (persistent) radical and a propagating (transient) radical. According to Fischer *et al.*,[22-25] the persistent radical can only react with transient radical, whereas the transient radicals are able to combine with transient radicals (irreversible termination). At the very beginning of the

polymerization, the concentration of the nitroxide radicals and the propagating radicals are low enough that irreversible terminations can be neglected; both concentrations increase linearly with time. However, after some time reversible and irreversible termination reactions start to occur resulting in a decrease of the transient radicals and a further increase of the persistent radicals. Since the concentration of persistent and transient radicals is dependent on time, the ideal nitroxide-mediated polymerization is not a steady state system.[22-26] The monomer conversion $\ln([M]_0/[M])$ itself does not depend linearly on time, but to its 2/3 order, which has been experimentally confirmed.[27]

3.2.1.1 Polymerization of styrenics

The terpyridine-functionalized alkoxyamine is perfectly suitable for the synthesis of styrenic homopolymers. However, considering the fact that styrene is able to spontaneously generate radicals, loss of end group functionality and larger PDI values are expected in particular for high molar mass polymers. The thermal self-initiation of styrene involves a preliminary dimer formation via a Diels-Alder reaction, followed by a hydrogen atom transfer to a third monomer generating two radicals.[28] That means that a controlled growth of the polystyrene chains is achieved by a steady state between auto-initiation reactions (producing new transient radicals which, as a result, lead to non-functionalized polymer chains) and irreversible termination reactions (consuming existing transient radicals).

Styrene first had to be purified to remove inhibitors and impurities, which can have a detrimental effect on the reaction, before it was used for the polymerization. The monomer was passed over a column of activated basic aluminum oxide adsorbing the inhibitor and impurities. Terpyridine-functionalized polystyrene **III-2a-c** (PS-[) was prepared in three different chain lengths according to the kinetic data reported elsewhere.[29] The degrees of polymerization were calculated by integrating the aromatic signals of the polystyrene (region between 7.5 to 6.3 ppm) and the signals of the terpyridine ligand that are clearly resolved between 9 and 7 ppm in the ^{1}H NMR spectrum. Special focus was on end group functionality of the resulting polymers with respect to the initiating fragment containing the terpyridine ligand as well as the mediating nitroxide. The nitroxide is attached to the polystyrene as can be observed from the weak resonances between 4.6 and 4.3, at 3.3 and at 0.5 ppm (Figure 3.3).

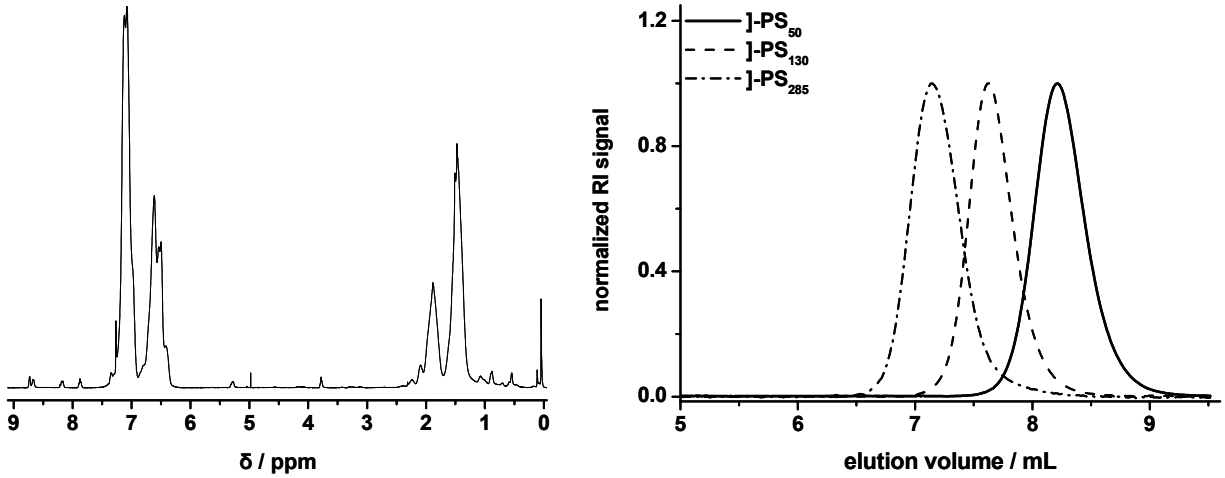

Figure 3.3 *^{1}H NMR spectrum of the synthesized terpyridine-functionalized polystyrene (**III-2b**) in $CDCl_3$ (left) and GPC traces of the polymers **III-2a-c** with varying molar masses (right).*

The obtained GPC chromatograms of the three polymers revealed narrow molar mass distributions with PDI values of 1.13 ($M_{n\ GPC}$ = 4,600 g/mol, M_{NMR} = 5,800 g/mol for **III-2a** and $M_{n\ GPC}$ = 12,700 g/mol, M_{NMR} = 14,100 g/mol for **III-2b**) and 1.17 ($M_{n\ GPC}$ = 23,900 g/mol, M_{NMR} = 30,200 g/mol for **III-2c**), respectively. The M_n values determined by GPC using standard polystyrene calibrations are generally lower compared to the M_n values obtained by integration of the ^{1}H NMR spectra. This can be due to the previously discussed auto-initiation of styrene which leads to non-functionalized polymer chains. Consequently, ^{1}H NMR spectroscopy provides overestimated M_n values since the determination is based on the polymer end groups.

Furthermore, the TIPNO-based alkoxyamine has been adapted for the polymerization of fluorinated styrenic monomers (*para*-trifluoromethylstyrene and 2,3,4,5,6-pentafluorostyrene, respectively) which resulted in well-defined polymers with unimodal and narrow molar mass distributions and polydispersity indices well below 1.3. Nowadays, fluorinated polymers find applications in microelectronic devices, or as antifouling and antifogging agents due to their specific properties, including high thermal stability, chemical resistance, excellent mechanical properties at extreme temperatures, superior weatherability and low flammability.[30] Similarly to styrene, the monomers were purified by passing them over an activated basic aluminum oxide column. Afterwards, 2,3,4,5,6-pentafluorostyrene was polymerized for 5 h at 120 °C in the presence of the terpyridine-functionalized unimolecular alkoxyamine **III-1** in THF and then stopped ([M]/[I] = 70). The composition of polymer **III-3** was determined by ^{1}H NMR spectroscopy revealing an experimental degree of polymerization of 30, which corresponds to the theoretical value of 35 at 50% conversion. GPC revealed a narrow molar mass distribution with a PDI value below 1.10 (the GPC chromatogram is omitted because it will be shown later in Sections 3.2.3 and 3.2.4.). The obtained homopolymer is particularly suitable for further chemical modification reactions since it exhibits several functionalities. Section 3.2.3 will demonstrate the use of the homopolymer as a macroinitiator for the preparation of well-defined block copolymers. Furthermore, such a polymer provides the possibility to make use of the terpyridine ligand which can form metallo-supramolecular complexes with transition metals in low oxidation states (see Chapter 4). Moreover, the polymer backbone itself can be chemically modified using nucleophilic substitution reactions (Section 3.2.4).

As mentioned before, the terpyridine-functionalized alkoxyamine initiator **III-1** was also applied for the polymerization of *para*-trifluoromethylstyrene. The polymerization has been performed at 120 °C for 2 h reaching a conversion of 51% ([M]/[I] = 100) as determined by ^{1}H NMR spectroscopy. The obtained polymers **III-4** exhibit narrow molar mass distributions as can be seen in Figure 3.4, with polydispersity indices below 1.20.

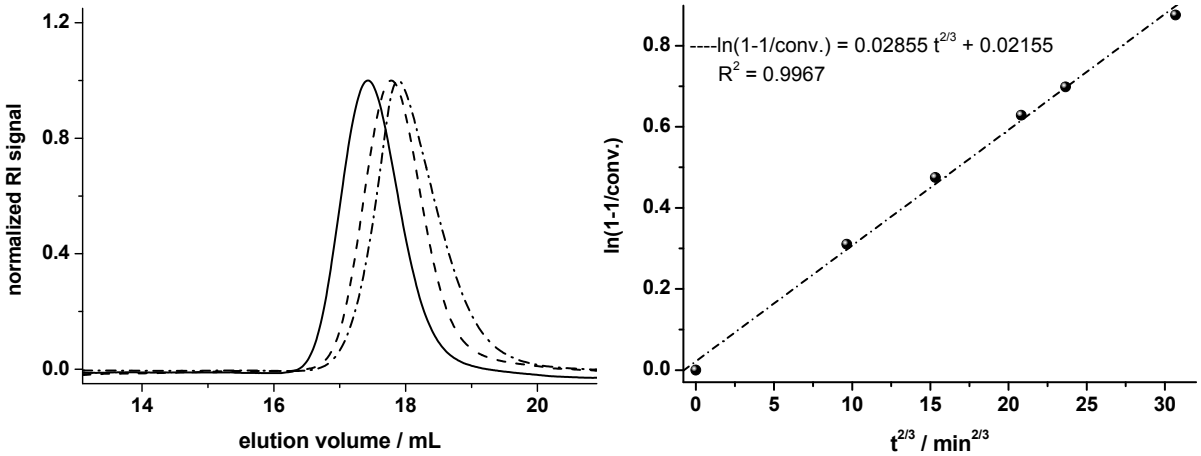

Figure 3.4 *GPC-traces of samples taken during the polymerization of para-trifluoromethylstyrene (solid line represents the final polymer) (left). Linear dependency of the monomer conversion on the 2/3rd power of time (persistent radical effect) (right).*

The basic kinetic behavior of this polymerization is controlled and regulated by persistent radicals: a continuous decrease of the propagating radicals through termination results in a $t^{2/3}$ dependence of ln(1-1/conv.) which was described by Fischer.[25] Samples were taken in short time intervals and the conversion was evaluated by ^{1}H NMR spectroscopy. Indeed, fitting the data with a $t^{2/3}$ dependence revealed a perfect linear relationship (Figure 3.4). In a separate experiment, the polymerization of this monomer was repeated using similar conditions. The polymerization was stopped after 1.6 h and the polymer was precipitated twice into ice-cold methanol. ^{1}H NMR spectroscopy revealed an average degree of polymerization of 42 which corresponds to a M_n value of 7,800 g/mol, including the initiating fragment (terpyridine ligand and mediating nitroxide, respectively). Molar mass determination by GPC (M_n = 7,100 g/mol; PDI = 1.16) revealed again a lower value in comparison to ^{1}H NMR spectroscopy. This can be attributed again to auto-initiation of the polymer or to hydrodynamic volume differences since the M_n value was determined using a polystyrene calibration. Further characterization of this polymer, besides ^{1}H NMR spectroscopy and GPC, included MALDI-TOF MS and a UV-vis titration experiment (Figure 3.5).

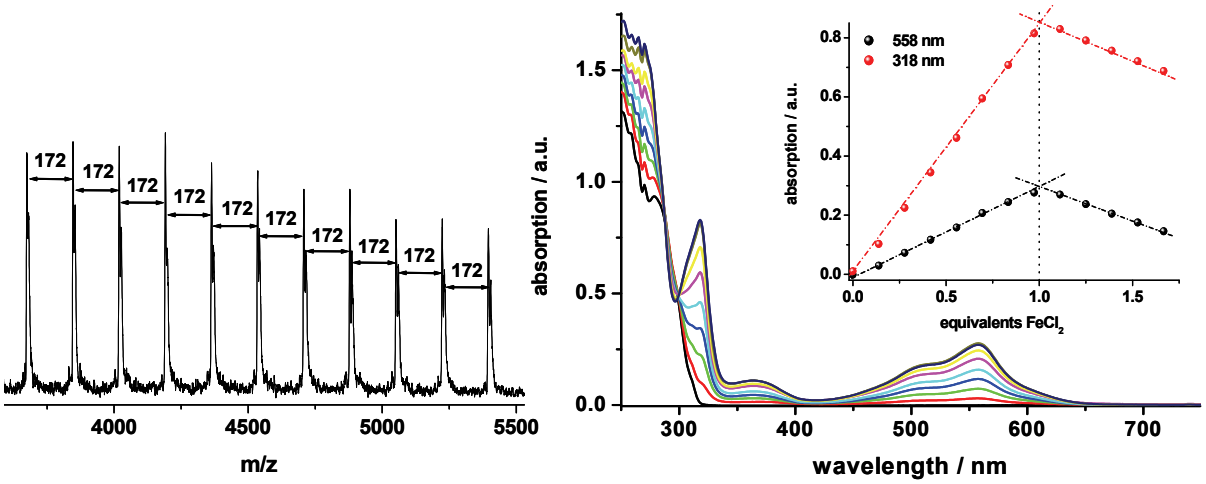

Figure 3.5 *Part of the MALDI-TOF mass spectrum of (**III-4**) (left) and UV-vis titration experiment with $FeCl_2$ in methylene chloride (right).*

Although it was not possible to observe an unimodal molar mass distribution in the MALDI-TOF MS of this polymer, the distance between the peaks is 172 which corresponds to the molar mass of *para*-trifluoromethylstyrene. It was reported in literature that the detection of the species is depending on the analytical conditions of the measurement.[31,32] In particular, polymers which are capped with TIPNO are not stable during the MALDI-TOF measurement and undergo fragmentation upon ionization. Moreover, the peaks in the spectrum could not be assigned to the supposed nitroxide group fragmentation, which results in loss of the *t*-butyl group.[33] In the UV-vis titration experiment, iron(II) chloride ($FeCl_2$) dissolved in methanol was added stepwise to a solution of a predetermined amount of the terpyridine-functionalized polytrifluoromethylstyrene (**III-4**) in chloroform. An increase of the metal-to-ligand charge transfer (MLCT) of the *bis*-terpyridine iron(II) complex was observed at 560 nm; a plateau was reached at the equivalence point after a linear increase. The equivalence point is observed at a ligand:metal ratio of 2:1. Assuming that one terpyridine ligand is attached to each polymer chain, it can be calculated how much $FeCl_2$ has to be added to reach the equivalence point. In this way, the M_n value of the polymer was calculated (M_n = 7,200 g/mol). The result is in good agreement with the values obtained by ^{1}H NMR spectroscopy and GPC. It can be concluded that the UV-vis titration experiment represents a valuable supplementary tool for the characterization of terpyridine-based polymers.

3.2.1.2 Polymerization of acrylates

Traditionally, the limitation of NMP, when using TEMPO-based initiators, was the selection of the monomer, which had to be styrene-derivatives. However, the development of new stable radicals, such as SG1 and TIPNO, has expanded the range of polymerizable monomers. They have shown to afford better control over polymerizations of acrylic monomers and dienes compared to TEMPO-derivatives. This second-generation nitroxides are responsible for the decreasing polymerization times due to an increasing rate of C-O bond dissociation between the polymer chain and the nitroxide moiety. The terpyridine-functionalized NMP initiator used for this study has the TIPNO-nitroxide connected to a functionalized styrene fragment. In literature it was reported that the rate constant for dissociation from the styrene fragment is 10 times higher than from a *t*-butyl acrylate fragment (k_d = 3.3 × 10^{-3} and 2.5 × 10^{-4} s^{-1} for TIPNO at 120 °C, respectively).[21] These results are beneficial for controlling polymerizations of acrylic monomers such as *t*-butyl acrylate using the terpyridine-functionalized NMP initiator since one key factor for controlled radical polymerizations is the fast initiation with respect to the propagation reaction. The faster the initiation, the faster the equilibrium concentrations for transient and persistent radicals are reached resulting in a better control over the polymerization. For TEMPO, the dissociation constants k_d for the polymerization of styrene and *t*-butyl acrylate are of the same order of magnitude; however, the absolute value is much lower. Moreover, the recombination rate constant is much higher for TEMPO leading to an equilibrium between dormant and transient radicals which is shifted towards the dormant species. Therefore, the question rises how a different initiator affects the polymerization of acrylic monomers. Irreversible termination reactions during the polymerization lead to a decrease of transient radicals. In case TEMPO is used as persistent nitroxide radical, the polymerization cannot proceed anymore and the conversion stops due to the lower rate of propagation (in comparison to the second-generation nitroxides) and the increased amount of free TEMPO in combination with the high recombination rate. In contrast, the TIPNO-based dormant species exhibit a higher C-O bond dissociation rate resulting in the continuation of the polymerization. Generally speaking, the propagation rates of acrylates are much higher compared to styrene[34] leading to rather high polydispersitiy indices when using TIPNO.[16] An improved control over the polymerization can be gained simply by adding a certain amount of free nitroxide radicals.[16,35] The excess of nitroxide radicals significantly slows down the polymerization process, because it increases the probability to transform the growing polymer chain into the dormant species. In addition, it decreases the probability to generate irreversible termination reactions.

In the following paragraph the application of the terpyridine-functionalized NMP initiator for the polymerization of three acrylates, namely *t*-butyl acrylate, methyl acrylate and 2-ethylhexyl acrylate, is presented. By taking into account the aforementioned requirements, *i.e.* addition of free nitroxide to the system, well-defined homopolymers were obtained with the initiating fragment of the alkoxyamine being attached at the α-chain end and the nitroxide-fragment at the ω-chain end, respectively. The polymerizations of all three monomers were performed at 120 °C with the addition of 5% free radical yielding the well-defined polymers **III-5a, III-5b**, **III-6** and **III-7**. Gel permeation chromatography (GPC) revealed in all cases narrow molar mass distributions with polydispersity indices below 1.3 (see Table 1: M_n values were determined using PMMA calibrations). Moreover, the integration of the terpyridine signals with respect to the signals of the polymer backbone in the ^{1}H NMR spectra proves that every chain was initiated by the terpyridine-functionalized initiator. The probability that two propagating polymer chains recombine is low since the conversion was kept low in all cases and also because of the excess of free nitroxide. Comparing the M_n values obtained by GPC with the values obtained by ^{1}H NMR spectroscopy shows that the PMMA calibration is a good candidate for the determination of molar masses because both values were very similar (Table 1).

Table 1 *M_n determination of the obtained polymers by ^{1}H NMR spectroscopy and GPC.*

	Polymer	$M_{n\ NMR}$ (g/mol)	conv. (%)	$M_{n\ th}$ (g/mol)	$M_{n\ GPC}$ (g/mol) / PDI*
III-5a	P*t*BA$_{40}$	5,600	23	24,000	4,400 / 1.11
III-5b	P*t*BA$_{66}$	9,100	35	26,000	8,000 / 1.10
III-6	PMA$_{60}$	4,100	21	19,000	3,000 / 1.20
III-7	P2EHA$_{18}$	3,900	17	23,000	2,700 / 1.28

*GPC eluent: mixture of chloroform, triethylamine, and 2-propanol (94:4:2), poly(methyl methacrylate) (PMMA) calibration.

3.2.1.3 Polymerization of acrylamides

N,N-Dimethylacrylamide (DMAA) and *N*-isopropylacrylamide (NIPAA) also have much higher propagation rate constants as compared to styrene and *n*-butyl acrylate.[36,37] Thus, a similar approach as for the polymerization of acrylic monomers was undertaken affording well-defined homopolymers (**III-8** and **III-9**) with narrow molar mass distributions and low polydispersity indices. Even though the M_n values obtained by GPC were slightly lower than those determined by integration of the ^{1}H NMR spectra, a good agreement was found. The results are summarized in Table 2.

Table 2 *M_n weight determination of the obtained polymers by ^{1}H NMR spectroscopy and GPC.*

	Polymer	$M_{n\ NMR}$ (g/mol)	conv. (%)	$M_{n\ th}$ (g/mol)	$M_{n\ GPC}$ (g/mol) / PDI*
III-8	PDMAA$_{36}$	4,700	25	19,000	3,400 / 1.30
III-9	PNIPAA$_{29}$	3,900	29	13,000	2,700 / 1.28

*GPC eluent: mixture of chloroform, triethylamine, and 2-propanol (94:4:2), PMMA calibration.

3.2.2 Synthesis of styrene-based copolymers

In this section the preparation of a luminescent terpyridine-functionalized copolymer is presented. This required the modification of a benzylic monomer. For this purpose, *para*-vinylbenzylchloride seemed to be a suitable candidate since the chloro-functionality can easily undergo nucleophilic substitution reactions. According to a previously reported procedure,[38] it was reacted with 9-hydroxymethylanthracene in order to obtain the corresponding macromonomer **III-10** by etherification. The synthesis involved the *in situ* generation of the highly reactive alkoxide by reacting the primary hydroxy-group of anthracenemethanol with the strong base sodium hydride (NaH). Subsequently, the powerful nucleophile reacts via a S_N2 reaction to form the corresponding ether (Williamson ether reaction). After purification, a yellow crystalline compound **III-10** was obtained in 55% yield which was recrystallized from methanol. Figure 3.6 shows the synthetic approach for the preparation of the anthracene-functionalized monomer together with the assigned ^{1}H NMR spectrum.

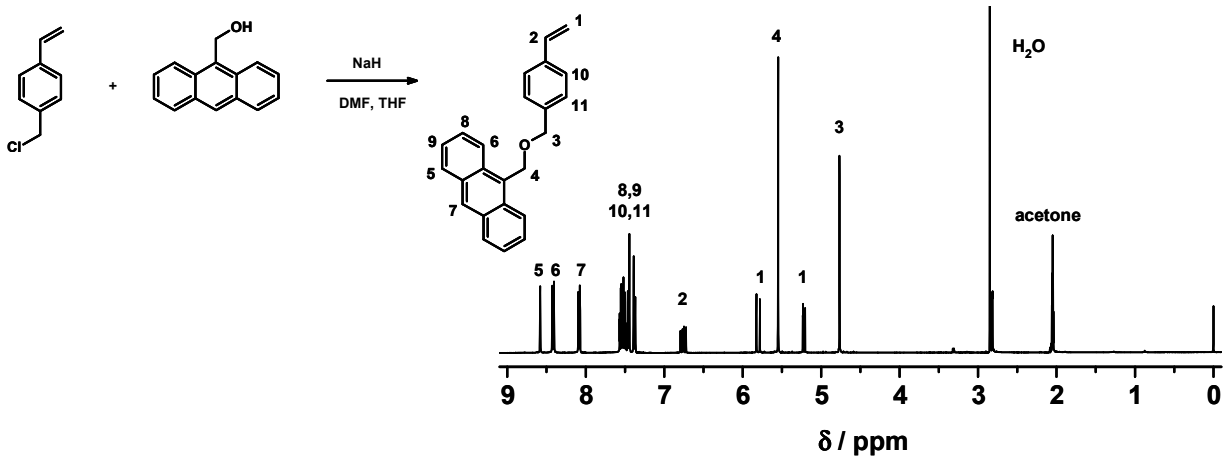

Figure 3.6 *Schematic representation of the synthesis of the anthracene-functionalized monomer **III-10** and assignment of the signals in the ^{1}H NMR spectrum (in d_6-acetone).*

Single crystals of **III-10** were obtained by crystallization allowing the characterization by X-ray diffraction analysis. Figure 3.7 shows the molecular structure of the compound in the ORTEP presentation and its special arrangement which clearly reveals an assembly of the molecules via π-π interaction.

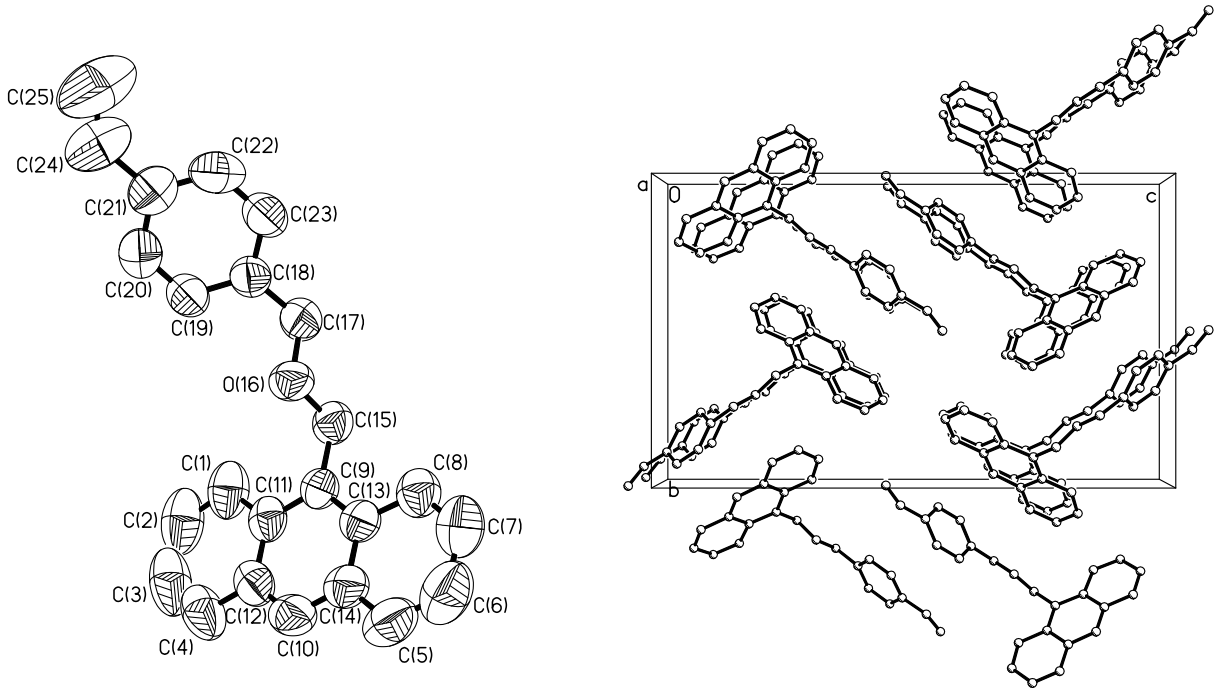

Figure 3.7 *Single crystal x-ray structure of the synthesized anthracene-monomer **III-10** with thermal ellipsoids (left) and the elementary cell of the crystal (right).*

Subsequently, a copolymerization with styrene (styrene-to-anthracene-monomer ratio of 7:1) was performed in bulk at 120 °C for 6 h using the terpyridine-functionalized NMP initiator. Afterwards, the polymerization was stopped and the polymer was precipitated twice from chloroform into methanol. The obtained slightly yellow polymer powder indicated the successful incorporation of the anthracene-monomer into the polymer **III-11**. A first real proof for the incorporation of the anthracene-modified monomer was revealed by GPC measurements using

two detector types: refractive index as well as UV-vis (at 365 nm). The obtained GPC-traces eluted at the same elution volume. This means that the performed copolymerization with the antracene-modified macromonomer was effective since polystyrene does not show any absorption at 365 nm. However, those measurements are only qualitative. In order to determine quantitatively how many macromonomers were incorporated, ^{1}H NMR spectroscopy measurements were performed. The integration over the signals belonging to the terpyridine end group as well as to the anthracene moieties with respect to the polymer backbone allowed the determination of the degree of polymerization (]-PS_{48}-*co*-$PS_{anthr\ 4}$). The M_n value determined by ^{1}H NMR spectroscopy was confirmed by a UV-vis titration measurement which is displayed in Figure 3.8. Upon addition of Fe(II) ions, a rise in the characteristic absorption band at 560 nm was observed until the equivalence point at a metal-to-ligand ratio of 1:2 was reached.

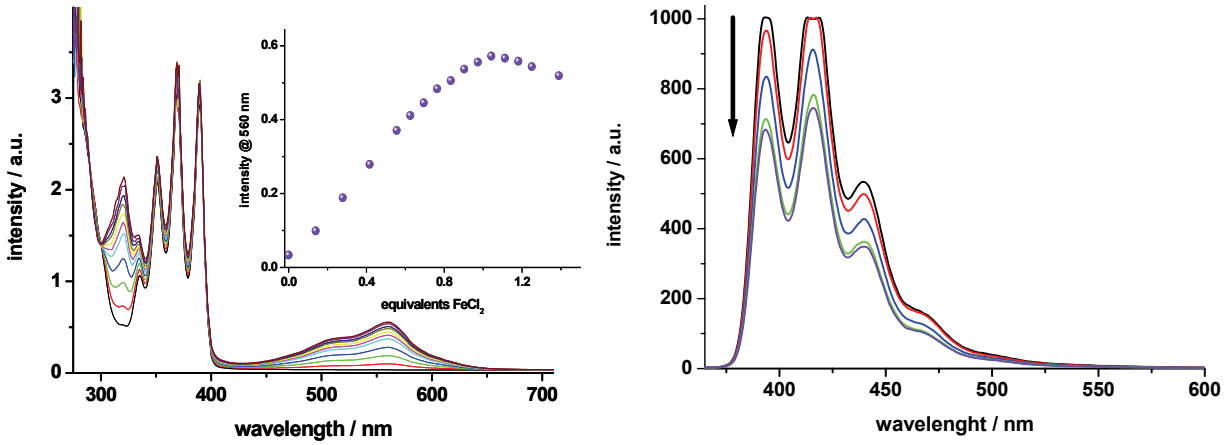

Figure 3.8 *Titration of $FeCl_2$ to the terpyridine-functionalized copolymer **III-11** in methylene chloride followed by UV-vis and emission spectroscopy.*

Anthracene is a well-known polycyclic aromatic compound possessing specific photophysical properties. Therefore, anthracene containing polymers have been used for various optoelectronic materials,[39] chemiluminescent fluorophores,[40,41] electroluminescent devices,[42] photoresist and channel waveguide applications.[43] Figure 3.9 represents the characteristic absorption and emission bands of the synthesized copolymer which can be attributed to the anthryl moiety. The appearance of the vibrationally spaced absorption bands at 335, 351, 369 and 389 nm can be assigned to $\pi \rightarrow \pi^*$ transitions. Upon long-wave UV irradiation (310 - 390 nm) photons are absorbed and the molecules rapidly relax to the lowest excited singlet state. There are three different possibilities: (1) anthracene molecules can emit photons converting back to the ground state (fluorescence), (2) they can convert the excess energy into heat or (3) they can undergo a photochemically allowed [$4\pi_s + 4\pi_s$] cycloaddition resulting in the formation of dimers. The aromatic middle ring of anthracene looses its aromaticity by connecting two monomers across the 9 and 10 positions, respectively. As a consequence, the absorption above 300 nm disappears, as can be seen in Figure 3.9.

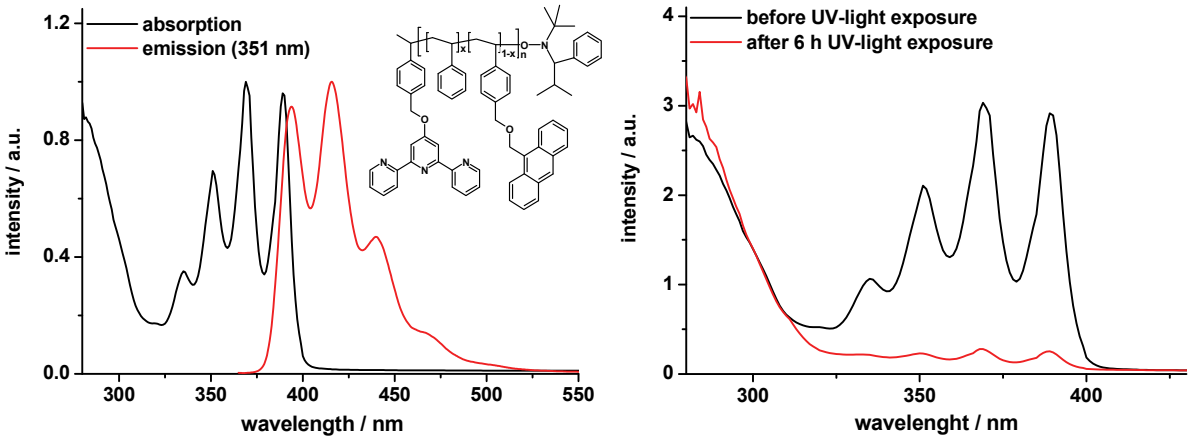

Figure 3.9 *Absorption and emission spectra in methylene chloride (left) and UV-vis spectrum before and after UV-light treatment (right).*

Since there are more than two anthracene units connected to each polymer chain, the polymer solution cross-links upon dimer formation. This was confirmed by GPC measurements. As expected, the molar mass and the polydispersity index were increasing (from M_n = 5,700 g/mol (1.14) to M_n = 8,400 g/mol (1.50)). Due to the fact that the concentration of the copolymer solution was low we only observed a broadened GPC-trace which additionally shifted to higher molar mass rather than cross-linking. In principle, short-wave UV irradiation (254 nm) or heating can invert the dimerization reaction.[44] However, other groups also reported that this process is only partially reversible.[45,46] A second titration with $FeCl_2$ was performed in order to investigate the emission behavior of the copolymer **III-11** upon complexation. Upon addition of iron(II) ions the octahedral *bis*-terpyridine iron complex was formed. As a result, approximately 30% of the emission was quenched since there was a non-radiative transition of the excited triplet metal-to-ligand charge transfer (^{3}MLCT) state via a triplet metal-centered (^{3}MC) state to the ground state.[47] Apparently, only the emission of anthracene groups in close proximity to the formed *bis*-terpyridine metal complex was quenched. The emission of the remaining anthracene groups stayed intact. Therefore, 70% emission was observed after reaching the equivalence point at a metal-to-ligand ratio of 1:2, *i.e.* full conversion to the *bis*-terpyridine metal complex (Figure 3.8).

3.2.3 Synthesis of block copolymers

In the previously described sections the preparation of various homopolymers and copolymers with well-defined molecular characteristics (predetermined molar mass, narrow molar mass distribution, end group control, and architecture) was highlighted. In the following section the focus lies on the preparation of terpyridine-functionalized block copolymers by reinitiating the respective homopolymers. Ideally, all homopolymer chains should have the same composition and chain-end functionality. In order to ensure this very important requirement, the polymerizations have to be stopped before reaching 80% conversion since otherwise the probability to form dead polymer chains by irreversible termination becomes too significant. Another criterion for a successful block copolymerization is an efficient cross-over reaction from the macroinitiator to the monomer. This implies a fast reinitiation with respect to the propagation according to the polymerization conditions of the first block. However, this requisite is sometimes difficult to fulfill due to the reactivity differences of various monomers. For instance, it has already been discussed before that acrylates are far more reactive than styrenes. Therefore, it can be

expected that a polystyrene macroinitiator will not as efficiently reinitiate the polymerization of, *e.g.*, *n*-butyl acrylate as it would be the case for the reinitiation of poly(*n*-butyl acrylate) with styrene.[10] Certainly, the addition of free nitroxide (see Section 3.2.1.2) to the polymerization mixture represents a powerful method here to force a shift of the equilibrium towards the dormant species. In this way, high propagation rate constants are suppressed and the sequence of the respective blocks can be effectively altered.[48]

3.2.3.1 Synthesis of diblock copolymers

The next section points out the seemingly unlimited potential to create a wide range of well-defined block copolymers simply by using different monomers and by controlling the molecular features of the material. Polystyrene was used as a macroinitiator for the polymerization of *t*-butylacrylate, methyl acrylate, *para*-trifluoromethylstyrene, 2,3,4,5,6-pentafluorostyrene and 2-vinylpyridine, respectively (Figure 3.10).

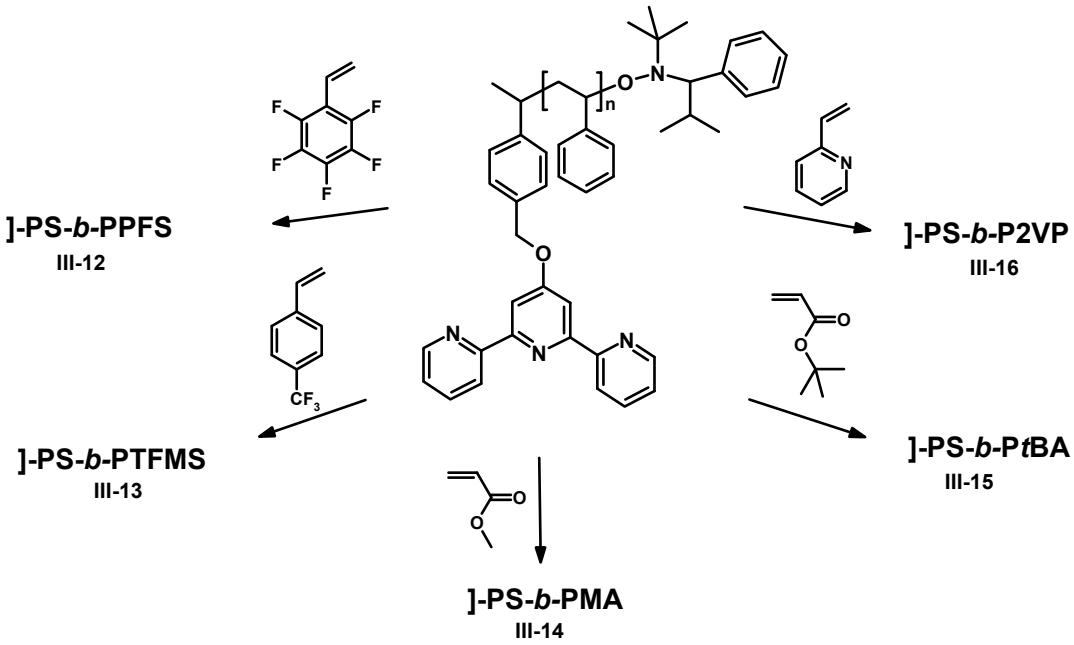

Figure 3.10 *Schematic representation of all block copolymers prepared by nitroxide mediated polymerization utilizing polystyrene as macroinitiator.]- represents the terpyridine ligand.*

The basis for the block copolymerizations of 2,3,4,5,6-pentafluorostyrene and *para*-trifluoromethylstyrene was a relatively short polystyrene macroinitiator with 50 repeating units. The polymerizations were performed in bulk without the addition of extra free nitroxide assuming a similar reactivity of these monomers and styrene. After the polymerization was stopped the block copolymers (**III-12** and **III-13**) were precipitated twice from chloroform into ice-cold methanol. The GPC-traces of the corresponding block copolymers remained narrow and revealed low polydispersity indices in the range of 1.20. Moreover, the curves shifted to higher molar masses. The composition of the respective block copolymers was determined by ^{1}H NMR spectroscopy revealing an average of 34 TFMS units for the one polymer and 80 units PFS for the other polymer. Table 3 summarizes the results of the M_n values obtained by ^{1}H NMR spectroscopy and GPC for all synthesized block copolymers.

Another example for effective block copolymerization using the polystyrene as the macroinitiator was performed using methyl acrylate and *t*-butyl acrylate. As it was already

mentioned before, acrylate monomers possess a very high rate of polymerization compared to styrene. In order to gain control over the polymerization, a certain amount of free nitroxide radical (4%) is required, which sufficiently slows down the propagation of the acrylate with respect to the initiation of the polystyrene macroinitiator and, thus, ensures an efficient crossover reaction from the macroinitiator to the propagating species. If this additional nitroxide is not present inefficient initiation takes place and the control over molar mass and polydispersity index is poor. Hence, by addition of free nitroxide the resulting GPC chromatograms indicated block copolymer formation through clean chain extension (Figure 3.11).

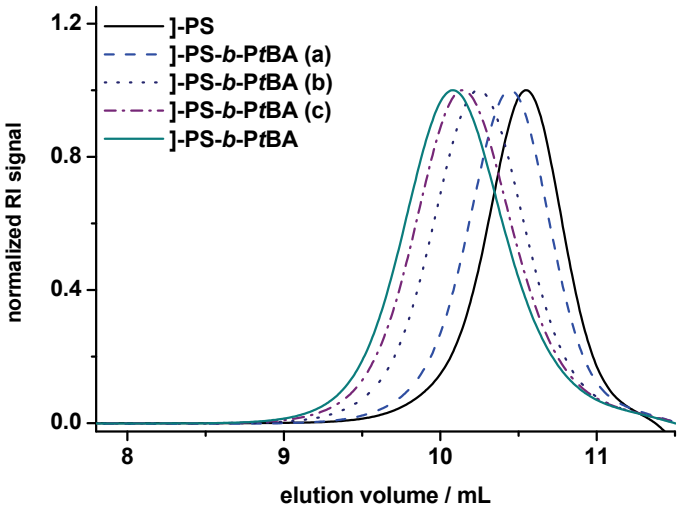

Figure 3.11 *Normalized GPC-traces of the polymer **III-15** obtained during the polymerization of t-butyl acrylate using the]-PS as macroinitiator (a, b and c correspond to intermediate samples) showing successful chain extensions.*

Unfortunately, the controlled polymerization of 2-vinylpyridine was not as straightforward as the examples discussed above. Good control over molar mass and polydispersity index could not be achieved by simply adding an excess of nitroxide. Instead, a decrease in the temperature to 110 °C was necessary in order for the polymerization to proceed in a controlled fashion (see Table 3).

Table 3 *M_n determination of the block copolymers using polystyrene as macroinitiator by ^{1}H NMR spectroscopy and GPC.*

	Polymer	$M_{n\ NMR}$ (g/mol)	$M_{n\ GPC}$ (g/mol) / PDI*
III-12	PS_{50}-*b*-$PPFS_{80}$	20,700	11,300[a] / 1.23
III-13	PS_{50}-*b*-$PTFMS_{34}$	11,700	10,200[a] / 1.17
III-14	PS_{34}-*b*-PMA_{54}	38,700	31,900[b] / 1.23
III-15	PS_{160}-*b*-P*t*BA_{90}	28,000	32,900[c] / 1.17
III-16	PS_{85}-*b*-$P2VP_{130}$	23,100	27,500[d] / 1.16

[a] GPC eluent: DMA with LiCl (2.1 g/L), PS calibration.
[b] GPC eluent: chloroform, triethylamine, and 2-propanol (94:4:2), PMMA calibration.
[c] GPC eluent: DMF with NH_4PF_6 (0.8 g/L), PMMA calibration.
[d] GPC eluent: DMF with NH_4PF_6 (0.8 g/L), PS calibration.

Successful block copolymerization was also realized using poly(*t*-butylacrylate) as macroinitiator for the polymerization of styrene. The macroinitiator was obtained according to the polymerization procedure described in Section 3.2.1.2. The polymer was characterized by ^{1}H NMR spectroscopy as well as GPC (M_{NMR} = 11,500 g/mol, $M_{n\ GPC}$ = 10,300, PDI = 1.10). The example presented here shows that the respective blocks can be efficiently altered using nitroxide-mediated polymerization. In order to gain insight in the polymerization a kinetic study was performed using an automated ASW2000 synthesizer. The polymerization was conducted in solution to prevent high viscosity that would reduce the efficiency of automated sampling. Anisole was used as solvent because of its high boiling point (154 °C) to prevent evaporation. A stock solution was prepared with a concentration of 2 M in anisole and a monomer-to-initiator ratio of 200. The reaction mixture was heated to 118 °C and samples were taken at different times. All samples were characterized by GC and GPC to determine the conversion of the monomer, the molar mass, and the molar mass distribution, respectively. As can be seen in Figure 3.12 the polymerization proceeds in a controlled fashion. However, due to the high dilution of the polymerization mixture a conversion of only 30% was reached after 20 hours. Applying the model of the persistent radical effect, the monomer conversion depends linearly on time$^{2/3}$, as it is demonstrated in the right graph of Figure 3.12.

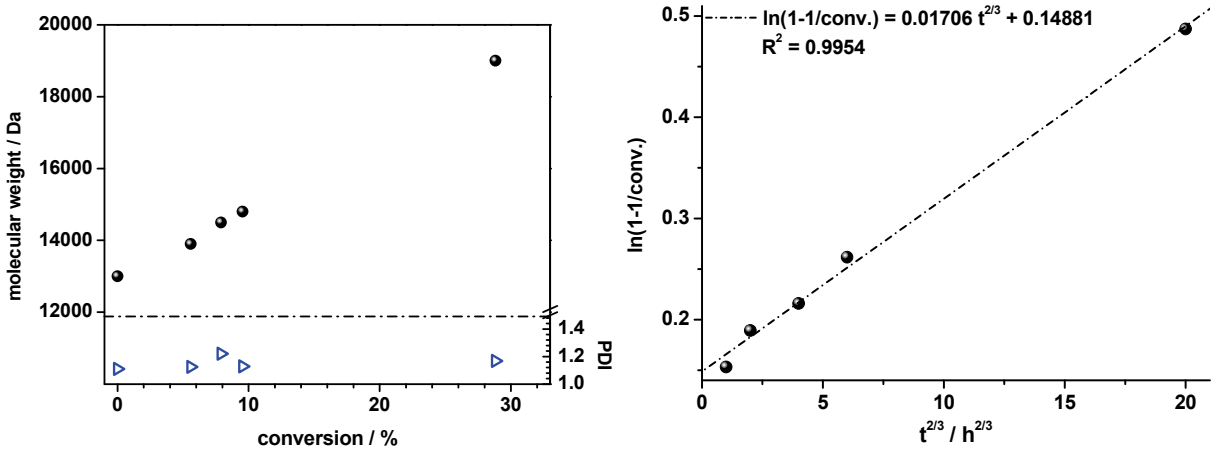

Figure 3.12 *Left: PDI values and M_n values (GPC) obtained during the block copolymerization of]-PtBA$_{85}$ with styrene plotted against the conversion. Right: Linear dependency of the monomer conversion on the 2/3rd power of time.*

In a different experiment, the polymerization was performed in bulk conditions. For this purpose, the monomer-to-initiator ratio was increased to 400. Here, the monomer also acts as a solvent for the growing polymer. After 45 minutes a conversion of 58% was reached and the polymerization was stopped. The block copolymer **III-17** was precipitated twice into ice-cold methanol and dried *in vacuo* before it was characterized by ^{1}H NMR spectroscopy revealing a composition of 85 units *t*-butyl acrylate and 230 styrene units. The respective data obtained by ^{1}H NMR spectroscopy and GPC is shown in Table 4. The obtained block copolymer is of special importance when supramolecular block copolymer complexes are formed. The relatively soft poly(*t*-butyl acrylate) chain linked to the significantly harder polystyrene block makes it an interesting system for morphological (phase separation) and mechanical properties. Therefore, the morphology of the synthesized block copolymer was investigated by atomic force microscopy (AFM).

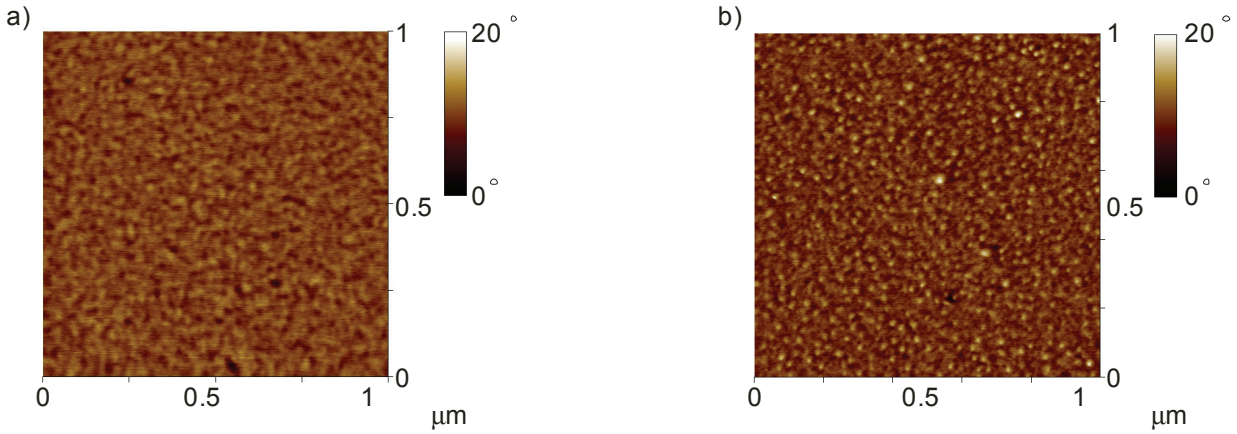

Figure 3.13 *Phase images of spincoated thin films of]-PtBA$_{85}$-b-PS$_{230}$ block copolymer **III-17** (a) and PS$_{230}$-b-PtBA$_{85}$-[Fe]-PtBA$_{85}$-b-PS$_{230}$ (b).*

Figure 3.13a shows the phase image of the spincoated block copolymer **III-17** where phase separation is hardly observed. In order to improve the phase separation behavior of the block copolymer, a complexation strategy from supramolecular chemistry was applied to extend the system. This approach involved the formation of a metallo-supramolecular block copolymer using iron(II) ions. The iron complexed A-B-[Fe]-B-A block copolymer was obtained by refluxing iron acetate with the terpyridine functionalized block copolymer in a solvent mixture of methanol and chloroform. The phase behavior was indeed improving (Figure 3.13b); however, the phase separation cannot be attributed to a distinct morphology. Nevertheless, a cylindrical morphology was suggested from the phase image, which would be in good agreement with the theoretical predictions since a volume fraction of 69% polystyrene was calculated.[37,49] Recently, it was reported in literature that the presence of charged complexes within a block copolymer has a strong impact on the self-assembly and effects the orientation of the cylinders and the ordering process.[50] Therefore, it could be assumed that all cylinders are oriented vertically. The longer chains of the complexed system remarkably improve the formation of the cylinders, as more and more ordered features are obtained.

Polymers consisting of *t*-butyl acrylate groups rise special interest since the facile cleavage of the *t*-butyl group results in the formation of acrylic acid functional groups.[51,52] In case of the synthesized]-P*t*BA$_{85}$-*b*-PS$_{230}$ block copolymer **III-17**, this chemical post-modification leads to the design of an amphiphilic block copolymer **III-18**. The deprotection of the *t*-butyl groups was performed in methylene chloride using trifluoroacetic acid. The conversion of the ester groups to carboxylic acid functionalities was confirmed by IR-spectroscopy which revealed the disappearance of the ester resonances (1725 cm^{-1}) and the appearance of a new broad signal characteristic for the carboxylic acid functionality (1711 cm^{-1}). Furthermore, the stretching bands of the *t*-butyl groups at ca. 1390 and 1366 cm^{-1} disappeared (Figure 3.14).

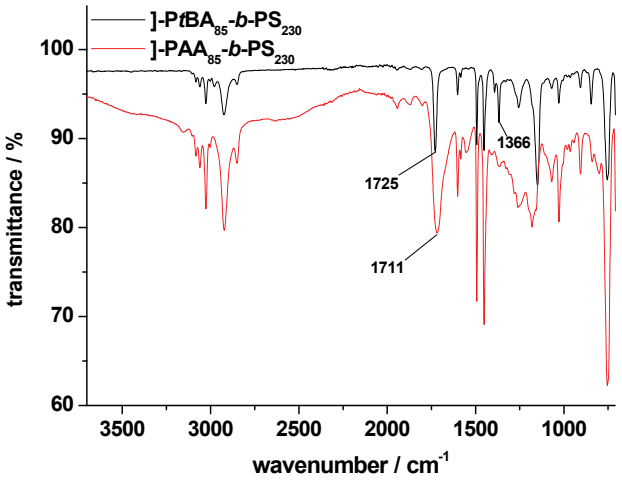

Figure 3.14 *IR-spectra of]-PtBA-b-PS (**III-17**) and the deprotected]-PAA-b-PS (**III-18**) demonstrating the successful post-polymerization modification reaction.*

The accordingly obtained poly(*t*-butyl acrylate) was further used as a macroinitiator for the polymerization of isoprene. The polymerization proceeded slowly with the addition of 5% free nitroxide at 120 °C. Narrow molar mass distributions were obtained with polydispersity indices below 1.20. The vinylic protons (between 5.3 and 4.6 ppm) are clearly visible in the ^{1}H NMR spectrum (Figure 3.15) and were integrated with respect to the terpyridine signals that appear in the region between 8.7 and 7.6 ppm. Figure 3.15 represents the GPC chromatograms of the]-P*t*BA macroinitiator **III-5a** and the resulting diblock copolymer **III-19**. The unimodal trace of the diblock copolymer shifted slightly to lower elution volumes indicating a successful block copolymerization. The results are shown is Table 4.

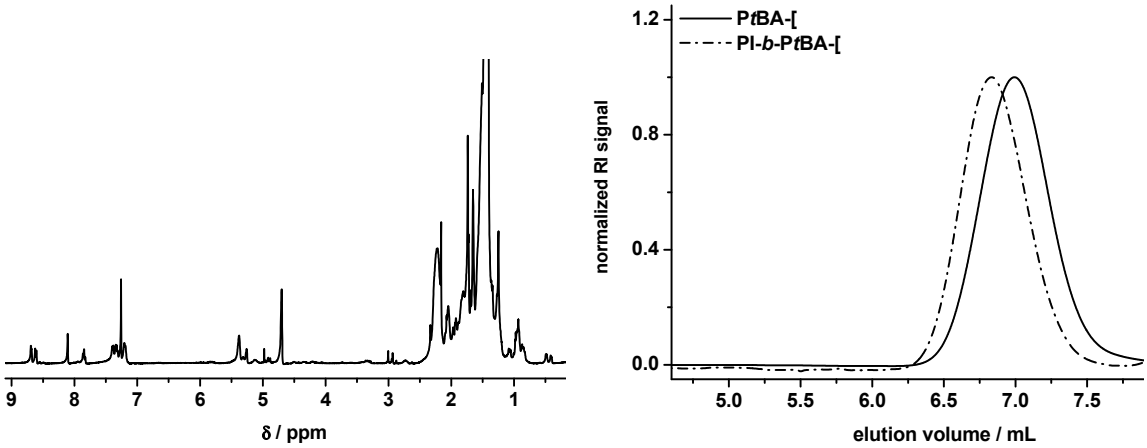

Figure 3.15 *^{1}H NMR spectrum (in $CDCl_3$) of the terpyridine-functionalized PtBA-b-PI block copolymer **III-19** in $CDCl_3$ (left) and GPC traces of the PtBA macroinitiator **III-5a** and the obtained diblock copolymer **III-19** (right). GPC eluent: $CHCl_3$, triethylamine, and 2-propanol (94:4:2).*

Moreover, polypentafluorostyrene (**III-3**) and polytrifluoromethylstyrene (**III-4**) have been used for the preparation of well-defined block copolymers. Both homopolymers initiated successfully the polymerization of styrene resulting in the corresponding block copolymers]-PPFS-*b*-PS **III-20** and]-PTFMS-*b*-PS **III-21**. The polymerizations were performed at 120 °C without the addition of free nitroxide radicals due to the similar reactivity of the monomers with respect to styrene. The polymers **III-20** and **III-21** were precipitated twice in ice-cold methanol and characterized by GPC

(see Figure 3.16) as well as ^{1}H NMR spectroscopy in order to determine the composition of the respective blocks (see Table 4). Although the GPC traces of both diblock copolymers are not completely separated from their corresponding macroinitiator, the molar mass distributions do not show shoulders or tailing. Therefore, chain coupling and incomplete initiation can be excluded. Hence, the majority of the macroinitiator chains initiated the polymerization of the second monomer resulting in a terpyridine-functionalized diblock copolymer.

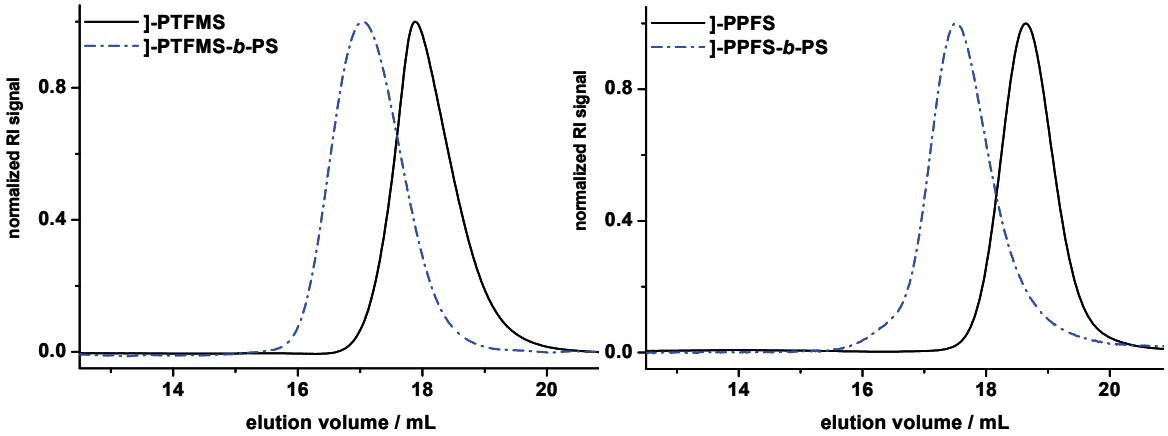

Figure 3.16 *GPC chromatograms of the macroinitiators (**III-3** and **III-4)** and the respective block polymers showing a successful chain extension:]-PPFS-b-PS **III-20** (right) and]-PTFMS-b-PS **III-21** (left).*

The bulk morphology of the diblock copolymer **III-21** was investigated by atomic force microscopy (AFM). The diblock copolymer was spin-coated from chloroform (2 mg/mL) onto a silicon wafer and annealed at 120 °C. Based on the volume fractions (48% PTFMS, 52% PS) a lamellar phase separation is expected. Although the AFM images revealed a more pronounced phase separation after annealing, the structural morphology was difficult to assign. Nonetheless, a clear phase separation was observed demonstrating the demixing of the PS and PTFMS phases. Polytrifluoromethylstyrene was further used as macroinitiator to polymerize *t*-butyl acrylate. Once again, due to the higher reactivity of the monomer, the polymerization could only proceed in a controlled fashion by the addition of 4% free nitroxide. The block copolymer **III-22** was purified by multiple precipitations into ice-cold methanol. Subsequently, it was characterized by ^{1}H NMR spectroscopy and GPC. Table 4 summarizes the results of all the block copolymers.

Table 4 *M_n determination of the block copolymers using poly(t-butyl acrylate), polytrifluoromethylstyrene and polypentafluorostyrene as respective macroinitiators.*

	Polymer	$M_{n\ NMR}$ (g/mol)	$M_{n\ GPC}$ (g/mol) / PDI*
III-17	P*t*BA$_{85}$-*b*-PS$_{230}$	32,800	30,400[a] / 1.13
III-19	P*t*BA$_{40}$-*b*-PI$_{22}$	10,600	8,900[b] / 1.17
III-20	PPFS$_{30}$-*b*-PS$_{73}$	14,000	9,900[c] / 1.22
III-21	PTFMS$_{42}$-*b*-PS$_{76}$	15,700	13,100[c] / 1.18
III-22	PTFMS$_{81}$-*b*-P*t*BA$_{110}$	28,800	15,500[c] / 1.23

[a] GPC eluent: DMF with NH_4PF_6 (0.8 g/L), polystyrene (PS) calibration.
[b] GPC eluent: mixture of chloroform, triethylamine, and 2-propanol (94:4:2), PS calibration.
[c] GPC eluent: DMA with LiCl (2.1 g/L), PS calibration.

3.2.3.2 Synthesis of triblock copolymers

All described block copolymers of Section 3.2.3.1 still possess the terpyridine end group and the nitroxide as it was confirmed by ^{1}H NMR spectroscopy. That means that the obtained polymers are able to reinitiate the polymerization of a third monomer. Indeed, the reinitiation of two diblock copolymers was accomplished resulting in new ABC triblock copolymers. The]-PS_{35}-*b*-PMA_{54} diblock copolymer was used to reinitiate 2,3,4,5,6-pentafluorostyrene and the]-PS_{35}-*b*-P*t*BA_{25} diblock copolymer enabled chain extension with *para*-trifluoromethylstyrene. Both polymerizations were performed in bulk at 120 °C. After precipitation the triblock copolymers (**III-23** and **III-24**) were analyzed by ^{1}H NMR spectroscopy as well as GPC (Table 5). The GPC chromatograms revealed in both cases a slight tailing on the lower molar mass side indicating that not all macroinitiator chains initiated the polymerization. However, the majority did initiate. The molar mass distributions are somewhat broader compared to the molar mass distributions of the corresponding macroinitiators (Figure 3.17). However, still acceptable polydispersity indices were obtained (PDI = 1.28 and 1.33, respectively), indicating a polymerization in a controlled fashion.

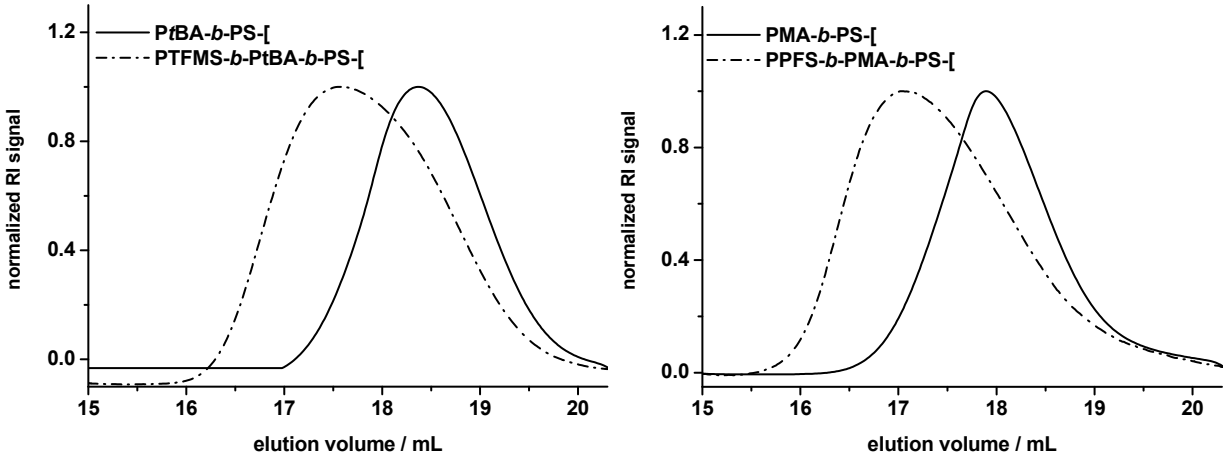

Figure 3.17 *GPC-chromatograms of the two triblock copolymers (**III-23** and **III-24**) and their corresponding macroinitiators obtained via NMP.*

Table 5 *M_n determination of the obtained triblock copolymers by ^{1}H NMR spectroscopy and GPC.*

	Polymer	$M_{n\ NMR}$ (g/mol)	$M_{n\ GPC}$ (g/mol) / PDI*
III-23	PS_{35}-*b*-PMA_{54}-*b*-$PPFS_{97}$	28,000	12,600 / 1.28
III-24	PS_{35}-*b*-P*t*BA_{25}-*b*-$PTFMS_{20}$	10,900	8,700 / 1.33

* GPC eluent: DMA with LiCl (2.1 g/L), PS calibration.

The bulk morphology of the triblock copolymer **III-23** was investigated by atomic force microscopy (AFM). The triblock copolymer was spin-coated from chloroform (2 mg/mL) onto a silicon wafer. A lamellar phase separation was observed after solvent annealing using chloroform as can be seen in Figure 3.18.

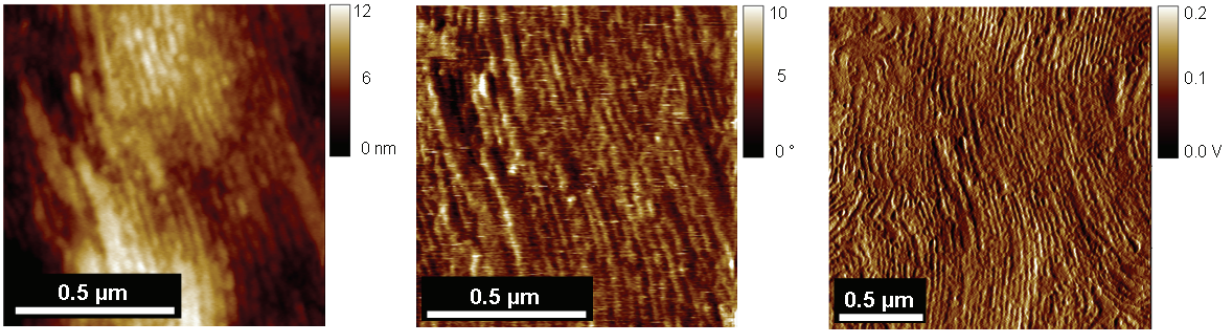

Figure 3.18 *Height image (left), phase image (center) and amplitude image (right) of the triblock copolymer after solvent annealing revealing a lamellar phase separation.*

The sample was measured using tapping mode, *i.e.* the oscillating cantilever is lowered to the surface until the amplitude is reduced to a pre-determined set-point. The topography image is made by scanning the tip over the surface of the sample keeping the amplitude of oscillation constant. The height image in Figure 3.18 demonstrates brighter areas belonging to the softer PMA block and darker areas belonging to the harder PS and PPFS blocks, respectively. The distances of the lamellae are fitting to the calculated lengths for each block: PPFS ≈ 15 nm, PMA ≈ 8 nm and PS ≈ 5 nm; however, it is difficult to assign the exact organization of the triblock copolymer to the pattern since PS and PPFS are both hard blocks. In order to make a more specific statement on the phase separation, TEM investigations should be performed with specific staining of the blocks.

In summary, a large variety of monomers can be polymerized in a controlled fashion using the terpyridine functionalized NMP initiator. The obtained homopolymers can be effectively used as macroinitiators for the preparation of well-defined diblock copolymers as well as triblock copolymers, which offer two useful functionalities: the nitroxide moiety for further controlled radical polymerizations at the one chain end and the terpyridine ligand for supramolecular self-assembly processes at the other end. Moreover, NMP provides the possibility to design polymers with diverse properties such as the combination of high and low Tg blocks (PS and P*t*BA). Beyond this, the incorporation of *t*-butyl acrylate segments allows the facile preparation of amphiphilic block copolymers by cleaving the *t*-butyl groups. In addition, block copolymers containing other functionalities such as crosslinkable systems (PI), water-soluble blocks (PDMAA) and stimuli-responsive systems including pH-responsive P4VP and temperature-responsive PNIPAM (LCST) as well as PTFMS (UCST) can be easily prepared. In particular, pentafluorostyrene segments are favored building blocks since nucleophilic substitution in *para*-position permits the incorporation of functional molecules (Section 3.2.4).

3.2.4 Synthesis of graft copolymers on the PPFS backbone

It is well-known in organic chemistry that the labile *para*-fluorine of pentafluorophenyl groups can undergo nucleophilic substitution reactions with primary amino groups.[53-56] The introduction of electron-donating substituents, such as amines, thiols or alcohols, occurs with high yield and selectivity since the *para*-group is far more reactive than the respective *meta* or *ortho*-position. Furthermore, after the introduction of the electron-donating group, the corresponding tetrafluorophenyl-group becomes less reactive towards nucleophiles. This synthetic route is frequently employed in porphyrin chemistry. This reaction type could therefore also be considered

as a kind of “click” reaction[57-59] since it is easy to perform, uses readily available reagents and it is insensitive to oxygen and water. Surprisingly, this strategy has not yet been applied as versatile tool to synthesize graft copolymers. A general reaction scheme is shown in Scheme 3.3.

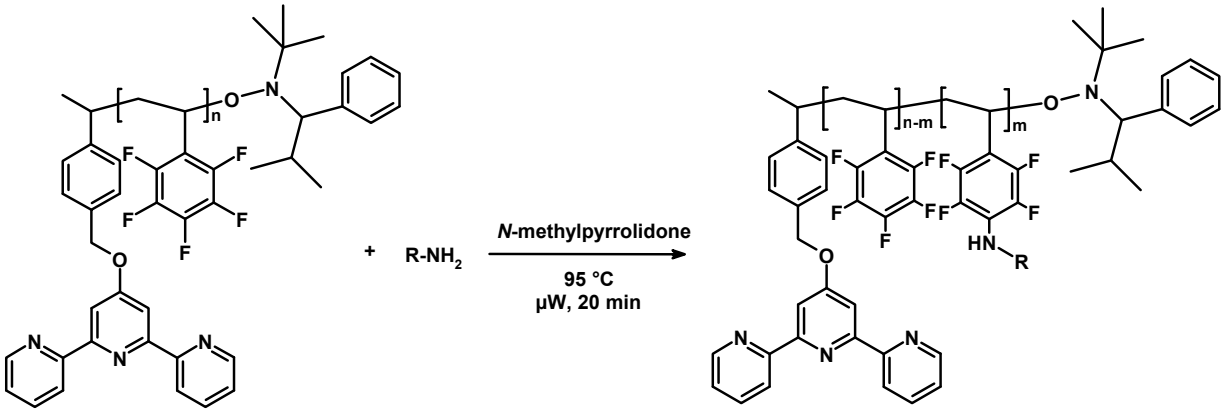

Scheme 3.3 *Schematic representation of the post-modification reaction using primary amines and the terpyridine-functionalized PPFS derived by NMP.*

The possibility of accurately tuning material properties by controlling the macromolecular structure raised significant attention. In particular in the field of polymer science there is a tremendous search for new efficient ways to functionalize and combine different polymer structures. The introduction of click chemistry has lead to major advantages for polymer coupling and functionalization. However, to be able to perform copper-catalyzed Huisgen-type click reactions onto a polymer backbone new acetylene and azide functionalized monomers have to be prepared and incorporated into the polymers. Hence, a straightforward polymer post-modification method was applied which requires amino-functionalized monomers (commercially available) and proceeds without the addition of transition metal catalysts since the coupling is base catalyzed.

3.2.4.1 Grafting supramolecular binding motifs “onto” the PPFS backbone

As a proof of priciple,]-PPFS was reacted with 5-(2,2’:6’2”-terpyridine-4’-yloxy)-pentylamine. The substitution reaction was performed in *N*-methylpyrrolidone (NMP) in a closed reaction vessel for 20 minutes at 95 °C under microwave irradiation based on a recent publication.[60] After purification by precipitation into methanol the post-functionalized polymer **III-25** was characterized by ^{1}H NMR spectroscopy and GPC (Figure 3.19). The GPC-trace shifted slightly to lower elution volumes, indicating the successful transformation. The ^{1}H NMR spectrum provides the evidence that terpyridine-moieties were effectively incorporated into the side-chain since an increasing intensity of the terpyridine signal is clearly visible. In addition, ^{1}H NMR spectroscopy was used to calculate the actual amount of *para*-substitutions by integrating over the corresponding signals. Of interest hereby is the signal at 8.05 ppm which can be attributed to the protons in the 3’- and 5’-position of the terpyridine end-group belonging to the polymer. An average of six terpyridines is present in the side-chain of the polymer, as it was determined from the integral ratios. High conversions can be obtained in a relatively short time using this simple post-modification reaction. In the described experiment above, seven equivalents of terpyridine-functionalized amine were used for the reaction, from which six equivalents were inserted into the polymer backbone.

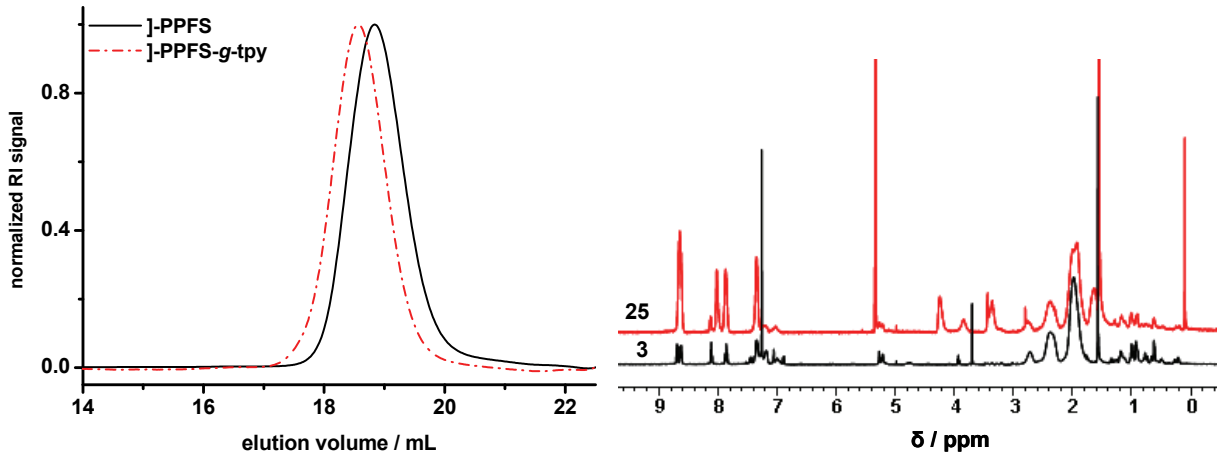

Figure 3.19 *^{1}H NMR spectra of]-PPFS before (**III-3** in $CDCl_3$) and after (**III-25** in CH_2Cl_2) the post-modification reaction (right) and GPC chromatograms of the respective polymers (left). Both demonstrate the successful transformation.*

The incorporation of chelating ligands, such as terpyridines, has been extensively exploited for the preparation of "smart" materials with tunable properties. The "grafted" terpyridine moieties in the side chain of the polymer can act as supramolecular cross-linker when transition metal ions are present, leading to the formation of octahedral *bis*-terpyridine complexes with high stability constants.[1,61,62] In this particular case, a pre-determined amount of iron(II) ions (1 Fe(II) ion : 2 terpyridine ligands) was added to a solution of the post-modified polymer **III-25** in chloroform (50 mg/mL), resulting in a deep-purple gel (Scheme 3.4).

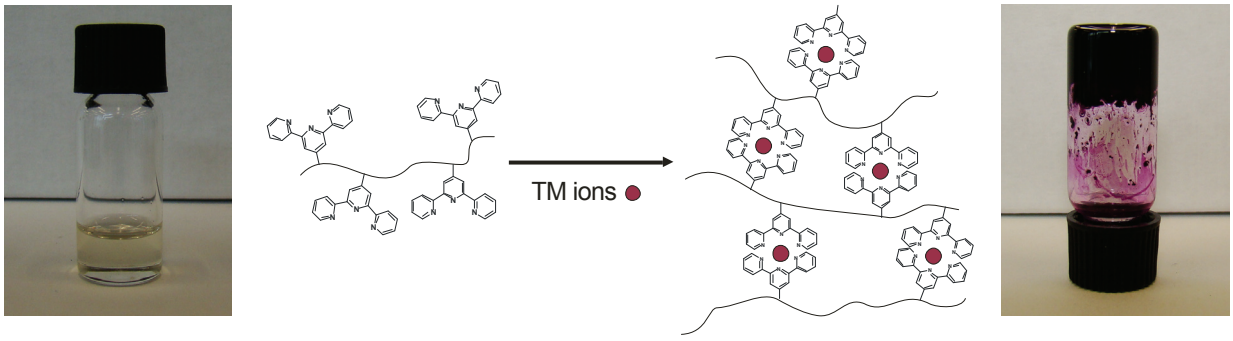

Scheme 3.4 *Schematic representation of metallo-supramolecular crosslinking.*

The same synthetic "clicking" procedure has been followed for the synthesis of a block copolymer consisting of "grafted" phoshorescent iridium complexes (Scheme 3.5). For this purpose, an amino-functionalized Ir-complex was reacted with]-PS_{39}-*b*-$PPFS_{89}$ using similar conditions as for the incorporation of the uncomplexed terpyridine ligand. Subsequently, the product **III-26** was purified by precipitation and analyzed by ^{1}H NMR spectroscopy. By integrating over the signals belonging to the iridium complex with respect to the polymer backbone an average of three incorporated iridium complexes was determined. Interestingly, the terpyridine ligand which is part of the main chain is still available in this material for further modification reactions, *e.g.* complexation with other metal ions such as ruthenium, osmium or zinc.

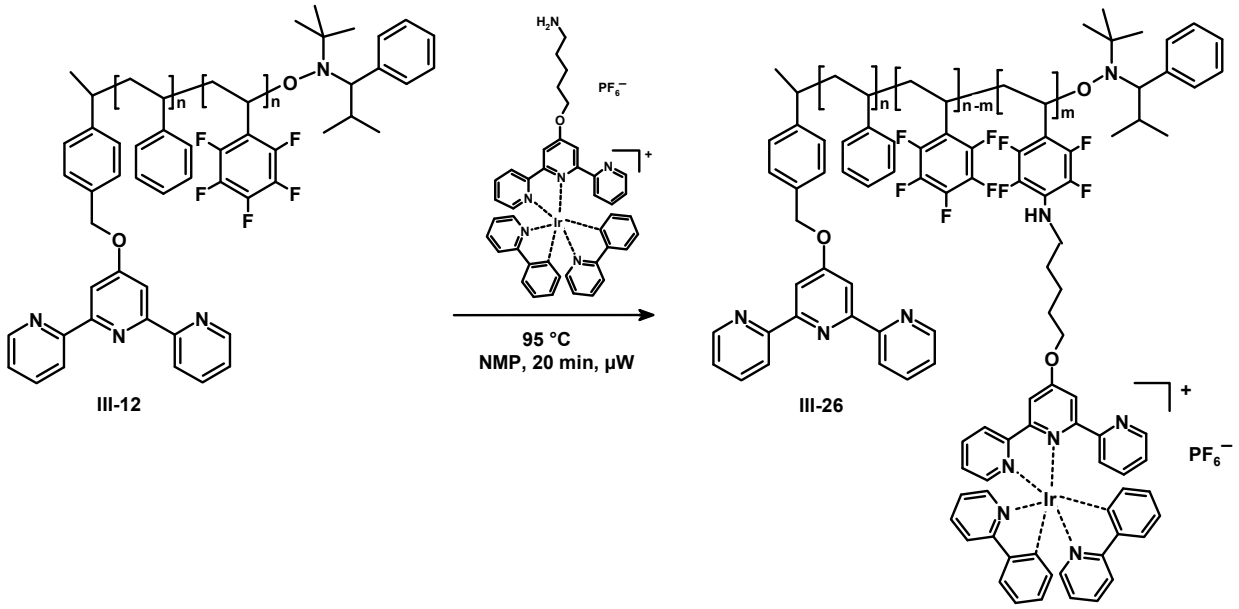

Scheme 3.5 *Schematic representation of the synthesis of a terpyridine-functionalized block copolymer consisting of inserted iridium complexes (**III-26**).*

The post-modified polymer **III-26** gains its optical properties from the incorporated iridium complex. The iridium(III) complex shows a strong absorption band at 260 nm, which is attributed to the ligand centered π → π* transitions on the chelating ligand and on the cyclometallating 2-phenyl-pyridine. The broad absorption bands at lower energy (around 380 nm) are due to typical spin-allowed metal-to-ligand charge transfer transitions (^{1}MLCT, (dπ(Ir) → π*) terpyridine and phenylpyridine transitions. The shoulder tailing to 440 nm was assigned to spin-forbidden ^{3}MLCT (dπ(Ir) → π*) terpyridine transitions.[63] Excitation at 380 nm revealed an emission band with a maximum located at 586 nm (Figure 3.20).

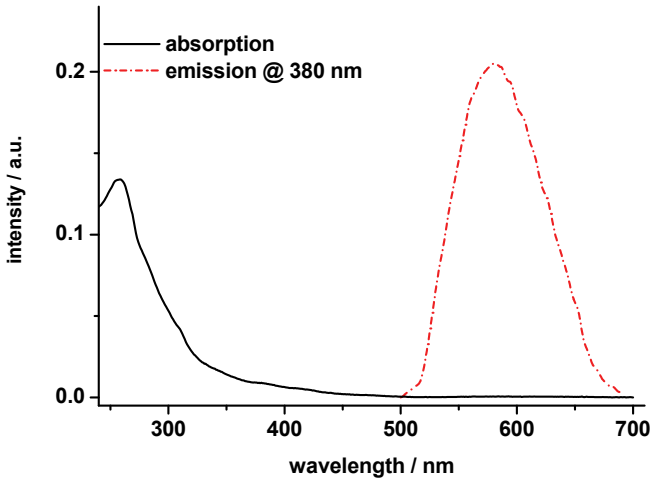

Figure 3.20 *Absorption and emission properties of the iridium(III)-modified block copolymer **III-26** in CH_2Cl_2.*

3.2.4.2 Grafting polymers "onto" the PPFS backbone

Complex macromolecular architectures, such as graft copolymers, are known to exhibit good phase separation[64,65] and are, therefore, used for a variety of applications, *i.e.* impact-resistant materials, compatibilizers, emulsifiers and thermoplastic elastomers. These polymeric architectures are easily accessible using the discussed synthetic pathway for the modification of pentafluorostyrene building blocks with primary amines.

In order to obtain an amphiphilic graft copolymer, the terpyridine-functionalized PPFS was reacted with amino-functionalized poly(ethylene glycol) (M_w = 3,400 g/mol, PDI = 1.08) using the same conditions as described in Section 3.2.4.1. Purification of the graft copolymer **III-27** was carried out by precipitation and preparative SEC in order to remove unreacted PEG. The accordingly measured GPC-chromatograms show a clear chain extension indicating the successful insertion of several PEG macromolecules (Figure 3.21). The number of attached PEG chains was determined by ^{1}H NMR spectroscopy revealing an average of 10 grafted side chains per pentafluorostyrene backbone.

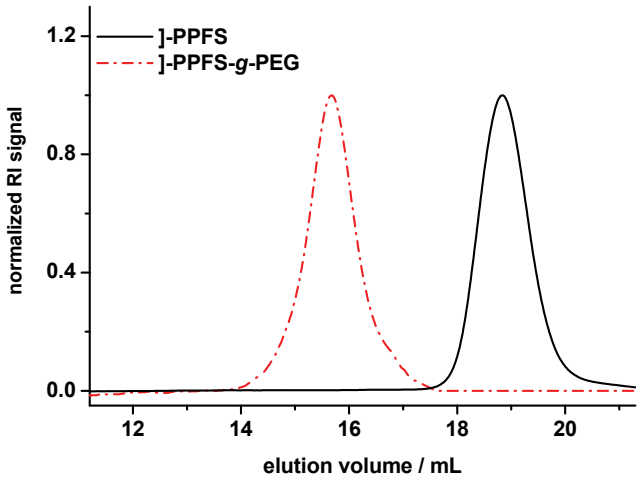

Figure 3.21 *GPC-chromatograms of PPFS before (**III-3**) and after the amine-coupling with polyethylene glycol (**III-27**).*

3.2.4.3 Grafting "from" pre-functionalized PPFS backbone

The scope of this synthetic concept was extended by introducing several functional groups into the side chain of the polymer which allow direct access to a wide variety of chemical modifications including concepts and strategies from organic and polymer chemistry. For this purpose, polypentafluorostyrene was reacted with 5-aminopentanol which leads to the introduction of several hydroxy groups (**III-28**). Subsequently, these hydroxy functionalities were exploited for a ring opening polymerization of *L*-lactide (**III-29**). The polymerization was performed at 100 °C for 5 h in the presence of stannous octoate as catalyst and some drops of dry toluene to ensure a sufficent solubility of the polymer. The polymerization was monitored over time by GPC revealing an increase of the molar mass in time with narrow molar mass distributions, as it is expected for a controlled polymerization process. Figure 3.22 displays the GPC-traces of all involved polymers: homopolymer **III-3**, polypentafluorostyrene substituted with 5-aminopentanol **III-28** and the post-modified polymer with grafted polylactide arms **III-29**. All polymers were characterized by ^{1}H NMR spectroscopy demonstrating that on average nine aminopentanol units were attached per polymer chain and that all hydroxy groups initiated a PLA graft. Moreover, a

degree of polymerization of approximately 11 per graft was also determined by ^{1}H NMR spectroscopy.

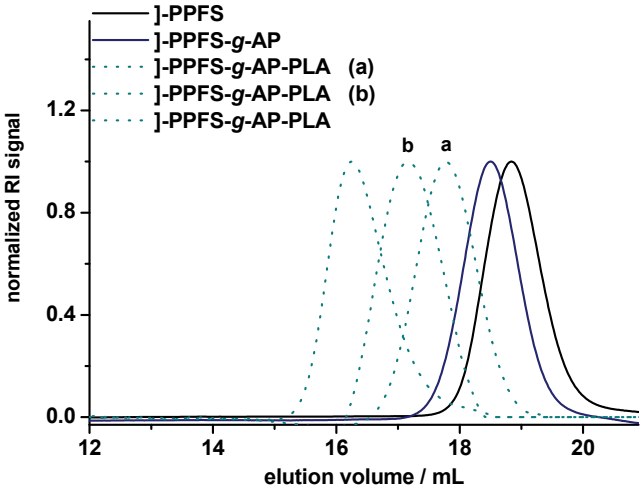

Figure 3.22 *Normalized GPC-traces of the graft copolymer **III-29** (a and b correspond to intermediate samples obtained after 1 h and 3 h polymerization time, respectively) showing successful chain extensions after each reaction.*

The full potential of the here presented methodology is demonstrated by the subsequent combination of a nitroxide mediated block copolymerization and ATRP of a macromonomer resulting in a blocky "graft-on-graft" architecture. In a similar reaction as before mentioned, a terpyridine-functionalized block copolymer **III-20** was reacted with 5-aminopentanol to yield a polymer with hydroxyl functionalities in the side chain (**III-30**). The ^{1}H NMR spectrum after precipitation into methanol revealed an average of eight inserted aminopentanol groups per chain by integration over the corresponding signals. Accordingly, the hydroxy groups were readily converted into *α*-bromoesters by reacting the pre-polymer **III-30** with 2-bromoisobutyryl bromide in the presence of triethylamine. This quantitative esterification reaction incorporates the necessary bromo-functionality into the polymer (**III-31**), as demonstrated by ^{1}H NMR spectroscopy which can be used to initiate a subsequent ATRP. The ^{1}H NMR spectrum revealed that the reaction proceeded quantitatively because the signal attributed to the CH_2-OH shifted downfield to 4.2 ppm. The slightly lower retention time in the GPC after esterification is most likely due to the decreased solubility (decreased hydrodynamic volume) of the grafts in DMA (Figure 3.23). In the next step, the controlled radical polymerization of oligo(ethylene oxide) methacrylate (OEGMA 475) was carried out in toluene at 75 °C for 5 hours with *N*,*N*,*N*′,*N*″,*N*‴-pentamethyldiethylenetriamine (PMDETA) and CuBr as catalytic system. The resulting unimodal GPC-trace (Figure 3.23) indicates that the polymerization proceeded in a controlled fashion. Due to the fact that the terpyridine group is still linked to the polymer (which can form complexes with any kind of transition metal ions in low oxidation states) a loss of control during the ATRP might be expected. Therefore, the ATRP was performed using a large excess of copper ions so that sufficient free copper was available after all terpyridine moieties are complexed. After removing the copper from the graft copolymer by treating the polymer solution with the strong chelating ligand hydroxyethyl ethylenediaminetriacetic acid (HEEDTA), the polymer **III-32** was precipitated twice into ice-cold hexane. A subsequent ^{1}H NMR spectroscopy measurement revealed the incorporation of 70 OEGMA units into the polymer: Approximately 9 OEGMA molecules were "grafted-from" each arm assuming an uniform distribution.

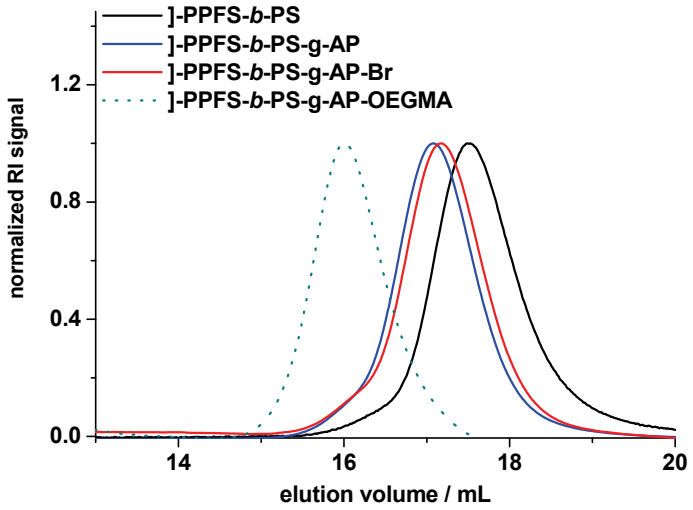

Figure 3.23 *Normalized GPC-traces of the polymers **III-20**, **III-30**, **III-31** and **III-32** utilized for the construction of the "graft-on-graft" copolymer.*

Table 6 summarizes the characteristics for all eight polymers (from Sections 3.2.4.2 and 3.2.4.3) determined by ^{1}H NMR spectroscopy and GPC, whereby it should be noted that all these polymers still bear the terpyridine at one chain end and the nitroxide at the other. In addition, Figure 3.24 provides an overview over the synthesized polymers using the "grafting onto" and the "grafting from" appoach.

Table 6 *M_n determination of the polymers by ^{1}H NMR spectroscopy and GPC.*

	Polymer	$M_{n\ NMR}$ (g/mol)	$M_{n\ GPC}$ (g/mol) / PDI*
III-3	$PPFS_{30}$	6,400	4,500 / 1.09
III-20	$PPFS_{30}$-*b*-PS_{73}	14,000	9,900 / 1.22
III-27	$PPFS_{30}$-*g*-$(PEG_{75})_9$	40,200	27,700 / 1.12
III-28	$PPFS_{30}$-*g*-AP_9	7,200	5,800 / 1.13
III-29	$PPFS_{30}$-*g*-AP_9-PLA_{11}	21,600	27,200 / 1.12
III-30	$PPFS_{30}$-*g*-AP_7-*b*-PS_{73}	14,700	13,400 / 1.18
III-31	$PPFS_{30}$-*g*-$(AP\text{-}Br)_7$-*b*-PS_{73}	15,900	12,600 / 1.19
III-32	$PPFS_{30}$-*g*-$(AP\text{-}OEGMA_{10})_7$-*b*-PS_{73}	49,100	27,700 / 1.15

* GPC in DMA with LiCl (2.1 g/L), polystyrene calibration.

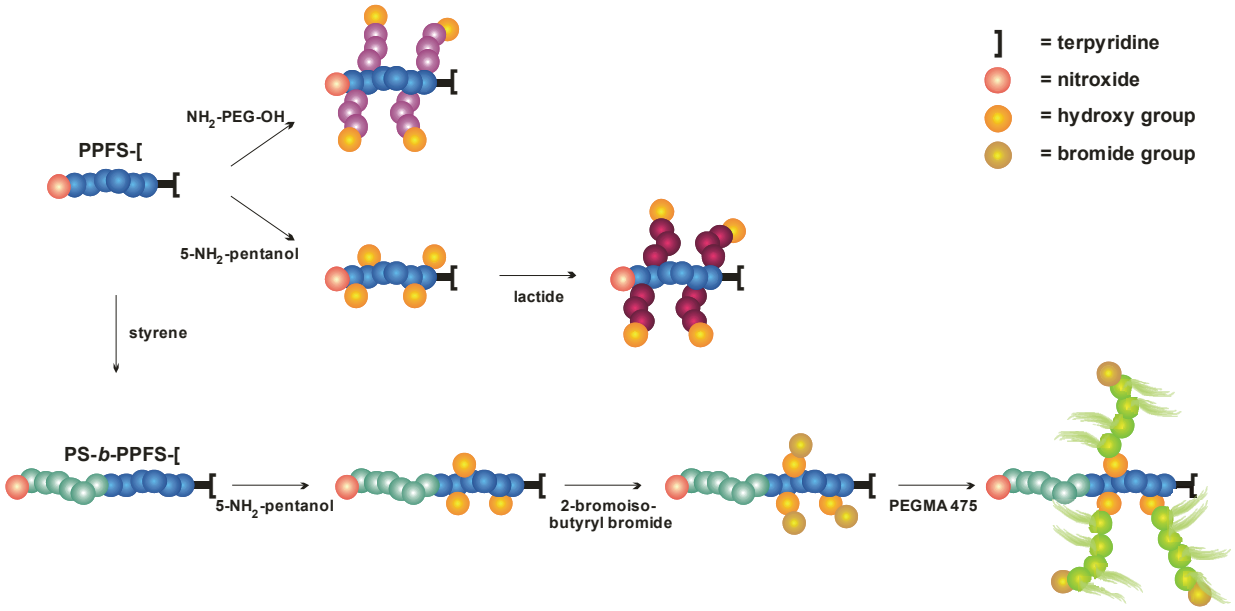

Figure 3.24 *Schematic representation of the synthesized polymers.*

3.3 Conclusions

This chapter has been devoted to the preparation of terpyridine-functionalized polymers using the nitroxide mediated radical polymerization procedure. The unimolecular initiator bearing the supramolecular chelating ligand was capable of the controlled radical polymerization of several monomers leading to a toolbox of well-defined homopolymers and (block) copolymers. It was demonstrated that monomers with very high propagation rates can be polymerized in a controlled fashion by adding an excess of free nitroxide radical in order to achieve an efficient cross-over reaction from the (macro)initiator to the monomer. Moreover, several of the synthesized polymers offer the possibility for post-modification as it was demonstrated for PS-*b*-PtBA, PS-*b*-PTFMS and PS-*b*-PPFS, respectively. In this way, a variety of highly functional materials were synthesized. All of them contain the terpyridine end group which can be exploited for supramolecular chemistry. In the last part special focus was given to polypentafluorostyrene. A facile and versatile approach towards graft copolymers with different side chains was developed by taking advantage of the selective replacement of the *para*-fluorine groups. This strategy of controlled multi-functionalization allows the fine-tuning of polymer architectures as well as properties, and opens avenues towards new tailor-made functional materials.

3.4 Experimental

Chemicals were received from Aldrich, Fluka, Fluorochem Ltd., Shearwater and Apollo Scientific. All monomers were purified by filtration column chromatography (basic Al_2O_3) prior to use in order to remove the inhibitor. Amino-functionalized poly(ethylene glycol) (Shearwater Polymers, Inc.) and 5-aminopentanol (Fluka) were utilized as received from the suppliers. *L*-Lactide was recrystallized from toluene and OEGMA 474 was treated with an inhibitor-remover (Aldrich) before usage. Solvents were purchased from Biosolve. For preparative size exclusion chromatography, Bio-Rad SX-1 Beads swollen in CH_2Cl_2 or THF were used. Proton nuclear magnetic resonance spectra (^{1}H-NMR) were

recorded on a Varian Gemini 400 MHz spectrometer at room temperature. Chemical shifts are given in parts per million (ppm) downfield from an internal standard tetramethylsilane (TMS). Coupling constants (*J* values) are reported in Hertz (HZ). GPC measurements were performed on a Shimadzu system with a SCL-10A system controller, a LC-10AD pump, a RID-6A refractive index detector and a Polymer Laboratories PLgel 5 µm Mixed-D column using *N,N*-dimethylacetamide (DMA) as eluent at a flow rate of 0.5 mL/min, on a Waters system with a 1515 pump, a 2414 refractive index detector, and a Waters Styragel HT4 column utilizing a *N,N*-dimethylformamide (DMF) / 5 mM NH_4PF_6 mixture as eluent at a flow rate of 0.5 mL/min at 50 °C and on a Shimadzu system equipped with a SCL-10A system controller, a LC-10AD pump, a RID-6A refractive index detector and a PLgel 5 µm Mixed-D column with chloroform as the eluent containing 4 vol% Et_3N and 2 vol% 2-propanol as additives to reduce column interactions at a flow of 1 mL/min. Molar masses were calculated against polystyrene or poly(methyl methacrylate) standards. UV-Vis spectra were recorded on a Perkin Elmer Lambda 45P spectrophotometer. Emission spectra were recorded on a Perkin Elmer LS50B Luminescence spectrometer. Matrix assisted laser desorption/ionization mass spectra were obtained using an Ultraflex III TOF/TOF (Bruker Daltonics, Bremen, Germany). The instrument was equipped with a Nd:YAG laser and a collision cell. All spectra were measured in the positive reflector mode. For the MS/MS mode, argon was used as the collision gas at a pressure of 2×10^{-6} mbar. The instrument was calibrated prior to each measurement with an external standard PMMA from PSS Polymer Standards Services GmbH (Mainz, Germany). MS and MS/MS data were processed using PolyTools 1.0 (Bruker Daltonics) and Data Explorer 4.0 (Applied Biosystems). IR-spectra were measured on a Perkin Elmer 1600 FT-IR in attenuated total reflection (ATR) mode. Elemental analysis was carried out on an Eurovector Euro EA Elemental Analyzer equipped with an EuroCAP 40-2 autosampler. TGA was conducted using a Netzsch TG209 F1 under nitrogen atmosphere at a heating rate of 10 °C min^{-1}. GC-MS were recorded with a Shimadzu GC17A connected to a MS. AFM investigations were conducted on a NanoScope IIIa Multimode system (DI, Santa Barbara, US) in tapping mode. Commercially available AFM tips, purchased from µ-masch (Estonia), were used for imaging. Determination of the step height was performed by omitting imaging processing artifacts. All reactions were carried out under argon atmosphere unless stated otherwise.

Synthesis of the terpyridine functionalized initiator (2,2,5-trimethyl-3-(1-(4'-(4''-terpyridinyloxy)-methyl)-phenylethoxy)-4-phenyl-3-azahexane) (III-1)

To a suspension of 2,6-*bis*-(2'pyridyl)-4-pyridone (3.25 g, 13 mmol) and K_2CO_3 (6.95 g, 52 mmol) in dry DMF (35 mL) at 50 °C, a solution of 2,2,5-trimethyl-3-(1-(4'-chloromethyl)phenylethoxy)-4-phenyl-3-azahexane (4.2 g, 11.4 mmol) in dry DMF (10 mL) was added dropwise. Stirring at 50 °C was continued overnight, after which the reaction mixture was cooled to room temperature, poured into cold water (300 mL) and extracted with dichloromethane (3 times). The combined organic layers were dried over Na_2SO_4, filtered and removed *in vacuo*. The light brown residue was subjected to a filtration column (Al_2O_3, hexane/dichloromethane 1:1). The solvent was removed *in vacuo* and 3.96 g (60.2%) of a polycrystalline white powder was obtained (Yield = 61%).[2]

The presence of diastereomers makes the normally well-defined *J*-couplings in the terpyridine region loose the fine splitting into ddd, td or dd so that only multiplets or dublets remained. ^{1}H-NMR ($CDCl_3$, 400 MHz): δ (ppm) = 8.69 (d, 4 H, *J* = 5.2 Hz, $H_{6,6''}$), 8.61 (d, 4 H, *J* = 7.6 Hz, $H_{3,3''}$), 8.13 (s, 2 H, $H_{3',5'}$, major), 8.12 (s, 2 H, $H_{3',5'}$, minor), 7.84 (t, 4 H, *J* = 7.6 Hz, $H_{4,4''}$), 7.48-7.14 (m, 22 H, aromatic & $H_{5,5''}$), 5.35 (s, 2 H, tpyOCH_2, minor), 5.30 (s, 2 H, tpyOCH_2, major), 4.94 (q + q, 2 H, *J* = 6 Hz, *H*C-ON, both diastereomers), 3.42 (d, 1 H, *J* = 10.8 Hz, ON-C*H*, major), 3.28 (d, 1 H, *J* = 10.4 Hz, ON-C*H*, minor), 2.34 (m, 1 H, CH_3CHCH_3, major), 1.63 (d, 3 H, *J* = 6.4 Hz, CH_3CH-ON, major), 1.55 (d, 3 H, *J* = 6.4 Hz, CH_3CH-ON, minor), 1.39 (m, 1 H, CH_3CHCH_3, minor), 1.31 (d, 3 H, *J* = 6.8 Hz, CH_3CHCH_3, major), 1.04 (s, 9 H, C(CH_3)$_3$, minor), 0.89 (d, 3 H, *J* = 6.0 Hz, CH_3CHCH_3, major), 0.77 (s, 9 H, C(CH_3)$_3$, major), 0.54 (d, 3 H, *J* = 6.4 Hz, CH_3CHCH_3, minor), 0.17 (d, 3 H, *J* = 6.8 Hz, CH_3CHCH_3, minor). ^{13}C-NMR ($CDCl_3$, 125 MHz): δ (ppm) = 166.9 ($C_{4'}$), 157.0 ($C_{2',6'}$), 155.9 ($C_{2,2''}$), 148.9 ($C_{6,6''}$), 145.7, 144.9, 142.3, 142.1 (q, C aromatic), 136.7 ($C_{3',5'}$), 135.0, 134.3 (q, C aromatic), 130.9, 130.8, 127.3-126.1 (*C*-H aromatic), 123.7 ($C_{3,3''}$), 121.3 ($C_{4,4''}$), 107.7 , 107.6 ($C_{5,5''}$), 83.1 (*C*-O-N, major), 82.3 (*C*-O-N, minor), 72.1 (O-N-*C*, major), 72.0 (O-N-*C*, minor), 69.9 (tpyO*C*H_2, major), 69.8 (tpyO*C*H_2, minor), 60.4 (*C*(CH_3)$_3$, major), 60.3 (*C*(CH_3)$_3$, minor), 31.9, 31.6, 28.3 (C(*C*H_3)$_3$, minor), 28.2 (C(*C*H_3)$_3$, major), 24.5, 23.0, 22.0, 21.9, 21.1, 20.9. Elemental analysis calcd.for $C_{38}H_{42}N_4O_2$ (586,7771 g/mol): 77.78% C, 7.21% H, 9.55% N; found: 77.51% C, 7.17% H, 9.22% N; MALDI-TOF MS (dithranol): m/z: 591 ($M+H^+$, 100%), 366 (M^+-nitroxide, 55%). UV-vis (CH_2Cl_2): λ (nm) (ε (mol^{-1} cm^{-1})): 278 (20100), 240 (25300). IR (ATR): ν (cm^{-1}): 3060 (CH_2, CH_3); 2973, 2868 (CH), 1600, 1582, 1563 (C-C, C-N terpyridine), 1516, 1468, 1385, 1354, 1195, 1063, 1015, 821, 793, 743, 733, 701.

Terpyridine-functionalized polystyrene]-PS_{68} **(III-2)**

The initiator was dissolved in purified styrene. A degree of polymerization of 100 was targeted. Three freeze-pump-thaw cycles were applied for removal of oxygen before the reaction vessels were immersed in an oilbath of 125 °C. The polymerization was carried out for a certain amount of time and then stopped according to the kinetic data obtained previously. The polymers were precipitated twice from CH_2Cl_2 into cold methanol. Yield (3.84 g, 77%). ^{1}H-NMR ($CDCl_3$): δ (ppm) = 8.68 (m, 2 H; $H_{6:6''}$), 8.62 (m, 2 H; $H_{3:3''}$), 8.21 (m, 2 H; $H_{3':5'}$), 7.93 (m, 2 H; $H_{4:4''}$), 7.47-6.32 (m, 353 H; $H_{PS\ backbone\ aromatic}$; $H_{aromatic}$, $H_{5,5''}$), 5.34 (m, 2 H; tpyOCH_2), 4.27-4.07 (broad, 1 H; *H*C-ON), 3.50-3.15 (m, 1 H; ON-C*H*), 2.45-0.40 (m, 225 H, $H_{PS\ backbone\ aliphatic}$; C(C$H_3$)$_3$; C$H_3$C*H*C$H_3$; C$H_{3\ initiating\ fragment}$). GPC (eluent $CHCl_3$, triethylamine, and 2-propanol (94:4:2): M_n = 7,700 g/mol, PDI = 1.08.

Terpyridine-functionalized poly(pentafluorostyrene)]-$PPFS_{30}$ **(III-3)**
The initiator (180 mg, 3.1×10^{-4} mol was dissolved in purified 2,3,4,5,6-pentafluorostyrene (4.1 g, 0.02 mol, M/I = 70). Three freeze-pump-thaw cycles were applied for removal of oxygen before the reaction vessels were immersed in an oilbath of 120 °C for 5 hours. The polymer was precipitated twice from CH_2Cl_2 into cold methanol. ^{1}H-NMR (CD_2Cl_2): δ (ppm) = 8.68 (m, 2 H; $H_{6:6''}$), 8.65 (m, 2 H; $H_{3:3''}$), 8.13 (m, 2 H; $H_{3':5'}$), 7.89 (m, 2 H; $H_{4:4''}$), 7.45-6.95 (m, 11 H; $H_{aromatic}$, $H_{5,5''}$), 5.30-5.20 (m, 2 H; tpyOCH_2),4.78 (m, 1 H; *H*C-ON, both diastereomers), 3.54-3.20 (m, 1 H; ON-C*H*, major & minor), 3.09-1.70 (m, 91 H; $H_{PPFS\ backbone}$, CH_3CHCH_3 major), 1.60-0.15 (m, 18 H; $C(CH_3)_3$; CH_3CHCH_3 minor, CH_3CHCH_3; CH_3CH-ON). GPC (eluent DMA with LiCl 2.1 g/L): M_n = 4,500 g/mol, PDI = 1.09.

Terpyridine-functionalized poly(trifluoromethylstyrene)]-$PTFMS_{42}$ **(III-4)**
The unimolecular nitroxide initiator (100 mg, 1.7×10^{-4} mol) was dissolved in *p*-trifluoromethlstyrene (3.0 g, 0.017 mol, M/I = 100). Three freeze-pump-thaw cycles were applied for removal of oxygen before the closed reaction vessel was immersed in an oilbath of 120 °C for 1.6 hours. The polymer was precipitated twice from CH_2Cl_2 into cold methanol. ^{1}H NMR (CD_2Cl_2): δ (ppm) = 8.67 (m, 2H; $H_{6:6''}$), 8.64 (m, 2H; $H_{3:3''}$), 8.14 (m, 2H; $H_{3':5'}$), 7.88 (m, 2H; $H_{4:4''}$), 7.60-6.30 (m, 179H; $H_{PTFMS\ backbone}$, $H_{aromatic}$, $H_{5,5''}$), 5.30-5.20 (m, 2H; tpyOCH_2), 4.78 (m, 1H; *H*C-ON, both diastereomers), 3.54-3.20 (m, 1H; ON-C*H*, major & minor), 2.30-0.00 (m, 145H; $H_{PTFMS\ backbone}$, $C(CH_3)_3$; CH_3CHCH_3 major & minor, CH_3CHCH_3; CH_3CH-ON). GPC (eluent DMA with LiCl 2.1 g/L): M_n = 7,100 g/mol, PDI = 1.16.

Terpyridine-functionalized poly(*t*-butyl acrylate)]-P*t*BA_{40} **(III-5)**
A mixture of initiator (100 mg, 0.17 mmol), the corresponding free nitroxide (1.5 mg, 0.04 equiv. with respect to initiator), and *t*-butyl acrylate (4.1 g, 32 mmol) were degassed by three freeze-pump-thaw cycles, sealed under argon and heated at 120 °C for 22 h. The reaction mixture was concentrated and finally dried at 40 °C for 24 h. Yield (0.4 g, 21%). ^{1}H-NMR (CD_2Cl_2): δ (ppm) = 8.60 (m, 2 H; $H_{6:6''}$), 8.54 (m, 2 H; $H_{3:3''}$), 8.05 (m, 2 H; $H_{3':5'}$), 7.79 (m, 2 H; $H_{4:4''}$), 7.40-7.04 (m, 11 H; $H_{aromatic}$, $H_{5,5''}$) 5.19 (m, 2 H; tpyOCH_2), 4.25-4.03 (broad, 1 H; *H*C-ON), 3.37-3.21 (m, 1 H; ON-C*H*), 2.30-0.30 (m, 489 H, $H_{tBA\ backbone\ aliphatic}$; $C(CH_3)_3$; CH_3CHCH_3; CH_3 $_{initiating\ fragment}$). GPC (eluent $CHCl_3$, triethylamine, and 2-propanol (94:4:2): M_n = 4,400 g/mol, PDI = 1.11.

Terpyridine-functionalized poly(methyl acrylate)]-PMA_{60} **(III-6)**
A mixture of initiator (100 mg, 0.17 mmol), the corresponding free nitroxide (1.5 mg, 0.04 equiv. with respect to initiator), and methyl acrylate (1.5 g, 58 mmol) were degassed by three freeze-pump-thaw cycles, sealed under argon and heated at 120 °C for 20 h. The reaction mixture was concentrated, precipitated into ice-cold hexane and dried at 40 °C for 24 h. Yield (0.7 g, 44%). ^{1}H-NMR (CD_2Cl_2): δ (ppm) = 8.60 (m, 2 H; $H_{6:6''}$), 8.54 (m, 2 H; $H_{3:3''}$), 8.05 (m, 2 H; $H_{3':5'}$), 7.79 (m, 2 H; $H_{4:4''}$), 7.40-7.04 (m, 11 H; $H_{aromatic}$, $H_{5,5''}$) 5.19 (m, 2 H; tpyOCH_2), 4.25-4.03 (broad, 1 H; *H*C-ON), 3.70-3.40 (m, 180 H, O-CH_3), 3.37-3.21 (m, 1 H; ON-C*H*), 2.40-0.30 (m, 199 H, $H_{PMA\ backbone\ aliphatic}$; $C(CH_3)_3$; CH_3CHCH_3; CH_3 $_{initiating\ fragment}$). GPC (eluent $CHCl_3$, triethylamine, and 2-propanol (94:4:2): M_n = 3,000 g/mol, PDI = 1.20.

Terpyridine-functionalized poly(2-ethylhexyl acrylate)]-$P2EHA_{18}$ **(III-7)**
A mixture of initiator (50 mg, 0.085 mmol), the corresponding free nitroxide (0.75 mg, 0.04 equiv. with respect to initiator), and 2-ethylhexyl acrylate (2 g, 11 mmol) were degassed by three freeze-pump-thaw cycles, sealed under argon and heated at 120 °C for 20 h. The reaction mixture was concentrated, precipitated into ice-cold hexane and dried at 40 °C for 24 h. Yield (0.25 g, 10%). ^{1}H-NMR ($CDCl_3$): δ (ppm) = 8.60 (m, 2 H; $H_{6:6''}$), 8.54 (m, 2 H; $H_{3:3''}$), 8.05 (m, 2 H; $H_{3':5'}$), 7.79 (m, 2 H; $H_{4:4''}$), 7.40-7.04 (m, 11 H; $H_{aromatic}$, $H_{5,5''}$) 5.19 (m, 2 H; tpyOCH_2), 4.25-4.03 (broad, 1 H; *H*C-ON), 3.70-3.40 (m, 36 H, O-CH_2-CH), 3.37-3.21 (m, 1 H; ON-C*H*), 2.70-0.35 (m, 55 H, $H_{P2EHA\ backbone\ aliphatic}$; $C(CH_3)_3$; CH_3CHCH_3; CH_3 $_{initiating\ fragment}$). GPC (eluent $CHCl_3$, triethylamine, and 2-propanol (94:4:2): M_n = 2,700 g/mol, PDI = 1.28.

Terpyridine-functionalized poly(dimethyl acrylamide)]-$PDMAA_{36}$ **(III-8)**
A mixture of initiator (100 mg, 0.17 mmol), the corresponding free nitroxide (2.6 mg, 0.07 equiv. with respect to initiator), and *N,N*-dimethyl acrylamide (2.5 g, 25 mmol) were degassed by three freeze-pump-thaw cycles, sealed under argon and heated at 120 °C for 7 h. The polymer was precipitated twice from $CHCl_3$ into ice-cold diethyl ether. Yield (0.25 g, 10%). ^{1}H-NMR ($CDCl_3$): δ (ppm) = 8.68 (m, 2 H; $H_{6:6''}$), 8.61 (m, 2 H; $H_{3:3''}$), 8.09 (m, 2 H; $H_{3':5'}$), 7.84 (m, 2 H; $H_{4:4''}$), 7.44-7.08 (m, 11 H; $H_{aromatic}$, $H_{5,5''}$) 5.30 (m, 2 H; tpyOCH_2), 4.25-4.03 (broad, 1 H; *H*C-ON), 3.52-2.08 (m, 259 H, $N(CH_3)_2$ $_{PDMAA\ backbone}$, CH $_{PDMAA\ backbone}$, ON-C*H,* CH_3 $_{initiating\ fragment}$, CH_3CHCH_3 major, CH_3CHCH_3 minor), 2.05-0.40 (m, 84 H, CH_2 $_{PDMAA\ backbone}$, $C(CH_3)_3$, CH_3CHCH_3 minor, CH_3CHCH_3 major). GPC (eluent $CHCl_3$, triethylamine, and 2-propanol (94:4:2): M_n = 3,400 g/mol, PDI = 1.30.

Terpyridine-functionalized poly(isopropyl acrylamide)]-PNIPAM$_{29}$ **(III-9)**
A mixture of initiator (75 mg, 0.13 mmol), the corresponding free nitroxide (0.8 mg, 0.03 equiv. with respect to initiator), *N,N*-dimethyl acrylamide (1.4 g, 13 mmol) and dry toluene (12 mL) were degassed by three freeze-pump-thaw cycles, sealed under argon and heated at 120 °C for 20 h. The polymer was precipitated twice from $CHCl_3$ into ice-cold diethyl ether. Yield (0.4 g, 29%). ^{1}H-NMR ($CDCl_3$): δ (ppm) = 8.68 (m, 2 H; $H_{6:6"}$), 8.61 (m, 2 H; $H_{3:3"}$), 8.09 (m, 2 H; $H_{3':5'}$), 7.84 (m, 2 H; $H_{4:4"}$), 7.44-7.08 (m, 11 H; $H_{aromatic}$, $H_{5,5"}$) 5.30 (m, 2 H; tpyOCH_2), 4.25-3.85 (broad, 30 H; *H*C-ON, NH-C*H*-$(CH_3)_2$), 3.53-3.08 (m, 30 H; ON-C*H*, major & minor, N*H*-CH-$(CH_3)_2$), 2.44-0.15 (m, 280 H; CH_2-C$H_{PNIPAM\ backbone}$, NH-CH-(CH_3)$_2$, CH_3CHCH_3 major, C(CH_3)$_3$; CH_3CHCH_3 minor, CH_3CHCH_3; CH_3CH-ON). GPC (eluent $CHCl_3$, triethylamine, and 2-propanol (94:4:2): M_n = 3,400 g/mol, PDI = 1.30.

Synthesis of the anthracene-containing macromonomer (III-10)
To an ice cooled solution of anthracenemethanol (6 g, 28.7 mmol) in THF and DMF (300 mL + 180 mL) NaH (1.7 g, 43 mmol as 60% purity in oil) was added and the mixture was stirred for 30 min. To this suspension 4-vinyl benzylchloride (4.09 mL, 29 mmol) was then added. The mixture was allowed to warm to room temperature and stirred for 24 h. The reaction was quenched by addition of a saturated NaCl solution. The product was extracted with ethyl acetate (50 mL × 3) and dried over anhydrous Na_2SO_4. The crude product obtained upon evaporation of the solvent was subjected to flash chromatography (silica gel, *n*-hexane/ethyl acetate, 9/1). The product was recrystallized from methanol. 5.12 g of the product was obtained as yellow crystals in 55% yield. ^{1}H-NMR (d_6 acetone): δ (ppm) = 8.58 (s, 1 H), 8.41 (d, 2 H; *J* = 8.8 Hz), 8.08 (d, 2 H; *J* = 7.6 Hz), 7.60-7.48 (m, 4 H), 7.45 (d, 2 H; *J* = 8.0 Hz), 7.38 (d, 2 H; *J* = 8.0 Hz), 6.75 (dd, 1 H; *J* = 18.0 Hz, 10.8 Hz), 5.80 (d, 1 H; *J* = 17.6 Hz),5.55 (s, 2 H), 5.22 (d, 1 H; *J* = 11.0 Hz), 4.77 (s, 2H).

Terpyridine-functionalized PS-*stat*-PS$_{anthracene}$]-PS$_{48}$-*stat*-PS$_{anthr\ 4}$ **(III-11)**
The nitroxide initiator (100 mg, 1.7 × 10^{-4} mol) and the macromonomer (500 mg, 1.5 × 10^{-3} mol) were dissolved in purified styrene (1.75 g, 16.8 mmol) and 1 mL dry toluene. Three freeze-pump-thaw cycles were applied, and the reaction mixture was heated for 6 hours at 120 °C. The statistical copolymer was precipitated twice from dichloromethane into methanol. The precipitate was collected and dried under vacuum to yield the desired copolymer. Yield (3.84 g, 77%). ^{1}H-NMR (CD_2Cl_2): δ (ppm) = 8.70 (m, 4 H; $H_{6:6"}$, $H_{3:3"}$), 8.51 (m, 3.6 H; anthr.), 8.34 (m, 7.2 H; anthr.), 8.17 (m, 2 H; $H_{3':5'}$), 8.06 (m, 7.2 H; anthr.), 7.89 (m, 2 H; $H_{4:4"}$), 7.70-6.10 (m, 271 H; $H_{PS\ backbone\ aromatic}$; $H_{aromatic}$, $H_{5,5"}$, $H_{aromatic\ macromonomer}$, $H_{anthr.}$), 5.60-5.10 (m, 9.2 H; tpyOCH_2, OCH_2-anthr), 4.93-4.05 (broad, 8.2 H; *H*C-ON, PhCH_2O), 3.50-3.15 (m, 1 H; ON-C*H*), 2.50-0.15 (m, 174 H, $H_{PS\ \&\ PS\ anthr.\ backbone\ aliphatic}$; C(C$H_3$)$_3$; C$H_3CHCH_3$; C$H_3$ initiating fragment). GPC (eluent $CHCl_3$, triethylamine, and 2-propanol (94:4:2): M_n = 5,000 g/mol, PDI = 1.14. Quantum yield = 15% (bulk).

Terpyridine-functionalized poly(styrene-*block*-pentafluorostyrene)]-PS$_{50}$-*b*-PPFS$_{80}$ **(III-12)**
The polystyrene macroinitiator (135 mg, 2.3 × 10^{-5} mol, M_n = 5,800 g/mol, PDI = 1.13) was dissolved in purified 2,3,4,5,6-pentafluorostyrene (2.3 g, 11.8 mmol, M/I = 500) and 1.3 g dry THF. Three freeze-pump-thaw cycles were applied, and the reaction mixture was heated for 3 hours at 120 °C. The block copolymer was precipitated twice from dichloromethane into ice-cold methanol. The precipitate was collected and dried under vacuum to yield the desired block copolymer. ^{1}H-NMR (CD_2Cl_2): δ (ppm) = 8.70 (m, 2 H; $H_{6:6"}$), 8.66 (m, 2 H; $H_{3:3"}$), 8.16 (m, 2 H; $H_{3':5'}$), 7.88 (m, 2 H; $H_{4:4"}$), 7.58-6.31 (m, 261 H; $H_{aromatic}$,$H_{PS\ aromatic}$ $H_{5,5"}$), 5.30-5.20 (m, 2 H; tpyOCH_2), 4.78 (m, 1 H; *H*C-ON, both diastereomers), 3.54-3.20 (m, 1H; ON-C*H*, major & minor), 2.91-0.24 (m, 409 H; $H_{PPFS\ \&\ PS\ backbone}$, C(C$H_3$)$_3$; CH_3CHCH_3 major & minor, CH_3CHCH_3 major & minor; CH_3CH-ON). GPC (eluent DMA with LiCl 2.1 g/L): M_n = 11,300 g/mol, PDI = 1.23.

Terpyridine-functionalized poly(styrene-*block*-trifluoromethylstyrene)]-PS$_{50}$-*b*-PTFMS$_{34}$ **(III-13)**
The polystyrene macroinitiator (100 mg, 1.7 × 10^{-5} mol, M_n = 5,800 g/mol, PDI = 1.13) was dissolved in purified *para*-trifluoromethylstyrene (420 mg, 2.4 mmol, M/I = 140). Three freeze-pump-thaw cycles were applied, and the reaction mixture was heated for 2 hours at 120 °C. The block copolymer was precipitated twice from dichloromethane into ice-cold methanol. The precipitate was collected and dried under vacuum to yield the desired block copolymer. ^{1}H-NMR (CD_2Cl_2): δ (ppm) = 8.70 (m, 2 H; $H_{6:6"}$), 8.66 (m, 2 H; $H_{3:3"}$), 8.16 (m, 2 H; $H_{3':5'}$), 7.88 (m, 2 H; $H_{4:4"}$), 7.59-6.30 (m, 397 H; $H_{aromatic}$,$H_{PS\ \&\ PTFMS\ aromatic}$ $H_{5,5"}$), 5.30-5.20 (m, 2 H; tpyOCH_2), 4.78 (m, 1 H; *H*C-ON, both diastereomers), 3.54-3.20 (m, 1H; ON-C*H*, major & minor), 2.30-0.24 (m, 271 H; $H_{PTFMS\ \&\ PS\ backbone}$, C(C$H_3$)$_3$; CH_3CHCH_3 major & minor, CH_3CHCH_3 major & minor; CH_3CH-ON). GPC (eluent DMA with LiCl 2.1 g/L): M_n = 10,200 g/mol, PDI = 1.17.

Terpyridine-functionalized poly(styrene-*block*-methyl acrylate)]-PS$_{34}$-*b*-PMA$_{54}$ **(III-14)**
The polystyrene macroinitiator (200 mg, 4.4 × 10^{-5} mol, M_n = 4,500 g/mol, PDI = 1.12) was dissolved in purified methyl acrylate (1.0 g, 11.6 mmol, M/I = 250). Three freeze-pump-thaw cycles were applied, and the reaction mixture was heated for 6 hours at 120 °C. The block copolymer was precipitated twice from dichloromethane into methanol. The precipitate was collected and dried under vacuum to yield the desired block copolymer. ^{1}H-NMR

(CD_2Cl_2): δ (ppm) = 8.70 (m, 2 H; $H_{6:6''}$), 8.66 (m, 2 H; $H_{3:3''}$), 8.16 (m, 2 H; $H_{3':5'}$), 7.88 (m, 2 H; $H_{4:4''}$), 7.59-6.30 (m, 181 H; $H_{aromatic}$,$H_{PS\ aromatic}$ $H_{5,5''}$), 5.30-5.20 (m, 2 H; tpyOCH_2), 4.78 (m, 1 H; *H*C-ON, both diastereomers), 3.93-3.20 (m, 163 H; ON-C*H*, major & minor, $OCH_{3\ MA}$), 2.50-0.80 (m, 280 H; $H_{PS\ backbone}$, $H_{PMA\ backbone}$, CH_3CHCH_3 major, $C(CH_3)_3$; CH_3CHCH_3 minor, CH_3CHCH_3 major, CH_3CHCH_3 minor, CH_3CH-ON), 0.55-0.40 (d, 3 H, CH_3CHCH_3 minor, CH_3CHCH_3 major). GPC (eluent DMA with LiCl 2.1 g/L): M_n = 7,500 g/mol, PDI = 1.23.

Terpyridine-functionalized poly(styrene-*block*-*t*-butyl acrylate)]-PS_{160}-*b*-P*t*BA_{90} **(III-15)**
The polystyrene starting block (200 mg, 1.2 × 10^{-5} mol, M_n = 16,600 g/mol, PDI = 1.07) was redissolved in *t*-butyl acrylate (2.4 g, 18.75 mmol), an appropriate amount of free nitroxide (0.05 equiv with respect to macroinitiator) was added, three freeze-pump-thaw cycles were applied, and the reaction mixture was heated at 120 °C for 22 h. The block copolymer was precipitated twice from dichloromethane into methanol. The precipitate was collected and dried under vacuum to yield the desired block copolymer. ^{1}H-NMR (CD_2Cl_2): δ (ppm) = 8.68 (m, 2 H; $H_{6:6''}$), 8.65 (m, 2 H; $H_{3:3''}$), 8.05 (m, 2 H; $H_{3':5'}$), 7.79 (m, 2 H; $H_{4:4''}$), 7.50-6.22 (m, 811 H; $H_{PS\ backbone\ aromatic}$; $H_{aromatic}$, $H_{5,5''}$), 5.34 (m, 2 H; tpyOCH_2), 4.27-4.07 (broad, 1 H; *H*C-ON), 3.50-3.15 (m, 1 H; ON-C*H*), 2.26-0.39 (m, 2259 H, $H_{PS\ backbone\ aliphatic}$; $C(CH_3)_3$; CH_3CHCH_3; CH_3 $_{initiating\ fragment}$, $H_{PtBA\ backbone}$).
GPC (eluent DMF with NH_4PF_6 (0.8 g/L)): M_n = 32,900 g/mol, PDI = 1.17.

Terpyridine-functionalized poly(styrene-*block*-2-vinylpyridine)]-PS_{85}-*b*-$P2VP_{130}$ **(III-16)**
The polystyrene starting block (50 mg, 5.5 × 10^{-6} mol, M_n = 9,100 g/mol, PDI = 1.05) was redissolved in 2-vinylpyridine (1.2 g, 11.4 mmol), an appropriate amount of free nitroxide (0.1 equiv with respect to macroinitiator) was added, three freeze-pump-thaw cycles were applied, and the reaction mixture was heated at 110 °C for 1.5 h. The block copolymer was precipitated twice into ice-cold diethyl ether. The precipitate was collected and dried under vacuum to yield the desired block copolymer which was further characterized by ^{1}H-NMR and GPC (UV-detector). Yield (55 mg, 43%).^{1}H-NMR ($CDCl_3$): δ (ppm) = 8.65 (m, 2 H; $H_{6:6''}$), 8.57 (m, 2 H; $H_{3:3''}$), 8.43-8.07 (m,125 $H_{P2VP\ backbone\ aromatic}$; $H_{3':5'}$), 7.79 (m, 2 H; $H_{4,4''}$), 7.29-6.47 (m; 827 $H_{PS\ backbone\ aromatic}$; $H_{P2VP\ backbone\ aromatic}$, $H_{5,5''}$), 3.96 (m, 2 H; tpyOCH_2), 3.79 (m, 2 H; tpyOCH_2CH_2), 2.42-0.56 (m; 664 H $_{P2VP\ \&\ PS\ backbone}$ $C(CH_3)_3$; CH_3CHCH_3; CH_3 $_{initiating\ fragment}$). GPC (eluent DMF with NH_4PF_6 (0.8 g/L)): M_n = 27,500 g/mol, PDI = 1.16.

Terpyridine-functionalized poly(*t*-butyl acrylate-*block*-styrene)]-P*t*BA_{85}-*b*-PS_{230} **(III-17)**
The poly(*t*-butylacrylate) starting block (350 mg, 3.85 × 10^{-5} mol, M_n = 9,100 g/mol, PDI = 1.10) was redissolved in styrene (1.6 g, 15.4 mmol), three freeze-pump-thaw cycles were applied, and the reaction mixture was heated at 120 °C for 12 h. The block copolymer was precipitated twice into methanol. The precipitate was collected and dried under vacuum to yield the desired block copolymer. Yield (890 mg, 46%). ^{1}H-NMR ($CDCl_3$): δ (ppm) = 8.60 (m, 2 H; $H_{6:6''}$), 8.55 (m, 2 H; $H_{3:3''}$), 8.05 (m, 2 H; $H_{3':5'}$), 7.79 (m, 2 H; $H_{4:4''}$), 7.50-6.22 (m, 353 H; $H_{PS\ backbone\ aromatic}$; $H_{aromatic}$, $H_{5,5''}$), 5.34 (m, 2 H; tpyOCH_2), 4.27-4.07 (broad, 1 H; *H*C-ON), 3.50-3.15 (m, 1 H; ON-C*H*), 2.26-0.39 (m, 225 H, $H_{PS\ backbone\ aliphatic}$; $C(CH_3)_3$; CH_3CHCH_3; CH_3 $_{initiating\ fragment}$, $H_{PtBA\ backbone}$). GPC (eluent DMF with NH_4PF_6 (0.8 g/L)): M_n = 30,400 g/mol, PDI = 1.13.

Terpyridine-functionalized poly(acrylic acid-*block*-styrene)]-PAA_{85}-*b*-PS_{230} **(III-18)**
The terpyridine-functionalized poly(*t*-butyl acrylate-*b*-styrene) block copolymer (0.2 g, 5.65 × 10^{-6} mol, M_n = 35,400 g/mol, PDI = 1.13) was added to anhydrous CH_2Cl_2 (10 mL) at 0 ºC and allowed to stir for 1 h. A 10-fold molar excess (relative to *t*-butyl acrylate side-chain units) of trifluoroacetic acid was added dropwise to the stirred solution, which was then allowed to warm to room temperature. Stirring was continued for 1 day, after which air was blown over the solution to remove the CH_2Cl_2 and trifluoroacetic acid. The product was collected as a white solid after dialysis with distilled water / THF. IR: v (cm^{-1}): 3025, 2927, 1711, 1600, 1580, 1564, 1493, 1452, 1405, 1247, 1170, 1027, 796, 758, 697.

Terpyridine-functionalized poly(*t*-butyl acrylate-*block*-isoprene)]-P*t*BA_{40}-*b*-PI_{22} **(III-19)**
The poly(*t*-butylacrylate) starting block (40 mg, 7.14 × 10^{-6} mol, M_n = 5,600 g/mol, PDI = 1.11) was redissolved in isoprene (1.0 g, 14.26 mmol), 0.07 equiv (with respect to macroinitiator) of free nitroxide was added, three freeze-pump-thaw cycles were applied, and the reaction mixture was heated at 120 °C for 13 h. The excess of monomer was removed *in vacuo* to yield the desired block copolymer. Yield (170 mg, 15%). ^{1}H-NMR (CD_2Cl_2): δ (ppm) = 8.60 (m, 2 H; $H_{6:6''}$), 8.54 (m, 2 H; $H_{3:3''}$), 8.05 (m, 2 H; $H_{3':5'}$), 7.79 (m, 2 H; $H_{4:4''}$), 7.60-7.02 (m, 11 H; $H_{nitroxide}$, $H_{initiating\ fragment}$, $H_{5,5''}$), 5.77 (m, 2 H; tpyOCH_2), 5.42-4.63 (m, 20 H; PI backbone), 4.53 (m, 2 H; H_2C-ON minor), 4.37 (m, 2 H; H_2C-ON major), 4.25-4.03 (broad, 1 H; ON-C*H* minor), 3.42-3.21 (m, 1 H; ON-C*H*, major), 3.00-0.30 (m, 653 H, $H_{tBA\ backbone\ aliphatic}$; $C(CH_3)_3$; CH_3CHCH_3; CH_3 $_{initiating\ fragment}$, CH_3 $_{isoprene}$). GPC (eluent $CHCl_3$, triethylamine, and 2-propanol (94:4:2): M_n = 8,900 g/mol, PDI = 1.17.

Terpyridine-functionalized poly(pentafluorostyrene-*block*-styrene)]-$PPFS_{30}$-*b*-PS_{73} **(III-20)**
The poly(pentafluorostyrene) macroinitiator (250 mg, 3.9 × 10^{-5} mol, M_n = 6,400 g/mol, PDI = 1.09) was dissolved in purified styrene (700 mg, 6.7 mmol, M/I = 170). Three freeze-pump-thaw cycles were applied, and the reaction

mixture was heated for 3 hours at 120 °C. The block copolymer was precipitated twice from dichloromethane into methanol. The precipitate was collected and dried under vacuum to yield the desired block copolymer. ^{1}H-NMR (CD_2Cl_2): δ (ppm) = 8.68 (m, 2 H; $H_{6:6''}$), 8.65 (m, 2 H; $H_{3:3''}$), 8.13 (m, 2 H; $H_{3':5'}$), 7.89 (m, 2 H; $H_{4:4''}$), 7.45-6.30 (m, 376 H; $H_{PS\ backbone}$, $H_{aromatic}$, $H_{5,5''}$), 5.30-5.20 (m, 2 H; tpyOCH_2),4.78 (m, 1 H; *H*C-ON, both diastereomers), 3.54-3.20 (m, 1 H; ON-C*H*, major & minor), 2.90-0.10 (m, 328 H; $H_{PPFS\ \&\ PS\ backbone}$, CH_3CHCH_3 major, C(CH_3)$_3$; CH_3CHCH_3 minor, CH_3CHCH_3; CH_3CH-ON). GPC (eluent DMA with LiCl 2.1 g/L): M_n = 13,100 g/mol, PDI = 1.18.

Terpyridine-functionalized poly(trifluoromethylstyrene-*block*-styrene)]-$PTFMS_{42}$-*b*-PS_{76} **(III-21)**
The poly(trifluoromethylstyrene) macroinitiator (250 mg, 3.2 × 10^{-5} mol, M_n = 7,900 g/mol, PDI = 1.16) was dissolved in purified styrene (0.9 g, 8.6 × 10^{-3} mol, M/I = 260) and 0.5 mL dry toluene. Three freeze-pump-thaw cycles were applied, and the reaction mixture was heated for 2 hours in a closed reaction vessel at 120 °C and then stopped. The block copolymer was precipitated twice from dichloromethane into methanol. The precipitate was collected and dried under vacuum to yield the desired block copolymer. ^{1}H NMR (CD_2Cl_2): δ (ppm) = 8.68 (m, 2H; $H_{6:6''}$), 8.65 (m, 2H; $H_{3:3''}$), 8.14 (m, 2H; $H_{3':5'}$), 7.88 (m, 2H; $H_{4:4''}$), 7.58-6.21 (m, 559 H; $H_{PS\ backbone}$, $H_{PTFMS\ backbone}$, $H_{aromatic}$, $H_{5,5''}$), 5.30-5.20 (m, 2H; tpyOCH_2), 4.78 (m, 1H; *H*C-ON, both diastereomers), 3.54-3.20 (m, 1H; ON-C*H*, major & minor), 2.37-0.10 (m, 373H; $H_{PTFMS\ \&\ PS\ aliphatic\ backbone}$, CH_3CHCH_3 major, C(CH_3)$_3$; CH_3CHCH_3 minor, CH_3CHCH_3; CH_3CH-ON). Elemental analysis: calcd. composition: 78.18% C, 6.05% H, 0.36% N; found: 77.47% C, 5.72% H, 0.42% N. GPC (eluent DMA with LiCl 2.1 g/L): M_n = 9,900 g/mol, PDI = 1.22.

Terpyridine-functionalized poly(trifluoromethylstyrene-*block*-*t*-butyl acrylate)]-$PTFMS_{81}$-*b*-P*t*BA_{110} **(III-22)**
The poly(trifluoromethylstyrene) macroinitiator (500 mg, 4.3 × 10^{-5} mol, M_n = 11,500 g/mol, PDI = 1.18) was dissolved in purified *t*-butyl acrylate (1.5 g, 0.023 mol, M/I = 260) and 0.5 mL dry toluene. Three freeze-pump-thaw cycles were applied, and the reaction mixture was heated for 4 hours in a closed reaction vessel at 120 °C and then stopped. The block copolymer was precipitated twice from dichloromethane into methanol. The precipitate was collected and dried under vacuum to yield the desired block copolymer. ^{1}H NMR (CD_2Cl_2): δ (ppm) = 8.68 (m, 2H; $H_{6:6''}$), 8.65 (m, 2H; $H_{3:3''}$), 8.14 (m, 2H; $H_{3':5'}$), 7.88 (m, 2H; $H_{4:4''}$), 7.50-6.40 (m, 335 H; $H_{PTFMS\ backbone}$, $H_{aromatic}$, $H_{5,5''}$), 5.30-5.20 (m, 2H; tpyOCH_2), 4.78 (m, 1H; *H*C-ON, both diastereomers), 3.54-3.20 (m, 1H; ON-C*H*, major & minor), 2.37-0.10 (m, 1582 H; $H_{PTFMS\ aliphatic\ backbone}$, H_{tBA} CH_3CHCH_3 major, C(CH_3)$_3$; CH_3CHCH_3 minor, CH_3CHCH_3; CH_3CH-ON). GPC (eluent DMA with LiCl 2.1 g/L): M_n = 15,500 g/mol, PDI = 1.23.

Terpyridine-functionalized poly(styrene-*block*-methyl acrylate-*block*-pentaflurostyrene)
]-PS_{35}-*b*-PMA_{54}-*b*-$PPFS_{97}$ **(III-23)**
The poly(styrene-*b*-methyl acrylate) macroinitiator (100 mg, 1.1 × 10^{-5} mol, M_n = 9,100 g/mol, PDI = 1.23) was dissolved in purified 2,3,4,5,6-pentafluorostyrene (1.5 g, 7.7 mmol, M/I = 700) and 1 mL dry THF. Three freeze-pump-thaw cycles were applied, and the reaction mixture was heated for 3 hours at 120 °C. The block copolymer was precipitated twice from dichloromethane into methanol. The precipitate was collected and dried under vacuum to yield the desired block copolymer. ^{1}H-NMR (CD_2Cl_2): δ (ppm) = 8.68 (m, 2 H; $H_{6:6''}$), 8.65 (m, 2 H; $H_{3:3''}$), 8.13 (m, 2 H; $H_{3':5'}$), 7.89 (m, 2 H; $H_{4:4''}$), 7.45-6.35 (m, 186 H; $H_{PS\ backbone}$, $H_{aromatic}$, $H_{5,5''}$), 5.30-5.20 (m, 2 H; tpyOCH_2),4.78 (m, 1 H; *H*C-ON, both diastereomers), 3.93-3.20 (m, 175 H; ON-C*H*, major & minor, $OCH_{3\ MA}$), 2.90-0.15 (m, 586 H; $H_{PPFS\ \&\ PS\ \&\ PMA\ backbone}$, CH_3CHCH_3 major, C(CH_3)$_3$; CH_3CHCH_3 minor, CH_3CHCH_3; CH_3CH-ON). GPC (eluent DMA with LiCl 2.1 g/L): M_n = 12,600 g/mol, PDI = 1.28.

Terpyridine-functionalized poly(styrene-*block*-*t*-butyl acrylate-*block*-trifluoromethylstyrene)
]-PS_{35}-*b*-P*t*BA_{25}-*b*-$PTFMS_{20}$ **(III-24)**
The poly(styrene-*b*-*t*-butyl acrylate) macroinitiator (150 mg, 1.1 × 10^{-5} mol, M_n = 7,400 g/mol, PDI = 1.15) was dissolved in purified *para*-trifluoromethylstyrene (530 mg, 3.0 mmol, M/I = 150). Three freeze-pump-thaw cycles were applied, and the reaction mixture was heated for 2.5 hours at 120 °C. The block copolymer was precipitated twice from dichloromethane into methanol. The precipitate was collected and dried under vacuum to yield the desired block copolymer. ^{1}H-NMR (CD_2Cl_2): δ (ppm) = 8.68 (m, 2 H; $H_{6:6''}$), 8.65 (m, 2 H; $H_{3:3''}$), 8.13 (m, 2 H; $H_{3':5'}$), 7.89 (m, 2 H; $H_{4:4''}$), 7.45-6.35 (m, 266 H; $H_{PS\ backbone}$, $H_{aromatic}$, $H_{5,5''}$), 5.30-5.20 (m, 2 H; tpyOCH_2),4.78 (m, 1 H; *H*C-ON, both diastereomers), 3.54-3.20 (m, 1H; ON-C*H*, major & minor), 2.90-0.41 (m, 586 H; $H_{PPFS\ \&\ PS\ \&\ PMA\ backbone}$, CH_3CHCH_3 major, C(CH_3)$_3$; CH_3CHCH_3 minor, CH_3CHCH_3; CH_3CH-ON). GPC (eluent DMA with LiCl 2.1 g/L): M_n = 8,700 g/mol, PDI = 1.33.

General procedure of the post-modification reaction by microwave irradiation
The polypentafluorostyrene containing polymer and the corresponding amine-functionalized compound were dissolved in *N*-methylpyrrolidone (NMP). The mixture was heated for 20 min at 95 °C in a sealed microwave vial.

Terpyridine-functionalized poly(pentafluorostyrene-*graft*-terpyridine)]-$PPFS_{30}$-*g*-tpy_6 **(III-25)**
Polypentafluorostyrene (350 mg, M_n = 6,400 g/mol, PDI = 1.09) and 5-(2,2':6'2"-terpyridine-4'-yloxy)-pentylamine (200 mg) were dissolved in 2.5 mL NMP. The polymer was purified by precipitation into ice-cold methanol. ^{1}H-NMR (CD_2Cl_2): δ (ppm) = 8.64 (m, 28 H; $H_{6:6''}$, $H_{3:3''}$), 8.12 (m, 2 H; $H_{3':5'\ end\ group}$), 8.02 (m, 12 H; $H_{3':5'}$), 7.86 (m, 14

H; $H_{4:4''}$), 7.45-6.90 (m, 23 H; $H_{aromatic}$, $H_{5,5''}$), 5.30-5.20 (m, 2 H; tpyOCH_2), 4.78 (m, 1 H; *H*C-ON, both diastereomers), 4.35-4.05 (m, 12 H; OCH_2), 3.55-3.20 (m, 13 H; ON-C*H*, major & minor, Ph-NCH_2), 3.00-0.10 (m, 145 H; $H_{PPFS\ backbone}$, CH_3CHCH_3 major, C(CH_3)$_3$; CH_3CHCH_3 minor, CH_3CHCH_3; CH_3CH-ON, O-CH_2CH_2 CH_2CH_2 CH_2N). GPC (eluent DMA with LiCl 2.1 g/L): M_n = 5,500 g/mol, PDI = 1.13.

Terpyridine-functionalized poly(styrene-*block*-pentafluorostyrene-*graft*-(tpy)Ir(ppy)$_2$)]-PS_{39}-*b*-$PPFS_{89}$-*g*-[(tpy)Ir(ppy_2)]$_{2.5}$ **(III-26)**
Terpyridine-functionalized poly($styrene_{39}$-*b*-$pentafluorostyrene_{89}$) (100 mg, M_n = 21,900 g/mol, PDI = 1.20) and Iridium(III)-(2,2':6'2"-terpyridine-4'-yloxy)-pentylamine)(ppy_2) (PF_6) (20 mg) were dissolved in 0.5 mL NMP. The polymer was purified by precipitation into ice-cold methanol. ^{1}H-NMR (CD_2Cl_2): δ (ppm) = 8.88 (m, 1 H; H^6-ppy), 8.66 (m, 4 H; $H_{6:6''}$, $H_{3:3''}$), 8.20-6.20 (m, 265 H; $H_{3':5'}$, $H_{4:4''}$, $H_{aromatic}$, $H_{5,5''}$, H^5-ppy, H^4-ppy, H^3-ppy, H^5-ppy, H^4-ppy, $H^{3'}$-ppy, Ir-complexed tpy), 5.91 (m, 1 H; $H^{6'}$-ppy), 5.46 (m, 1 H; $H^{6'}$-ppy), 5.30-5.20 (m, 2 H; tpyOCH_2), 4.78 (m, 1 H; *H*C-ON, both diastereomers), 4.27 (m, 5 H; OCH_2), 3.60-3.20 (m, 6 H; ON-C*H*, major & minor, Ph-NCH_2), 3.00-0.10 (m, 418 H; $H_{PPFS\ \&\ PS\ backbone}$, CH_3CHCH_3 major, C(CH_3)$_3$; CH_3CHCH_3 minor, CH_3CHCH_3; CH_3CH-ON, O-CH_2CH_2 CH_2CH_2 CH_2N).

Terpyridine-functionalized poly(pentafluorostyrene-*graft*-ethylene glycol)]-$PPFS_{30}$-*g*-$(PEG_{75})_9$ **(III-27)**
Polypentafluorostyrene (100 mg, M_n = 6,400 g/mol, PDI = 1.09) and NH_2-functionalized poly(ethylene glycol) (600 mg, M_w = 3,400 g/mol) were dissolved in 0.7 mL NMP. The polymer was purified by preparative SEC and precipitation into ice-cold diethyl ether. ^{1}H-NMR (CD_2Cl_2): δ (ppm) = 8.68 (m, 2 H; $H_{6:6''}$), 8.65 (m, 2 H; $H_{3:3''}$), 8.13 (m, 2 H; $H_{3':5'}$), 7.89 (m, 2 H; $H_{4:4''}$), 7.45-6.95 (m, 11 H; $H_{aromatic}$, $H_{5,5''}$), 5.30-5.20 (m, 2 H; tpyOCH_2),4.78 (m, 1 H; *H*C-ON, both diastereomers), 4.20-3.20 (m, 2701 H; OC$H_{2\ PEG\ backbone}$, ON-C*H*, major & minor), 3.09-1.70 (m, 91 H; $H_{PPFS\ backbone}$, CH_3CHCH_3 major), 1.60-0.15 (m, 18 H; C(CH_3)$_3$; CH_3CHCH_3 minor, CH_3CHCH_3; CH_3CH-ON). GPC (eluent DMA with LiCl 2.1 g/L): M_n = 27,700 g/mol, PDI = 1.12.

Terpyridine-functionalized poly(pentafluorostyrene-*graft*-pentanol)]-$PPFS_{30}$-*g*-$(AP)_9$ **(III-28)**
Polypentafluorostyrene (100 mg, M_n = 6,400 g/mol, PDI = 1.09) and NH_2-pentanol (17 mg, M = 103 g/mol) were dissolved in 0.5 mL NMP. The polymer was precipitated into cold methanol. ^{1}H-NMR ($CDCl_3$): δ (ppm) = 8.80 (m, 4 H; $H_{6:6''}$ & $H_{3:3''}$), 8.24 (m, 2 H; $H_{3':5'}$), 8.02 (m, 2 H; $H_{4:4''}$), 7.65-6.89 (m, 11 H; $H_{aromatic}$, $H_{5,5''}$), 5.47-5.24 (m, 2 H; tpyOCH_2), 4.64 (m, 1 H; *H*C-ON, both diastereomers), 3.67 (m, 18 H; CH_2OH) 3.54-3.20 (m, 19 H; CH_2NH, ON-C*H*, major & minor), 3.09-1.70 (m, 109 H; $H_{PPFS\ backbone}$, CH_3CHCH_3 major, CH_2NH, CH_2OH), 1.69-0.15 (m, 72 H; C(CH_3)$_3$; CH_3CHCH_3 minor, CH_3CHCH_3; CH_3CH-ON, (CH_2)$_3CH_2$OH). GPC (eluent DMA with LiCl 2.1 g/L): M_n = 5,800 g/mol, PDI = 1.13.

Terpyridine-functionalized poly(pentafluorostyrene-*graft*-lactide)]-$PPFS_{30}$-*g*-$(PLA_{11})_9$ **(III-29)**
Terpyridine-functionalized poly(pentafluorostyrene-*g*-pentanol) (40 mg, M_n = 5,800 g/mol, PDI = 1.09), *L*-lactide (150 mg, M = 144 g/mol) and 0.4 mL dry toluene were added to a polymerization tube and stirred at 100 °C for 10 minutes. Subsequently, the polymerization was started by adding three drops of the catalyst stannous octoate. The desired graft copolymer was purified from residual monomer by precipitation into cold hexane. ^{1}H-NMR ($CDCl_3$): δ (ppm) = 8.60 (m, 4 H; $H_{6:6''}$ & $H_{3:3''}$), 8.05 (m, 2 H; $H_{3':5'}$), 7.82 (m, 2 H; $H_{4:4''}$), 7.40-6.85 (m, 11 H; $H_{aromatic}$, $H_{5,5''}$), 5.47-5.24 (m, 2 H; tpyOCH_2), 5.19-4.99 (m, 200 H, lactide C*H* (CH_3)O), 4.64 (m, 1 H; *H*C-ON, both diastereomers), 4.26 (m, 11 H; lactide-end group C*H*(CH_3)OH), 3.67 (m, 18 H; CH_2O-lac) 3.54-3.20 (m, 19 H; CH_2NH, ON-C*H*, major & minor), 3.09-0.30 (m, 736 H; $H_{PPFS\ backbone}$, CH_3CHCH_3 major, CH_2NH, CH (CH_3)O, C(CH_3)$_3$; CH_3CHCH_3 minor, CH_3CHCH_3; CH_3CH-ON, CH_2CH_2OH). GPC (eluent DMA with LiCl 2.1 g/L): M_n = 27,200 g/mol, PDI = 1.12.

Terpyridine-functionalized poly((pentafluorostyrene-*graft*-pentanol)-*block*-styrene)]-$PPFS_{30}$-*g*-$(AP)_7$-*b*-PS_{73} **(III-30)**
Poly(pentafluorostyrene-*b*-styrene) (200 mg, M_n = 14,000 g/mol, PDI = 1.18) and NH_2-pentanol (15 mg, M = 103 g/mol) were dissolved in 0.5 mL NMP. The polymer was precipitated into cold methanol. ^{1}H-NMR (CD_2Cl_2): δ (ppm) = 8.69 (m, 2 H; $H_{6:6''}$), 8.66 (m, 2 H; $H_{3:3''}$), 8.13 (m, 2 H; $H_{3':5'}$), 7.89 (m, 2 H; $H_{4:4''}$), 7.60-6.30 (m, 376 H; $H_{PS\ backbone}$, $H_{aromatic}$, $H_{5,5''}$), 5.30-5.20 (m, 2 H; tpyOCH_2),4.78 (m, 1 H; *H*C-ON, both diastereomers), 3.98-3.56 (m, 14 H; CH_2OH), 3.54-3.20 (m, 15 H; CH_2NH, ON-C*H*, major & minor), 2.90-0.32 (m, 384 H; $H_{PPFS\ \&\ PS\ backbone}$, CH_3CHCH_3 major, C(CH_3)$_3$; CH_3CHCH_3 minor, CH_3CHCH_3; CH_3CH-ON, CH_2NH, CH_2OH, (CH_2)$_3CH_2$OH). GPC (eluent DMA with LiCl 2.1 g/L): M_n = 13,400 g/mol, PDI = 1.18.

Terpyridine-functionalized poly((pentafluorostyrene-*graft*-Br)-*block*-styrene)]-$PPFS_{30}$-*g*-$(Br)_7$-*b*-PS_{73} **(III-31)**
Terpyridine-functionalized poly((pentafluorostyrene-*g*-pentanol)-*b*-styrene) (100 mg, M_n = 13,400 g/mol, PDI = 1.18) was dissolved in 2 mL of methylene chloride (CH_2Cl_2). Triethylamine (37 mg, M = 101 g/mol) was added to the mixture. Afterwards 2-bromoisobutyryl bromide (90 mg, M = 230 g/mol) diluted in 1 mL methylene chloride was added dropwise to the mixture and was stirred at room temperature for 24 hours. The polymer was purified by precipitation into methanol. ^{1}H-NMR ($CDCl_3$): δ (ppm) = 8.73 (m, 4 H; $H_{6:6''}$ & $H_{3:3''}$), 8.18 (m, 2 H; $H_{3':5'}$), 7.92

(m, 2 H; $H_{4:4"}$), 7.55-6.28 (m, 376 H; $H_{aromatic}$, $H_{5,5"}$), 5.43-5.18 (m, 2 H; tpyOCH_2), 4.64 (m, 1 H; *H*C-ON, both diastereomers), 4.28-4.07 (m, 14 H; CH_2O-CO) 3.65-3.20 (m, 15 H; CH_2NH, ON-C*H*, major & minor), 3.13-0.26 (m, 419 H; $H_{PPFS\ \&\ PS\ backbone}$, CH_3CHCH_3 major, $C(CH_3)_3$; CH_3CHCH_3 minor, CH_3CHCH_3; CH_3CH-ON, CH_2NH, $(CH_2)_3CH_2O$, CO-CBr$(CH_3)_2$). GPC (eluent DMA with LiCl 2.1 g/L): M_n = 12,600 g/mol, PDI = 1.19.

Terpyridine-functionalized poly((pentafluorostyrene-*graft*-OEGMA)-*block*-styrene)
]-$PPFS_{30}$-*g*-$(POEGMA_{10})_7$-*b*-PS_{73} **(III-32)**
Terpyridine-functionalized poly((pentafluorostyrene-*g*-Br)-*b*-styrene) (60 mg, M_n = 12,600 g/mol, PDI = 1.19) and OEGMA (800 mg, M_n = 475 g/mol) were dissolved in 4 mL dry toluene and deoxygenated by bubbeling argon though the polymer solution for 5 minutes. In a different vial, a mixture of PMDETA (6.6 mg, M_n = 173 g/mol), CuBr (5 mg, M_n = 143 g/mol) and toluene were also deoxygenated in the same way. Afterwards, the polymer solution was transferred to the catalyst solution and heated to 70 °C for 5 h. The solution was filtered over basic aluminium oxide, the excess solvent was removed and the polymer was precipitated twice into ice-cold hexane. ^{1}H-NMR (CD_2Cl_2): δ (ppm) = 8.69 (m, 2 H; $H_{6:6"}$), 8.66 (m, 2 H; $H_{3:3"}$), 8.13 (m, 2 H; $H_{3':5'}$), 7.89 (m, 2 H; $H_{4:4"}$), 7.60-6.30 (m, 376 H; $H_{PS\ backbone}$, $H_{aromatic}$, $H_{5,5"}$), 5.43-5.18 (m, 2 H; tpyOCH_2), 4.64 (m, 1 H; *H*C-ON, both diastereomers), 4.25-3.95 (m, 140 H; CH_2O-CO), 3.90-3.20 (m, 2535 H; $H_{OEGMA\ backbone}$, CH_2NH, ON-C*H*, major & minor), 3.10-0.30 (m, 769 H; $H_{PPFS\ \&\ PS\ backbone}$, $H_{OEGMA\ aliph.\ backbone}$, CH_3CHCH_3 major, $C(CH_3)_3$; CH_3CHCH_3 minor, CH_3CHCH_3; CH_3CH-ON, CH_2NH, $(CH_2)_3CH_2O$, CO-C$(CH_3)_2$). GPC (eluent DMA with LiCl 2.1 g/L): M_n = 27,700 g/mol, PDI = 1.15.

3.5 References

1 B.G.G. Lohmeijer, U.S. Schubert, *J. Polym. Sci., Part A: Polym. Chem.* **2003**, *41*, 1413.
2 B.G.G. Lohmeijer, U.S. Schubert, *J. Polym. Sci., Part A: Polym. Chem.* **2004**, *42*, 4016.
3 C. Ott, B.G.G. Lohmeijer, D. Wouters, U.S. Schubert, *Macromol. Chem. Phys.* **2006**, *207*, 1439.
4 A.D. Ievins, X. Wang, A.O. Moughton, J. Skey, R.K. O'Reilly, *Macromolecules* **2008**, *41*, 2998.
5 K.J. Calzia, G.N. Tew, *Macromolecules* **2002**, *35*, 6090.
6 K.A. Aamer, G.N. Tew, *Macromolecules* **2004**, *37*, 1990.
7 R. Shunmugam, G.N. Tew, *J. Polym. Sci., Part A: Polym. Chem.* **2005**, *43*, 5831.
8 K. Matyjaszewski, J. Xia, *Chem. Rev.* **2001**, *101*, 2921.
9 M. Kamigaito, T. Ando, M. Sawamoto, *Chem. Rev.* **2001**, *101*, 3689.
10 C.J. Hawker, A.W. Bosman, E. Harth, *Chem. Rev.* **2001**, *101*, 3661.
11 H. Fischer, *Chem. Rev.* **2001**, *101*, 3581.
12 G. Moad, E. Rizzardo, S.H. Thang, *Polymer* **2008**, *49*, 1079.
13 G. Moad, D.H. Solomon, *The Chemistry of Free Radical Polymerization*, 2nd ed.; Elsevier: Amsterdam, **2006**.
14 D.H. Solomon, E. Rizzardo, P. Cacioli, US Patent 4, 581, 429, **1985**.
15 M.K. Georges, R.P.N. Veregin, P.M. Kazmaier, G.K. Hamer, *Macromolecules* **1993**, *26*, 2987.
16 D. Benoit, V. Chaplinski, R. Braslau, C.J. Hawker, *J. Am. Chem. Soc.* **1999**, *121*, 3904.
17 D. Benoit, E. Harth, P. Fox, R.M. Waymouth, C.J. Hawker, *Macromolecules* **2000**, *33*, 363.
18 A.W. Bosman, R. Vestberg, A. Heumann, J.M.J. Fréchet, C.J. Hawker, *J. Am. Chem. Soc.* **2003**, *125*, 715.
19 M. Rodlert, E. Harth, I. Rees, C.J. Hawker, *J. Polym. Sci., Part A: Polym. Chem.* **2000**, *38*, 4749.
20 E. Harth, C.J. Hawker, W. Fan, R.M. Waymouth, *Macromolecules* **2001**, *34*, 3856.
21 S. Marque, C. Le Mercier, P. Tordo, H. Fischer, *Macromolecules* **2000**, *33*, 4403.
22 H. Fischer, *J. Am. Chem. Soc.* **1986**, *108*, 3925.
23 H. Fischer, *Macromolecules* **1997**, *30*, 5666.
24 T. Kothe, S. Marque, R. Martschke, M. Popov, H. Fischer, *J. Chem. Soc. Perkin Trans. 2* **1998**, 503.
25 H. Fischer, *J. Polym. Sci., Part A: Polym. Chem.* **1999**, *37*, 1885.
26 T. Fukada, A. Goto, K. Ohno, *Macromol. Rapid Commun*. **2000**, *21*, 151.
27 J.-F. Lutz, P. Lacroix-Desmazes, B. Boutevin, *Macromol. Rapid Commun*. **2001**, *22*, 189.
28 F.R. Mayo, *J. Am. Chem. Soc.* **1968**, *90*, 1289.

29 S. Schmatloch, A.M.J. van den Berg, A.S. Alexeev, H. Hofmeier, U.S. Schubert, *Macromolecules* **2003**, *36*, 9943.
30 J. Scheirs, *"Modern Fluoropolymers: High Performance Polymers for Diverse Applications",* John Wiley & Sons: Chichester, **1997**.
31 M.A. Dourges, B. Charleux, J.P. Vairon, J.C. Blais, G. Bolbach, J.C. Tabet, *Macromolecules* **1999**, *32*, 2495.
32 A. Bartsch, W. Dempwolf, M. Bothe, S. Flakus, G. Schmidt-Naake, *Macromol. Rapid Commun*. **2003**, *24*, 614.
33 W. Dempwolf, S. Flakus, G. Schmidt-Naake, *Macromol. Symp*. **2007**, *259*, 416.
34 C.R. Becer, R.M. Paulus, R. Hoogenboom, U.S. Schubert, *J. Polym. Sci., Part A: Polym. Chem.* **2006**, *44*, 6202.
35 M. Souaille, H. Fischer, *Macromolecules* **2002**, *35*, 248.
36 A.M. North, A.M. Scallan, *Polymer* **1964**, *5*, 447.
37 J. Brandrup, E.H. Immergut, E.A. Grulke, *Polymer Handbook*, 4th ed., Wiley-Interscience, **1999**.
38 D. Jayaprakash, Y. Kobayashi, S. Watanabe, T. Arai, H. Sasai, *Tetrahedron*: *Asymmetry* **2003**, *14*, 1587.
39 Q. Tran-Cong, *Photochromic Reactions, Polarization-induced, Polymeric Materials Encyclopedia*, CRC: New York, **1996**.
40 D.W. Kim, C.W. Lee, M.S. Gong, *J. Lumin.* **2002**, *99*, 205.
41 C.W. Lee, S.W. Joo, J. Ko, J.S. Kim, S.S. Lee, M.S. Gong, *Synth. Met.* **2002**, *126*, 97.
42 S. Satoh, H. Suzuki, Y. Kimata, A. Kuriyama, *Synth. Met.* **1996**, *79*, 97.
43 S. Paul, O. Halle, H. Einsiedel, B. Menges, K. Müllen, W. Knoll, *Thin Solid Films* **1996**, *288*, 150.
44 D. Cao, H. Meier, *Angew. Chem. Int. Ed.* **2001**, *40*, 186.
45 J. Matsui, Y. Ochi, K. Tamaki, *Chem. Lett.* **2006**, *35*, 80.
46 Y. Zheng, M. Micic, S.V. Mello, M. Mabrouki, F.M. Andreopoulos, V. Konka, S.M. Pham, R.M. Leblanc, *Macromolecules* **2002**, *35*, 5228.
47 J.P. Sauvage, J.P. Collin, J.C. Chambron, S. Guillerez, C. Coudret, V. Balzani, F. Barigelletti, L. De Cola, L. Flamigni, *Chem. Rev.* **1994**, *94*, 993.
48 P. Lacroix-Desmazes, J.-P. Lutz, F. Chauvin, R. Severac, B. Boutevin, *Macromolecules* **2001**, *34*, 8866.
49 M.L. Miller, C.E. Rauhut, *J. Polym. Sci.* **1959**, *38*, 63.
50 C.-A. Fustin, P. Guillet, M.J. Misner, T.P. Russell, U.S.Schubert, J.-F. Gohy, *J. Polym. Sci., Part A: Polym. Chem.* **2008**, *46*, 4719.
51 K.A. Davis, K. Matyjaszewski, *Macromolecules* **2000**, *33*, 4039.
52 Q. Ma, K.L. Wooley, *J. Polym. Sci., Part A: Polym. Chem.* **2000**, *38*, 4805.
53 R.D. Chambers, J.S. Waterhouse, D.L.H. Williams, *J. Chem. Soc. Perkin II* **1977**, 585.
54 R.D. Chambers, D. Close, D.L.H. Williams, *J. Chem. Soc. Perkin II* **1980**, 778.
55 K.M. Kadish, C. Araullo-McAdams, B.C. Han, M.M. Franzen, *J. Am. Chem. Soc.* **1990**, *112*, 8364.
56` P. Battioni, O. Brigaud, H. Desvaux, D. Mansuy, T.G. Taylor, *Tetrahedron Lett.* **1991**, *32*, 2893.
57 H.C. Kolb, M.G. Finn, K.B. Sharpless, *Angew. Chem. Int. Ed.* **2001**, *40*, 2004.
58 H.C. Kolb, K.B. Sharpless, *Drug Discovery Today* **2003**, *8*, 1128.
59 D. Fournier, R. Hoogenboom, U.S. Schubert, *Chem. Soc. Rev.* **2007**, *36*, 1369.
60 D. Samaroo, C.E. Soll, L.J. Todaro, C.M. Drain, *Org. Lett.* **2006**, *8*, 4985.
61 M. Rehahn, *Acta Polym.* **1998**, *49*, 201.
62 D.G. Kurth, M. Schütte, J. Wen, *Colloids Surf., A* **2002**, *198-200*, 633.
63 E. Holder, V. Marin, M.A.R. Meier, U.S. Schubert, *Macromol. Rapid Commun*. **2004**, *25*, 1491.
64 A.V. Dobrynin, I.Y. Erukhimovich, *Macromolecules* **1993**, *26*, 276.
65 H. Shinoda, P.J. Miller, K. Matyjaszewski, *Macromolecules* **2001**, *34*, 3186.

CHAPTER 4

Metallo-supramolecular (block) copolymers: Synthesis and self-assembly investigations in solution

Abstract

In this chapter the complexation strategies described in Chapter 2 were applied to the polymers synthesized in Chapter 3 by nitroxide-mediated radical polymerization (NMRP) resulting in the construction of new polymeric materials. The ability to form heteroleptic complexes provides a straightforward synthetic pathway to synthesize a large variety of metal-containing block copolymers. Commercially available poly(ethylene glycol) was post-functionalized with the terpyridine entity and represented a reliable building block for the targeted synthesis of well-defined amphiphilic block copolymers, including A-[Ru]-B diblock copolymers, A-B-[Ru]-C triblock terpolymers as well as A-B-C-[Ru]-D tetrablock quaterpolymers. The synthesized block copolymers were characterized by means of ^{1}H NMR and UV-vis spectroscopy as well as GPC. Due to the amphiphilic character of the materials, micelles could be obtained in different solvents which were subsequently investigated by AFM and TEM, respectively. In addition, terpyridine-functionalized polymers provided the opportunity to prepare a series of light-emitting iridium(III) compounds which were accomplished by a bridge-splitting reaction of dimeric iridium(III) precursor complexes. The utilization of differently substituted cyclometallating ligands allows the facile approach to tune the optical properties of the polymers.

Parts of this chapter have been and will be published: C. Ott, B.G.G. Lohmeijer, D. Wouters, U.S. Schubert, *Macromol. Chem. Phys.* **2006**, *207*, 1439-1449; C. Ott, D. Wouters, H.M.L. Thijs, U.S. Schubert, *J. Inorg. Organometal. Polym. Mater.* **2007**, *17*, 241-249; C. Ott, R. Hoogenboom, U.S. Schubert, *Chem. Commun.* **2008**, 3516-3518; C. Ott, R. Hoogenboom, S. Hoeppener, D. Wouters, J.-F. Gohy, U.S. Schubert, *Soft Matter* **2009**, in press.

4.1 Introduction

The previous chapter dealt with the synthesis and characterization of various polymers with different compositions and architectures (homopolymers, block copolymers, graft copolymers and random copolymers). Even though the polymers are composed of different blocks, all of them have the initiating fragment containing the terpyridine ligand in common. The main focus in this chapter will be on a relatively new type of block copolymer. Usually, block copolymers are defined to consist of two or more blocks of different monomers connected via covalent bonds. In this work, block copolymers consisting of metallo *bis*-terpyridine complexes as supramolecular linkers between two of the constituting blocks are described. A schematic representation of this typical polymeric structure is shown in Scheme 4.1.

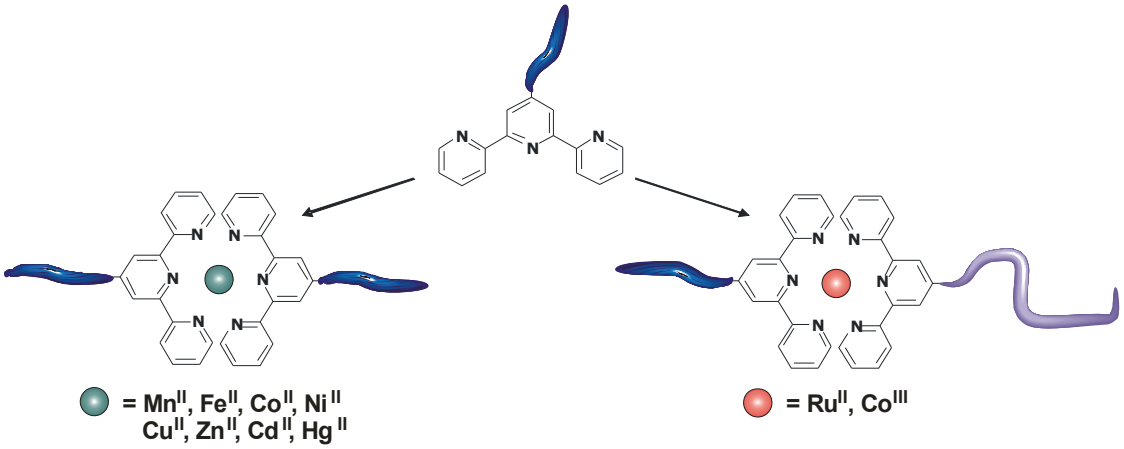

Scheme 4.1 *Schematic representation of the bis-terpyridine complex formation. The left route displays the synthetic approach for the preparation of A-[•]-A homo-dimers whereas the right pathway shows an effective method towards the synthesis of A-[•]-B block copolymers.*

An important feature of metallo-supramolecular block copolymers is the reversibility of the metal-to-ligand coordination, due to the relatively weak non-covalent interaction between the incorporated metal ion and the respective ligand. This property is essential for the design and the application of smart and switchable materials.[1] In supramolecular chemistry, the appropriate choice of the metal and the ligand permits to specifically control the strength of the non-covalent interactions as well as the resulting properties. Therefore, a careful selection of the coordinating system is necessary to allow the targeted introduction of any desired electrical, photophysical or conductivity properties. The vast majority of compounds synthesized in this chapter possesses ruthenium(II) as transition metal ion. Ruthenium(II) *bis*-terpyridine complexes feature very high stability constants and are therefore considered as inert metal ions which allow a stepwise construction of the metal complex using differently substituted ligands (see Chapter 2). In case of terpyridine-functionalized polymers, this leads to the formation of block copolymers, where the metal complex is located at the interface between the two blocks. Of course, this requires the synthesis of a polymer *mono*-complex, which is described in Section 4.2. So far, mostly linear poly(ethylene glycol) (PEG) and polystyrene (PS) were utilized as constituting polymers. Section 4.3 demonstrates the optimization of the complexation reaction between PEG and PS. The optimized conditions were subsequently applied to prepare a small library of PS_x-[Ru]-PEG_{70}. Moreover, the same section contains the preparation and characterization of several A-[Ru]-B diblock copolymers, A-B-[Ru]-C triblock terpolymers as well as A-B-C-[Ru]-D tetrablock quaterpolymers using the well-defined polymers from Chapter 3 as building blocks. Section 4.4 represents the micellization behavior of one particular triblock terpolymer. In the last section

(Section 4.5), the synthesis and characterization of iridium-containing polymers will be discussed. Differently substituted cyclometallating ligands were used for the complexation with various terpyridine-functionalized polymers. This approach leads to light-emitting polymeric materials revealing interesting optical properties.

4.2 Polymeric ruthenium(III) *mono*-complexes

As it was already demonstrated in Chapter 2, terpyridine *mono*-complexes are readily prepared by reaction with $RuCl_3$. Small terpyridine-functionalized organic molecules precipitate from the reaction mixture after the *mono*-complex had been formed. Simple filtration and thorough washing of the residue afforded the analytically pure compound. When terpyridine-functionalized polymers are converted into the corresponding *mono*-complexes, the solubility of the compound is governed by the polymer itself and not by the complex. A procedure for the successful formation of ruthenium(III) *mono*-complexes is described in literature.[2] Here, anhydrous $RuCl_3$ is partially dissolved and partially suspended in dry *N,N*-dimethylformamide (DMF). The salt-solvent mixture is heated to 130 °C for 30 minutes where a color change of the solution from black to blue to green to dark brown can be observed. Although, the exact intermediates are not clarified yet, the bluish and greenish colors are thought to originate from ruthenium clusters with metal-metal interactions, whereas the brown color presumably originates from molecularly dissolved ruthenium(III) having three chloride ligands and up to three solvent ligands attached.[3-6] In order to prepare the corresponding *mono*-complexes the terpyridine ligand had to be first introduced into the end of a polymer chain. For this purpose, hydroxy-functionalized poly(ethylene glycol) was reacted with commercially available 4'-chloro-2,2':6'2"-terpyridine.[7-9] This synthetic approach usually allows a straightforward access to end group functionalized monomers as well as polymers and afforded **1** in high yield (85%). Since PEG is a very hygroscopic polymer, traces of water were removed in an azeotropic mixture with toluene. Subsequently, the terpyridine-functionalized PEG was added dropwise to a solution of pre-heated degassed *N,N*-dimethylacetamide (DMA) containing a slight excess of $RuCl_3$ (Scheme 4.2).

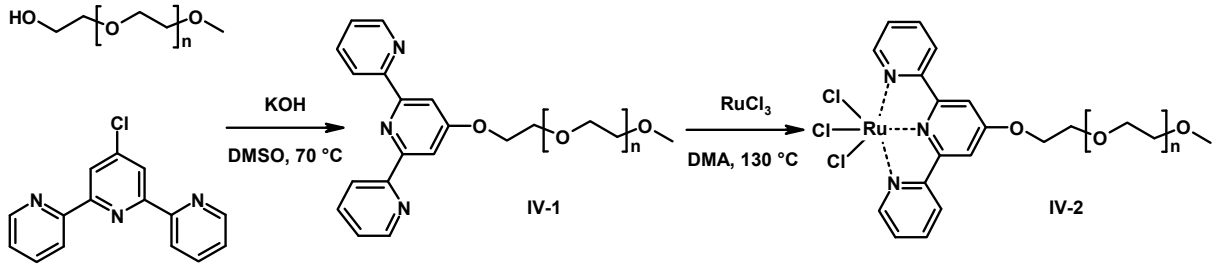

Scheme 4.2 *Schematic representation of the synthetic approach for the preparation of terpyridine-functionalized poly(ethylene glycol) and its corresponding mono-complex.*

The formation of the *mono*-complex **IV-2** can be followed by UV-vis spectroscopy since a characteristic absorption band appears at approximately 400 nm which can be attributed to a metal-to-ligand charge transfer. On the other hand, ^{1}H NMR spectroscopy is a suitable tool to quantitatively determine the conversion of the reaction (Figure 4.1). Thereby, the characteristic terpyridine signals disappear in time in the region between 7 to 9 ppm due to the paramagnetic nature of the Ru(III) metal ion.[10-12] The polymer was further characterized by GPC using a photo-diode array detector (PDA). An UV-vis spectrum of the eluent (containing the analyte) is measured at any retention time. Figure 4.1 shows the corresponding three dimensional elution

profile of the polymeric *mono*-complex. An extracted UV-vis spectrum at the maximum elution volume (10.35 mL) is displayed in the inset revealing the typical MLCT-band for *mono*-terpyridine Ru(III) complexes at around 400 nm.

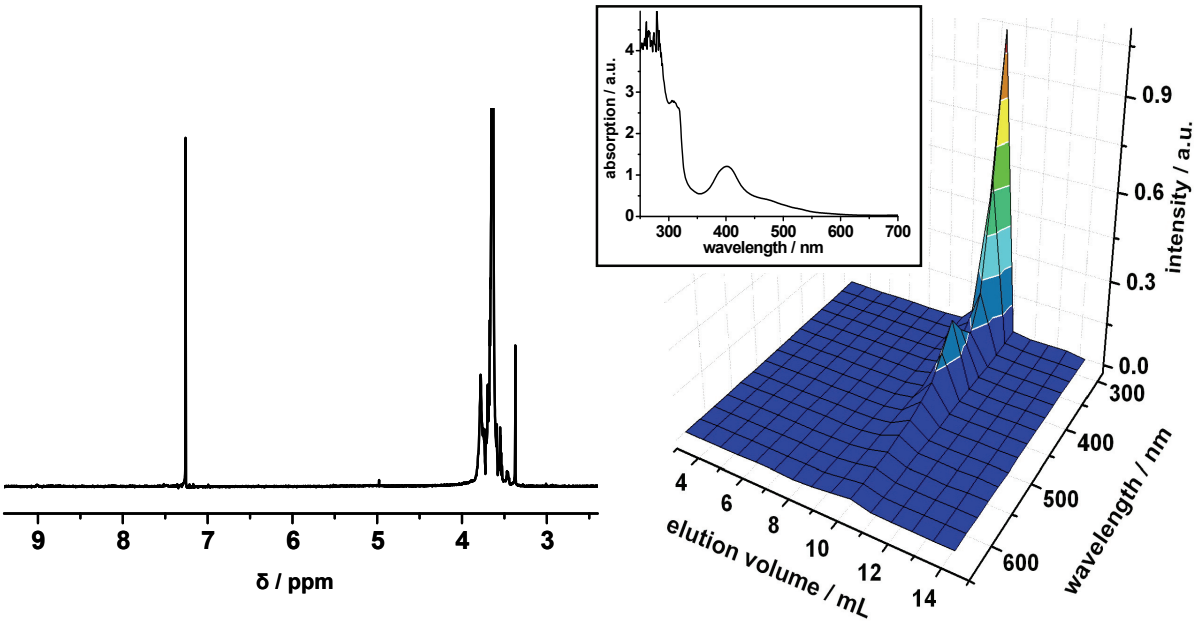

Figure 4.1 *^{1}H NMR spectrum of PEG_{70}-[$RuCl_3$* ***IV-2*** *proving the formation of the mono-complex since the terpyridine signals vanished. The three dimensional GPC-chromatogram (coupled in-line with a photo-diode array detector) reveals the characteristic absorption band at 400 nm (right).*

As it could be demonstrated by the different characterization techniques, the preparation of polymeric *mono*-complexes is feasible when working under dry and oxygen-free conditions. In the following section, the successfully prepared PEG_{70}-[$RuCl_3$ *mono*-complex **IV-2** was utilized as a key compound for the design of several amphiphilic block copolymers which are linked together *via* the metal complex.

4.3 Block copolymers based on ruthenium *bis*-terpyridine complexes

Block copolymers are composed of at least two chemically different blocks that are covalently linked to each other.[13,14] If the block copolymer consists of thermodynamically incompatible blocks, a wide range of microstructures in bulk[14] and in solution[15-17] can emerge due to the inherent immiscibility of the different polymer blocks within the same material. The chemical link between the different segments prevents phase separation at the macroscopic length scale; however, regular structures can be designed with periodicities of the phases in the nanometer scale. Depending on the composition of the block copolymers and the interactions between the blocks different morphologies can be adjusted, whereby the microstructures contribute to the physical and chemical properties of the corresponding material. Such systems are employed in (industrial) applications ranging from high impact plastics,[18,19] thermoplastic elastomers,[20] additives,[21] porous materials[22,23] as well as drug delivery systems[24] and information storage.[21,25] Generally, block copolymers are prepared by the addition of a second monomer to “living” or controlled polymerization processes. However, these methods suffer from restrictions due to monomer incompatibility as well as incomplete re-initiation of the second block. Hence, the

application of metallo-supramolecular chemistry[26] is an ideal approach to connect individual blocks together. The non-covalent bond interactions of chelating ligands such as terpyridines in combination with the respective Ru(III)/Ru(II)-chemistry[27] ensures the formation of the desired architectures due to the high complex stability caused by the strong metal-to-ligand (d-π*) back donation.[24,28]

4.3.1 Optimization of the complexation reaction: PS-[Ru]-PEG

The complexation process for the construction of heteroleptic polymeric *bis*-terpyridine ruthenium complexes still poses a challenge because harsh conditions are required to reduce the Ru(III) to Ru(II) ions. This usually results in low yields (35-50%) of the *bis*-terpyridine ruthenium complex due to an incomplete conversion unless highly optimized reaction conditions are employed.[27,29] Above all, the required purification of the product is rather difficult when using high molar mass polymers. For this reason, the optimization of the reaction conditions and the subsequent purification of the crude product are discussed in this section using terpyridine-functionalized polystyrene and the previously described PEG Ru(III) *mono*-complex as a model system. The complexation reaction is performed in a mixture of chloroform and methanol as it is demonstrated in Scheme 4.3.

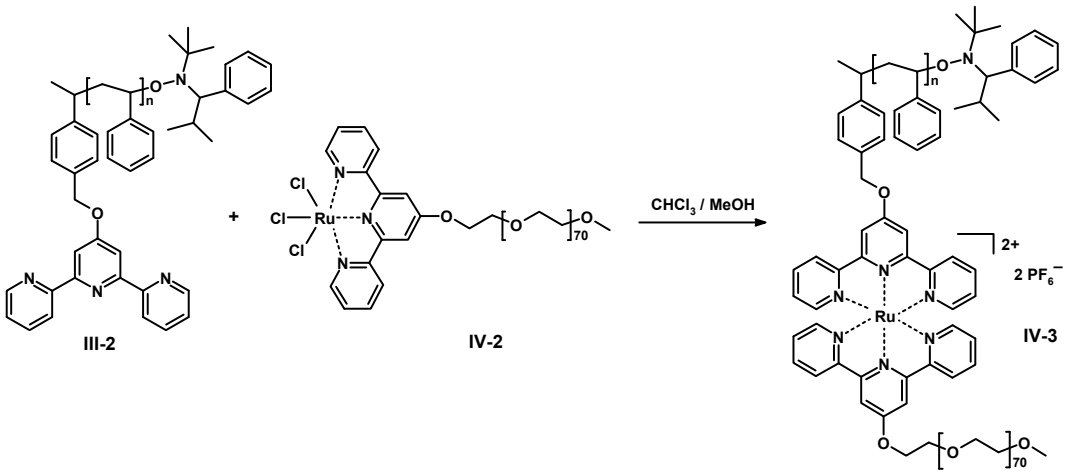

Scheme 4.3 *Schematic representation of the A-[Ru]-B block copolymer synthesis where the A-block represents the polystyrene and the B-block represents the poly(ethylene glycol).*

Typically, a catalytic amount of *N*-ethylmorpholine is added to the reaction mixture which is stirred under reflux for several hours. The effectiveness of *N*-ethylmorpholine was checked thoroughly. Two reactions were started with exactly the same conditions (temperature, volume and concentration using a mixture of chloroform and methanol as solvent); one with the addition of the catalyst and the other without, leading to the conclusion that *N*-ethylmorpholine has no real influence on the reaction in this particular case. Therefore, all further reactions were performed without the addition of *N*-ethylmorpholine. In order to compare the following results all reactions were performed using a microwave synthesizer to ensure a better control over the reaction time and temperature. Microwave energy consists of an electric field and a magnetic field. Polar molecules display the property that they can be oriented along an electric field (dipolar polarization phenomenon). As the applied field oscillates, the dipole field attempts to follow these oscillations and the energy is lost in the form of heat.[30] Subsequently, the heat is dissipated homogeneously through the whole reaction mixture due to frictional forces occurring between the

polar molecules (solvent, reagents or complexes, solid supports) and the rotational velocity. The main advantage of microwave heating over conventional heating is the fast and uniform heating throughout the reaction mixture. Moreover, all process parameters are controlled and stored which guarantees a better reproducibility. Sealed microwave vials were used for the reaction which can be heated above the boiling temperature of the solvent. First of all, the influence of the applied temperature was investigated. The progress of the reaction was determined by using GPC as can be seen in Figure 4.2. It is obvious that higher temperatures promote the formation of the *bis*-complex; however, only conversions below 50% with respect to the PEG_{70}-[$RuCl_3$ *mono*-complex **IV-2** were achieved.

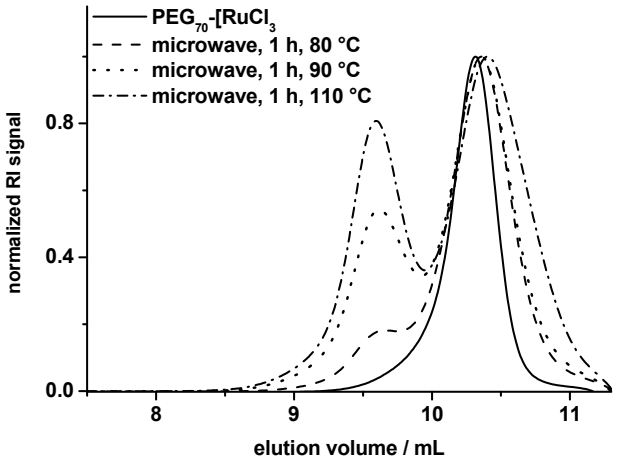

Figure 4.2 *GPC-chromatograms of the block copolymer formation at varying temperatures (eluent: DMF with 0.8 g/L NH_4PF_6).*

It should be mentioned that it was crucial for these investigations to utilize an optimized GPC system that suppresses the interaction of the charged supramolecular analytes with the column material.[31] By increasing the temperature, the *bis*-terpyridine ruthenium(II) complex was formed to a greater extent. However, it can be also seen that the trace of the starting material was shifting to lower molar mass which might be explained by decomposition at too high temperatures which limits the use of higher temperatures. The efficiency of the complexation reaction was also followed by UV-vis spectroscopy. By increasing the reaction temperature an increasing MLCT band at around 490 nm (formation of the *bis*-terpyridne ruthenium(II) complex) and a decreasing MLCT band at 390 nm (starting material) were observed (see Figure 4.3).

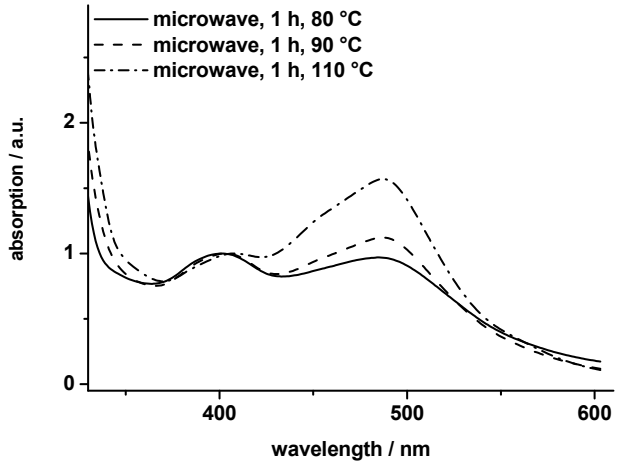

Figure 4.3 *UV-vis spectra of the block copolymer formation at varying temperatures (in CH_2Cl_2).*

The GPC curves do not reveal more *bis*-complex formation when longer reaction times are applied; only an enhanced decomposition of the PEG terpyridine ruthenium *mono*-complex can be observed. It is known that PEG is susceptible to thermo-oxidative degradation at elevated temperatures resulting in the reduction of the molar mass and the formation of low molar mass oxygenated products.[32-35] Due to the fact that the solutions have not been degassed by applying freeze-pump-thaw cycles, it is possible that a small amount of oxygen remained in the solution causing the decomposition. The concentration of the sample plays a significant role; the higher the concentration the better the yield of the *bis*-terpyridine ruthenium(II) complex. For the previous discussed reaction a solvent mixture of chloroform and methanol (8:1) was utilized. It was found that an increased amount of methanol, which is acting as reducing agent, promotes the *bis*-complex formation. However, the amount of methanol cannot be increased endlessly because methanol is a precipitant for a wide range of polymers. With the optimized parameters the conversion was increased up to 73% within one hour (see Figure 4.4).

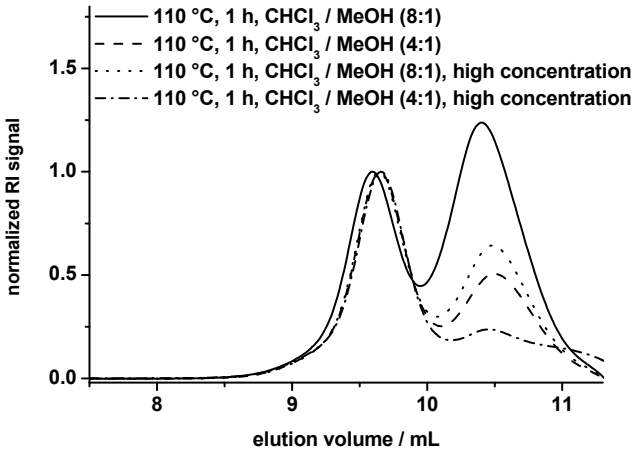

Figure 4.4 *GPC traces taken during the optimization of the reaction parameters (eluent: DMF with 0.8 g/L NH_4PF_6).*

Instead of chloroform, THF can also be used in a mixture with methanol (4:1), which provides slightly better conversions. All reactions up to this point were carried out at 110 °C; however for the preparation of the block copolymers the temperature was reduced to 90 °C to suppress degradation of the PEG starting material. Counterion exchange was performed by the addition of NH_4PF_6 to the reaction mixture. Unfortunately, the standard purification of the obtained polymers by preparative size exclusion chromatography (Bio-beads) did not work well due to the maximum exclusion limit of these materials of 14,000 g/mol. Also several re-precipitations and extractions were unsuccessful. We finally succeeded to purify the three PS_n-[Ru]-PEG_{70} block copolymers (**IV-3a** with n = 50, **IV-3b** with n = 130, **IV-3c** with n = 285) by preparative size exclusion chromatography with automated fractionation. It has already been described in literature[31] that GPC analysis of *bis*-terpyridine metal-complexes is rather difficult due to strong interactions with the column material (caused by the nitrogen atoms and the charged complex). Pure solvents often lead to fragmentation of the metal-ligand bond. Sometimes even oxidation to the Ru(III) *mono*-complex has been observed. But with the adjustment of temperature, flow rate and use of additives like NH_4PF_6 nearly all column interactions were suppressed in the preparative SEC. However, *N,N'*-dimethylformamide (DMF) is not a recommendable candidate for the fractionation *via* SEC/GPC because of its low volatility. For this reason, the fractionation was carried out with tetrahydrofuran (THF). 50 mg of the corresponding block copolymer were dissolved in 1 mL of THF (containing NH_4PF_6) and injected onto a PSS Gram preparative 100 Å column. Fractions were taken in equal time intervals and collected with a fraction collector. The collected fractions

were then measured with a conventional GPC with DMF as eluent. Figure 4.5 displays the GPC-chromatograms of the three different PS_n-[Ru]-PEG_{70} diblock copolymers before and after fractionation. The purified metallo-supramolecular block copolymers reveal PDI values below 1.1.

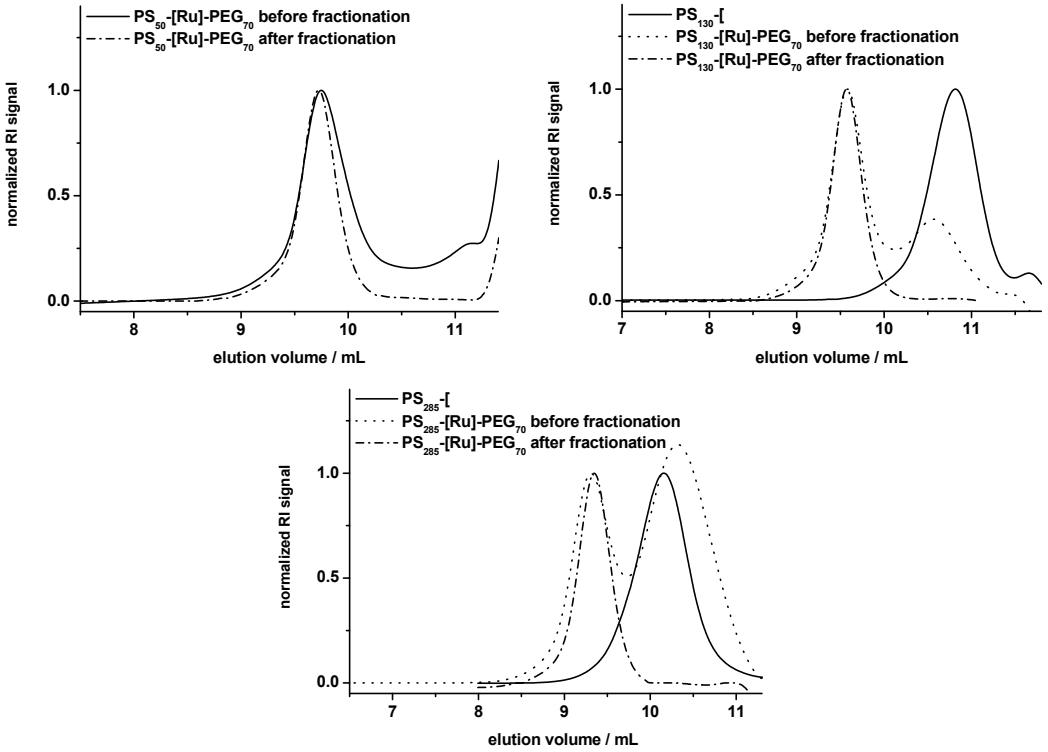

Figure 4.5 *GPC-chromatograms of the PS_n-[Ru]-PEG_{70} diblock copolymers **IV-3a, IV-3b** and **IV-3c**. After fractionation the traces reveal a unimodal molar mass distribution (eluent: DMF with 0.8 g/L NH_4PF_6).*

4.3.2 Synthesis of A-[Ru]-B diblock copolymers

The last section has demonstrated that the formation of non-covalently bonded block copolymers based on ruthenium(II) *bis*-terpyridine complexes is feasible. In this part, the preparation of other amphiphilic diblock copolymers is presented, namely $PTFMS_{42}$-[Ru]-PEG_{70} (**IV-4**) and $PPFS_{30}$-[Ru]-PEG_{70} (**IV-5**) (Figure 4.6). The terpyridine-functionalized fluorinated building blocks for the complexation with PEG_{70}-[$RuCl_3$ were obtained by a nitroxide-mediated polymerization process (see Chapter 3). Both complexation reactions were performed in closed microwave vessels at 80 °C for 10 hours. Prior to the reaction, the utilized solvent mixture (chloroform or tetrahydrofuran and methanol 4:1) was degassed by a gentle flow of argon through the solution for 5 minutes. A 1.2 fold excess of the *mono*-complex was taken in order to facilitate the purification of the product since the presence of uncoordinated terpyridine-functionalized fluoropolymer can be excluded. Even though, the preparation of the three PS_n-[Ru]-PEG_{70} diblock copolymers (**IV-3a-c**) was carried out without the addition of *N*-ethylmorpholine, the complexation reactions of $PPFS_{30}$-[and $PTFMS_{42}$-[were performed with *N*-ethylmorpholine. In the case of the PS_n-[Ru]-PEG_{70} diblock copolymers, *N*-ethylmorpholine did not influence the performance of the complexation reaction. But it could not be excluded that it could have a promoting effect for the complexation reactions of PPFS and PTFMS. After the reaction, a counter-ion exchange was performed by the addition of a methanolic solution containing a ten-fold excess of NH_4PF_6. In

order to remove the excess of salt from the product, the block copolymer was washed three times with water. The purification from unreacted materials was carried out by preparative size exclusion chromatography on BioBeads and/or column chromatography on AlOx (Al_2O_3). The last mentioned method worked best for the charged metallo-supramolecular polymers. Due to the strong interaction with the column material, the polymer could not elute from the column. However, the interactions diminished with the addition of a tiny amount of methanol to the eluent. A small fraction of the brown *mono*-complex was collected before the deep red block copolymer complex eluted.

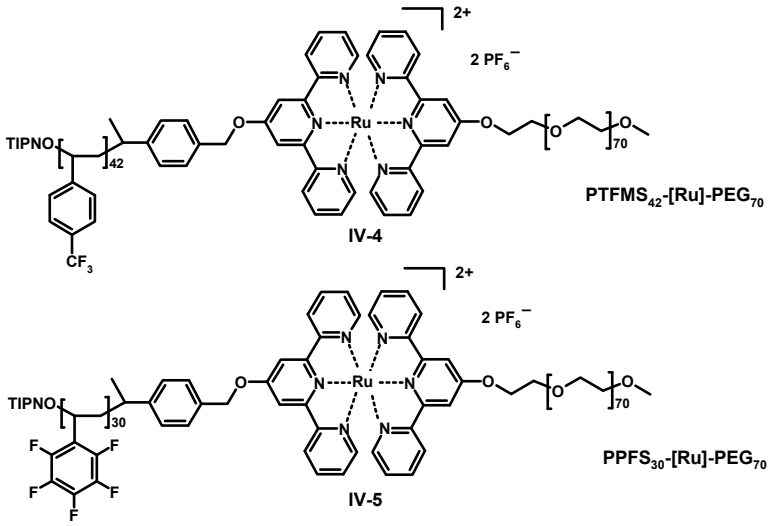

Figure 4.6 *Schematic representation of the two types of A-[Ru]-B diblock copolymers.*

Afterwards, the collected fractions were analyzed by GPC using 5 mM NH_4PF_6 in DMF as eluent.[31] Both metallo-supramolecular block copolymers (**IV-4**) and (**IV-5**) revealed unimodal molar mass distributions. Moreover, GPC evidenced that the PEG *mono*-complex was effectively separated from the desired product. The GPC measurement was repeated for both polymers using the connected photo-diode array (PDA) detector. This method provides an even better insight into the purity of the obtained block copolymers. The graph clearly reveals the typical MLCT-band for *bis*-terpyridine Ru(II) complexes at around 490 nm (Figure 4.7).

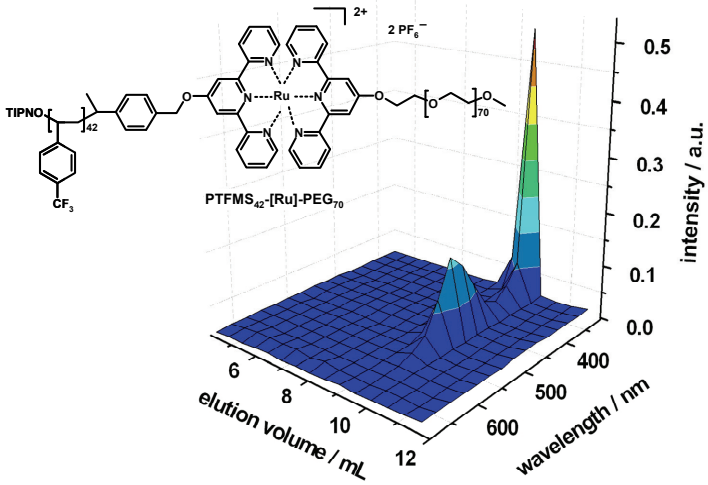

Figure 4.7 *3-Dimensional plot obtained by GPC with a PDA detector for the metallo-supramolecular diblock copolymer (**IV-4**) demonstrating both a unimodal molar mass distribution as well as the characteristic metal-to-ligand charge transfer band at 490 nm.*

4.3.3 Synthesis of A-B-[Ru]-C triblock copolymers

The same synthetic approach as described in Section 4.3.2 has been utilized for the construction of metallo-supramolecular triblock copolymers. For this purpose, well-defined diblock copolymers from Chapter 3 provided the basis for the complexation with the PEG Ru(III) *mono*-complex **2**. In general, block copolymers provide unique solid state and solution properties due to their different blocks (often incompatible) which, in turn, lead to various applications. ABC triblock copolymers are of special interest because a larger number of possible morphologies compared to diblock copolymers can be observed which can be explained by the existence of three different Flory-Huggins interaction parameters χ_{AB}, χ_{BC} and χ_{AC}. Advances in the field of controlled radical polymerization (CRP) techniques have simplified the design of macromolecules. Hence, a large variety of well-defined architectures can be synthetically accessed. In particular, block sequence plays a crucial role in ABC triblock copolymers. Different morphologies and phase transitions may be accessed simply by changing the respective blocks from ABC to ACB or BAC.[36,37] The increase in architectural complexity results in multiple self-assembled microphase structures. The phase separation of an AB diblock copolymer can lead to the formation of four different morphologies: lamellar, gyroid, cylindrical and spherical (Figure 4.8); each depending on the composition *f* of the AB block copolymer and the Flory-Huggins interaction parameter χN. In the case of triblock copolymers, the combination of block sequence, composition and block molar masses provide tremendous potential for the creation of new morphologies. Self-assembly of amphiphilic block copolymers in aqueous or organic media lead to the formation of micellar aggregates with a large variety of different morphologies (see Figure 4.8). The solvent incompatible blocks are located in the core of the polymeric micelle surrounded by a corona of the solvent-compatible blocks. The morphology of the micellar aggregates basically depends on three factors: (1) the swelling and stretching of the involved core-forming and corona-forming blocks, (2) the core-corona interfacial energy and (3) the repulsion among coronal chains.[38] A change in one of these three parameters directly affects the free energy of the micelles. In other words, the micelles become thermodynamically unstable and modify their morphology in order to reach another stable state.

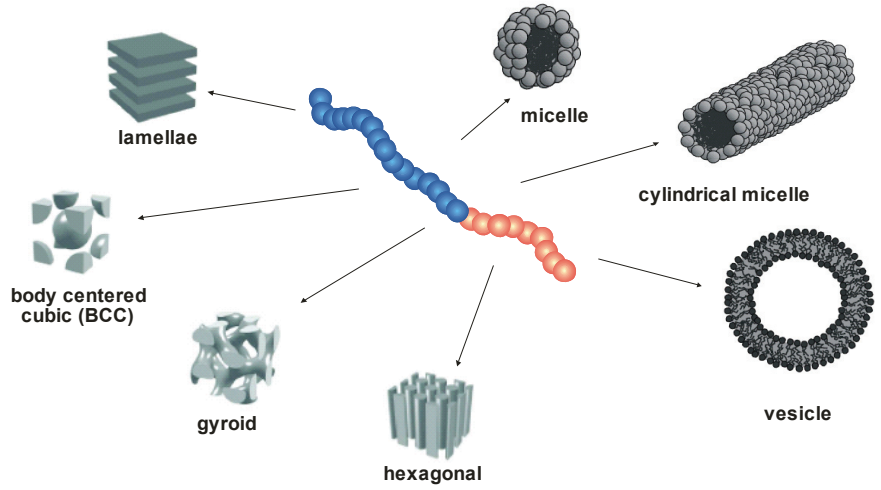

Figure 4.8 *Morphologies for linear diblock copolymers in bulk and in solution (in analogy to Förster et al.[39]).*

In total six different amphiphilic triblock terpolymers (**IV-6 to IV-11**) were prepared using the supramolecular complexation approach. Four of the synthesized polymers are of special interest since they are composed of a hydrophilic, a hydrophobic and a fluorophilic block. This is of particular importance for self-assembly investigations in bulk and in solution. Demixing of the

three different blocks could lead to the formation of three segregated domains. Hence, multicompartment micelles[40-44] composed of a phase-separated micellar core might be obtained in solution which are able to encapsulate hydrophobic and/or fluorophilic compounds in the segregated core. The block sequence was changed in those four examples. The PEG-block (C) served as an end block and the respective hydrophobic and fluorophilic blocks were reversed resulting in the formation of A-B-[Ru]-C and B-A-[Ru]-C triblock terpolymers. Figure 4.9 displays the synthesized metallo-supramolecular triblock copolymers. Poly(ethylene glycol) is a commonly used block in block copolymers because of its versatility: it features useful properties, such as biocompatibility and solubility in water as well as organic solvents, which makes the molecule extremely valuable for applications in various fields of science including biomedical applications.[45] Anionic polymerization is a suitable tool to prepare this polymer. However, due to its nucleophilicity it is difficult to grow a different polymer block onto PEG. For this reason, it is usually employed as end block. In order to construct an amphiphilic ABC block copolymer where PEG is located between two other blocks requires the employment of various polymerization techniques and modification steps.[46] On the other hand, supramolecular chemistry offers an easy pathway to obtain polymers consisting of a PEG middle block. Such macromolecular structures can be realized simply by the modification of commercially available α,ω-hydroxy functionalized PEG with chloro-2,2':6'2"-terpyridine.[7] This approach was applied for the preparation of A-[Ru]-B-[Ru]-A triblock copolymers where B represents PEG as a soft middle block between two hard blocks (see Chapter 5).

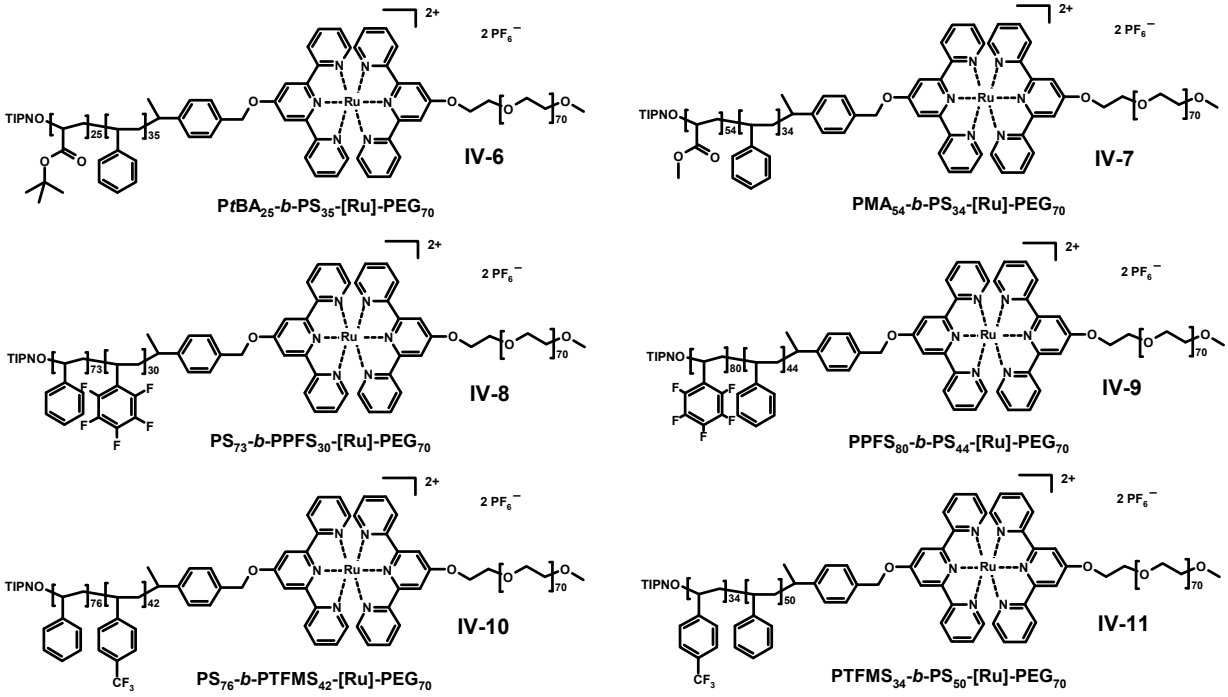

Figure 4.9 *Schematic representation of the six triblock copolymers that were prepared by combining controlled radical polymerization with supramolecular chemistry.*

The synthesis of the six triblock terpolymers was performed as it was described for the metallo-supramolecular A-[Ru]-B diblock copolymers in Section 4.3.2. After reacting the corresponding terpyridine-functionalized diblock copolymer with **IV-2** at 80 °C, an anion exchange was performed using NH_4PF_6 and the desired product was obtained by column chromatography (Al_2O_3). The polymers were subsequently analyzed by ^1H NMR spectroscopy and GPC. The former technique reveals the characteristic shifts in the terpyridine region for all of the

synthesized triblock copolymers indicating the successful complex formation. The most interesting signal shifts upon coordination are the protons in 3':5' and 6:6" position of the terpyridine ligand due to the influence of the electrons of the metal center on the magnetic field. Of course, the signals belonging to the PEG backbone could be observed in the region between 3.9 and 3.1 ppm. ^{1}H NMR spectroscopy also allows the determination of the block ratios; however, sometimes this is not straightforward as the signals are overlaying as it is the case for]-PS-*b*-PTFMS. The GPC chromatograms of the triblock copolymers reveal a unimodal molar mass distribution (Figure 4.10).

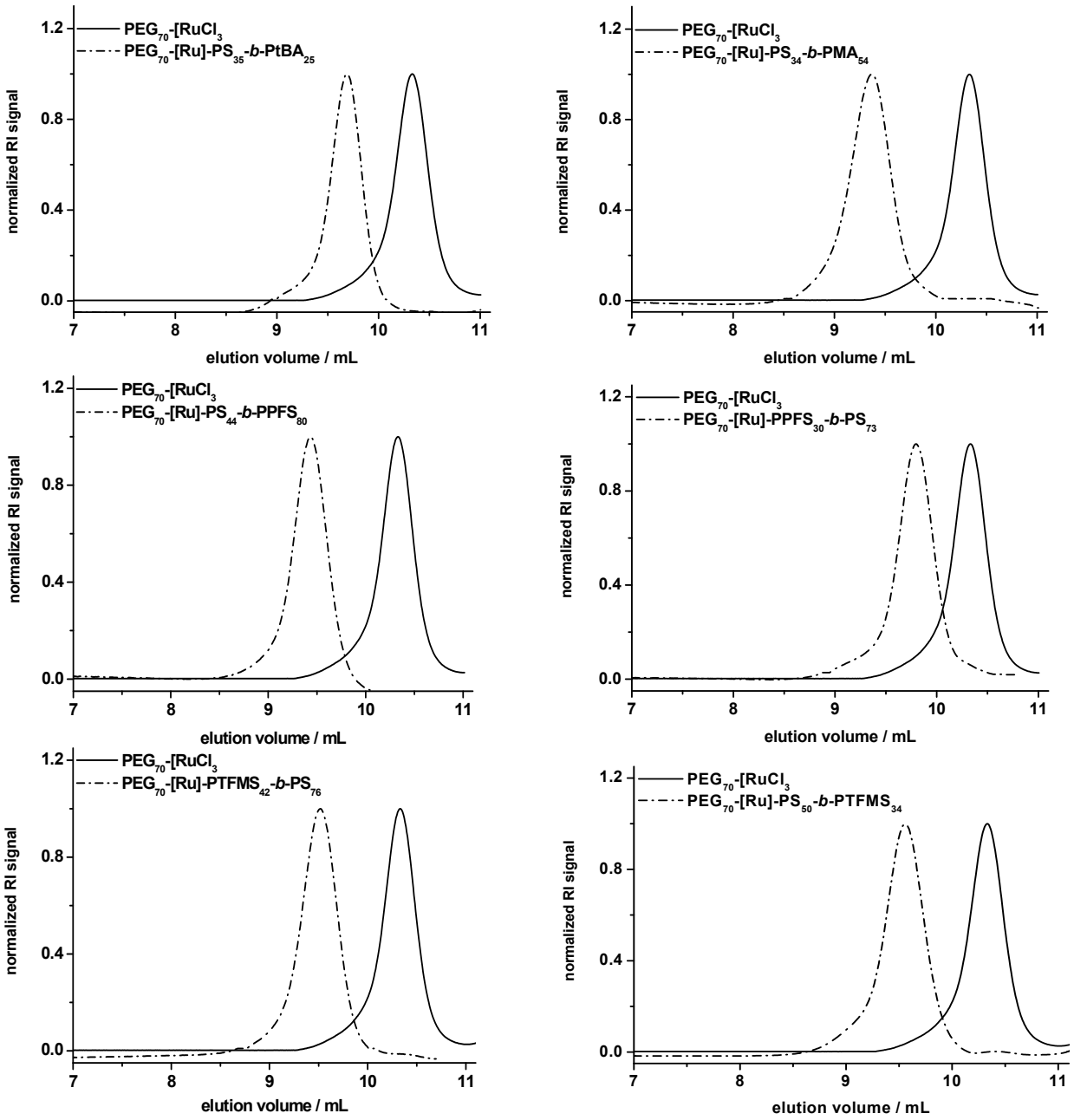

Figure 4.10 *GPC-chromatograms of the six metallo-supramolecular triblock copolymers (**IV-6** to **IV-11**) reveal the successful chain extension by the complex formation.*

Normally, a short tailing on higher molar mass side is observed. However, this can be attributed to the PEG starting material which was used as received from the supplier. Its characteristic shape is reflected in all stages of the synthesis towards the desired end product starting with the hydroxy-functionalized PEG, the terpyridine-functionalized PEG (**IV-1**), the PEG *mono*-complex (**IV-2**) and, finally, the *bis*-terpyridine ruthenium(II) complex. Figure 4.10 shows the GPC measurements with the RI detector. The GPC chromatograms do not include the traces of the corresponding]-A-*b*-B diblock copolymer since this GPC system (with DMF and NH_4PF_6 as eluent) is in particular suitable for the metal-containing polymers. In some cases the diblock copolymer (starting material) even partially overlaid with the solvent signal. For this reason, the uncomplexed diblock copolymers were measured on the GPC containing DMA and LiCl as eluent. Additionally, GPC measurements were performed using the photo-diode array detector revealing the characteristic MLCT band at around 490 nm for *bis*-terpyridine ruthenium(II) complexes.

Analytical ultracentrifugation (AUC) is a suitable characterization technique for both uncomplexed materials as well as metal-complexed materials. It is not strongly influenced by the presence of charges as for example GPC. Since this method relies on the sedimentation coefficient of macromolecules which, in turn, depends on the molar mass of the involved species, it provides useful information about the purity of the material including the possible formation of homo-dimers. In an experiment with PEG_{70}-[Ru]-PTFMS-*b*-PS (**IV-10**) the absence of homo-dimers was confirmed by the single sedimentation distribution which is attributed to the triblock copolymer. Figure 4.11 demonstrates the normalized distributions of the intrinsic sedimentation coefficients of all involved polymers which were obtained with interference optics. Table 1 summarizes the hydrodynamic data obtained from these measurements demonstrating that this technique is an efficient tool to determine the molar mass. The molar mass M_{fs} of the complex is in agreement with the sum of the molar masses of the starting materials. M_{fs} was determined using the values of the frictional ratio (f/f_{sph}) and the intrinsic sedimentation coefficient [s] which is only dependent on the macromolecule (the sedimentation coefficient s_0 on the other hand is dependent on the macromolecule and the solvent). The small difference between the calculated molar mass and the determined value can be due to the Ru(II) ion and the PF_6^- counterions that are also included upon complexation.

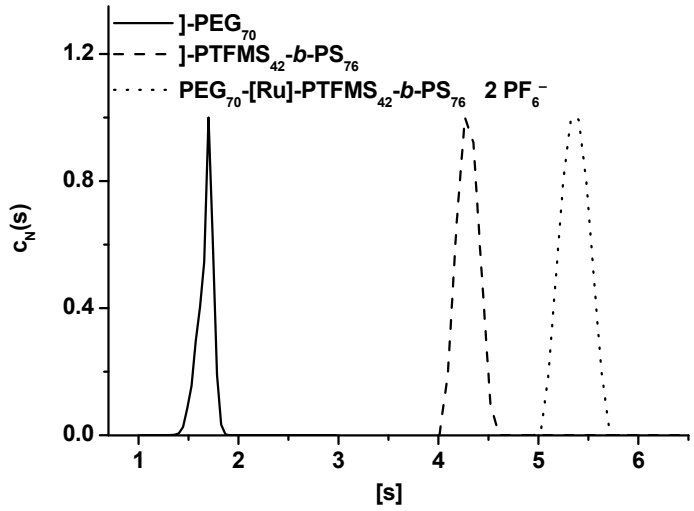

Figure 4.11 *Results of the AUC experiment revealing the intrinsic sedimentation coefficient for terpyridine-functionalized PEG_{70} (**IV-1**) (solid line), terpyridine-functionalized]-$PTFMS_{42}$-b-PS_{76} (**III-21**) (dashed line) and the respective heteroleptic polymer-complex (**IV-10**) (dotted line).*

Table 1 *Hydrodynamic data of the measured polymers including the determination of the molar mass M_{fs}, the intrinsic viscosity [η] and the partial specific volume υ_{bar}.*

Polymer	$s_0 \times 10^{13}$ (s)	[s] × 10^{15} (g/cm)	[η] (cm^3/g)	f/f_{sph}	υ_{bar} (cm^3/g)	M_{fs} (g/mol)	M_{NMR} (g/mol)
IV-1 [a]	1.96	1.7	9.6	1.62	0.78	3,100	3,400
III-21 [b]	2.60	4.5	11.4	1.63	0.81	13,600	15,800
IV-10 [b]	3.20	5.4	-	1.63	0.80	17,700	19,600

[a] measured in acetone.
[b] measured in tetrahydrofuran (THF).

4.3.4 Synthesis of A-B-C-[Ru]-D tetrablock copolymers

The synthetic strategy can be even further extended to prepare metallo-supramolecular tetrablock copolymers using the two terpyridne-functionalized triblock terpolymers that were described in Chapter 3.2.3.2. In a complexation reaction with **IV-2** under reducing conditions, two tetrablock copolymers **IV-12** and **IV-13** were prepared. Purification by column chromatography in methylene chloride and addition of small amounts of methanol yielded the well-defined tetrablock copolymers. The polymers were characterized by means of ^{1}H NMR spectroscopy and GPC, respectively. The characteristic shift of the terpyridine signals indicated a successful complex formation. The latter mentioned method revealed a shift of the GPC trace to higher molar mass in comparison to the GPC traces of the starting materials. The GPC traces of both tetrablock copolymers revealed narrow molar mass distributions with PDI values of 1.15 and 1.08, respectively. Furthermore, both materials were investigated by GPC with accompanying PDA detector proving their successful synthesis (Figure 4.12).

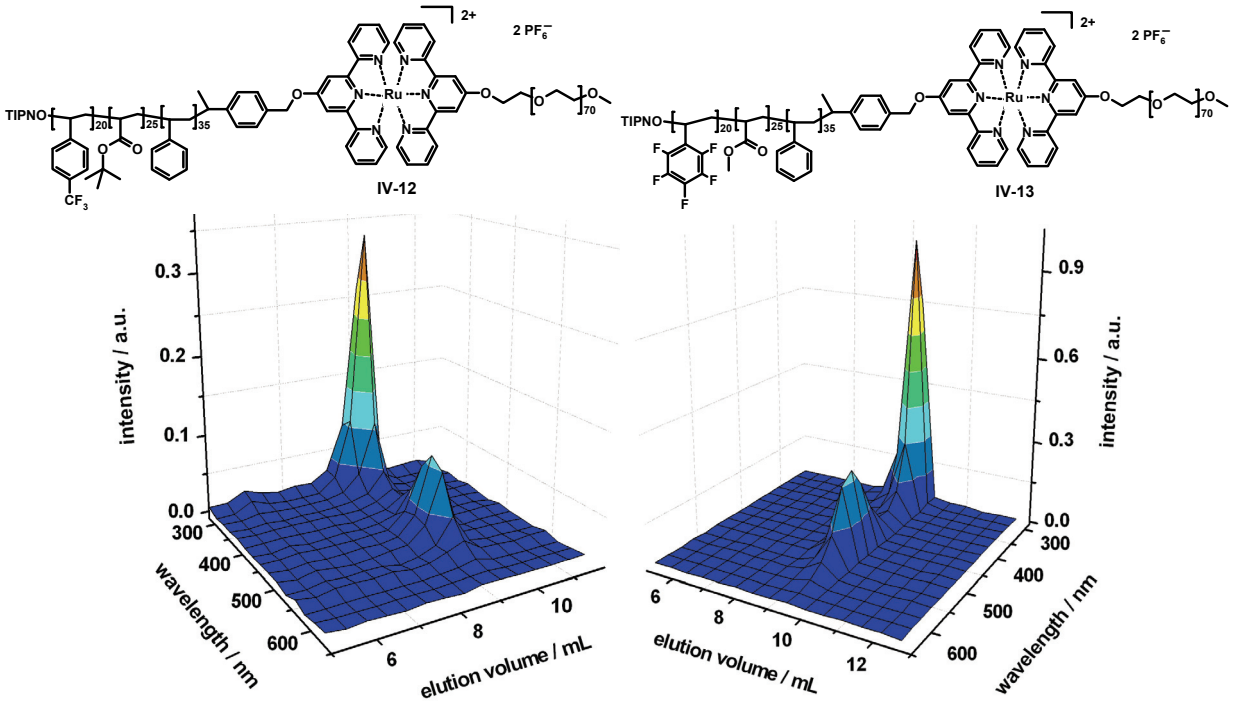

Figure 4.12 *GPC-PDA results of the metallo-supramolecular tetrablock copolymers **IV-12** and **IV-13**.*

Both of the tetrablock quaterpolymers revealed a unimodal molar mass distribution which displays at the same time the UV-vis spectrum of the block copolymer with its representative metal-to-ligand charge transfer band at around 490 nm. Both polymers are composed of a fluorophilic, a hydrophilic block and two hydrophobic blocks. The hydrophobic blocks within the polymers (PS and PMA[47] as well as PS and P*t*BA[48]) are known to form segregated domains. Self-assembly of those materials in solution would possibly lead to the formation of multicompartment micelles due to strong demixing of the blocks. In principle, the tetrablock copolymer containing the poly(*t*-butyl acrylate) block could be easily converted to a hydrophilic poly(acrylic acid) block by cleaving the *t*-butyl groups under acidic conditions. Consequently, this post-modification would afford a new polymer with alternating hydrophilic and hydrophobic segments.

4.4 Self-assembly in solution

When block copolymers with incompatible blocks are dissolved in a thermodynamically good solvent for one of the blocks and a bad solvent for the other block(s) the copolymer chains associate reversibly to form diverse microstructures in solution,[13] such as spherical micelles, worm-like micelles,[49] vesicles[16,50,51] and bilayers.[52,53] The most commonly driving force for this process is amphiphilicity. The system experiences thereby a decrease in free energy due to the removal of hydrophobic segments from the polar environment. As a result, the micellar core is protected from the polar media by the hydrophilic blocks. The properties of the formed aggregates are in many aspects the same as for classical micelles resulting from low molar mass surfactants. The self-assembly of block copolymer chains in solutions can usually be initiated either by increasing concentration (micelles form at a critical micelle concentration at a fixed temperature, CMC) or by changing the temperature (micelles form at a critical micelle temperature at a fixed concentration, CMT). Both CMC and CMT are the fundamental parameters which characterize the solution behavior of block copolymers. The CMC of block copolymers is usually much lower compared to that of conventional surfactants. In contrast to surfactant micelles, micelles of block copolymers are often kinetically frozen, *i.e.* there is no exchange of block copolymers between different micelles. The control over the aggregate architecture can be achieved by adjusting the solution conditions *i.e.* water content in the solvent mixture, the solvent nature and composition, the presence of additives and the polymer concentration.[54,55] Moreover, polymer parameters like the molar mass, the hydrophobic-to-hydrophilic relative block length, and the chain architecture play an important role in respect to aggregate size and morphology.[40,56-59] Two different micelle types can be classified for A-B block copolymers where B is the insoluble block and hence forms the core of the micelle.[17,60] Micelles in which the degree of polymerization for the insoluble block (N_B) is smaller than the soluble block (N_A) are called “hairy” micelles. The other type in which N_A is smaller than N_B is referred to as “crew-cut” micelles.

Scaling theories were developed to predict the correlations between the molecular characteristics of a given block copolymer, and characteristics, such as the core radius R_c, the corona thickness R_s and the aggregation number Z of the corresponding micelle. Assuming uniformly stretched coronal chains the radius (R_c) for “crew-cut”-type micelles can be predicted by

$$R_c \propto \gamma \cdot N_B^{2/3} \cdot a \qquad\qquad Z \propto \gamma \cdot N_B$$

where γ is the A/B interfacial tension and a the segment length.[17,61]

If the condition $N_A > N_B^{4/5}$ in a good solvent for A blocks is fulfilled, the aggregates can be regarded as “hairy” micelles, where the following correlations are valid:

$$Z \propto N_B^{4/5} \qquad\qquad R_c \propto N_B^{3/5} \qquad\qquad R_S \propto N_A^{3/5} \cdot N_B^{6/25}$$

All metallo-supramolecular block copolymers presented in this chapter are amphiphiles due to the non-covalently connected PEG block. Thus, most of the materials were investigated towards their micellization behavior in aqueous or polar organic media. The results of this research are discussed in the following sections.

4.4.1 Block copolymer micelles of the PS_n-[Ru]-PEG_{70} library

Micelles were prepared of the three amphiphilic block copolymers **IV-3a** to **IV-3c** (Section 4.3.1) by dissolving the copolymer in the common solvent DMF followed by the dropwise addition of the selective solvent (deionized water). The solubility of the polystyrene block decreases with increasing amount of water leading to the formation of aggregates. In the beginning there is a thermodynamic equilibrium between single polymer chains and micelles. However, the structure becomes kinetically frozen when more water is added.[62] Ammonium hexafluorophosphate (NH_4PF_6), which is an additive in the eluent of the preparative GPC, and the residual unselective solvent were then effectively removed by dialysis. The size of the micelles was investigated by means of dynamic light scattering (DLS), atomic force microscopy (AFM), and transmission electron microscopy (TEM). DLS is a suitable characterization technique to investigate the micelles in solution. It is well-known that micelles prepared from metallo-supramolecular block copolymers tend to aggregate; however, this is dependent on the polymer and the metal ion involved.[62,63] In fact, two different populations were observed with the CONTIN size distribution analysis for **IV-3c** (PS_{285}–[Ru]–PEG_{70}): the first peak corresponds to single micelles and small aggregates and the second very broad peak is attributed to large aggregates. A mean hydrodynamic radius (D_h) of 93 nm was observed for the ‘‘crew-cut’’ behaving PS_{285}–[Ru]–PEG_{70} micelle. With decreasing polystyrene block length, also decreasing values for the mean D_h were found (62 nm for PS_{130}–[Ru]–PEG_{70} (**IV-3b**) and 24 nm for PS_{50}–[Ru]–PEG_{70} (**IV-3a**), respectively). In addition, AFM and TEM imaging was used to visualize the micelles. The AFM measurements were performed in dry state. After dropcasting the micellar solution onto mica the sample was dried under a gentle stream of nitrogen. In AFM the diameter of the micelle can be estimated from the observed height.[64] The height of the measured micelles approximates the size of the core for two reasons: firstly, the flexible PEG chains of the corona should collapse upon drying and secondly, the short length of the PEG chains is not expected to have an influence on the size of the micelle, especially for larger PS chains. Figure 4.13 displays the AFM images of the three PS_n–[Ru]–PEG_{70} block copolymers. The images exemplify clustering of single micelles that exhibit an average height of 55 nm (left), 35 nm (center) and 25 nm (right), respectively.

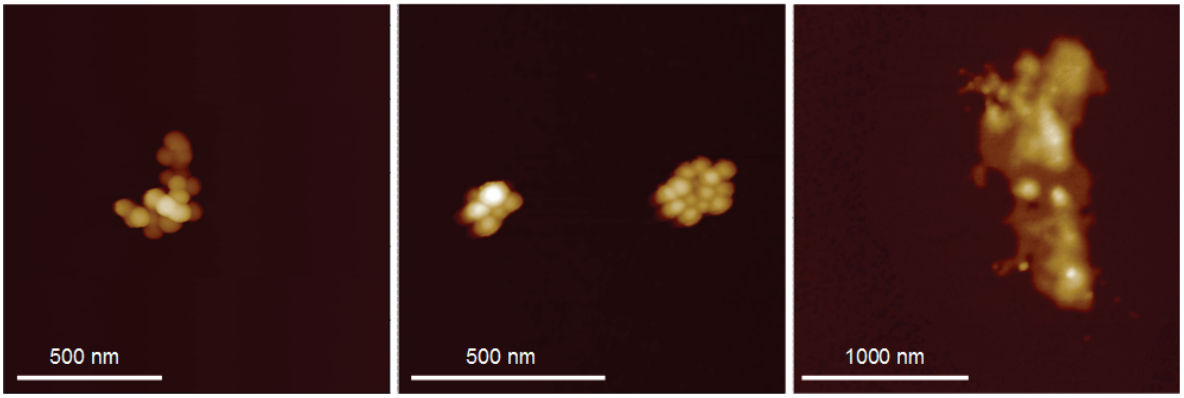

Figure 4.13 *AFM height images of PS_{285}-[Ru]-PEG_{70} (left), PS_{130}-[Ru]-PEG_{70} (center) and PS_{50}-[Ru]-PEG_{70} (right).*

For TEM imaging, no contrasting agent was required to visualize the micelles due to the presence of the Ru(II) ions. TEM displays the core of the micelles like in AFM because it was measured in dry state and the short PEG-arms are supposed to collapse upon drying. Spherical micelles were observed by TEM for two of the three block copolymers (Figure 4.14). The left TEM picture shows once more the evidence that metallo-supramolecular micelles form large aggregates. The size of the individual spherical micelles is rather uniform; however, also much larger micelles are formed as can be seen in the right TEM image. The micelle size determined by TEM is approximately 55 nm for PS_{285}–[Ru]–PEG_{70} and 40 nm for PS_{130}–[Ru]–PEG_{70}. The aggregation numbers for the above discussed micelles have been calculated using the density of amorphous polystyrene (0.95 g/cm^3). **IV-3c** reveals an aggregation number of 1650, and **IV-3b** an aggregation number of 1360, respectively. The values are in good agreement with those described in literature.[65] No stable micelles were observed in the dry state for the sample with the smallest polystyrene block length **IV-3a**, neither on the hydrophilic TEM-grid nor on the hydrophilic mica support. Although hints of spherical objects were found, no reliable results could be obtained with these techniques. Cryo-TEM would possibly be a more suitable technique to visualize the micelles of **IV-3a** since it gives direct access to the micellar morphology and eliminates influences from the drying process.[66] Generally, the data obtained by AFM and TEM are in good agreement revealing values in the same range. In comparison to AFM and TEM, the micelle sizes obtained by DLS are somewhat higher due to the fact that DLS measures the size of the complete micelle (core and the corona) in solution where the coronal chains are swollen.

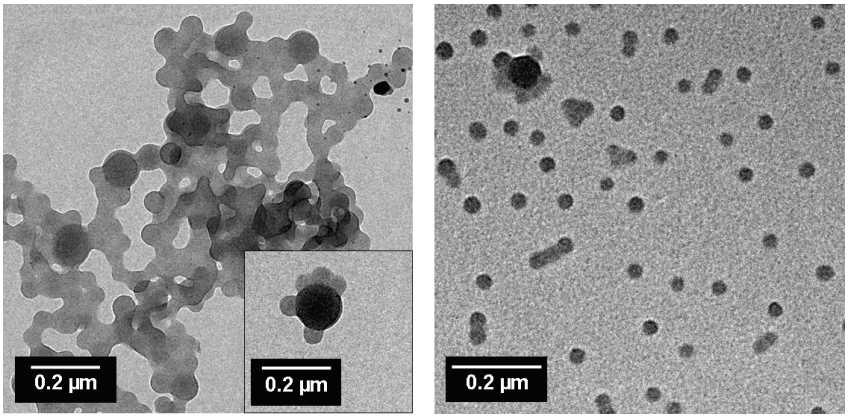

Figure 4.14 *TEM images of the unstained micelles in water: PS_{285}-[Ru]-PEG_{70} (left) and PS_{130}-[Ru]-PEG_{70} (right).*

4.4.2 Block copolymer micelles in aqueous media

One attractive goal of supramolecular chemistry is to control the molecular self-assembly ("bottom-up" approach) in order to obtain specific structures for sophisticated applications. Access to control the structure can be achieved by considering four general points. First of all, the design of the macromolecule including number and chemical identity of molecules, molecular weight, composition and architecture, plays an important role. The second necessary component is the composition of the mixture which comprises among other things the selectivity of the added solvent and the miscibility or immiscibility of different polymeric components. Thirdly, external stimuli such as temperature, pressure, pH and ionic strength may be used to tune the structure. Finally, the use of external fields, such as shear and extensional flow, electric and magnetic fields, may contribute to the desired self-assembled structure. The micelles obtained from the

before described PS_n-[Ru]-PEG_{70} system were found to be spherical micelles independent of the length of the hydrophobic block. It was shown that a change of the hydrophilic-to-hydrophobic block length ratio only affected the size of the formed spherical micelles. The block copolymer micelles presented in this section were all prepared by the dissolution of the block copolymer in a common solvent for all blocks (THF) and the subsequent addition of the selective solvent (deionized H_2O). The investigated block copolymers are composed of a fluorophilic segment (either PTFMS or PPFS) which may change the interaction between the involved polymer blocks. Moreover, the investigation also included more complicated structures such as metallo-supramolecular triblock copolymers as well as one example of a tetrablock quaterpolymer. Standard micelle concentrations of 1 mg/mL were prepared for all samples. Figure 4.15 shows the TEM images of the investigated block copolymers. The images clearly demonstrate the changes in the morphology that occurred by modifying the design variables of the polymer structure.

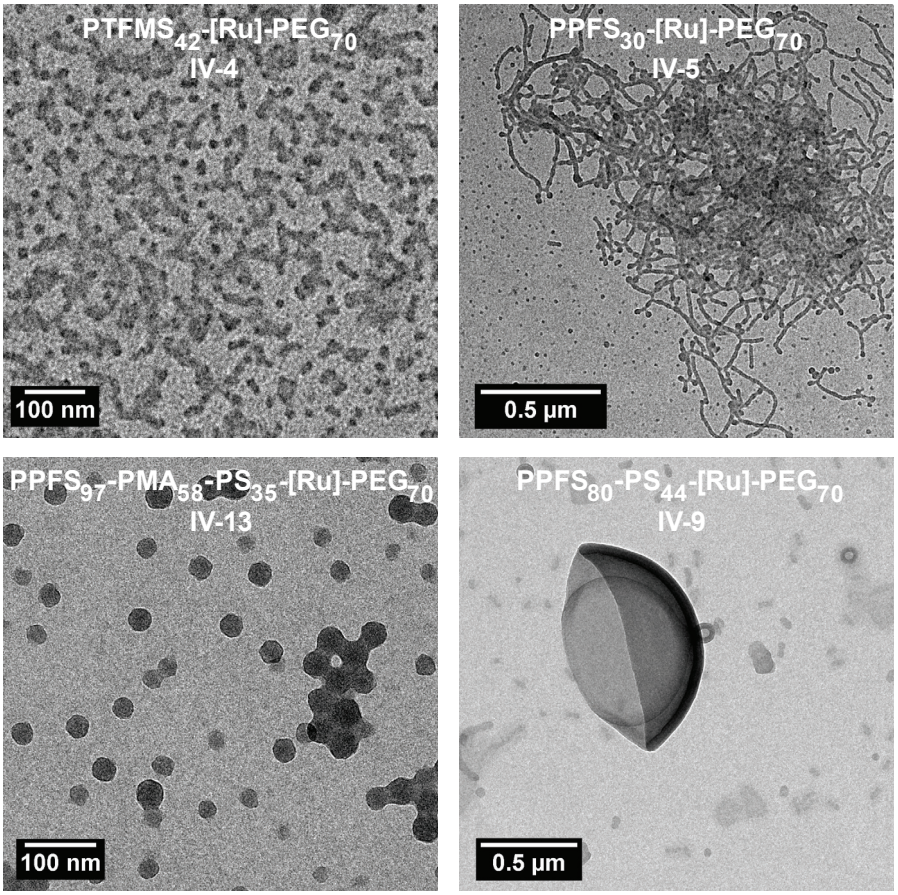

Figure 4.15 *TEM images of different metallo-supramolecular diblock (**IV-4** and **IV-5**), triblock (**IV-9**) and tetrablock (**IV-13**) copolymer micelles in water (1 mg/mL) demonstrating a variety of morphologies: spherical micelles, worm-like micelles and vesicles.*

The chemical identity of the involved polymer blocks plays indeed an important role for the formation of self-assembled nanostructures. In contrast to the micellization experiments of PS_{50}-[Ru]-PEG_{70} (**IV-3a**), where no stable micelles could be obtained in the dried state, the corresponding block copolymers with PTFMS (**IV-4**) and PPFS (**IV-5**) clearly show the formation of spherical micelles and worm-like micelles. Surprisingly, these micelles were formed even though the fluorine-containing block has a smaller degree of polymerization than polystyrene

(**IV-3a**). A possible explanation for this observation could be a stronger demixing effect caused by the fluorinated block. It is well-known that fluoro-containing compounds are highly water repellent. Therefore, in case of the two fluoro-containing diblock copolymers, where the fluoro-block forms the core of the micelle and the PEG-block the corona, strong demixing from the water is only provided when the micelle is densely packed whereby a large number of water-soluble PEG-chains shield the core of the micelle from the water. As a result, aggregation numbers within the micelles are increased. This assumption would also explain why diblock copolymer **IV-4** forms micelles whereas diblock copolymer **IV-5** forms coexisting spherical micelles and wormlike micelles. Presumably, PPFS is more hydrophobic compared to the PTFMS block due to its higher number of fluoro-atoms within the monomer. A higher aggregation number leads to an increase in micelle size accompanied by a transformation from spherical micelles to wormlike micelles (Figure 4.15). The TEM image of triblock copolymer **IV-9** reveals a coexistence of spherical micelles, short worm-like micelles and a few vesicles. On the other hand, only spherical micelles with rather uniform sizes were observed from the tetrablock copolymer **IV-13**. Both materials (**IV-9** and **IV-13**) have a relatively long PPFS end-block, which is shielded from the water by an additional hydrophobic PS-block as well as PS-PMA-block. For this reason, the size of the aggregates is relatively small and the majority of the formed aggregates are spherical micelles since demixing between water and PS occurs at the interface of the core and corona. A possible reason why three different morphologies are observed for **IV-9** could be the much shorter length of the hydrophobic block in comparison to **IV-13**. In contrast to the A-B-[Ru]-C triblock copolymer **IV-9**, the B-A-[Ru]-C triblock copolymer **IV-8** was exclusively forming large vesicles which can be seen from the TEM and SEM images in Figure 4.16. Upon sequence change of the PS-PPFS-block, the fluorinated block borders directly on the hydrophilic block. Consequently, the aggregate number increases in order to protect the fluorophilic part from the water leading to a transformation from micelles to vesicles. For SEM imaging, the micellar solution was blotted onto a purified glass slide. The spherical particles are stable both in solution as well as on the surface which was confirmed by a control-measurement after 2 months. The fact that most of the particles are “broken” can be an effect of the drying process that is included in the sample preparation.

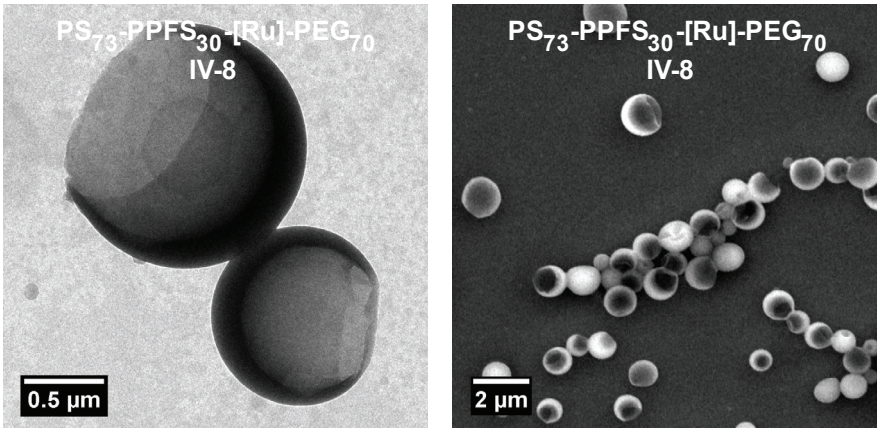

Figure 4.16 *TEM image (left) and SEM image (right) of the metallo-supramolecular triblock copolymer **IV-8**. Both measurements reveal spherical hollow objects with diameters around 1 µm.*

These examples show that the morphology of a given block copolymer is strongly depending on the interaction between the polymer blocks itself as well as the interaction between the polymer blocks and the solvent. However, the more complex the block copolymer, the more difficult it becomes to predict the materials morphology. Moreover, the preparation method used for micelle preparation essentially leads to kinetically trapped micellar structures that do not represent an equilibrium state in the final pure water solution. Therefore, it becomes difficult to predict a

micellar structure on the basis of “thermodynamic” arguments for the aggregates prepared in this section.

4.4.3 Block copolymer micelles in polar organic media

In the present study, the influence of the solvent on the micelle formation was investigated by applying a single solvent procedure[55] onto the metallo-supramolecular triblock copolymer **IV-10** (PEG_{70}-[Ru]-$PTFMS_{42}$-b-PS_{76}) which consists of a hydrophilic, a fluorophilic and a hydrophobic polymer block. Various alcohols including methanol, ethanol, 1-propanol, 2-propanol and 1-butanol were selected as potential solvents for micellization. Since the investigated triblock terpolymer was poorly soluble in those alcohols at room temperature, the solutions (1 mg/mL) were heated in closed reaction vessels to 140 °C for 5 minutes and slowly cooled to room temperature. The resulting self-assembly into discrete nanostructures upon cooling was then visualized by transmission electron microscopy (TEM, Figure 4.17).

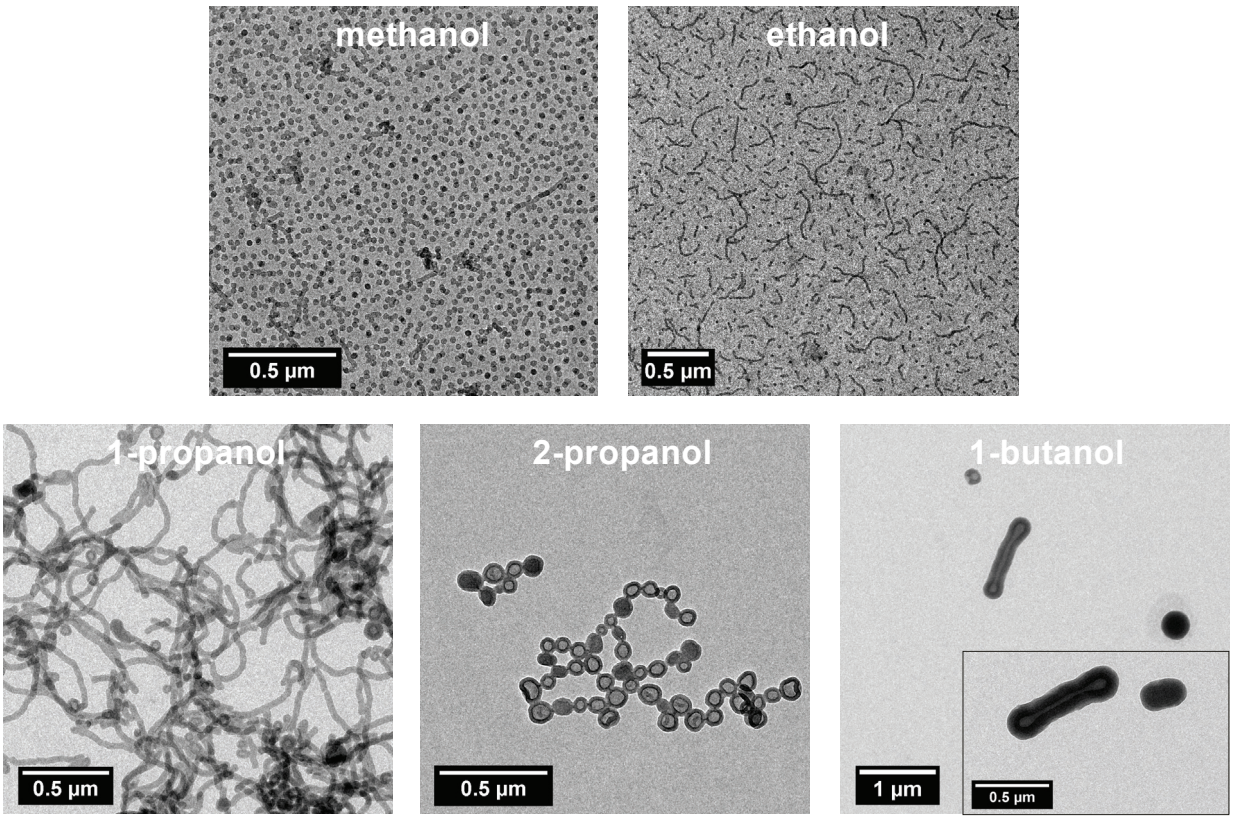

Figure 4.17 *Unstained TEM images of **IV-10** in different solvents demonstrating the strong influence of the solvent on the micellar morphology. All basic morphologies were obtained: spherical micelles in methanol, spherical and wormlike micelles in ethanol, wormlike micelles and vesicles in 1-propanol, vesicles in 2-propanol and coexisting large compound micelles and hollow tubes in 1-butanol.*

From the results shown in Figure 4.17, it is clear that the micellar morphology is strongly dependent on the alcohol used. In methanol, a vast majority of small spherical micelles was formed whereas in ethanol a coexistence of spherical micelles and wormlike micelles was observed. However, much larger aggregates including vesicles, hollow tubes and large compound micelles (LCM’s) were detected in the solutions of 1-propanol, 2-propanol and

1-butanol, respectively. The micellar solutions in those latter solvents had a cloudy appearance while the methanol and ethanol-based solutions seemed to be optically transparent. The reason for the different morphologies has to be found in the solubility of the constituting polymer blocks of the triblock terpolymer in the respective solvents. The poly(ethylene glycol) block is soluble in all utilized solvents already at room temperature. As expected, the polystyrene block is neither soluble at room temperature nor at higher temperature in all the used solvents (up to 90 °C). On the other hand, the polytrifluoromethylstyrene (PTFMS) block was found to have an upper critical solution temperature (UCST) in the less polar alcohols, *i.e.* 1-propanol, 2-propanol and 1-butanol while it is fully soluble in methanol and ethanol. In order to shed light on this temperature-dependent behavior, solubility measurements were performed by measuring the turbidity of a synthesized model polymer]-$PTFMS_{81}$ in the above mentioned alcohols as a function of temperature in a wide temperature range (Figure 4.18).

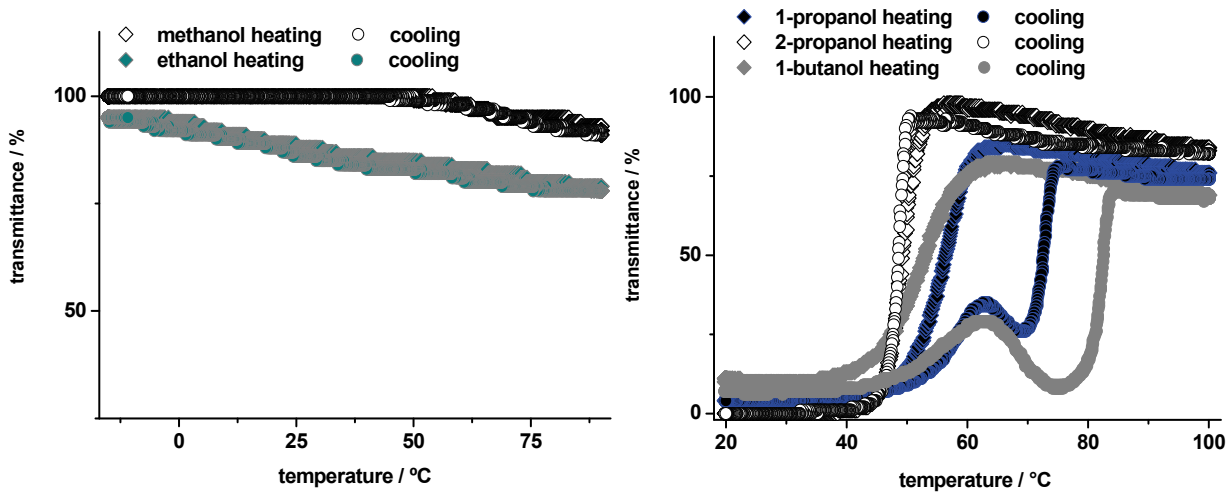

Figure 4.18 *Turbidity measurements of polytrifluoromethylstyrene (]-$PTFMS_{81}$) in methanol, ethanol, 1-propanol, 2-propanol and 1-butanol in the range from –20 °C to 100 °C.*

The resulting turbidity curves, together with a visual inspection of the solutions, revealed complete solubility of PTFMS in methanol and ethanol from –20 °C to 90 °C. Basically, transparent solutions, *i.e.* the polymer is fully dissolved, reveal a transmittance above 75% which is the case for both solvents. Furthermore, it can be assumed that methanol is a slightly better solvent for the polymer since the polarity is higher. In this case, the major part of **IV-10** is solubilized in the solvent. Therefore it is not surprising to observe a spherical morphology for the micelles in methanol consisting of a PS_{76} core surrounded by $PTFMS_{42}$-[Ru]-PEG_{70} coronal chains. Since the solubility of the PTFMS is slightly reduced in ethanol compared to methanol, the coexistence of spherical micelles and wormlike micelles in ethanol can be explained by the decreased hydrodynamic volume of the PTFMS block. With a decreasing polarity of the solvents, PTFMS became less soluble; the polymer only dissolved in 2-propanol, 1-propanol and 1-butanol at higher temperatures, indicating that PTFMS exhibits an UCST in these solvents (48.6 °C in 2-propanol, 72.5 °C in 1-propanol and 82.6 °C in 1-butanol, respectively; determined at 50% transmittance during cooling), whereby the UCST increases with decreasing solvent polarity. In other words, the investigated metallo-supramolecular triblock terpolymer **IV-10** is able to change the solvophilic to solvophobic block ratio depending on the utilized solvent system; here a transition from spherical micelles to wormlike micelles to vesicles and hollow tubes can be observed when going from methanol to ethanol to 1-propanol to 2-propanol to 1-butanol. Using methanol and ethanol as solvents for the triblock terpolymer, two polymer blocks are solvophilic (PEG and PTFMS), whereas only the PEG block is solvophilic at room temperature in the less

polar solvents, *i.e.* 1-propanol, 2-propanol and 1-butanol (Figure 4.19). On closer inspection, the turbidity curves of PTFMS in 1-propanol and 1-butanol in Figure 4.18 reveal strong hysteresis, which is absent for the UCST transition observed in 2-propanol. This difference might be due to the hydrogen bond acidity of the different solvents that affects the formation of weak hydrogen bonds between the hydroxyl-group of the solvent and the fluorine atoms of the PTFMS. It might be speculated that the higher hydrogen-bond acidity of 1-propanol and 1-butanol results in better solvation of the precipitated polymer upon heating compared to the 2-propanol that has a lower hydrogen bond acidity.[67] In contrast, the precipitation of the polymer upon cooling seems to be related to the solvent polarity. The exact nature of these observed differences should be investigated in detail in future work. These future studies should also focus on the multiple transitions that are observed at around 62 °C in the cooling run for 1-propanol and 1-butanol that might be related to the formation of large highly solvated aggregates followed by the formation of denser aggregates upon further cooling and finally macroscopic precipitation resulting in 0% transmittance. Nonetheless, the existence of an upper critical solution temperature in 1-propanol, 2-propanol and 1-butanol is the main important observation for the current study since it explains the observed morphological transformations for the triblock terpolymer.

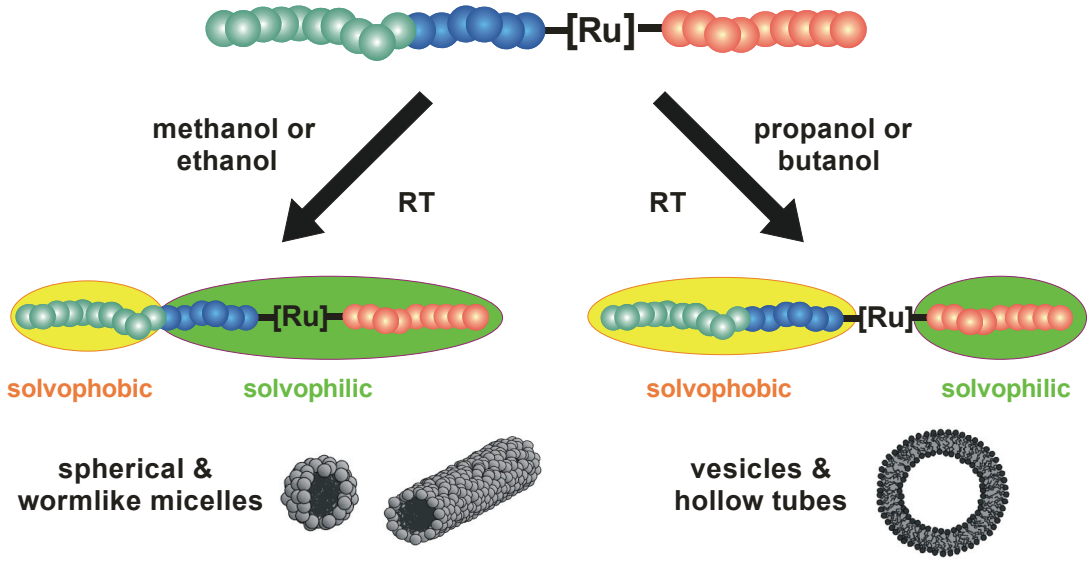

Figure 4.19 *Schematic representation of the solvophilic and solvophobic blocks within the triblock copolymer using different solvents.*

In general, transitions from spherical micelles to wormlike micelles to vesicles go along with a decrease of the core-corona interfacial curvature. A decrease in interfacial curvature could directly result from an increase in hydrophobic block length.[68,69] This is actually also the case in this study: the solvophobic block length in the investigated triblock terpolymer increases when altering the solvent from methanol or ethanol to propanol or butanol (Figure 4.19). The decrease of the solvent compatible blocks leads to a reduced corona crowding and, therefore, allows a larger aggregation number. However, an unlimited expansion of the micelle is prevented due to a large entropy penalty caused by the stretching of the solvophobic blocks in the core domain. In order to satisfy the interfacial curvature requirement, the micelle undergoes a transition towards wormlike micelles and vesicles rather then forming larger spherical micelles (Figure 4.17). Since those morphologies are formed during the cooling of the solution, which is realized at a given speed, we can not exclude the kinetic trapping of non-equilibrium morphologies during this step. This could explain why different morphologies are coexisting in each TEM picture of Figure 4.17. The nanostructures formed at room temperature in 1-propanol, 2-propanol and 1-butanol possess

the PS-block and the PTFMS-block in the core domain. Since those blocks phase-separate into coexisting hydrocarbon and fluorocarbon microdomains (as it was confirmed by the bulk phase separation, see Chapter 3), it might be speculated that multicompartment micelles and vesicles are formed in these solvents. Unfortunately, it was not possible to visualize these multicompartment structures by staining in TEM due to the presence of ruthenium in the polymer, but future investigations will be directed to prove the formation of multicompartment structures by, *e.g.*, dye-encapsulation studies.[69]

Due to the fact that PTFMS exhibits an UCST in 1-propanol, 2-propanol and 1-butanol, thermoreversible switching of the morphologies was investigated in 2-propanol. Therefore, the micellar solution was not cooled to room temperature after heating to 140 °C but only to 75 °C. The solution was left at 75 °C for 12 hours in order to allow the system to reach the equilibrium. Afterwards, the solution was drop-casted onto a heated TEM-grid. After evaporation of the solvent in the oven, the morphologies are kinetically frozen and the corresponding TEM image clearly reveals the formation of spherical micelles instead of vesicles that were present at room temperature (Figure 4.20). Above the UCST temperature in the less polar solvents, the triblock terpolymer behaves like in methanol and ethanol at room temperature, *i.e.* the PEG-block and the PTFMS-block are solubilized and accommodated in the corona of the micelle. Thus, the interfacial curvature increases and causes a transition from vesicles to spherical micelles. The larger aggregates in the image are believed to have been formed upon cooling of the micelle solution during the blotting onto the TEM grid since the clear solution turned slightly cloudy indicating changes in the particle size.

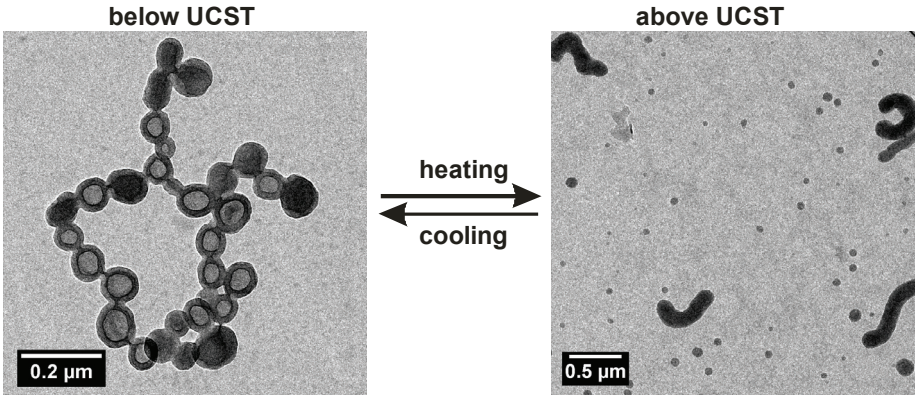

Figure 4.20 *TEM images of **IV-10** in 2-propanol at room temperature (left) and at 75 °C (right) representing the thermoreversible character of the formed aggregates.*

4.5 Polymeric terpyridine-based iridium(III) complexes

The combination of inorganic metal-containing units and macromolecules lead to supramolecular systems with new and exciting photo-and electrochemical properties.[70,71] In particular, the design of luminescent and redox-active transition-metal complexes is of interest and has been extensively studied in the last years because of their potential application in light-emitting devices[72-76] and solar cells.[77,78] Iridium(III) polypyridyl complexes are highly appealing due to their remarkable properties, such as high quantum yields and long lifetimes.[71] As a result of the metal-to-ligand based radiation, different emission colors can be observed depending on the introduced ligand. The incorporation of metal complexes into polymers prevents the formation of aggregates, which often leads to self-quenching and to reduced device lifetimes. Moreover, polymeric metal complexes feature the properties of the respective polymer and ensure easy processing of the

materials.[75] For this purpose, terpyridine-functionalized polymers obtained by NMP (Chapter 3) are suitable candidates since they are known to form mixed-ligand complexes with iridium.[79] Bridge-splitting reactions of iridium(III) precursor complexes with *N,N*-chelating ligands or *N,C*-cyclometallating ligands are common procedures to incorporate the orthometallated $[Ir(ppy)_2]$ fragment (ppy = phenyl pyridine) into mononuclear or multinuclear species.[80] The preparation of the iridium(III) precursor complexes of the type $[Ir(ppy)_2\text{-}\mu\text{-}Cl]_2$, was carried out according to literature reports.[81] Three different iridium(III) precursor complexes with various *N,C*-cyclometallating ligands have been prepared and used for the preparation of polymeric mixed-ligand iridium(III) complexes (Scheme 4.8). Therefore, the precursor complexes were reacted with the corresponding terpyridine-functionalized polymers (polystyrene (]-PS_{39}) and polystyrene-based copolymer **III-11** (]-PS_{48}-*co*-$PS_{anthr\ 3.6}$), respectively) under reflux conditions in a mixture of methylene chloride and methanol.[79] A counter ion exchange was performed by the addition of an excess of NH_4PF_6. The purification from unreacted materials was carried out by preparative size exclusion chromatography on BioBeads (SX-1, methylene chloride) and subsequent precipitation into ice-cold methanol. The polymers were dried *in vacuo* and subsequently characterized by means of ^{1}H NMR spectroscopy, GPC, UV-vis and emission spectroscopy. Figure 4.21 displays an overview of the starting materials used to obtain three different iridium-containing polymers.

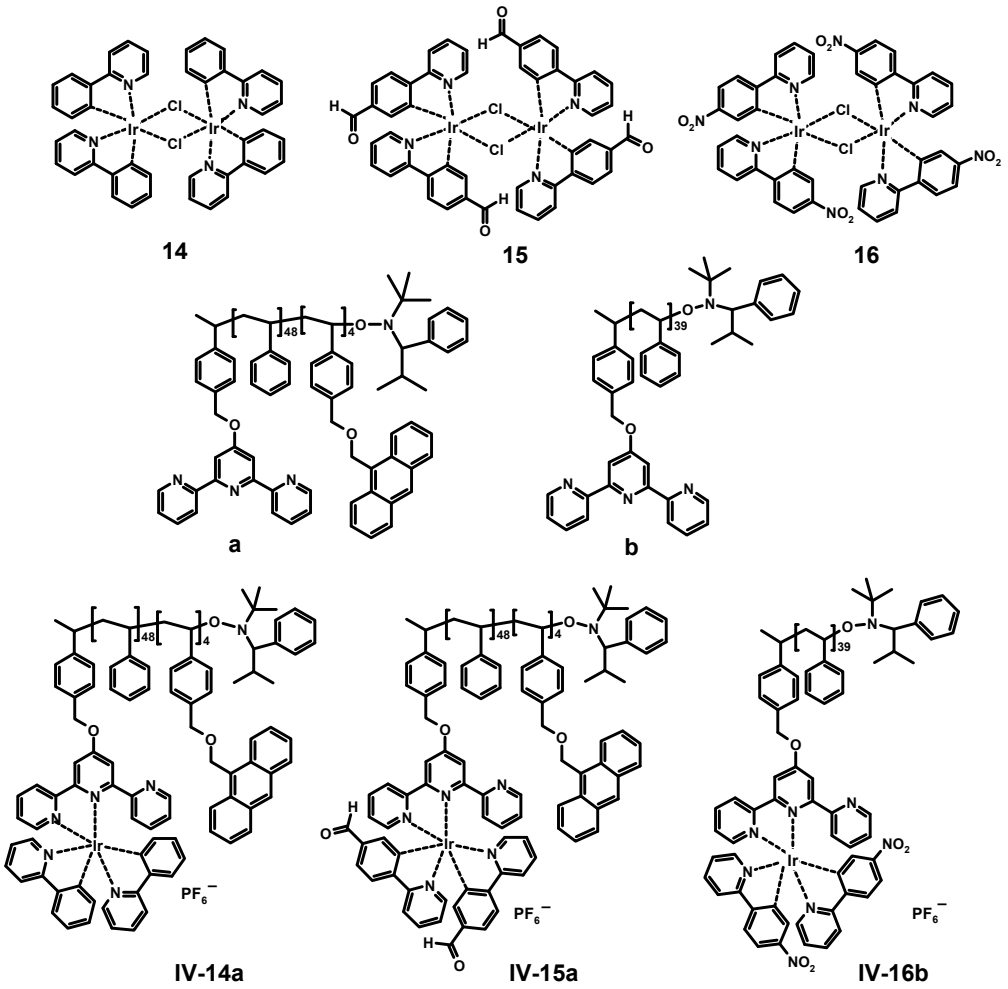

Figure 4.21 *Schematic representation of the synthesized light-emitting polymers based on mixed-ligand iridium(III) complexes. It displays the utilized iridium(III) precursor complexes (top row), the terpyridine-functionalized polymers (middle row) and the resulting functionalized mono-terpyridine Ir(III) complexes.*

The characterization by ^{1}H NMR spectroscopy shows clearly the formation of the desired polymeric complex (Figure 4.22). The signal of the cyclometallating ligand $H^{6'}$ which is next to the electron withdrawing nitro-group has been shifted upfield to 6.1 ppm. Furthermore, the signal which can be attributed to H^6 shifted slightly downfield to 9.35 ppm. GPC measurements were performed using a mixture of chloroform, triethylamine and 2-propanol as eluent (94:4:2). When the GPC-traces of the starting material are compared with those of the product, no real shift can be observed which would indicate that the complexation reaction was not successful. However, the obtained product revealed the typical yellow color as well as the emissive properties upon excitation with UV light. Therefore, the sample was injected a second time and the eluting fraction between 8 and 11 minutes was collected using the fraction collector. The collected eluent appeared yellow and it maintained the light-emissive behavior, indicating that the complex did not undergo fragmentation during the measurement. In general, charged complexes interact strongly with the column material; however, it seems that it is not the case for this particular compound. On the other hand, the GPC investigation of **IV-14a** and **IV-15a** reveal a small shift towards shorter elution volumes suggesting the desired complexation of the terpyridine-functionalized polymer with iridium. Observing unfragmented complexes in GPC clearly demonstrates the stability of the investigated supramolecular polymers.

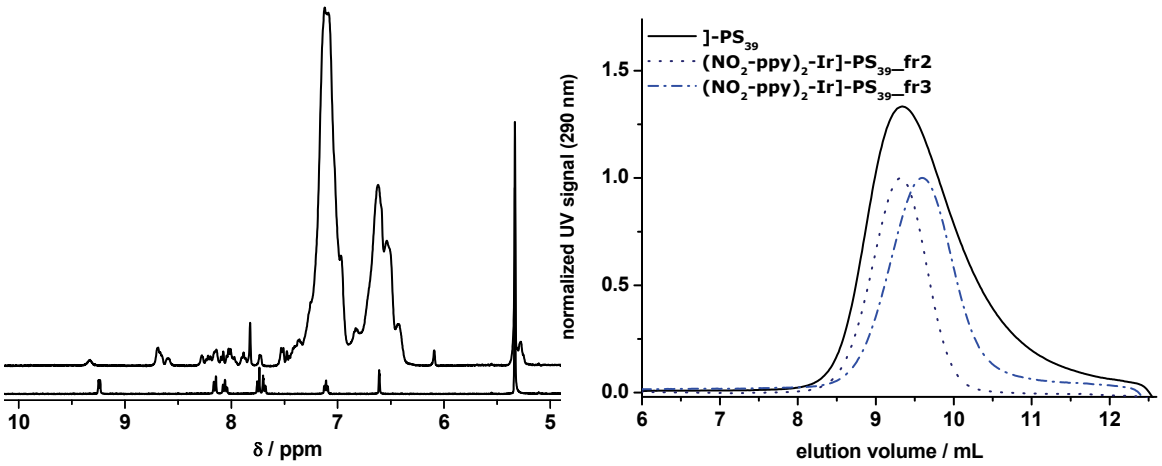

Figure 4.22 *Left: ^{1}H NMR spectra (in CD_2Cl_2) of the iridium(III) precursor complex (bottom) and the polymeric mixed-ligand iridium(III) complex* ***IV-16b*** *(top). Right: GPC chromatogram of the terpyridine-functionalized PS and the resulting complexed polymer* ***IV-16b****.*

The UV-vis spectra of the three synthesized polymers, **IV-14a**, **IV-15a** and **IV-16b**, display a strong absorption band at about 270 nm, which is attributed to the ligand centered π→π* transitions on the chelating ligand and on the cyclometallating phenyl pyridine (ppy) ligand. The broad absorption bands at lower energy (around 370 nm) are due to typical spin-allowed metal-to-ligand charge transfer transitions (^{1}MLCT, (dπ(Ir)→π*) tpy and ppy transitions). The shoulder tailing to approximately 440 nm was assigned to spin forbidden ^{3}MLCT (dπ(Ir)→π*) tpy and ppy transitions. Figure 4.23 shows the emission properties of the polymeric complexes in methylene chloride solution.

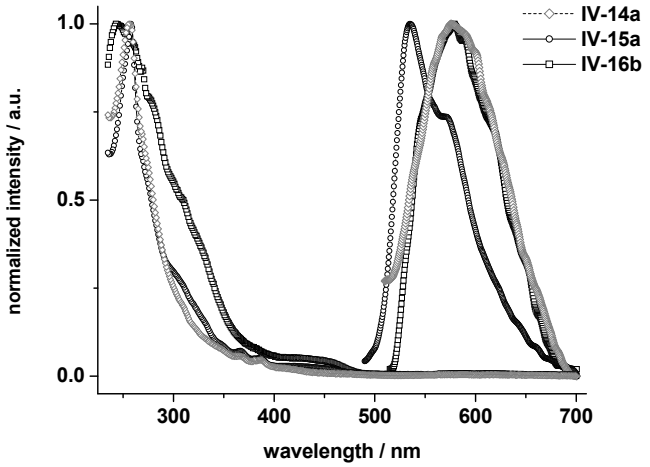

Figure 4.23 *Absorption and emission properties of the iridium-containing polymers in methylene chloride.*

Excitation of the polymeric iridium(III) complexes at 370 nm (^{1}MLCT) revealed broad emission bands due to ^{3}IC π→π* transitions on the cyclometallating ligand excited states. Moreover, there might be some ^{3}MLCT (dπ(Ir)→π* ppy) excited states involved. For the materials **IV-14a** and **IV-16b** this results in a broad band with a maximum at 580 nm. The emission band of compound **IV-15a** reveals an emission maximum at 535 nm and a shoulder with a maximum at 550 nm. Depending on the incorporated cyclometallating ligand and its resulting metal-to-ligand based radiation, different emission colors can be observed. Complex **IV-14a** showed a yellow emission, **IV-15a** a yellow-orange emission and **IV-16b** an orange emission, respectively. The synthesized iridium-containing materials combine the beneficial properties for light-emitting applications: the processability attributed to the polymer backbone as well as optical properties caused by the complex. For applications in light-emitting devices, the film formation plays a crucial role. The required smooth films are usually obtained by spin-coating from *ortho*-dichlorobenzene (ODCB).

4.6 Conclusions

This chapter has demonstrated the exploitation of the supramolecular terpyridine moiety. In the first part, metal directed self-assembly processes allowed the construction of metallo-supramolecular block copolymers where the metal complex is located at the junction between the constituting polymer blocks. A variety of macromolecular architectures were easily accessed including well-defined metallo-supramolecular diblock, triblock and tetrablock copolymers. All of the presented block copolymers were created by applying the Ru(III)/Ru(II) method, a well-known strategy for the formation of hetero-complexes. Subsequently, techniques such as ^{1}H NMR spectroscopy, GPC (using 5 mM NH_4PF_6 in DMF) also in combination with the photo-diode array detector and analytical ultracentrifugation have been successfully applied to characterize the obtained macromolecules. As a result of the amphiphilic nature of the block copolymers, micelles have been formed in aqueous and polar organic media, consisting of an insoluble core and a soluble corona. Characterization techniques such as DLS, AFM and TEM are suitable tools to analyze the formed microstructures. The self-organization in solution of more complex architectures, *e.g.* A-B-C triblock copolymers, revealed all basic micellar morphologies (spherical micelles, wormlike micelles, vesicles). The PS_{76}-*b*-$PTFMS_{42}$-[Ru]-PEG_{70} metallo-supramolecular triblock terpolymer was extensively investigated towards the influence of the solvent on the micelle formation. This particular triblock copolymer allowed the formation of discrete nano

objects whose morphology can be reversibly tuned as a function of temperature due to the UCST behavior of the fluorinated middle block. In the last part of this chapter, iridium(III)-containing polymers were prepared by complexation to iridium(III) precursors, leading to the formation of polymeric mixed-ligand iridium(III) complexes which exhibit different emission colors depending on the functionality on the introduced cyclometallating ligand. The optical properties of these materials were investigated by absorption/emission spectroscopy.

4.7 Experimental

Solvents were purchased from Biosolve. Polymers used for the preparation of the metallo-supramolecular block copolymers were synthesized as described in Chapter 3. In addition to the experimental set-ups described in Chapter 3, the following specifications are applicable for the measurements described in this chapter. Microwave-assisted reactions were performed in capped reaction vials especially designed for the single-mode microwave system Emrys Liberator (Biotage, formerly Personal Chemistry). The pressure and the temperature inside the vial were monitored by a pressure sensor on the septum and an IR temperature sensor, respectively. All reactions were carried out under temperature control with variable microwave power (maximal 300 W). Gel permeation chromatography (GPC) was measured on a Waters system with a 1515 pump, a 2414 refractive index detector, a 2996 photo diode array (PDA) detector and a Waters Styragel HT4 column utilizing a *N,N*-dimethylformamide (DMF) / 5 mM NH_4PF_6 mixture as eluent at a flow rate of 0.5 mL/min at 50 °C. Preparative size exclusion chromatography was performed on an Agilent system consisting of an Agilent 1100 series Control Module, an Agilent 1100 series Isocratic Pump, an Agilent 1100 series RID refractive index detector, an Agilent 1100 series Manual Injector and a PSS Gram preperative 100 Å column utilizing THF and 5 mM NH_4PF_6 as eluent at a flow rate of 3 mL/min. UV-Vis spectra were recorded on a Perkin Elmer Lambda 45P spectrophotometer. Emission spectra were recorded on a Perkin Elmer LS50B Luminescence spectrometer. The absolute quantum yields of bulk materials were determined using a multi-channel analyzer Hamamatsu of the type C10027 equipped with a BT-CCD linear image sensor, a Czerny-Turner spectrograph and a xenon/mercury-xenon lamp as excitation light source.

Analytical ultracentrifugation was performed on a ProteomeLabTM XL-I (Beckman Coulter) with a rotor speed of 55 000 rpm in a double sector cell with 12 mm optical path length using interference optics. Interference scans were measured overnight in intervals of 2 to 5 min. Sedimentation coefficients s, and frictional ratios (f/f_{sph}) were otained with Sedfit.[82]

Dynamic light scattering (DLS) experiments were performed on a Malvern CGS-3 equipped with a He-Ne laser (633 nm) at a 90° angle and at room temperature (25 °C). Transmission microscopy measurements were performed on a FEI Tecnai 20, type Sphera TEM operating at 200 kV (LaB_6 filament). Images were recorded with a bottom mounted 1 k × 1 k Gatan CCD camera. 200 mesh carbon coated copper grids for TEM were purchased from SPI. Prior to blotting, the grids were made hydrophilic by surface plasma treatment using a Cressington 208 carbon coater operating at 5 mA for 40 s. For sample preparation a droplet of the micelle solution was blotted onto the grid and subsequently excess liquid was manually removed with filter paper. The samples for TEM measurements were not stained. Samples for AFM were prepared by drop casting the micelle solution onto freshly cleaved mica. Imaging was performed in intermittent contact mode on a multimode SPM (Digital Instruments, Santa Barbara, CA) using OLTESPA-type tips. Scanning electron microscopy measurements were performed on a FEG E-SEM XL30 (Philips, Eindhoven).

The solubility measurements were performed by heating the polymer (2.0 ± 0.1 mg) in the corresponding solvent (1.0 mL) from −20 °C to 90 °C (methanol and ethanol) or from 20 °C to 100 °C (1-propanol, 2-propanol, 1-butanol) with a heating rate of 1.0 °C per minute followed by cooling at a cooling rate of 1.0 °C per minute after keeping the temperature for 10 minutes at the maximum/minimum temperature. During these controlled heating cycles the transmission through the solutions was monitored in a Crystal16 from Avantium Technologies.[83] All vials were visually inspected after the heating program to facilitate interpretation of the observed transmission profiles. The upper critical solution temperature (UCST) was determined at 50% transmittance in the second cooling cycle.

Preparation of the micelles in aqueous solution
The block copolymers were dissolved in *N,N'*- dimethylformamide (DMF) or tetrahydrofuran (THF) at a concentration of 1 $g \cdot L^{-1}$. Subsequently, drops of water were added stepwise to induce aggregation of the hydrophobic block. After that an equal amount of water was added in one shot to “freeze” the micelles. Finally, the solution was dialyzed against water for 24 hours, replacing the water at least three times (Spectra-Por dialysis bags, cutoff 1,000 Da).

Preparation of the micelles in organic media
The solutions containing the respective alcohol and the block copolymer (1 mg/mL) were heated in a closed reaction vessel under classical heating to 140 °C for 5 minutes and cooled slowly back to room temperature. The corresponding aggregates formed upon cooling.

Terpyridine end-functionalized poly(ethylene oxide) PEG_{70}-[**(IV-1)**
Powdered KOH (0.56 g, 10 mmol) and *α*-methoxy-*ω*-hydroxy-poly(ethylene oxide) with M_n = 3,000 g/mol (10 g, 3.33 mmol) were stirred under argon in dry dimethyl sulfoxide (DMSO) at 70 °C.[9] After 30 minutes a two times excess of 4'-chloro-2,2':6',2"-terpyridine (1.78 g, 6.7 mmol) was added. The mixture was stirred for 24 h at the given temperature, then poured into cold water (precipitation) and extracted with CH_2Cl_2. The combined organic layers were dried over Na_2SO_4 and the solvent was removed *in vacuo*. The polymer was purified by a double precipitation from THF into diethyl ether. Yield: 8.72 g (78%).
^{1}H-NMR (400 MHz, $CDCl_3$): δ (ppm) = 8.68 (dd, 2 H, ^3J = 4.8 Hz, ^4J = 1.6 Hz; $H_{6,6''}$), 8.61 (dd, 2 H, ^3J = 7.6 Hz , ^4J = 1.2 Hz; $H_{3,3''}$), 8.04 (s, 2 H, $H_{3',5'}$), 7.85 (td, 2 H, ^3J = 8 Hz, ^4J = 2 Hz; $H_{4,4''}$), 7.34 (dd, 2 H, ^3J = 4.8 Hz, ^4J = 0.8 Hz; $H_{5,5''}$), 4.40 (m, 2 H; tpyOCH_2), 3.93 (m, 2 H; tpyOCH$_2CH_2$), 3.82-3.45 (m, 280 H; PEO backbone), 3.38 (s, 3 H, OCH_3).
UV-vis (H_2O): λ_{max} (ε) = 278 (13,200), 234 (17,000) nm (L·mol^{-1}·cm^{-1}). GPC (eluent DMF with NH_4PF_6 (0.8 g/L)): M_n = 7,000 g/mol, PDI = 1.07.

$RuCl_3$ poly(ethylene oxide) mono-complex PEG_{70}-[$RuCl_3$ **(IV-2)**
A three fold excess of anhydrous $RuCl_3$ (0.12 g, 0.58 mmol) with respect to the terpyridine end functionalized polymer was heated in dry degassed DMA (6 mL) to 130 °C. After the color of the suspension turned brown, a solution of the poly(ethylene oxide) (0.62 g, 0.19 mmol) in dry degassed *N,N*-dimethyl acetamide (DMA) was added dropwise. Stirring continued overnight at 130 °C under inert conditions and then the solution was allowed to cool to room temperature. The resulting mixture was partitioned between dichloromethane and water. The organic layer was separated, dried over Na_2SO_4, filtered and evaporated *in vacuo*. The brown residue was taken up in a minimum amount of THF and precipitated twice in ice-cold diethyl ether. Yield: 0.53 g (78%). ^{1}H-NMR and ^{13}C-NMR spectroscopy ($CDCl_3$): only polymer backbone signals were visible because of the paramagnetic nature of the Ru(III)-complex. GPC (UV): M_n (PDI): 3,420 g mol^{-1} (1.20). UV-vis ($CHCl_3$): λ_{max} (ε) = 401 (8,700), 311 (16,500), 276 (31,000) nm (L·mol^{-1}·cm^{-1}).

PS_n-[Ru]-PEG_{70} (IV-3)
Terpyridine-functionalized polystyrene and the $RuCl_3$ poly(ethylene oxide) mono-complex were reacted in a 1:1 molar ratio in a 4:1 solvent mixture of degassed tetrahydrofuran and methanol for 1 hour at 90 °C in a sealed vial. The reaction mixture was stirred for 10 minutes at room temperature after a 10-fold excess of NH_4PF_6 was added. The solution was poured into water and the aqueous layer was extracted twice with chloroform. The combined organic layers were dried over Na_2SO_4, filtered and evaporated *in vacuo*. The crude product was purified by fractionation via preparative SEC. ^{1}H-NMR (PS_{130}-[Ru]-PEG_{70}, 400 MHz, CD_2Cl_2): δ (ppm) = 8.60-8.37 (m, 8 H; $H_{3':5''}$,$H_{3:3''}$), 7.85 (m, 4 H; $H_{4:4''}$), 7.35 (m, 4 H; $H_{6:6''}$), 7.34-6.32 (m, 661 H; $H_{PS\ backbone\ aromatic}$; $H_{aromatic}$, $H_{5,5''}$), 5.34 (m, 2 H; tpyOCH_2), 4.27-4.07 (broad, 1 H; *H*C-ON), 3.90-3.15 (m, 281 H; ON-C*H*, O$CH_{2\ PEG\ backbone}$), 2.62-0.40 (m, 409 H, $H_{PS\ backbone\ aliphatic}$; C(C$H_3$)$_3$; C$H_3$C*H*C$H_3$; C$H_{3\ initiating\ fragment}$). UV-vis ($CH_2Cl_2$) λ_{max} (ε) = 305 (20,500), 485 (5,250) nm (L·mol^{-1}·cm^{-1}).
PS_{50}-[Ru]-PEG_{70}; Yield: 20 mg (35%). GPC (UV): M_n (PDI): 39,800 g mol^{-1} (1.05).
PS_{130}-[Ru]-PEG_{70}; Yield: 30 mg (38%). GPC (UV): M_n (PDI): 46,800 g mol^{-1} (1.05).
PS_{285}-[Ru]-PEG_{70}. Yield: 10 mg (19%). GPC (UV): M_n (PDI): 56,700 g mol^{-1} (1.06).

General procedure of the complexation with PEG_{70}-[$RuCl_3$
PEG_{70}-[$RuCl_3$ and the terpyridine-functionalized polymer were dissolved in a degassed mixture of THF:MeOH or $CHCl_3$:MeOH. Subsequently, the reaction mixture was heated to 85 °C for 30 minutes. A few drops of *N*-ethylmorpholine were added to the solution. Stirring under reflux was continued overnight, after which an excess of NH_4PF_6 was added. The solvent was removed *in vacuo* and the reaction mixture was partitioned between 25 mL water and 25 mL methylene chloride (CH_2Cl_2). The organic layer was washed with water (3 × 25 mL), dried over Na_2SO_4 and finally removed *in vacuo*. The metallo-supramolecular block copolymer was further purified by preparative size exclusion chromatography (BioBeads SX-1) and column chromatography (Al_2O_4).

$PTFMS_{42}$-[Ru]-PEG_{70} (IV-4)
PEG_{70}-[$RuCl_3$ (98 mg, M_n = 3,400 g/mol, PDI = 1.07) and the terpyridine-functionalized $PTFMS_{42}$-[(200 mg, M_n = 7,800 g/mol, PDI = 1.16) were dissolved in a mixture of 1 mL THF and 0.5 mL MeOH.
^{1}H NMR (CD_2Cl_2): δ (ppm) = 8.61-8.35 (m, 8H; $H_{3':5'}$,$H_{3:3''}$), 7.86 (m, 4H; $H_{4:4''}$), 7.60-6.30 (m, 185 H; $H_{PTFMS\ aromatic\ backbone}$, $H_{aromatic}$, $H_{6,6''}$, $H_{5,5''}$), 5.30-5.20 (m, 2H; tpyOCH_2), 4.78 (m, 1H; *H*C-ON, both diastereomers), 3.90-3.15 (m, 281 H; ON-C*H*, major & minor, O$CH_{2\ PEG\ backbone}$), 2.30-0.00 (m, 145H; $H_{PTFMS\ backbone}$, C(CH_3)$_3$; CH_3CHCH_3 major & minor, CH_3CHCH_3; CH_3CH-ON). Yield: 45%. GPC (eluent DMF with NH_4PF_6 (0.8 g/L)): M_n = 10,700 g/mol, PDI = 1.08.

$PPFS_{30}$-[Ru]-PEG_{70} (IV-5)
PEG_{70}-[$RuCl_3$ (63 mg, M_n = 3,400 g/mol, PDI = 1.07) and the terpyridine-functionalized $PPFS_{30}$-[(100 mg, M_n = 6,400 g/mol, PDI = 1.09) were dissolved in a mixture of 1 mL THF and 0.5 mL MeOH.
^{1}H-NMR (CD_2Cl_2): δ (ppm) = 8.60-8.37 (m, 8H; $H_{3':5'}$,$H_{3:3''}$), 7.86 (m, 4H; $H_{4:4''}$), 7.45-6.95 (m, 17 H; $H_{aromatic}$, $H_{6,6''}$, $H_{5,5''}$), 5.30-5.20 (m, 2 H; tpyOCH_2),4.78 (m, 1 H; *H*C-ON, both diastereomers), 3.90-3.15 (m, 281 H; ON-C*H*, major & minor, OCH_2 PEG backbone), 3.09-1.70 (m, 91 H; $H_{PPFS\ backbone}$, CH_3CHCH_3 major), 1.60-0.15 (m, 18 H; C(CH_3)$_3$; CH_3CHCH_3 minor, CH_3CHCH_3; CH_3CH-ON). Yield: 43%. GPC (eluent DMF with NH_4PF_6 (0.8 g/L)): M_n = 9,500 g/mol, PDI = 1.07.

P*t*BA_{25}-*block*-PS_{35}-[Ru]-PEG_{70} (IV-6)
PEG_{70}-[$RuCl_3$ (50 mg, M_n = 3,400 g/mol, PDI = 1.07) and the terpyridine-functionalized P*t*BA_{25}-*block*-PS_{35}-[(82 mg, M_n = 7,400 g/mol, PDI = 1.12) were dissolved in a mixture of 0.7 mL $CHCl_3$ and 0.5 mL MeOH.
^{1}H-NMR (CD_2Cl_2): δ (ppm) = 8.60-8.36 (m, 8H; $H_{3':5'}$,$H_{3:3''}$), 7.87 (m, 4H; $H_{4:4''}$), 7.50-6.22 (m, 192 H; $H_{PS\ aromatic\ backbone}$, $H_{aromatic}$, $H_{6,6''}$, $H_{5,5''}$), 5.34 (m, 2 H; tpyOCH_2), 4.27-4.07 (broad, 1 H; *H*C-ON), 3.90-3.15 (m, 281 H; ON-C*H*, major & minor, OCH_2 PEG backbone), 2.26-0.39 (m, 199 H, $H_{PS\ backbone\ aliphatic}$; C($CH_3$)$_3$; CH_3CHCH_3; CH_3 initiating fragment, $H_{PtBA\ backbone}$). Yield: 55%. GPC (eluent DMF with NH_4PF_6 (0.8 g/L)): M_n = 7,500 g/mol, PDI = 1.11.

PMA_{54}-*block*-PS_{34}-[Ru]-PEG_{70} (IV-7)
PEG_{70}-[$RuCl_3$ (83 mg, M_n = 3,400 g/mol, PDI = 1.07) and the terpyridine-functionalized PMA_{54}-*block*-PS_{34}-[(45 mg, M_n = 8,800 g/mol, PDI = 1.23) were dissolved in a mixture of 0.7 mL $CHCl_3$ and 0.5 mL MeOH.
^{1}H-NMR (CD_2Cl_2): δ (ppm) = 8.62-8.36 (m, 8H; $H_{3':5'}$,$H_{3:3''}$), 7.87 (m, 4H; $H_{4:4''}$), 7.59-6.30 (m, 187 H; $H_{PS\ aromatic\ backbone}$, $H_{aromatic}$, $H_{6,6''}$, $H_{5,5''}$), 5.30-5.20 (m, 2 H; tpyOCH_2), 4.78 (m, 1 H; *H*C-ON, both diastereomers), 3.93-3.15 (m, 443 H; ON-C*H*, major & minor, OCH_3 MA, OCH_2 PEG backbone), 2.50-0.80 (m, 280 H; $H_{PS\ backbone}$, $H_{PMA\ backbone}$, CH_3CHCH_3 major, C(CH_3)$_3$; CH_3CHCH_3 minor, CH_3CHCH_3 major, CH_3CHCH_3 minor, CH_3CH-ON), 0.55-0.40 (d, 3 H, CH_3CHCH_3 minor, CH_3CHCH_3 major). Yield: 50%. GPC (eluent DMF with NH_4PF_6 (0.8 g/L)): M_n = 10,900 g/mol, PDI = 1.11.

PS_{73}-*block*-$PPFS_{30}$-[Ru]-PEG_{70} (IV-8)
PEG_{70}-[$RuCl_3$ (28 mg, M_n = 3,400 g/mol, PDI = 1.07) and the terpyridine-functionalized PS_{73}-*block*-$PPFS_{30}$-[(120 mg, M_n = 14,000 g/mol, PDI = 1.18) were dissolved in a mixture of 1 mL THF and 0.5 mL MeOH.
^{1}H-NMR (CD_2Cl_2): δ (ppm) = 8.61-8.35 (m, 8H; $H_{3':5'}$,$H_{3:3''}$), 7.86 (m, 4H; $H_{4:4''}$), 7.45-6.30 (m, 382 H; $H_{PS\ aromatic\ backbone}$, $H_{aromatic}$, $H_{6,6''}$, $H_{5,5''}$), 5.30-5.20 (m, 2 H; tpyOCH_2),4.78 (m, 1 H; *H*C-ON, both diastereomers), 3.90-3.15 (m, 281 H; ON-C*H*, major & minor, OCH_2 PEG backbone), 2.90-0.10 (m, 328 H; $H_{PPFS\ \&\ PS\ backbone}$, CH_3CHCH_3 major, C(CH_3)$_3$; CH_3CHCH_3 minor, CH_3CHCH_3; CH_3CH-ON). Yield: 47%. GPC (eluent DMF with NH_4PF_6 (0.8 g/L)): M_n = 7,700 g/mol, PDI = 1.13.

$PPFS_{80}$-*block*-PS_{44}-[Ru]-PEG_{70} (IV-9)
PEG_{70}-[$RuCl_3$ (26 mg, M_n = 3,400 g/mol, PDI = 1.07) and the terpyridine-functionalized $PPFS_{80}$-*block*-PS_{44}-[(100 mg, M_n = 20,700 g/mol, PDI = 1.23) were dissolved in a mixture of 2 mL THF and 1 mL MeOH.
^{1}H-NMR (CD_2Cl_2): δ (ppm) = 8.62-8.36 (m, 8H; $H_{3':5'}$,$H_{3:3''}$), 7.86 (m, 4H; $H_{4:4''}$), 7.58-6.31 (m, 237 H; $H_{PS\ aromatic\ backbone}$, $H_{aromatic}$, $H_{6,6''}$, $H_{5,5''}$), 5.30-5.20 (m, 2 H; tpyOCH_2), 4.78 (m, 1 H; *H*C-ON, both diastereomers), 3.90-3.15 (m, 281 H; ON-C*H*, major & minor, OCH_2 PEG backbone), 2.91-0.24 (m, 391 H; $H_{PPFS\ \&\ PS\ backbone}$, C($CH_3$)$_3$; CH_3CHCH_3 major & minor, CH_3CHCH_3 major & minor; CH_3CH-ON). Yield: 49%. GPC (eluent DMF with NH_4PF_6 (0.8 g/L)): M_n = 13,100 g/mol, PDI = 1.08.

PS_{76}-*block*-$PTFMS_{42}$-[Ru]-PEG_{70} (IV-10)
PEG_{70}-[$RuCl_3$ (25 mg, M_n = 3,400 g/mol, PDI = 1.07) and the terpyridine-functionalized PS_{76}-*block*-$PTFMS_{42}$-[(95 mg, M_n = 15,800 g/mol, PDI = 1.22) were dissolved in a mixture of 1 mL THF and 0.5 mL MeOH.
^{1}H-NMR (CD_2Cl_2): δ (ppm) = 8.60-8.37 (m, 8H; $H_{3':5'}$,$H_{3:3''}$), 7.86 (m, 4H; $H_{4:4''}$), 7.58-6.21 (m, 565H; $H_{PS\ \&\ PTFMS\ aromatic\ backbone}$, $H_{aromatic}$, $H_{6,6''}$, $H_{5,5''}$), 5.30-5.20 (m, 2H; tpyOCH_2), 4.78 (m, 1H; *H*C-ON, both diastereomers), 3.90-3.15 (m, 281H; ON-C*H*, major & minor, OCH_2 PEG backbone), 2.37-0.10 (m, 373H; $H_{PTFMS\ \&\ PS\ aliphatic\ backbone}$, CH_3CHCH_3 major, C(CH_3)$_3$; CH_3CHCH_3 minor, CH_3CHCH_3; CH_3CH-ON). Yield: 49%. GPC (eluent DMF with NH_4PF_6 (0.8 g/L)): M_n = 11,000 g/mol, PDI = 1.10.

$PTFMS_{34}$-*block*-PS_{50}-[Ru]-PEG_{70} (IV-11)
PEG_{70}-[$RuCl_3$ (30 mg, M_n = 3,400 g/mol, PDI = 1.07) and the terpyridine-functionalized $PTFMS_{34}$-*block*-PS_{44}-[(86 mg, M_n = 11,700 g/mol, PDI = 1.17) were dissolved in a mixture of 1.2 mL $CHCl_3$ and 0.6 mL MeOH.
^{1}H-NMR (CD_2Cl_2): δ (ppm) = 8.61-8.35 (m, 8H; $H_{3':5'}$,$H_{3:3''}$), 7.85 (m, 4H; $H_{4:4''}$), 7.59-6.33 (m, 403 H; $H_{PS\ \&\ PTFMS\ aromatic\ backbone}$, $H_{aromatic}$, $H_{6,6''}$, $H_{5,5''}$), 5.30-5.20 (m, 2 H; tpyOCH_2), 4.78 (m, 1 H; *H*C-ON, both diastereomers), 3.90-3.15 (m, 281 H; ON-C*H*, major & minor, OCH_2 PEG backbone), 2.30-0.24 (m, 271 H; $H_{PTFMS\ \&\ PS\ backbone}$, C($CH_3$)$_3$; CH_3CHCH_3 major & minor, CH_3CHCH_3 major & minor; CH_3CH-ON). Yield: 53%. GPC (eluent DMF with NH_4PF_6 (0.8 g/L)): M_n = 11,400 g/mol, PDI = 1.12.

$PTFMS_{20}$-*block*-P*t*BA_{25}-*block*-PS_{35}-[Ru]-PEG_{70} (IV-12)
PEG_{70}-[$RuCl_3$ (30 mg, M_n = 3,400 g/mol, PDI = 1.07) and the terpyridine-functionalized $PTFMS_{20}$-*block*-P*t*BA_{25}-*block*-PS_{35}-[(67 mg, M_n = 10,900 g/mol, PDI = 1.33) were dissolved in a mixture of 0.6 mL $CHCl_3$ and 0.3 mL MeOH. ^{1}H-NMR (CD_2Cl_2): δ (ppm) = 8.62-8.37 (m, 8H; $H_{3':5'}$,$H_{3:3"}$), 7.86 (m, 4H; $H_{4:4"}$), 7.45-6.35 (m, 272 H; $H_{PS\ \&\ PTFMS\ aromatic\ backbone}$, $H_{aromatic}$, $H_{6,6"}$, $H_{5,5"}$), 5.30-5.20 (m, 2 H; tpyOCH_2),4.78 (m, 1 H; *H*C-ON, both diastereomers), 3.90-3.15 (m, 281 H; ON-C*H*, major & minor, OC$H_{2\ PEG\ backbone}$), 2.90-0.41 (m, 586 H; $H_{PPFS\ \&\ PS\ \&\ PMA\ backbone}$, CH_3CHCH_3 major, C(CH_3)$_3$; CH_3CHCH_3 minor, CH_3CHCH_3; CH_3CH-ON). Yield: 41%. GPC (eluent DMF with NH_4PF_6 (0.8 g/L)): M_n = 10,900 g/mol, PDI = 1.15.

$PPFS_{97}$-*block*-PMA_{58}-*block*-PS_{35}-[Ru]-PEG_{70} (IV-13)
PEG_{70}-[$RuCl_3$ (28 mg, M_n = 3,400 g/mol, PDI = 1.07) and the terpyridine-functionalized $PPFS_{97}$-*block*-PMA_{58}-*block*-PS_{35}-[(80 mg, M_n = 28,000 g/mol, PDI = 1.28) were dissolved in a mixture of 0.7 mL $CHCl_3$ and 0.4 mL MeOH. ^{1}H-NMR (CD_2Cl_2): δ (ppm) = 8.60-8.36 (m, 8H; $H_{3':5'}$,$H_{3:3"}$), 7.87 (m, 4H; $H_{4:4"}$), 7.58-6.21 (m, 192 H; $H_{PS\ aromatic\ backbone}$, $H_{aromatic}$, $H_{6,6"}$, $H_{5,5"}$), 5.30-5.20 (m, 2 H; tpyOCH_2),4.78 (m, 1 H; *H*C-ON, both diastereomers), 3.95-3.15 (m, 455 H; ON-C*H*, major & minor, $OCH_{3\ MA}$, OC$H_{2\ PEG\ backbone}$), 2.90-0.15 (m, 586 H; $H_{PPFS\ \&\ PS\ \&\ PMA\ backbone}$, CH_3CHCH_3 major, C(CH_3)$_3$; CH_3CHCH_3 minor, CH_3CHCH_3; CH_3CH-ON). Yield: 42%. GPC (eluent DMF with NH_4PF_6 (0.8 g/L)): M_n = 12,600 g/mol, PDI = 1.08.

(14) $[Ir(ppy)_2$-μ-$Cl]_2$ (15) $[Ir(ppy\text{-}CHO)_2$-μ-$Cl]_2$ (16) $[Ir(ppy\text{-}NO_2)_2$-μ-$Cl]_2$
The iridium(III) precursor complexes were synthesized according to published procedures.[81]

***Tetrakis*(2-phenylpyridine-C^2,N´)(μ-dichloro)diiridium (14)**
^{1}H-NMR (CD_2Cl_2): δ (ppm) = 5.79 (d, 4 H; $^3J_{H,H}$ = 8.8 Hz, $H^{6'}$), 6.50-6.54 (m, 4 H; $H^{5'}$), 6.71-6.76 (m, 8 H; $H^{4'}$, H^5), 7.46-7.49 (m, 4 H; $H^{3'}$), 7.69-7.74 (m, 4 H; H^4), 7.86 (d, 4 H; $^3J_{H,H}$ = 8.00 Hz, H^3), 9.17 (d, 4 H; $^3J_{H,H}$ = 5.60 Hz, H^6).

***Tetrakis*(2-phenyl-4-CHO-pyridine-C^2,N´)(μ-dichloro)diiridium (15)**
^{1}H-NMR ($CDCl_3$): δ (ppm) = 9.51 (s, 4 H; CHO), 9.25 (d, 4 H; H^6); 8.20-7.85 (m, 8 H, H^3, H^4); 7.68 (m, 4 H, $H^{3'}$); 7.32 (m, 4 H, $H^{4'}$); 6.95 (t, 4 H, H^5), 6.39 (s, 4 H; $H^{6'}$).

***Tetrakis*(2-phenyl-4-nitro-pyridine-C^2,N´)(μ-dichloro)diiridium (16)**
^{1}H-NMR (CD_2Cl_2): δ (ppm) = 6.61 (s, 4 H; $H^{6'}$); 7.11 (t, 4 H, H^5); 7.80-6.78 (m, 8H, H^3, H^4); 8.20-8.02 (m, 8 H, $H^{3'}$, $H^{4'}$); 9.23 (d, 4 H, H^6).

General procedure of the complexation with iridium(III) precursor complexes
The iridium(III) precursor complex and the terpyridine-functionalized polymer were added into a vial containing a mixture of degassed CH_2Cl_2 and MeOH. Subsequently, the reaction mixture was heated to 80 °C for 6 h. After cooling the reaction mixture to room temperature an excess of NH_4PF_6 was added. The solvent was removed *in vacuo* and the reaction mixture was partitioned between 25 mL water and 25 mL methylene chloride (CH_2Cl_2). The organic layer was washed with water (3 × 25 mL), dried over Na_2SO_4 and finally removed *in vacuo*. The metallo-supramolecular block copolymer was further purified by preparative size exclusion chromatography (BioBeads SX-1).

Iridium(III)[2,2':6'2"-terpyridine-4'-yloxy)-PS_{48}-*co*-$PS_{anthr3.6}$][ppy]$_2$ (PF_6) (IV-14a)
$[Ir(ppy)_2$-µ-$Cl]_2$ (12.3 mg, M = 1072 g/mol) and the terpyridine-functionalized]-PS_{48}-*co*-$PS_{anthr3.6}$ (105 mg, M_n = 5,000 g/mol, PDI = 1.14) are dissolved in a degassed mixture of 3 mL CH_2Cl_2 and 1 mL MeOH. ^{1}H-NMR (CD_2Cl_2): δ (ppm) = 8.75-8.63 (m, 1 H; H^6-ppy), 8.51 (m, 3.6 H; $H_{anthr.}$), 8.34-8.16 (m, 8.2 H; H^6-ppy, H_{anthr}), 8.11-7.92 (m, 9.2 H; H_6-tpy, H^5-ppy, $H_{anthr.}$), 7.84-6.10 (m, 291 H; $H_{3':5'}$-tpy, $H_{4:4"}$-tpy, $H_{6"}$-tpy, H_4-tpy, 2 × $H^{3'}$-ppy, $H_{PS\ backbone\ aromatic}$; $H_{aromatic}$, $H_{aromatic\ macromonomer}$, $H_{anthr.}$, $H_{3:3"}$-tpy, $H_{5:5"}$-tpy, 2 × H^3-ppy, 2 × H^4-ppy, H^5-ppy, 2 × H^4-ppy, 2 × H^5-ppy), 5.78 (m, 1H; $H^{6'}$-ppy), 5.60-5.10 (m, 10.2 H; tpyOCH_2, OCH_2-$_{anthr}$, $H^{6'}$-ppy), 4.93-4.05 (broad, 8.2 H; *H*C-ON, PhCH_2O), 3.50-3.15 (m, 1 H; ON-C*H*), 2.50-0.15 (m, 174 H, $H_{PS\ \&\ PS\ anthr.\ backbone\ aliphatic}$; C($CH_3$)$_3$; CH_3CHCH_3; $CH_{3\ initiating\ fragment}$). UV-Vis ($CH_2Cl_2$): λ_{max} (ε) = 256 (61,670), 268 (42,840), 364 (3,500), 439 (700) nm (L·mol^{-1}·cm^{-1}), Quantum yield: 0.01. GPC (eluent $CHCl_3$, triethylamine, and 2-propanol (94:4:2): M_n = 7,400 g/mol, PDI = 1.40.

Iridium(III)[2,2':6'2"-terpyridine-4'-yloxy)-PS_{48}-*co*-$PS_{anthr3.6}$][ppy-CHO]$_2$ (PF_6) (IV-15a)
$[Ir(ppy\text{-}CHO)_2$-µ-$Cl]_2$ (16.1 mg, M = 1184 g/mol) and the terpyridine-functionalized]-PS_{48}-*co*-$PS_{anthr3.6}$ (124 mg, M_n = 5,000 g/mol, PDI = 1.14) were dissolved in a degassed mixture of 3 mL CH_2Cl_2 and 1 mL MeOH. ^{1}H-NMR (CD_2Cl_2): δ (ppm) = 9.63 (s, 2 H; CHO), 8.75-8.63 (m, 1 H; H^6-ppy), 8.51 (m, 3.6 H; $H_{anthr.}$), 8.34-8.16 (m, 8.2 H; H^6-ppy, H_{anthr}), 8.11-7.92 (m, 9.2 H; H_6-tpy, H^5-ppy, $H_{anthr.}$), 7.84-6.10 (m, 289 H; $H_{3':5'}$-tpy, $H_{4:4"}$-tpy, $H_{6"}$-tpy, H_4-tpy, 2 × $H^{3'}$-ppy, $H_{PS\ backbone\ aromatic}$; $H_{aromatic}$, $H_{aromatic\ macromonomer}$, $H_{anthr.}$, $H_{3:3"}$-tpy, $H_{5:5"}$-tpy, 2 × H^3-ppy, 2 × H^4-ppy, H^5-ppy, 2 × H^4-ppy), 5.78 (m, 1H; $H^{6'}$-ppy), 5.60-5.10 (m, 10.2 H; tpyOCH_2, OCH_2-$_{anthr}$, $H^{6'}$-ppy), 4.93-4.05 (broad,

8.2 H; *H*C-ON, PhC*H*$_2$O), 3.50-3.15 (m, 1 H; ON-C*H*), 2.50-0.15 (m, 174 H, H$_{PS\ \&\ PS\ anthr.\ backbone\ aliphatic}$; C(C*H*$_3$)$_3$; C*H*$_3$C*H*C*H*$_3$; C*H*$_{3\ initiating\ fragment}$). UV-Vis ($CH_2Cl_2$): λ_{max} (ε) = 258 (99,554), 269 (61,890), 370 (7,010), 440 (2,526) nm (L·mol^{-1}·cm^{-1}). Quantum yield: 0.04. GPC (eluent $CHCl_3$, triethylamine, and 2-propanol (94:4:2): M_n = 5,200 g/mol, PDI = 1.38.

Iridium(III)[2,2':6'2"-terpyridine-4'-yloxy)-PS$_{39}$][ppy-NO$_2$]$_2$ (PF_6) (IV-16b)
[Ir(ppy-NO$_2$)$_2$-μ-Cl]$_2$ (23.2 mg, M = 1252 g/mol) and the terpyridine-functionalized]-PS$_{39}$ (155 mg, M_n = 4,600 g/mol, PDI = 1.16) were dissolved in a degassed mixture of 3 mL CH_2Cl_2 and 1 mL MeOH. ^{1}H-NMR (CD_2Cl_2): δ(ppm) = 9.35 (m, 1 H; H^6-ppy), 8.76-6.20 (m, 232 H; H^6-ppy, H$_6$-tpy, H^5-ppy, H$_{3':5'}$-tpy, H$_{4:4"}$-tpy, H$_{6"}$-tpy, H$_4$-tpy, 2 × H$^{3'}$-ppy, H$_{PS\ backbone\ aromatic}$; H$_{aromatic}$, , H$_{3:3"}$-tpy, H$_{5:5"}$-tpy, 2 × H^3-ppy, 2 × H^4-ppy, H^5-ppy, 2 × H$^{4'}$-ppy), 6.10 (m, 1H; H$^{6'}$-ppy), 5.34 (m, 2 H; tpyOC*H*$_2$), 4.27-4.07 (broad, 1 H; *H*C-ON), 3.50-3.15 (m, 1 H; ON-C*H*), 2.45-0.40 (m, 136 H, H$_{PS\ backbone\ aliphatic}$; C(C*H*$_3$)$_3$; C*H*$_3$C*H*C*H*$_3$; C*H*$_{3\ initiating\ fragment}$). UV-Vis ($CH_2Cl_2$): λ_{max} (ε) = 245 (55,960), 269 (49,060), 369 (5,586), 439 (2,712) nm (L·mol^{-1}·cm^{-1}). Quantum yield: 0.01. GPC (eluent $CHCl_3$, triethylamine, and 2-propanol (94:4:2): M_n = 4,000 g/mol, PDI = 1.09.

4.8 References

1 J.-F. Gohy, B.G.G. Lohmeijer, U.S. Schubert, *Chem. Eur. J.* **2003**, *9*, 3472.
2 D. Choudhury, R.F. Jones, G. Smith, D.J. Cole-Hamilton, *J. Chem. Soc., Dalton Trans.* **1982**, 1143.
3 T. Togano, N. Nagao, M. Tsuchida, H. Kumakura, K. Hisamatsu, F.S. Howell, M. Mukaida, *Inorg. Chim. Acta* **1992**, *195*, 221.
4 B.P. Sullivan, J.M. Calvert, T.J. Meyer, *Inorg. Chem.* **1980**, *19*, 1404.
5 F.P. Dwyer, H.A. Goodwin, E.C. Gyarfas, *Aust. J. Chem.* **1963**, *16*, 42.
6 A. Dovletoglou, S.A. Adeyemi, *Inorg. Chem.* **1996**, *35*, 4120.
7 U.S. Schubert, O. Hien, C. Eschbaumer, *Macromol. Rapid Commun.* **2000**, *21*, 1156.
8 U.S. Schubert, C. Eschbaumer, *Macromol. Symp.* **2001**, *163*, 177.
9 U.S. Schubert, S. Schmatloch, A.A. Precup, *Design. Monom. Polym.* **2002**, *5*, 211.
10 J.C. Dobson, B.P. Sullivan, P. Doppelt, T.J. Meyer, *Inorg. Chem.* **1988**, *27*, 3863.
11 C. Anderson, A.L. Beauchamp, *Can. J. Chem.* **1995,** *73*, 471.
12 P.J. Hore, *Nuclear magnetic resonance (Oxford chemistry primers, 32)*, Oxford University Press, Oxford, **1996**.
13 I.W. Hamley, *The Physics of Block Copolymers,* Oxford University Press, Oxford, **1998**.
14 F.S. Bates, G.H. Fredrickson, *Phys. Today* **1999**, *52*, 32.
15 J. Rodriguez-Hernandez, F. Chécot, Y. Gnanou, S. Lecommandoux, *Prog. Polym. Sci.* **2005**, *30*, 691.
16 D.E. Discher, A. Eisenberg, *Science* **2002**, *297*, 967.
17 G. Riess, *Prog. Polym. Sci.* **2003**, *28*, 1107.
18 R. Adhikari, R. Lach, G.H. Michler, R. Weidisch, W. Grellmann, K. Knoll, *Polymer* **2002**, *43*, 1943.
19 D.I. Bower, *An Introduction to Polymer Physics*, Cambridge University Press, Cambridge, **2002.**
20 J.G. Drobny, *Handbook of Thermoplastic Elastomers*, William Andrew Publishing, Norwich, **2007**.
21 N. Hadjichristidis, S. Pispas, G.A. Floudas, *Block Copolymers, Synthetic Strategies, Physical Properties, and Applications,* John Wiley & Sons, **2002**.
22 B. Smarsly, D. Grosso, T. Brezesinski, N. Pinna, C. Boissiere, M. Antionetti, C. Sanchez, *Chem. Mater.* **2004**, *16*, 2948.
23 R.E. Cohen, *Curr. Opin. Sol. State Mat. Sci.* **2000**, *4*, 587.
24 A.Rosler, G.W.M. Vandermeulen, H.-A. Klok, *Adv. Drug Deliv. Rev.* **2001**, *53*, 95.
25 A. Mortensen, *Concise Encyclopedia of Composite Materials,* Elsevier, Amsterdam, **2007**.
26 J.-M. Lehn, *Supramolecular Chemistry,* VCH, Weinheim, Germany, **1995**.
27 B.G.G. Lohmeijer, U.S. Schubert, *Angew. Chem. Int. Ed.* **2002**, *41*, 3825.
28 A.J. Goshe, I.M. Steele, C. Ceccarelli, A.L. Rheigold, B. Bosnich, *Proc. Natl. Acad. Sci.* **2002**, *99*, 4823.
29 M.A.R. Meier, D. Wouters, C. Ott, P. Guillet, C.-A. Fustin, J.-F. Gohy, U.S. Schubert, *Macromolecules* **2006**, *39*, 1569.
30 B.L. Hayes, *Microwave synthesis: Chemistry at the speed of light,* CEM publishing, Matthews (NC),

2002.
31 M.A.R. Meier, B.G.G. Lohmeijer, U.S. Schubert, *Macromol. Rapid Commun.* **2003**, *24*, 852.
32 A.M. Afifi-Effat, J.N. Hay, *Eur. Polym. J.* **1972**, *8*, 289.
33 G.G. Cameron, M.D. Ingram, M.Y. Qureshi, H.M. Gearing, *Eur. Polym. J.* **1989**, *25*, 779.
34 J. Scheirs, S.W. Bigger, O. Delatycki, *Eur. Polym. J.* **1991**, *27*, 1111.
35 S. Han, C. Kim, D. Kwon, *Polymer* **1997**, *38*, 317.
36 N. Stravrouli, A.I. Triftaridou, C.S. Patrickios, *Macromol. Rapid Commun.* **2007**, *28*, 560.
37 A.I. Triftaridou, M. Vamvakaki, C.S. Patrickios, *Polymer* **2002**, *43*, 2921.
38 L. Zhang, A. Eisenberg, *J. Am. Chem. Soc.* **1996**, *118*, 3168.
39 S. Förster, T. Plantenberg, *Angew. Chem. Int. Ed.* **2002**, *41*, 688.
40 J.-F. Gohy, N. Willet, S. Varshney, J.X. Zhang, R. Jérôme, *Angew. Chem. Int. Ed.* **2001**, *40*, 3214.
41 Y. Cai, S.P. Armes, *Macromolecules* **2004**, *37*, 7116.
42 V. Sfika, C. Tsitsilianis, A. Kiriy, G. Gorodyska, M. Stamm, *Macromolecules* **2004**, *37*, 9551.
43 Q. Ma, K.L. Wooley, *J. Polym. Sci., Part A: Polym. Chem.* **2000**, *38*, 4805.
44 A.K. Brannan, F.S. Bates, *Macromolecules* **2004**, *37*, 8816.
45 J. Milton Harris, *Poly(ethylene glcol) Chemistry: Biotechnical and Biomedical Apllications*, Plenum Press, New York, NY, **1992**.
46 S. Mahajan, B.-K. Cho, J. Allgaier, L. Fetters, G. Coates, U. Wiesner, *Macromol. Rapid Commun.* **2004**, *25*, 1889.
47 D.J. Pochan, Z. Chen, H. Cui, K. Hales, K. Qi, K.L. Wooley, *Science* **2004**, *306*, 94.
48 P. Wang, J.T. Koberstein, *Macromolecules* **2004**, *37*, 5671.
49 J.S. Pedersen, I.W. Hamley, C.Y. Ryu, T.P. Lodge, *Macromolecules* **2000**, *33*, 542.
50 B.M. Discher, Y.Y. Won, D.S. Ege, J.C.-M. Lee, F.S. Bates, D.E. Discher, D.A. Hammer, *Science* **1999**, *284*, 1143.
51 L. Yang, P. Alexandridis, *Curr. Opin. Colloid Interface Sci.* **2000**, *5*, 132.
52 M. Svensson, P. Alexandridis, P. Linse, *Macromolecules* **1999**, *32*, 637.
53 T.P. Lodge, J.A. Bang, Z.B. Li, M.A. Hillmyer, Y. Talmon, *Faraday Discuss.* **2005**, *128*, 1.
54 J.-F. Gohy, *Adv. Polym. Sci.* **2005**, *190*, 65.
55 L. Desbaumes, A. Eisenberg, *Langmuir* **1999**, *15*, 36.
56 C.J. Hawker, K.L. Wooley, *Science* **2005**, *309*, 1200.
57 Z.B. Li, E. Kesselman, Y. Talmon, M.A. Hillmyer, T.P. Lodge, *Science* **2004**, *306*, 98.
58 A. Kotzev, A. Laschewsky, P. Adriaensens, J. Gelan, *Macromolecules* **2002**, *35*, 1091.
59 Y. He, Z. Li, P. Simone, T.P. Lodge, *J. Am. Chem. Soc.* **2006**, *128*, 2745.
60 S. van der Burgh, A. de Keizer, M.A. Cohen Stuart, *Langmuir* **2004**, *20*, 1073.
61 A. Halperin, *Macromolecules* **1989**, *22*, 2403.
62 J.-F. Gohy, B.G.G. Lohmeijer, S.K. Varshney, U.S.Schubert, *Macromolecules* **2002**, *35*, 7427.
63 O. Regev, J.-F. Gohy, B.G.G. Lohmeijer, S.K. Varshney, D.H.W. Hubert, P.M. Frederik, U.S. Schubert, *Colloid. Polym. Sci.* **2004**, *282*, 407.
64 C. Guerrero-Sanchez, D. Wouters, C.-A. Fustin, J.-F. Gohy, B.G.G. Lohmeijer, U. S. Schubert, *Macromolecules* **2005**, *38*,10185.
65 G.A. McConnell, A.P. Gast, J.S. Huang, S.D. Smith, *Phys. Rev. Lett.* **1993**, *71*, 2103.
66 N. Pinna, K. Weiss, H. Sack-Kongehl, W. Vogel, J. Urban, M.P. Pileni, *Langmuir* **2001**, *17*, 7982.
67 M.H. Abraham, *Chem. Soc. Rev.* **1993**, 73.
68 L. Zhang, A. Eisenberg, *Polym. Adv. Technol.* **1998**, *9*, 677.
69 T.P. Lodge, A. Rasdal, Z. Li, M.A. Hillmyer, *J. Am. Chem. Soc.* **2005**, *127*, 17608.
70 L. Flamigni, F. Barigelletti, N. Armaroli, J.-P. Collin, I.M. Dixon, J.-P. Sauvage, J.A.G. Williams, *Coord. Chem. Rev.* **1999**, *190*, 671.
71 I.M. Dixon, J.-P. Collin, J.-P. Sauvage, L. Flamigni, S. Encinas, F. Barigelletti, *Chem. Soc. Rev.* **2000**, *29*, 385.
72 G. Kalyuzhny, M. Buda, J. McNeill, P. Barbara, A.J. Bard, *J. Am. Chem. Soc.* **2003**, *125*, 6272.
73 H. Rudman, S. Shimada, M.F. Rubner, *J. Appl. Phys.* **2003**, *94*, 115.
74 K.W. Lee, J.D. Slinker, A.A. Gorodetsky, S. Flores-Torres, H.D. Abruna, P.L. Houston, G.G. Malliaras, *Phys. Chem. Chem. Phys.* **2003**, *5*, 2706.
75 E. Holder, M.A.R. Meier, V. Marin, U.S. Schubert, *J. Polym. Sci., Part A: Polym. Chem.* **2003**, *41*, 3954.

76 X. Gong, J.C. Ostrowski, G.C. Bazan, D. Moses, A.J. Heeger, M.S. Liu, A.K.-Y. Jen, *Adv. Mater.* **2003**, *15*, 45.
77 K. Kalyanasundaram, M. Grätzel, *Coord. Chem. Rev.* **1998**, *177*, 347.
78 P. Wang, S.M. Zakeeruddin, J.E. Moser, M.K. Nazeeruddin, T. Sekiguchi, M. Grätzel, *Nature Mater*. **2003**, *2*, 498.
79 F. Neve, A. Crispini, S. Campagna, S. Serroni, *Inorg. Chem.* **1999**, *38*, 2250.
80 F. Neve, A. Crispini, *J. Inorg. Chem.* **2000**, *5*, 1039.
81 S. Sprouse, K.A. King, P.J. Spellane, R.J. Watts, *J. Am. Chem. Soc.* **1984,** *106*, 6647.
82 P. Schuck, *Biophysical J.* **2000**, *78*, 1606.
83 R. Hoogenboom, H.M.L. Thijs, D. Wouters, S. Hoeppener, U.S. Schubert, *Soft Matter* **2008**, *4*, 103.

CHAPTER 5

Well-defined terpyridine chain-end functionalized copolymers by anionic polymerization

Abstract

This chapter demonstrates the preparation of well-defined terpyridine end-functionalized polymers by employing anionic polymerization. Using this approach, access to differently composed polymers was achieved including homopolymers, alternating polymers as well as block copolymers. In the first part, 1,1-diphenylethylenene (DPE) was copolymerized with styrene to yield well-defined alternating copolymers which were terminated by reacting the "living" polymeric carbanion species with 4'-chloro-2,2':6'2"-terpyridine. Special focus was on chain end functionalization since the alternating copolymers served as a basis for the subsequent chemical transformation via the supramolecular binding motif. A series of non-covalently bonded block copolymers of the type P(S-alt-DPE)$_n$-[Ru]-PEG$_{70}$ were prepared and characterized in detail. Techniques such as ^{1}H NMR spectroscopy, GPC, MALDI-TOF MS, UV-vis spectroscopy as well as hydrodynamic methods were applied to determine the molar masses of the copolymers. Furthermore, the resulting block copolymers were investigated towards their thermal transitions and their mechanical properties, respectively. In the last part, the preparation of well-defined poly(styrene-b-isoprene) and poly(styrene-alt-DPE-b-isoprene) block copolymers by sequential monomer addition is described. In order to promote an efficient and straightforward chain end functionalization, DPE was reacted with the "living" polymer anion, before the addition of 4'-chloro-2,2':6'2"-terpyridine

Parts of this chapter will be published: C. Ott, G.M. Pavlov, C. Guerrero-Sanchez, U.S. Schubert, submitted; C. Ott, J.M. Kranenburg, C. Guerrero-Sanchez, S. Hoeppener, D. Wouters, U.S. Schubert, submitted.

5.1 Introduction

In 1956, Michael Szwarc discovered the living anionic polymerization of styrene with a naphthalene / sodium initiating system in THF induced by an electron transfer reaction.[1,2] The aromatic naphthalene is required to catalyze the process by accepting an electron from the alkali metal to form a radical anion. Subsequently, the radical is transferred to the monomer to create a radical anion which dimerizes upon radical combination resulting in a dianion with reactive groups at both ends. Alternatively, initiation can be achieved by using organo-metallic species. In order to obtain a fast and successful initiation, the energy of the initiation step must be favorable. Therefore, the choice of the initiator (*e.g* alkyl lithium) is a key step towards well-defined polymers, especially in the case of a weakly stabilized propagating anion. For this purpose, a powerful nucleophile such as *n*-butyl lithium is required as initiator. On the other hand, if the propagating species is strongly stabilized, a less powerful nucleophile like an alcoholate is sufficient to initiate the polymerization. The unique characteristic of organo lithium compounds is that the C-Li bond features covalent as well as ionic bond properties[3,4] due to the small radius of the lithium atom, the high electronegativity and the high ionization potential.[5] It has been reported in the literature that the reactivity of the alkyl lithium initiator is dependent on the degree of association which is affected by the structure of the organic moiety: the lower the degree of association the higher the reactivity of the initiator.[6] Stabilization of the propagating species is achieved by electron withdrawing groups or double bonds since they are able to stabilize the anion by resonance structures. Monomers that can be polymerized in a living fashion are *e.g.* styrene and styrene derivatives,[7-9] dienes,[10,11] and (meth)acrylates[12,13] (at low temperatures using bulky initiators). The mechanism of the polymerization is displayed in Scheme 5.1.

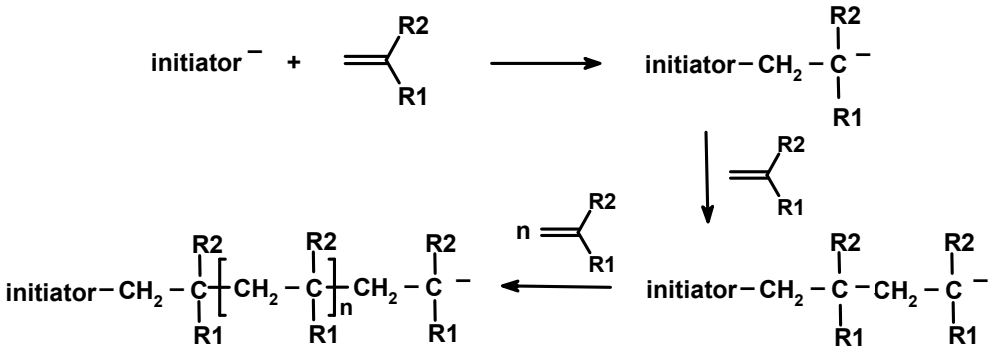

Scheme 5.1 *Schematic representation of the mechanism of the living anionic polymerization (counter ions are omitted for clarity).*

Despite the progressing development of new methods for the synthesis of well-defined polymers and copolymers (e.g. by controlled radical polymerization techniques[14]), anionic polymerization has been proven to be the most reliable and versatile technique for the synthesis of a wide variety of materials with a high degree of molecular and compositional homogeneity.[15-17] This advantage makes the polymerization technique very attractive for the synthesis of well-defined polymers that are needed for establishing structure-property relationships. The widespread utility of living anionic polymerization originates from the propagation reaction which proceeds without termination or chain transfer under the appropriate reaction conditions. Consequently, polymers are obtained with controlled chain length and narrow molar mass distributions. Apart from the absence of termination and chain transfer reactions the living chain end is also of great importance after monomer consumption. In fact, it provides the possibility to prepare well-defined block copolymers by sequential monomer addition as well as chain end-functionalized polymers

by the incorporation of electrophilic terminating agents. The complete monomer conversion is definitively an advantage of this polymerization technique in comparison to radical polymerization, since termination reactions between two polymer anions do not occur. However, the main drawback related to anionic polymerization (and other ionic polymerizations such as CROP[18]) is the extremely high reactivity of the anionic species towards impurities present in the involved chemical reagents and in the reaction environment (oxygen, moisture, and carbon dioxide).[19] In order to avoid spontaneous termination reactions of the reactive species, synthetic polymer chemists have developed specific experimental set-ups and techniques.[20-23] Nowadays, two major experimental techniques are applied when performing anionic polymerizations: high vacuum and inert atmosphere (schlenk technique). The polymerizations described in this chapter were performed using the latter technique. Even though anionic polymerization faces stringent requirements, it is frequently employed in academic research as well as industry. It has a high potential to synthesize complex macromolecular compounds with control over a wide range of compositional and structural parameters including molar mass, molar mass distribution, copolymer composition and microstructure, stereochemistry and chain-end functionality. These characteristic features are of special importance in the fields of polymer chemistry and material science since all these polymer variables affect the final polymer properties. In the first part of this chapter, the copolymerization of styrene with 1,1-diphenylethylene (DPE) is described (Section 5.2). It has been reported in literature that these two monomers can be copolymerized by anionic polymerization leading to almost alternating copolymers due to their specific reactivity ratios.[16] The incorporation of "bulky" comonomers, such as α-methylstyrene or 1,1-diphenylethylene, causes a change in the materials properties. The resulting copolymers exhibit improved long-term service temperatures compared to conventional polystyrene because of the increased stiffness due to the restricted mobility of the copolymer.[24,25] Since the copolymer chains retain their active centers when the monomer has been consumed, the possibility to incorporate an end-group functionality is provided. This end-capping possibility was exploited to introduce the terpyridine ligand at the end of the polymer chains allowing the construction of block copolymers by metal complexation (Section 5.3). Various alkyl lithium compounds are available for the initiation of anionic polymerization; however, they differ with respect to their relative reactivity. A fast initiation of the polymerization was achieved by utilizing *sec*-butyl lithium as initiator which furthermore allows the preparation of styrene-diene block copolymers (Section 5.5). These polymers are of special importance since non-covalently bonded A-B-[M]-B-A block copolymers (thermoplastic elastomers) can be prepared simply by the addition of a suitable transition metal ion. Excellent tensile strengths at room temperature have been reported for such ABA block copolymers, where B corresponds to a polydiene, such as polydiene.[26] Section 5.5 furthermore describes the synthesis of a thermoplastic elastomer obtained by anionic sequential polymerization.

5.2 Alternating terpyridine-endfunctionalized copolymers of styrene and diphenylethylene

A poly(styrene-*alt*-diphenylethylene) copolymer library was prepared by anionic polymerization using inert atmosphere schlenk techniques. As mentioned before, *sec*-butyl lithium was used to guarantee fast initiation and narrow molar mass distributions of the polymers. By using different amounts of initiator the synthesis of low and high molar mass copolymers could be achieved. First, DPE (1.1 equiv with respect to styrene) was added into a schlenk-flask containing a predetermined amount of cyclohexane under inert gas atmosphere. After the addition of the initiator, the reaction mixture turned deeply red indicating the formation of the diphenylethylenyl-anion. The reaction mixture was allowed to stir for 20 minutes at 55 °C before the second

monomer (styrene) was added. After 1,5 hours the polymerization stopped since all styrene monomer was consumed and DPE cannot homopolymerize due to steric hindrance.[27] The copolymer chains have the anionic DPE at the end of the chain because an excess of DPE was used for the polymerization. This facilitates the introduction of functional groups into the polymers,[16,28] which is of great importance since it makes the material suitable for further modifications. The addition of 4'-chloroterpyridine results in the formation of terpyridine-functionalized alternating copolymers, respectively. The synthetic approach of anionically obtained copolymers **V-1** is depicted in Scheme 5.2.

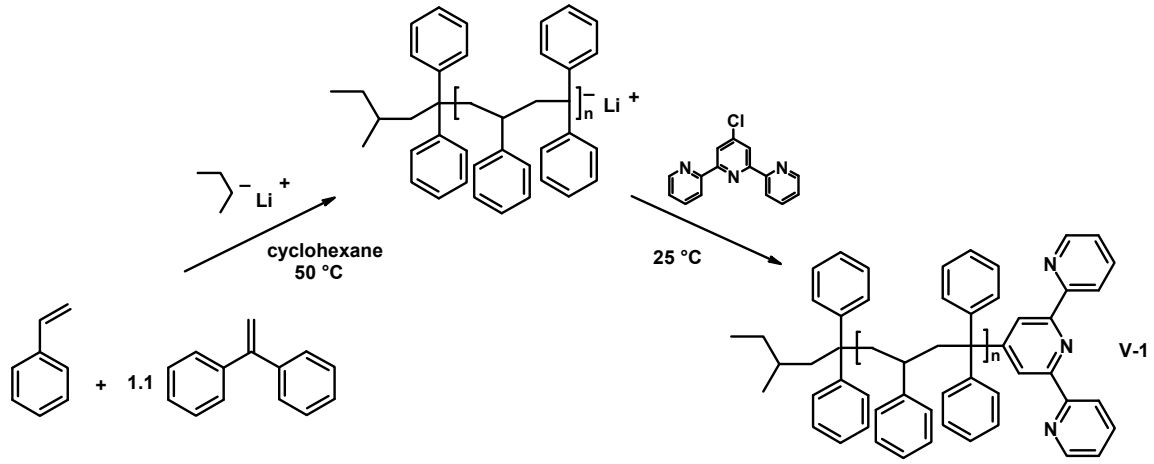

Scheme 5.2 *Schematic representation of the synthesis of terpyridine-terminated poly(styrene-alt-diphenylethylene) copolymers via anionic polymerization.*

The GPC traces of the synthesized copolymers after functionalization with the terpyridine moiety are shown in Figure 5.1 and reveal unimodal molar mass distributions with PDI values below 1.2 (see also Table 2). Hence, it can be concluded that the synthetic approach for the preparation of terpyridine-functionalized poly(styrene-*alt*-diphenylethylene) copolymers is successful and proceeds in a controlled fashion.

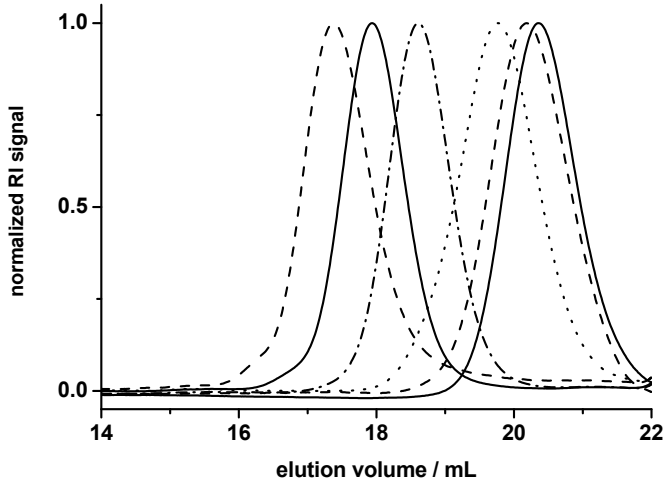

Figure 5.1 *Normalized GPC traces of P(S-alt-DPE)$_n$ copolymers (**V-1**) end-functionalized with terpyridine. GPC eluent: N,N"-dimethylacetamide with LiCl (2.1 g/mL).*

Various characterization techniques, including ^{1}H NMR spectroscopy, UV-vis spectroscopy and elemental analysis confirm that the supramolecular ligand was indeed effectively tethered to the

polymer chain end. Figure 5.2 represents the aromatic region of a ^{1}H NMR spectrum of a representative copolymer. The spectrum reveals the signals for the aromatic protons of the copolymer (region from 5.6 to 7.4 ppm) and the signals corresponding to the terpyridine moiety (region from 7.7 to 8.7 ppm). Another characteristic terpyridine signal partially overlaps with the aromatic signals of the polymer backbone at 7.3 ppm. The degrees of polymerization were calculated by integrating the clearly resolved signals of the terpyridine-ligand with respect to the aromatic signals of the polymer backbone. A polystyrene calibration was used to determine the M_n value by GPC. Generally, the M_n values obtained by GPC are lower compared to those calculated from the ^{1}H NMR spectra. The extra diphenylethylene units within the copolymer may change the hydrodynamic volume of the material, which may be a reason for the difference in molar mass observed by the two methods. Assuming complete conversion, the M_n values determined by ^{1}H NMR spectroscopy are more reliable, thus these values were taken into account for subsequent UV-vis titration experiments and elemental analysis. UV-vis titrations are an additional analysis method for determining the molecular weight of supramolecular materials as well as the degree of terpyridine end-group modification.[29] Figure 5.2 shows such a titration experiment with $FeCl_2$. Upon addition of iron(II) ions to the ligand, an increase of the metal-to-ligand charge transfer (MLCT) band of the iron(II) complex at 565 nm was observed. Another important absoption band appeared at 325 nm which originates from the all-*cis* configuration of the ligand. The titration process was controlled by following the appearance of the ligand centered band. After a linear increase of the intensity at 325 nm, a plateau was reached at the 1:2 metal-to-ligand ratio, indicating the formation of the iron *bis*-complex. In conclusion, the molar masses of the poly(styrene-*alt*-diphenylethylene) copolymers determined by UV-vis titration are in good agreement with those calculated from the ^{1}H NMR spectrum.

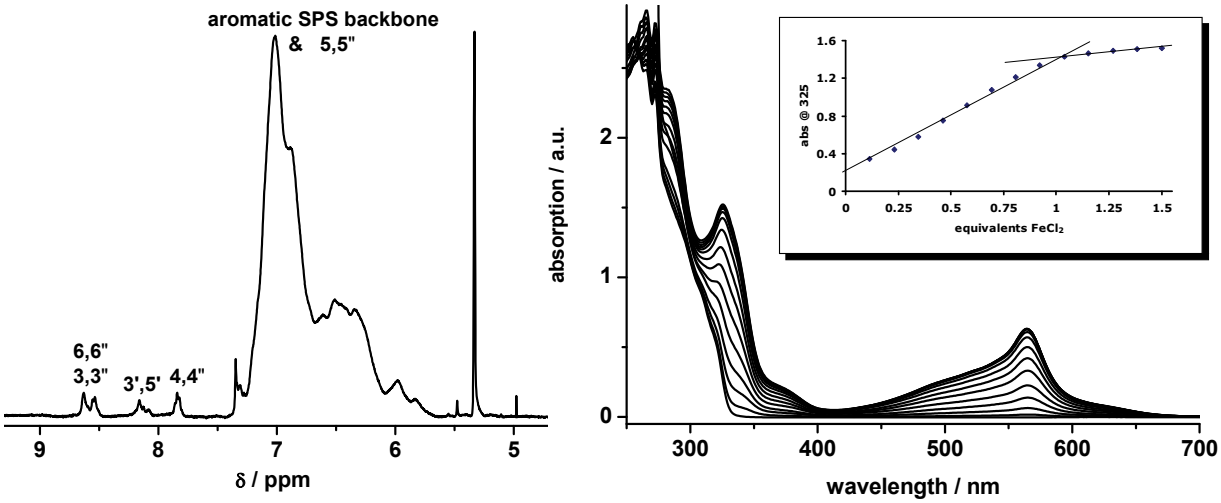

Figure 5.2 *^{1}H NMR spectrum of a terpyridine-terminated P(S-alt-DPE) copolymer in CD_2Cl_2 (left) and UV-vis titration of]-P(S-alt-DPE)$_{22}$ with $FeCl_2$ in $CHCl_3$ / MeOH.*

In addition, the functionalized polymers were investigated by elemental analysis (EA), which is an appropriate method to examine the efficiency of the functionalization reaction. Using the molar masses calculated from the ^{1}H NMR spectrum, the content of carbon, hydrogen and nitrogen can be determined. The measurements support the conclusion that the degree of functionalization is close to 100%. The nitrogen contents found in the materials are in good agreement with the expected nitrogen values. Moreover, elemental analysis contains information over the M_n value and hence information over the degree of polymerization (only terpyridine-functionalized chains can contribute to the nitrogen content since unfunctionalized polymer chains just consist of carbon and hydrogen atoms). Figure 5.3 demonstrates a high efficiency of the functionalization

reaction as investigated by elemental analysis. The theoretical line was calculated as reported in literature.[28]

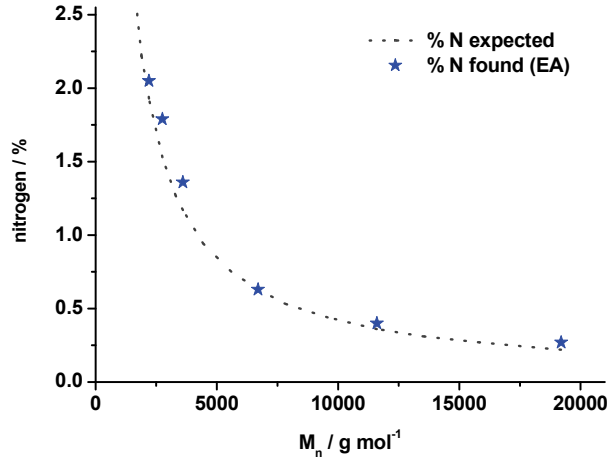

Figure 5.3 *Expected and found nitrogen values by elemental analysis of the synthesized poly(styrene-alt-diphenylethylene) copolymers functionalized with terpyridine.*

MALDI-TOF-MS is a well-known technique for end-group analysis and for the determination of the absolute molar mass.[30,31] Figure 5.4 shows an example for a MALDI-TOF MS spectrum of the]-P(S-*alt*-DPE)$_{22}$ copolymer. The spectrum reveals a narrow unimodal molar mass distribution. When zooming into the spectrum (Figure 5.4 right), multiple distributions are observed which can be explained from the reaction kinetics. Diverse species can be generated during the polymerization process: even though, DPE cannot homopolymerize due to steric hindrance, and the addition of a DPE unit to a polystyrylanion-end occurs very fast (in contrast, the addition of a styrene unit to a DPE-end is slow), it is possible that “defect structures” comprising of consecutive styrene-styrene units may form. This could explain the observed multiple distributions. However, also perfect alternating copolymers are obtained. One example can be found in the peak of the spectrum at 5865 Da, which perfectly matches an alternating copolymer with 19 repeating units (284 Da each repeating unit), including the starting *sec*-butyl group (57 Da) followed by one DPE unit (180 Da) and the terpyridine end-group (232 Da). Furthermore, the successful incorporation of both units, styrene and DPE, can be followed by the distance between the peaks corresponding to the mass of styrene (104 Da) and DPE (180 Da), respectively.

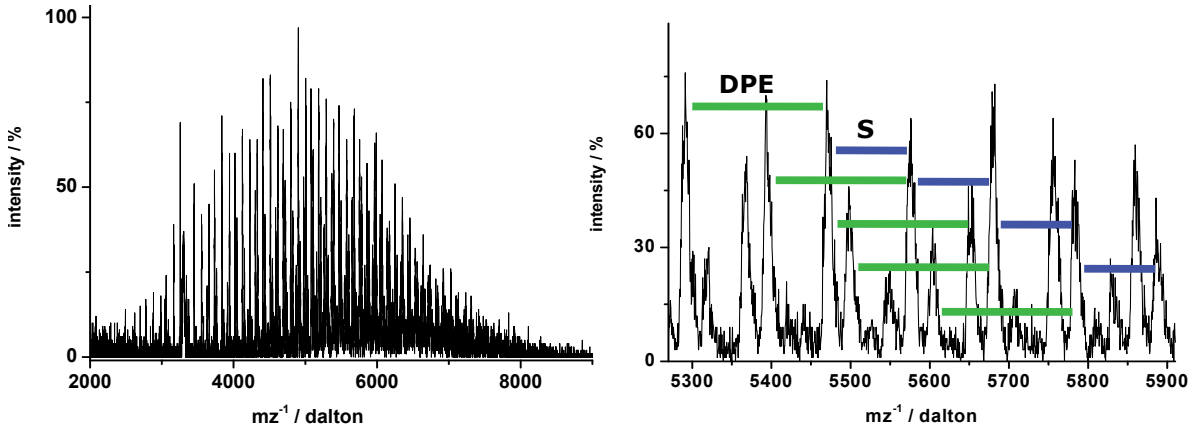

Figure 5.4 *MALDI-TOF-MS spectrum of the synthesized terpyridine-terminated]-P(S-alt-DPE)$_{22}$ copolymer by anionic polymerization.*

In principle, MALDI-TOF MS enables the rapid and facile determination of absolute molar masses, molar mass distributions, and end-groups of synthetic polymers.[32,33] However, the method also has its drawbacks since the analytic results obtained using this technique may differ depending on the investigated polymer and the used matrix/solvent combination. Moreover, as already mentioned before, analysis by GPC was performed using polystyrene calibrations which can certainly be used only as an estimate for the molar masses of the copolymers since the bulky phenyl rings in the polymer chain may considerably change the hydrodynamic volume of the material. To overcome these problems, the]-P(S-*alt*-DPE)$_n$ copolymers were analyzed by analytical ultracentrifugation as well as by other hydrodynamic measurements, all of them being absolute methods with respect to the determination of molar masses.

From density measurements the buoyancy factor (1 - $\bar{\upsilon}\,\rho_0$) = (0.266 ± 0.005) was obtained from the limiting slope of the plot of the solution density versus the concentration (Figure 5.5). Furthermore, the above described buoyancy factor allows the determination of the partial specific volume $\bar{\upsilon}$ = (0.848 ± 0.005) cm^3/g, which is a characteristic property of a material.[34] Values for partial specific volumes are required for the calculation of the molar mass from sedimentation velocity measurements. Thereby, the sedimentation coefficient, *s,* which can be related to the molar mass and to the frictional coefficient or shape of a macromolecule, can be obtained. Figure 5.5 also demonstrates the concentration dependence of the reciprocal sedimentation coefficients. Extrapolation to zero concentration results in the determination of the sedimentation coefficients at infinite dilution, s_0. As expected, the sedimentation coefficients increase with molar mass.

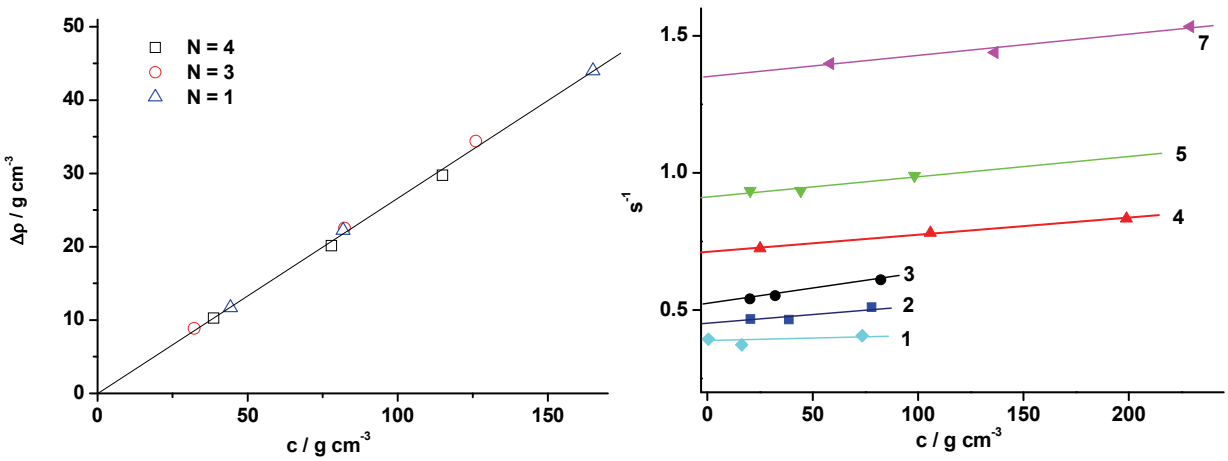

Figure 5.5 *Density increments $\Delta\rho$ / Δc = (1 - vρ_0) of the copolymers in toluene at 20 °C. The numbers correspond to the sample numbers in Table 1 and 2. $\Delta\rho = \rho - \rho_0$ where ρ and ρ_0 are the polymer solution and solvent densities, respectively (left). Concentration dependencies of the (reciprocal) sedimentation coefficients s^{-1} for the copolymer samples in toluene (right).*

The Gralen coefficients k_s[36-38] were obtained from the slope of the linear approximation. The actual measured data in the analytical ultracentrifugation is the time-dependent change of the polymer concentration as a function of sedimentation and diffusion in a centrifugal field. The obtained total number of fringes was superposed for all copolymer samples as a function of copolymer concentration. Furthermore, linear fitting of the frictional ratio f/f_{sph} was also used to obtain the frictional ratio extrapolated to infinite dilution $(f/f_{sph})_0$. The values s_0, k_s, and $(f/f_{sph})_0$ from the sedimentation velocity experiment for each sample are presented in Table 1.

Table 1 *Hydrodynamic data of the terpyridine-functionalized alternating copolymers (**V-1**) composed of styrene/diphenylethylene in toluene.*

N	[η] (cm^3/g)	k'	k''	$s_0 \times 10^{13}$ (s)	k_s (cm^3/g)	$(f/f_{sph})_0$
1	3.0 ± 0.2	3.10	0.70	0.75 ± 0.01	5.3 ± 1.0	1.20 ± 0.03
2	3.7 ± 0.1	1.20	0.40	0.83 ± 0.01	8.6 ± 2.0	1.31 ± 0.01
3	5.0 ± 0.1	0.32	-0.18	1.10 ± 0.02	8.0 ± 2.5	1.27 ± 0.04
4	5.9 ± 0.1	0.95	0.18	1.41 ± 0.01	8.8 ± 0.6	1.33 ± 0.07
5	8.3 ± 0.1	0.66	0.03	1.93 ± 0.01	21.7 ± 0.4	1.61 ± 0.01
6	10.4 ± 0.2	0.66	-0.04	2.25 ± 0.08	18.0 ± 7.0	1.61 ± 0.07
7	13.1 ± 0.2	0.69	0.00	2.74 ± 0.02	16.0 ± 2.0	1.81 ± 0.08

The molar masses of the copolymer series were evaluated using the transformed Svedberg equation below:[35-37]

$$M_{sf} = 9\pi 2^{1/2} N_A \left([s] \cdot \left(f / f_{sph} \right)_0 \right)^{3/2} \bar{\upsilon}^{1/2}$$

The calculated M_{sf} values for each copolymer and the corresponding M_n values obtained by ^{1}H NMR spectroscopy and GPC are shown in Table 2. The similarity of M_n and M_{sf} signifies a high degree of functionalization (also proven by EA) since analytical ultracentrifugation is a method which determines the absolute molar masses and the M_n values calculated from ^{1}H NMR spectroscopy are calculated from the end-group functionality (terpyridine signals).

Table 2 *Molar mass determination by ^{1}H NMR spectroscopy, AUC and GPC.*

N	$M_{n\,\mathrm{NMR}}$ (g/mol)	M_{sf} (g/mol)	$M_{n\,\mathrm{GPC}}$ (g/mol)	PDI_{GPC}
1	2,200	1,900	1,100	1.20
2	2,800	2,600	1,300	1.23
3	3,600	3,800	2,100	1.17
4	6,700	5,900	4,700	1.11
5	11,600	12,600	7,800	1.14
6	19,200	15,900	10,800	1.21
7	26,500	25,500	16,900	1.22

The refractive index increments $\Delta n/\Delta c$ were derived from the linear plots using intensity scans performed at 675 nm: $\Delta n/\Delta c$ = (0.145 ± 0.004) cm^3/g for the corresponding high molar mass samples (N = 3 – 7) and $\Delta n/\Delta c$ = (0.122 ± 0.005) cm^3/g for the two low molar mass samples (N = 1 and 2).[34] In addition, intrinsic viscosities [η] of the copolymer series were determined; which is a measure of the hydrodynamic volume of a macromolecule in solution. The values for [η] were obtained from the extrapolated Huggins (η_{sp}/c) and Kraemers ($\ln\eta_r/c$) plots to zero concentration (see Table 1).

The hydrodynamic characteristics scale with the molar mass following the Kuhn-Mark-Houwink-Sakurada relationships.[38,39] In Figure 5.6 the double logarithmic plots of sedimentation coefficient s_0, $(f/f_{sph})_0$ and intrinsic viscosity $[\eta]$ are shown. Linear fitting resulted in:

$$s_0 = K_s M^{bs} = 1.6210^{-15} \times M^{0.51\pm0.02}$$

$$[\eta] = K_\eta M^{b\eta} = 5.0310^{-2} \times M^{0.54\pm0.02}$$

$$\left(f / f_{sph}\right)_0 = K_f M^{bf} = 0.377 \times M^{0.15\pm0.02}$$

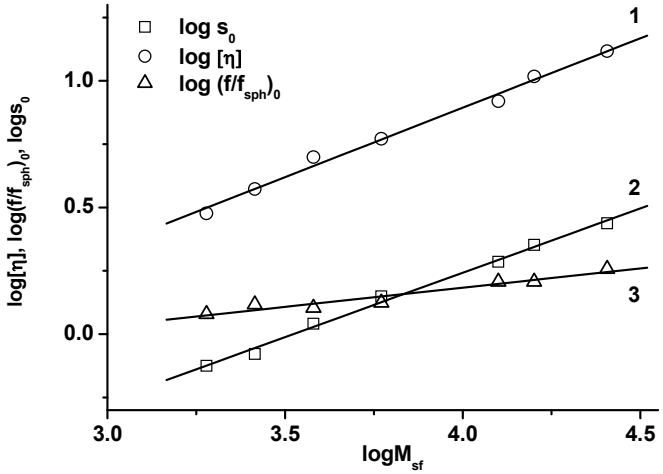

Figure 5.6 *Kuhn-Mark-Houwink-Sakurada scaling plots for]-P(S-alt-DPE)$_n$ copolymers in toluene: the double logarithmic plots of intrinsic viscosity [η] (1), the sedimentation coefficient s_0 (2) and the frictional ratio $(f/f_{sph})_0$ (3) vs. molar mass M_{sf}.*

The studied set of]-P(S-*alt*-DPE)$_n$ copolymers corresponds to the range of low molar mass polymers, where intrachain volume effects may be neglected. The worm-like cylinder model is the most adequate model for linear polymer chains without excluded volume. The parameters defining macromolecular dimensions are the contour length of the chain, *L*, its Kuhn statistical segment length, *A*, or the persistence length, *a = A/2,* and the cross-section diameter or thickness of the molecule, *d*. In case of very low molar mass chains (L/A < 2.28; L > d), a model of a weakly bending rod or cylinder can be used that provides the mass per unit length, $M_L = M/L$, and d through a linear regression:[40,41]

$$[s] = \left(\frac{M_L}{3\pi N_A}\right)\left[\ln M - \ln\left(M_L d\right) + 0.3863\right]$$

The dependency of [*s*] on ln*M* is shown in Figure 5.7. The following values for M_L and *d* were obtained: $M_L = (6 \pm 1) \times 10^9$ g cm^{-1} mol^{-1} and $d = (11 \pm 2) \times 10^{-8}$ cm, respectively. On the basis of these values, the partial specific volume may be estimated as $\bar{\upsilon} = N_A\pi d^2/4M_L = 0.83$ cm^3/g. This estimation is in good agreement with the received value $\bar{\upsilon} = 0.848$ cm^3/g from density measurements. Moreover, the M_L value is close to the value of $M_L = 5.6 \times 10^9$ g cm^{-1} mol^{-1}, which can be calculated for]-P(S-*alt*-DPE)$_n$ copolymers from the chemical structure, and their corresponding repeat unit length, $\lambda = 2.52 \times 10^{-8}$ cm, which is a common value for aliphatic polymer backbones.

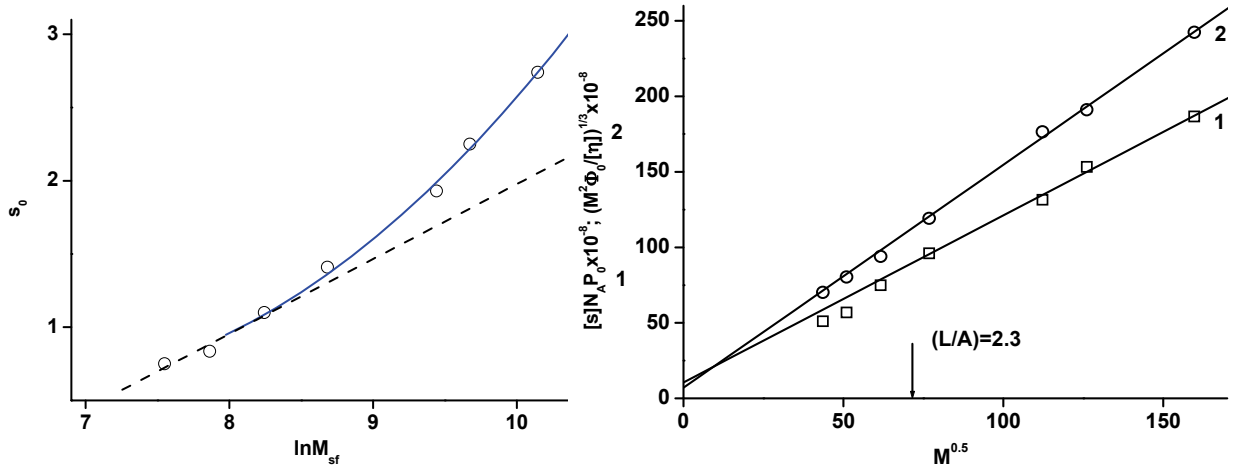

Figure 5.7 *Determination of M_L (ratio of molar mass M to contour length L), and the hydrodynamic diameter d of the]-P(S-alt-DPE)$_n$ copolymers from the plot [s] vs. lnM. The linear extrapolation (dashed line) was made using the samples of lowest molar mass (1, 2 and 3). The slope and intercept allow the determination of M_L and d (left). Dependencies of $(M^2\Phi_0/[\eta])^{1/3}$ (1) and $[s]N_AP_0$ (2) on $M^{1/2}$ (right). The slope and intercept of the curves were used to evaluate the Kuhn segment length A and the hydrodynamic diameter d using the worm-like cylinder model.*

The worm-like cylinder model does not consider intrachain volume effects, which is justified in the limit *L/A* < 50.[42] For all copolymers in the present study, the values of *L/A* are below 15. Therefore, the equilibrium rigidity can be evaluated quantitatively from the hydrodynamic data using the worm-like cylinder model without volume interaction. For linear chains in the limit *L/A* > 2.28, and without intramolecular volume interactions, *A* and *d* can be determined from the slopes and intercepts of the linear regressions using the equations below:[43]

$$[s]N_AP_0 = \left(\frac{M_L}{A}\right)^{1/2} M^{1/2} + \left(\frac{M_LP_0}{3\pi}\right)\left[\ln\left(\frac{A}{d}\right) - \varphi(0)\right] \text{ and}$$

$$\left(\frac{M^2\Phi_0}{[\eta]}\right)^{1/3} = [s]N_AP_0 = \left(\frac{M_L}{A}\right)^{1/2} M^{1/2} + \left(\frac{M_LP_0}{3\pi}\right)\left[\ln\left(\frac{A}{d}\right) - \varphi(0)\right]$$

where $\varphi(0) = 1.056$ considering the worm-like cylinder model.[43] The Kuhn segment length *A*, characterizing the equilibrium rigidity, and the hydrodynamic diameter *d* were obtained independently from the two plots (see Figure 5.7):[43-46] $(M^2\,\Phi_0\,/[\eta])^{1/3}$ and [*s*] *vs* $M^{1/2}$, using P_0 = 5.11 and $\Phi_0 = 2.87 \times 10^{23}$, respectively.[35,41] Both graphs keep a good linear behavior in the region L/A > 2.28.

Table 3 *Comparison of different structural parameters: Kuhn segment length A, hydrodynamic diameter d and parameter of steric hindrance σ* between]-P(S-*alt*-DPE)$_n$ *and polystyrene.*

method	translational friction		intrinsic viscosity		average		σ
parameter	**A ± ΔA (nm)**	**d ± Δd (nm)**	**A ± ΔA (nm)**	**d ± Δd (nm)**	**A ± ΔA (nm)**	**d ± Δd (nm)**	
copolymer (toluene)	4.9 ± 0.5	1.2 ± 0.2	2.8 ± 0.2	0.8 ± 0.1	4.0 ± 1	1.0 ± 0.2	3.2 ± 0.4
PS (toluene)	3.1 ± 0.1	0.5 ± 0.1	2.0 ± 0.05	0.7 ± 0.05	2.5 ± 0.6	0.6 ± 0.1	2.5 ± 0.3

Table 3 summarizes the characteristics of *A* and *d*, obtained from the two different measurements. Using the sets of P_0 and Φ_0 from Zimm,[47] the method of Garcia de la Torre *et al.*[48] or Oona and Kohmoto[49] provide slightly reduced values for *A* from experimental s_0 and *M*, and slightly larger values for *A* from experimental [*η*] and *M*. Concerning the value of the Kuhn segment length *A*, the values obtained from translational and rotational frictions are in the same order of magnitude, which is generally observed for flexible linear polymers.
Concluding, it seems worthwhile to compare the molecular and conformational properties of P(S-*alt*-DPE) copolymers ("super polystyrene")[50] with those of polystyrene. For this comparison, the equilibrium characteristics of polystyrene chains were calculated using the hydrodynamic data over a large range of M from literature.[51,52] Consequently, an algorithm was applied to obtain the estimation of equilibrium rigidity by taking the intrachain volume interactions in thermodynamically good solvents into account.[53] The estimations made from both, translational friction and intrinsic viscosity, demonstrate that the equilibrium rigidity as well as the hydrodynamic diameter are higher for the P(S-*alt*-DPE) copolymer chains in comparison with the chains of an atactic polystyrene (Table 3). Obviously, this effect is related to the higher concentration of phenyl rings in the P(S-*alt*-DPE) copolymer chains in comparison with those of standard PS. This leads to a restricted internal rotation in the chains of the copolymer. The following relationship represents the effect of steric hindrance on the average chain dimensions:

$$\sigma = \left(\frac{\langle h^2 \rangle_0}{\langle h^2 \rangle_{of}} \right)^{1/2} = \left(\frac{A}{A_{of}} \right)^{1/2}$$

where $\langle h^2 \rangle_0$ is the unperturbed mean-square end-to-end distance of the chain, and $\langle h^2 \rangle_{of}$ is the mean-square end-to-end distance of the freely rotating chain. The values of $\langle h^2 \rangle_{of}$ and A_{of} can be calculated from the given basic structure of the polymer chain.[34,54] The steric hindrance parameter, σ, was calculated using the average value of the statistical segment length and the theoretical value of A_{of} = 0.38 nm[55] (see Table 3). The value of σ for polystyrene is in good agreement with literature values.[34] As expected, the P(S-*alt*-DPE) copolymers exhibit a higher σ value which can be explained by the restricted internal rotation due to the extra phenyl rings.

5.3 Metallo-supramolecular complexes based on alternating copolymers composed of styrene and DPE

This section focuses on the synthesis and characterization of metallo-supramolecular polymeric complexes using the previously discussed]-P(S-*alt*-DPE) copolymers ("super polystyrene"[50] which will be abbreviated as SPS). Due to the fact that all polymers presented in Section 5.2 feature the supramolecular terpyridine moiety, the formation of non-covalently bonded block copolymers is feasible. As it was described in Chapter 4, *bis*-terpyridine ruthenium complexes are highly stable and therefore suitable candidates to construct metallo-supramolecular block copolymers of the type A-[Ru]-B. In order to form heteroleptic complexes with ruthenium, a two-step synthesis is required. In the first step, terpyridine-functionalized polyethylene glycol (]-PEG_{70}) is reacted with ruthenium(III) chloride to obtain the corresponding ruthenium(III) *mono*-complex. Subsequently, the *mono*-complex is reduced to Ru(II) in the presence of a reducing agent and the chlorides are replaced by the uncoordinated second terpyridine ligand.[56,57] The synthetic approach of the *bis*-complex formation is schematically depicted in Scheme 5.3.

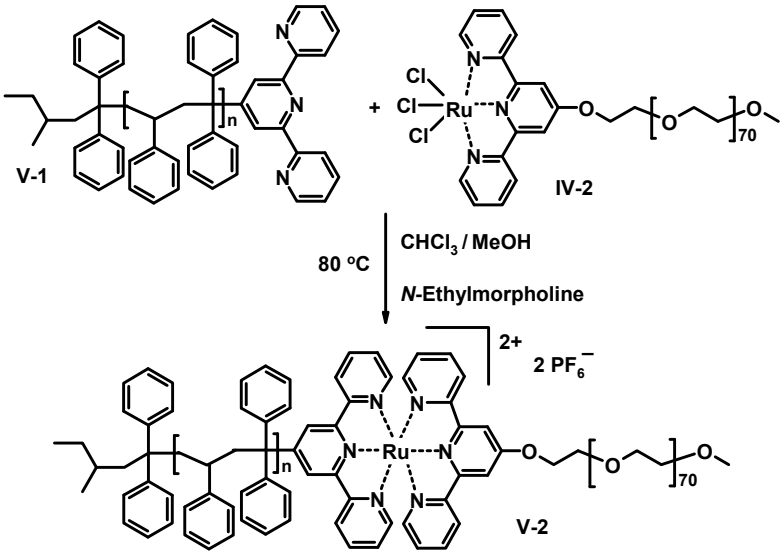

Scheme 5.3 *Schematic representation of the block copolymer formation using coordination chemistry.*

The obtained polymers were subsequently purified using column chromatography (Al_2O_3) to remove unreacted starting material. Evidence for the purity of the polymer was obtained by GPC. Even though, charged supramolecular polymers, such as *bis*-terpyridine ruthenium(II) complexes interact strongly with the column material, addition of 5 mM NH_4PF_6 to the GPC eluent (*N,N'*-dimethylformamide) minimizes this effect.[58] Since metallo-supramolecular polymers show a characteristic absorption in the visible region (at around 490 nm), the GPC measurements were also performed using a photo-diode-array detector providing an UV-vis spectrum for every retention time. This provides additional information about the purity of the material. Figure 5.8 displays the GPC spectra (RI detector) of five ruthenium-containing block copolymers which consist of varying styrene/diphenylethylene block lengths, as well as an example for the 3-dimensional GPC spectrum using the photo-diode-array detector which reveals the characteristic absorption band for ruthenium *bis*-terpyridine complexes at around 490 nm for all retention times of the polymer.

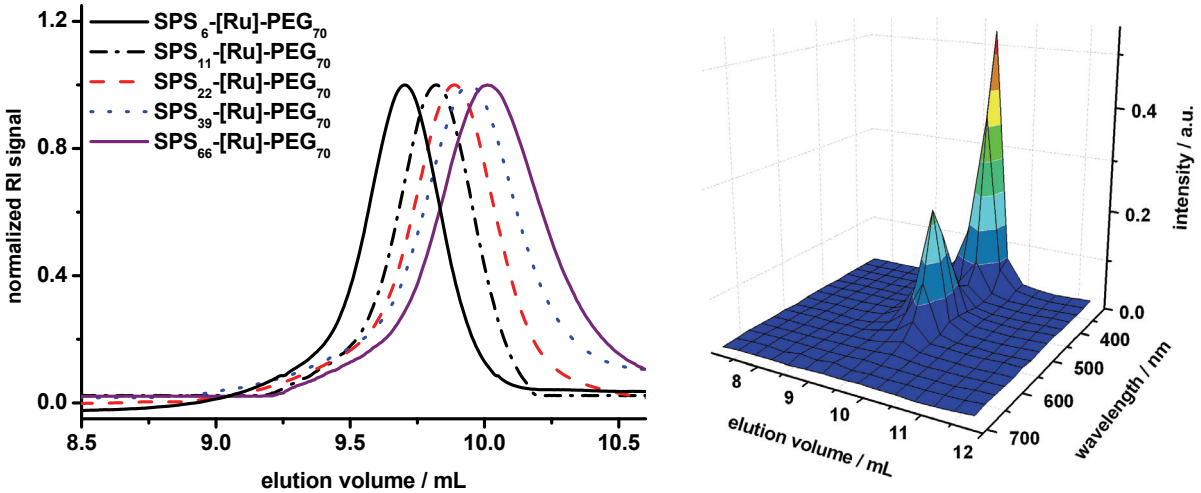

Figure 5.8 *Left: GPC chromatograms of the purified metallo-supramolecular block copolymers. Right: three-dimensional GPC of SPS_{22}-[Ru]-PEG_{70} using the PDA-detector. GPC eluent: N,N"-dimethylformamide with NH_4PF_6 (0.8 g/L).*

Interestingly, the GPC results of the metallo-supramolecular block copolymers show a decrease in molar mass with increasing length of the SPS block. This unusual retention time behavior can unfortunately not be explained, but it might be attributed to the solvent used for the GPC measurements. DMF is a poor solvent for the SPS block, resulting in the collapse of the SPS chain (the M_n value for SPS_{66}-[using DMF as solvent was found to be 2,200 g/mol). As a consequence smaller hydrodynamic radii are obtained for the block copolymers with a larger SPS chain resulting in longer elution times. ^{1}H NMR spectroscopy provided an additional indication for the successful complex formation. The terpyridine protons in 6,6"- and in the 3',5'- position are influenced most by the coordination of the two ligands in a meridonial fashion resulting in a significant shift of their resonances. Table 1 summarizes the M_n values of the starting materials and the corresponding block copolymers obtained by ^{1}H NMR spectroscopy and GPC.

Table 4 *M_n values and glass transition temperatures (T_g) of the SPS-copolymers and the corresponding metallo-supramolecular block copolymers.*

polymer	$M_{n\,NMR}$ (g/mol)	$M_{n\,GPC}$ (g/mol) / PDI	T_g (°C)
SPS_{11}-[	3,600	2,100 / 1.17[a]	137
SPS_{22}-[	6,700	4,700 / 1.11[a]	156
SPS_{39}-[	11,600	7,800 / 1.14[a]	164
SPS_{66}-[	19,200	10,800 / 1.21[a]	160
SPS_{11}-[Ru]-PEG_{70}	7,200	5,700 / 1.05[b]	n.d.
SPS_{22}-[Ru]-PEG_{70}	9,900	5,200 / 1.11[b]	126
SPS_{39}-[Ru]-PEG_{70}	15,200	4,700 / 1.12[b]	138
SPS_{66}-[Ru]-PEG_{70}	22,800	4,400 / 1.08[b]	142

[a] GPC in DMA with LiCl (2.1 g/L) as eluent using PS calibration.
[b] GPC in DMF with NH_4PF_6 (0.8 g/L) as eluent using PEG calibration.

In addition to the metallo-supramolecular diblock copolymers, A-[Ru]-B-[Ru]-A triblock copolymers were synthesized where block A corresponds to the alternating]-P(S-alt-DPE)$_n$ copolymer and block B to the midsegment, polyethylene glycol. Scheme 5.4 demonstrates the synthetic approach for this supramolecular triblock copolymer. Commercially available hydroxy-functionalized polyethylene glycol was post-functionalized with terpyridine units using a suspension of potassium hydroxide and 4-chloro-2,2':6,2"-terpyridine in DMSO at 70 °C to yield the corresponding terpyridine-terminated polyethylene glycol.[59,60] The terpyridine-functionalized alternating copolymer was reacted with $RuCl_3$ and converted into the corresponding Ru(III) *mono*-complex. The isolated polymer complex showed the characteristic MLCT-band for *mono*-complexes at approximately 400 nm. ^{1}H NMR spectroscopy revealed no terpyridine signals in the region between 7 to 9 ppm due to the paramagnetic nature of the complex proving for the formation of the desired complex. Subsequently, the polymer complex was utilized as an endcapper in the reaction with the terpyridine-functionalized polyethylene glycol to obtain the A-[Ru]-B-[Ru]-A triblock copolymers. Even though an excess of SPS-[$RuCl_3$ was used, the mononuclear complex was also obtained as a side product. Separation of the binuclear polymeric complex from the mononuclear complex was achieved by preparative size exclusion chromatography (BioBeads, SX-1, CH_2Cl_2) and column chromatography (Al_2O_3).

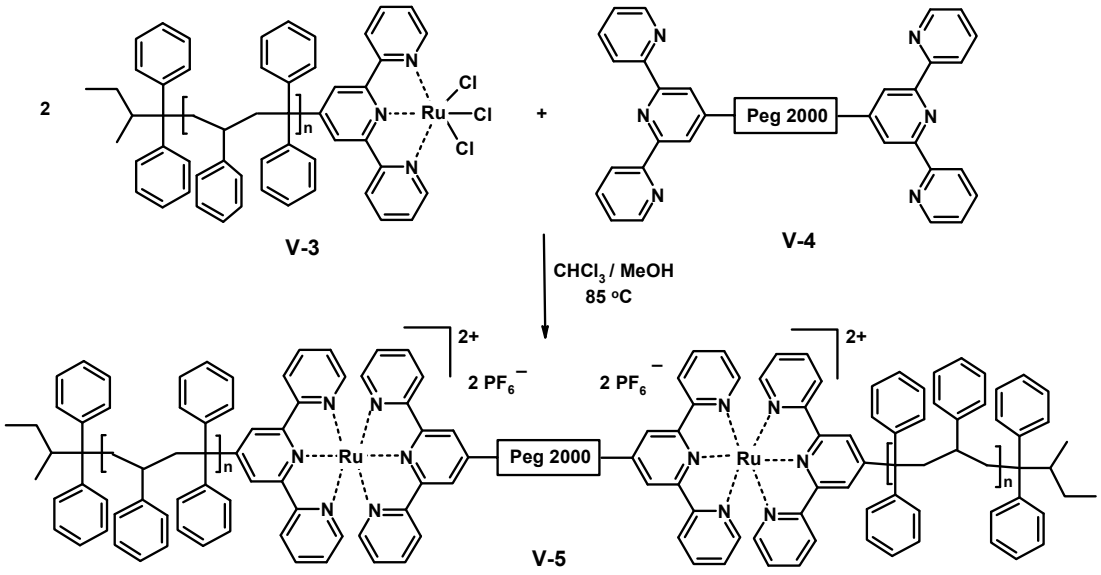

Scheme 5.4 *Schematic representation of the synthesis of ruthenium-containing triblock copolymers **V-5**.*

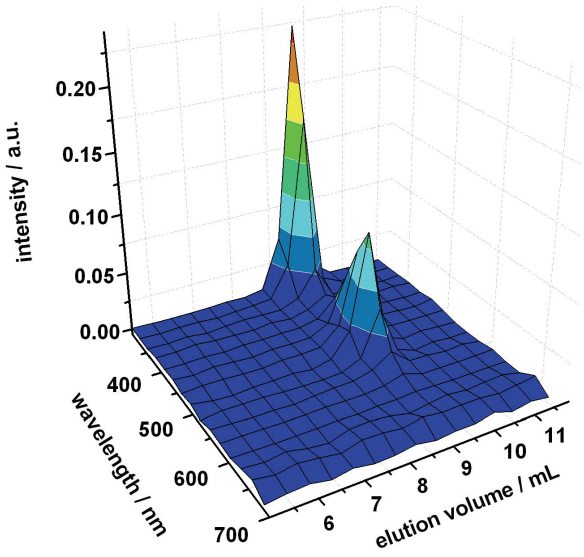

Figure 5.9 displays the results obtained from the SEC-coupled in-line photo diode array detector of the purified SPS_6-[Ru]-PEG_{44}-[Ru]-SPS_6 triblock copolymer. The graph clearly demonstrates the integrity of the supramolecular assembly over the complete polymer distribution as indicated by the MLCT band of the *bis*-terpyridine ruthenium(II) complex at 490 nm (M_n = 8,900 g/mol, PDI = 1.15). The analysis of the SPS_6-[$RuCl_3$ building block was also possible and revealed the presence of the MLCT-band at 400 nm in the whole polymer distribution.

Figure 5.9 *Photo-diode array size exclusion chromatogram of SPS_6-[Ru]-PEG_{44}-[Ru]-SPS_6 after purification by column chromatography.*

As a result of the above described reactions the hydrophilic polyethylene glycol block is chemically tethered to the hydrophobic block using non-covalent coordination interactions. The combination of thermodynamically incompatible blocks within the same material may lead to phase separation. In addition, amphiphilic block copolymers can form polymeric micelles in solution via association into nanoscopic core/shell structures. This was investigated by transmission electron microscopy (TEM) for the A-[Ru]-B materials based on PEG_{70}. For this purpose, the A-[Ru]-B block copolymers were dissolved in a minimum amount of THF. Subsequently, the selective solvent (H_2O) was added dropwise leading to the formation of the polymeric micelles. Afterwards, the common solvent (THF) was removed by dialysis against deionized water. Micelles with a rather uniform diameter of 19 to 27 nm were observed by TEM.

For TEM imaging, no contrast agent was necessary to visualize the spherical micelles due to the presence of ruthenium in the polymers. Figure 5.10 represents an example for the formed spherical micelles in water of SPS_{39}-[Ru]-PEG_{70}, demonstrating the different solubility of the PEG and SPS blocks. In these TEM pictures, the SPS core of the micelles corresponds basically to the micelle sizes shown in the image since the PEO coronal chains are expected to collapse on the core during the drying process. The micelles related to the largest sample (SPS_{66}-[Ru]-PEG_{70}) are of comparable size as the micelles of SPS_{39}-[Ru]-PEG_{70}. Indeed, it has been recently demonstrated that the size of the core of PS-[Ru]-PEG micelles did not scale with the 3/5 power of the degree of polymerization (DP) of the PS block as usually observed for "covalent" PS-*b*-PEO micelles. In fact, the micellar core size was observed to be constant for the DP of the PS block lower than 200. This effect was explained by the presence of the charged and bulky *bis*-terpyridine ruthenium(II) complexes (-[Ru]-) at the interface of the PS and PEO blocks that affected the micellar core size to a certain value.[61]

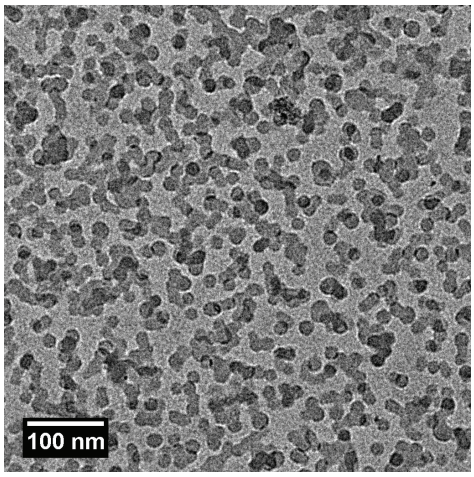

Figure 5.10 *TEM image of the unstained micelles of SPS_{39}-[Ru]-PEG_{70} in water*.

No stable micelles could be observed by TEM for the block copolymers consisting of a short hydrophobic block (SPS_{11}-[Ru]-PEG_{70} and smaller). In those cases, the core of the micelle collapsed upon evaporation of the solvent and a polymer film of uniform thickness is formed on the TEM-grid.

5.4 Thermal and mechanical properties of SPS copolymers and their metallo-supramolecular complexes

In the case of bulk materials, the relative block length relates to the volume fraction of the different blocks, which is, together with the interaction between the different polymers, expressed in the Flory Huggin's interaction parameter,[62] a governing parameter for the phase separation. The tendency to spontaneously separate into microphases affects many bulk properties. Therefore, it is possible to tailor the mechanical properties of the SPS_n-[Ru]-PEG_{70} by the variation of the block sizes or the number of hard/soft blocks within the copolymer.

Thermal transitions of the copolymers were investigated by differential scanning calorimetry (DSC). The glass transition (T_g) of the terpyridine-functionalized SPS increased from 137 °C for n = 11 to 165 °C for n = 66 (Figure 5.11, Table 1). This is in agreement with the common observation that the T_g is reduced for smaller chain lengths.[63] The SPS chains are expected to be

more rigid than polystyrene chains because the extra phenylring restricts its free rotation. Indeed, the glass transition temperature of the SPS was higher than for polystyrene: the T_g of conventional polystyrene of corresponding molar mass increases from 55 °C to 89 °C and reaches at higher molar mass a plateau-value of 100 °C.[55,64]

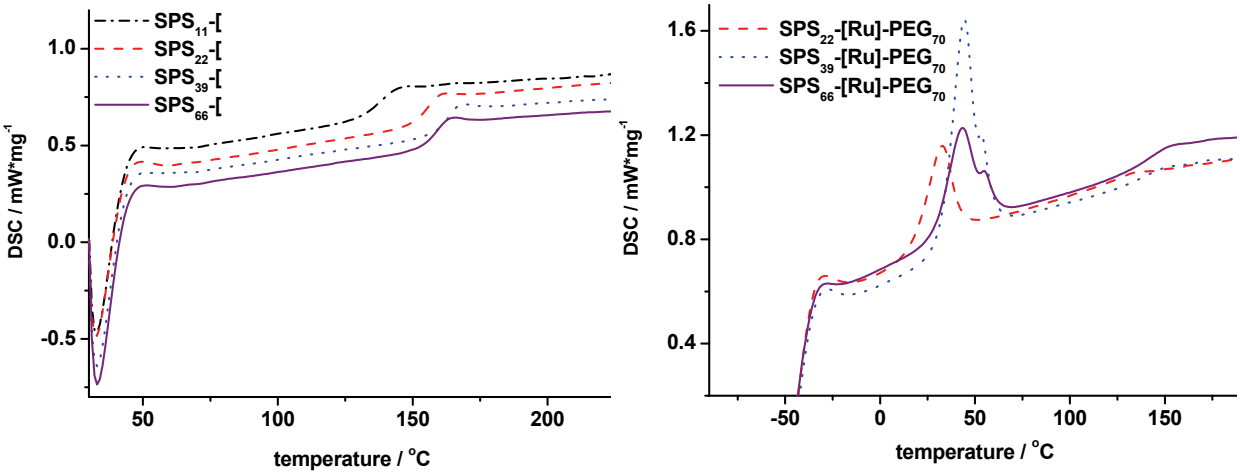

Figure 5.11 *Thermal transitions of a) the alternating terpyridine-functionalized copolymers and b) the complexed block copolymers, as measured by DSC.*

The SPS_n-[Ru]-PEG_{70} block copolymers show a decreased T_g compared to the corresponding SPS_n–[counterparts: due to the softer polyethylene glycol (PEG) present in or around the SPS-rich phase. Therefore, the change in phase segmental mobility already occurs at lower temperatures (Table 1). Moreover, the melting peak of polyethylene glycol at around 50 °C is clearly visible in the DSC graph (Figure 5.11b). Also the single complexed SPS_{11}-[Ru]-PEG_{44}–[showed a comparable melting point (at approximately 55 °C).[65]

One of the key mechanical properties for materials is the elastic modulus or Young's modulus. In order to study the elastic behavior of the SPS-[and the SPS-[Ru]-PEG materials, depth-sensing indentation (DSI) experiments were conducted. In spite of the gentle drying procedure after dropcasting, several supramolecular materials exhibited extensive cracking due to the volume change upon drying. One of the advantages of DSI is that spots where the film adhered to the substrate could be easily identified (from the absence of fringes in the optical image of the film) and indentation experiments could be successfully performed exactly on those spots. Only on the SPS_{66}-[Ru]-PEG_{70} samples, no suitable spots were found. Cracks in the films indicate brittleness of the material. For very brittle materials cracking may occur also on the smaller scale during the indentation experiment. In this case, the method employed to analyze the indentation load-displacement responses is not valid.[66] Therefore, for selected materials, the surface was imaged with the indenter tip after performing the indentation experiments. However, no fracture was observed at the corners of the indents or elsewhere around the indent. For SPS_n-[an indentation modulus of 5.91 GPa was measured with a standard deviation of 0.27 GPa. The variation in elastic modulus with the degree of polymerization *n* is small. The observed decrease in stiffness with increasing SPS length was smaller than one standard deviation, and might be caused by a tiny amount of solvent that remained trapped in the SPS with higher degree of polymerization *n*, but could be removed from the studied SPS samples with lower *n*. The absence of a clear dependency on the degree of polymerization also indicates that the effect of the terpyridine group on the material stiffness can be neglected. An E_i value of 4.2 GPa was measured for the commercial polystyrenes (indentation moduli for Styron 678, Styron 648 and N5000 were very close to each other), which corresponds well with the indentation moduli of

polystyrene reported in literature for indents to maximum indentation depths of 0.5 to 0.7 μm[67] (for polymers, the indentation modulus E_i exceeds the Young's elastic modulus E due to some material pile-up at the indent perimeter, non-linear viscoelasticity and some other factors).[68,69] Gausepohl *et al.*[70] observed a Young's modulus of 4.2 GPa for SPS compared to 3.2 GPa for polystyrene. A good agreement was observed between the ratio of the stiffnesses reported by Gausepohl, $E_{PS}/E_{SPS} = 0.76$, and the ratio discussed in this work, $E_{iPS}/E_{i,SPS} = 0.71 \pm 0.03$.

The elastic behavior of the obtained supramolecular A-[Ru]-B block copolymers was investigated as well. Figure 5.12 shows that upon loading to the same load, the displacement of the indenter probe into the surface of SPS_{22}-[Ru]-PEG_{70} is larger than into SPS_{39}-[Ru]-PEG_{70} reflecting its softer character. In Figure 5.13, the obtained indentation moduli are presented as a function of SPS content. This measure is calculated by dividing the mass of the SPS by the sum of the masses of the SPS, terpyridine moieties, counter ions, and PEG. It is worthwhile to note that the stiffness is usually modeled as a function of the volume fraction of the constituting phases.[71] Nevertheless, the weight fractions are plotted in Figure 5.13, since the density of SPS is unknown and the phases of some materials consist of a mixture of PEG and SPS.

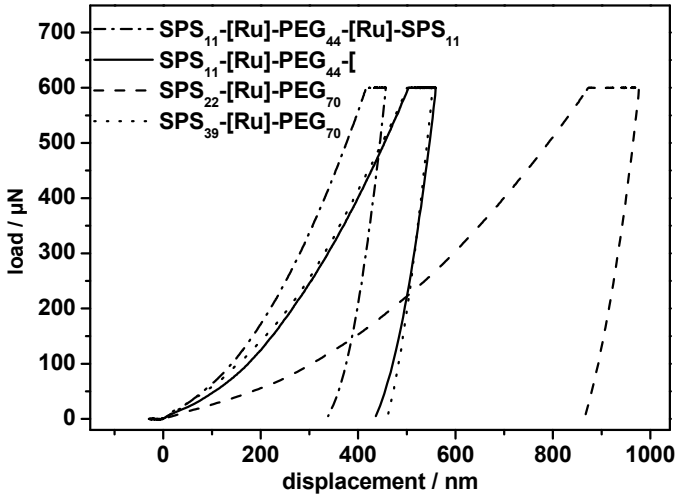

Figure 5.12 *Indentation load-displacement responses for selected supramolecular block copolymers.*

With increasing weight fraction of the hard-domain forming block, *i.e.*, with increasing length of the SPS blocks, the stiffness of the A-[Ru]-B block copolymer increases (filled circles in Figure 5.13). With increasing length of the SPS block, the weight fraction of the complexing Ru^{2+} ions and the PF_6^- counterions decreases. The weight fraction is demonstrated by the annotated numbers in Figure 5.13. These ions may influence the stiffness of the material, for instance through electrostatic interactions or by influencing the phase behavior of the material.[72,73] Polyethylene glycol is semicrystalline and, depending on the crystallinity, hygroscopic. This implies that the elastic properties of the PEG-containing materials may be affected by their processing history as well as by the humidity. To check the humidity influence on the stiffness of the supramolecular copolymers, the indentation measurements were repeated at 45% relative humidity. For apolar polymers such as polystyrene and SPS, the humidity did not have any effect on the load displacement responses, and thus also not on the modulus. The investigated A-[Ru]-B materials containing the hygroscopic PEG block did not show any significant decrease in modulus upon repeating the experiments at ambient humidity either. Therefore it can be concluded that the humidity can be neglected in these cases. Figure 5.12 and 5.13 also show the load-displacement responses and indentation moduli for SPS_{11}-[Ru]-PEG_{44}-[and SPS_{11}-[Ru]-PEG_{44}-[Ru]-SPS_{11}. These materials exhibit a higher stiffness than the A-[Ru]-B block copolymers

of comparable SPS content synthesized with *mono*-functionalized PEG_{70} (filled circles in Figure 5.13).[74]

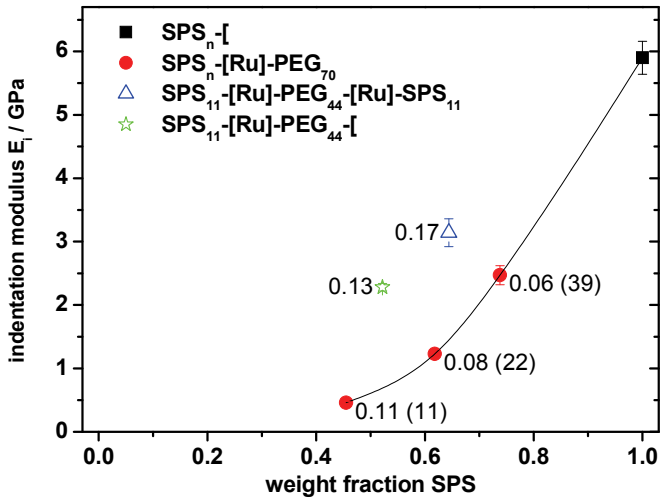

Figure 5.13 *Stiffness of the SPS and the supramolecular block copolymers as a function of the SPS weight fraction. The counterion and metal-ligand complex weight fraction is annotated to the data, and for the SPS-[Ru]-PEG$_{70}$, the degree of polymerization of the SPS is added in brackets.*

The higher stiffness of the materials containing the shorter PEG is attributed to their higher Ru^{2+} and PF_6^- ion contents. Small-angle X-ray scattering above the melting point of the PEG showed for PS_{20}-[Ru]-PEO_{70} that the metal-ligand complex (MLC) and the PF_6^- counterions form randomly located domains surrounded by a mixed PEG / PS phase.[72] For the PEG_{44} materials, the domains containing the MLC and counterions are located closer to each other and the MLC and counterion weight fraction is higher than for the PEG_{70} materials. Therefore, their effect on the deformation behavior increases. These domains are expected to increase the material stiffness through electrostatic interaction and/or by impeding the motion of the attached SPS and PEG chain. Moreover, the presence of the MLC and the counterions may induce changes in the phase-separation behavior of the PEG and SPS as well.[72,73] The smaller size of the PEG could also cause changes in the phase-separation (and crystallization) behavior compared to the materials consisting of the longer PEG_{70}-block.[62,75] This may change the relative amounts of the present phases and their thermal transition temperatures, which could thereby also influence the material stiffness.[76]

5.5 Synthesis of block copolymers by sequential monomer addition

One of the most important synthetic applications of living polymerizations is the synthesis of block copolymers by sequential monomer addition. In case of anionic polymerization, the ability to prepare block copolymers is a direct consequence of the stability of the carbanionic chain end which is strongly influenced by the carbanionic structure itself, the solvent and the temperature, respectively. In order to successfully design block copolymers, the order of monomer addition is of great importance. In general, a carbanionic chain end formed from one monomer will crossover to form the chain end of another monomer and initiate the polymerization of this monomer. However, the resulting carbanion has to be either of comparable stability or more stable than the previous carbanion. If these limitations are taken into consideration, living anionic polymerization provides a powerful synthetic technique for the preparation of block copolymers with well-defined

structures, including copolymer composition, block copolymer mass, molar mass distributions, block sequence, and low degrees of compositional heterogeneity.[19]

In this section, the synthesis of various block copolymers (including terpyridine-functionalized diblock copolymers PS-*b*-PI-[, SPS-*b*-PI-[and triblock copolymer PS-*b*-PI-*b*-SPS-[) by sequential monomer addition is discussed. The synthesis was performed at moderate reaction temperatures (20 °C to 55 °C) in cyclohexane. The applied synthetic method consists of the following steps: (1) predetermined amounts of styrene (and DPE in case of SPS) were polymerized in cyclohexane at 50 °C for 1.5 hours using *sec*-butyl lithium as initiator. (2) Subsequently, a predetermined amount of isoprene was slowly added into the schlenk-flask at 30 °C. (3) The resulting mixture was allowed to react for 6 hours before the endgroup functionalization was conducted at room temperature by the addition of 4'chloro-2,2':6'2"-terpyridine dissolved in dry toluene. Note that after the synthesis of each step samples were taken in order to determine the molar mass and to verify whether the formation of the block copolymer occurred successfully. The synthetic procedure is shown for the example PS-*b*-PI-[in Scheme 5.5.

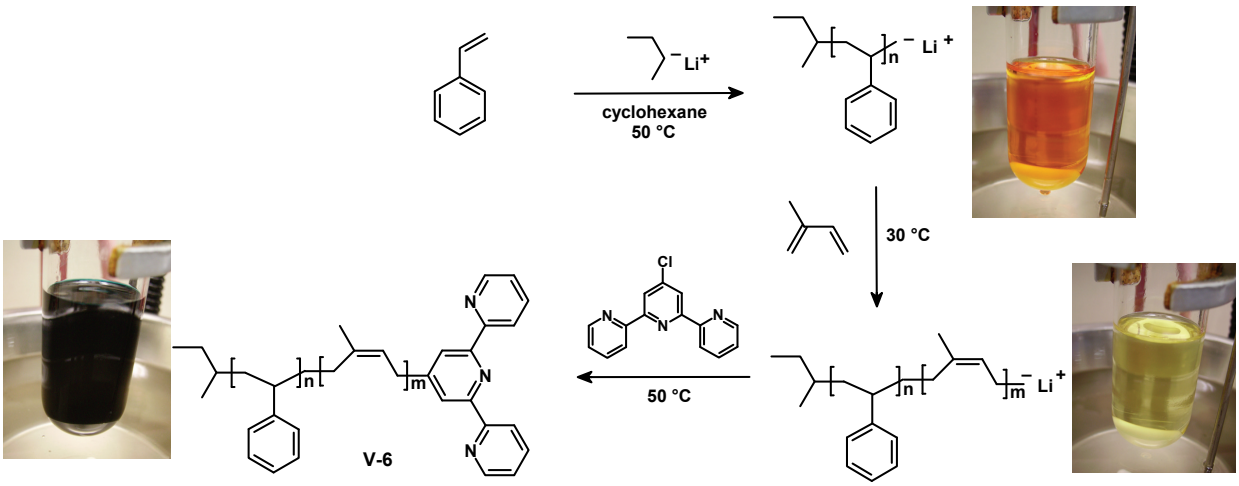

Scheme 5.5 *Schematic representation of the synthesis of poly(styrene-block-isoprene) block copolymers via sequential anionic polymerization. Images of the schlenk-flask were taken after every reaction step demonstrating the livingness of the process: polystyryl-anion orange, polyisoprenyl-anion yellow and functionalization with 4'-chloro-2,2':6'2"-terpyridine dark green.*

The differently colored reaction mixtures displayed in Scheme 5.5 demonstrate the livingness of the polymerization as well as the nature of the carbanion. The more intense the color of the mixture the higher is the concentration of the corresponding carbanions. If the color of the reaction mixture vanishes during the polymerization, the reactive carbanionic species possibly undergoes spontaneous termination in a reaction with electrophiles such as water. Therefore, it is extremely important to purify the monomers and the reaction flasks extensively before starting the polymerization. Poly(styrene-*block*-isoprene) and poly(styrene-*alt*-DPE-*block*-isoprene) were prepared according to Scheme 5.5. The GPC-traces of the homopolymers revealed to be unimodal with a PDI value below 1.10 (M_n = 6,200 g/mol for SPS and M_n = 9,900 g/mol for PS, respectively), whereas the GPC-traces of the terpyridine-functionalized diblock copolymers with the isoprene block as the second block showed that a few undesired coupling reactions occurred between the "living" polymer chains. This finding can be observed in the GPC trace of Figure 5.14 which represents a characteristic example for the performed experiments.

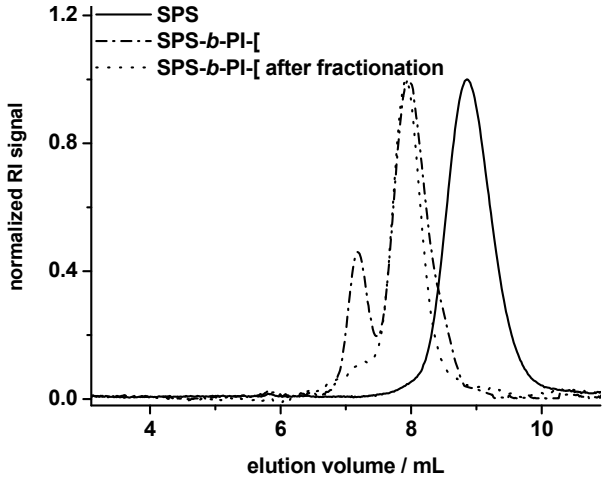

Figure 5.14 *Normalized GPC chromatograms of SPS-b-PI block copolymer: after complete monomer consumption of the first block (SPS, solid line), after the polymerization of isoprene including the functionalization step with 4'-chloro-2,2':6',2"-terpridine (dashed-dotted line) and after applying GPC/SEC to remove the undesired coupling product. GPC eluent: $CHCl_3$, triethylamine, 2-propanol (94:4:2).*

The molar mass distribution arising at lower elution volume can be attributed to the undesired coupling product revealing the double molar mass compared to the protonated PS-*b*-PI precursor (terminated using degassed methanol). Even though an intensive dark green color appeared upon the addition of the terpyridine solution to the block copolymer (which is supposed to originate from the electrophilic attack of the Cl-tpy to the "living" polymeric anion), ^{1}H NMR spectroscopy measurements evidenced only a low degree of functionalization since the intensity of the observed terpyridine signals in the region between 8.9 and 7.4 ppm was very low. Another proof for a low degree of functionalization was obtained when iron(II) ions were added to the diblock copolymer solution. This usually results in a very intense purple absorption due to the formation of *bis*-terpyridine iron(II) complexes; however, in this case the solution was poorly colored. The undesired coupling product could be easily removed by GPC using a fraction collector (Figure 5.15). The M_n values for both block copolymers were determined by GPC and were found to be 12,600 g/mol for PS-*b*-PI-[(PDI = 1.09) and 18,600 for SPS-*b*-PI-[(PDI = 1.05).

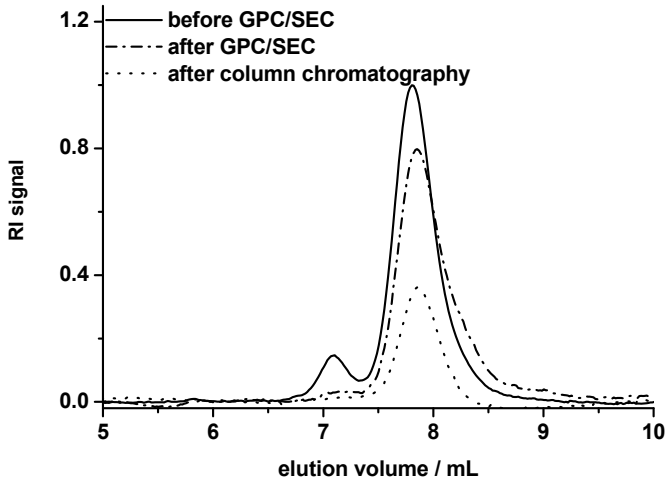

Figure 5.15 *GPC chromatograms obtained during the purification of the PS-b-PI-[block copolymer. Solid line: polymer after the functionalization process. Dashed-dotted line: polymer mixture after applying GPC/SEC. Dotted line: terpyridine-functionalized block copolymer after column chromatography. GPC eluent: $CHCl_3$, triethylamine, 2-propanol (94:4:2).*

As such, a mixture of terpyridine-functionalized and unfunctionalized diblock copolymer was obtained after using GPC/SEC. The separation of this polymer mixture was performed by column chromatography (Al_2O_3, CH_2Cl_2) since terpyridine-functionalized materials interact with the column material while the unfunctionalized polymer does not. After eluting the unfunctionalized polymer, the interaction between the terpyridine moiety and the Al_2O_3 is reduced upon the addition of small amounts of methanol to the eluent. ^{1}H NMR spectroscopy of the first eluted fraction indeed revealed the presence of only unfunctionalized polymer, since the characteristic terpyridine signals were missing in the aromatic region of the spectrum. The collected purified block copolymer was finally precipitated into methanol and dried *in vacuo*. Unfortunately, the block copolymer was obtained in a very low yield (9%) due to incomplete functionalization reaction and the multiple purification steps. Figure 5.16 demonstrates that the tailing on lower molecular side in the GPC-trace which is most likely due to unfunctionalized polymer and small amounts of "dead" polymer chains was successfully removed. Nonetheless, rather than this multistep purification process it would be preferred to improve the degree of functionalization during the synthesis procedure.

In order to improve the functionalization process, DPE was used as an intermediate synthetic step to end-cap the polyisoprenyl anions. It is reported in literature that DPE effectively reduces the reactivity of the respective carbanion.[16] The steric hindrance provided by the bulky phenyl rings and the fact that the resulting "new" chemical species are energetically more stable than the former carbanion decrease the occurrence of the undesired coupling reactions.[16,77] For this purpose, the reaction mixture was heated to 55 °C after the isoprene monomer was completely consumed and a predetermined amount of DPE was added. Stirring continued at the given temperature until the intensity of the developing orange/red solution did not change anymore. After cooling to room temperature, the terpyridine solution was added to the mixture, which thereupon changed its color to dark green. GPC measurements revealed that significantly less coupling reactions occurred when DPE was used as end-capper. Moreover, a higher degree of terpyridine functionalization was achieved as it was observed by ^{1}H NMR spectroscopy (Figure 5.16). However, complete functionalization (as it was reported in Section 5.2 for poly(styrene-*alt*-DPE)) could not be obtained. Elemental analysis revealed remarkably higher nitrogen contents compared to the experiment where DPE was not used as end-capper.

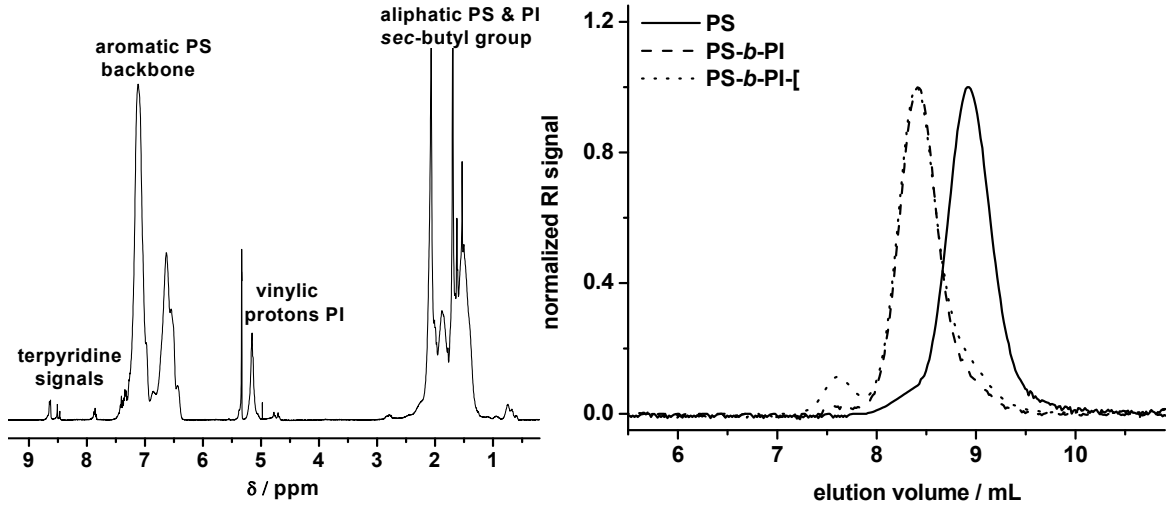

Figure 5.16 *Left: ^{1}H NMR spectrum of the terpyridine-functionalized PS-b-PI diblock copolymer synthesized by anionic polymerization in cyclohexane using DPE as end-capper (in CD_2Cl_2). Right: Normalized GPC traces obtained upon completion of each polymerization step: PS block (solid line), PS-b-PI diblock copolymer (dashed line) and the crude PS-b-PI diblock copolymer after functionalization (dotted line). GPC eluent: $CHCl_3$, triethylamine, 2-propanol (94:4:2).*

It is assumed that the generated “new” DPE-carbanion is energetically more stable than the polyisoprenyl anion but less stable than the SPS anion. This could be a potential explanation for both incidents: the improved degree of functionalization (approx. 70-85%) and the decrease of coupling reactions on the one hand and the lower degree of functionalization compared to SPS on the other hand. ^{1}H NMR spectroscopy clearly revealed that the terpyridine ligand is tethered to the polymer chain end. The signals related to the aromatic protons of the terpyridine moiety could be detected in the region between 7.3 to 8.7 ppm. Interestingly, the signal belonging to the $H_{3',5'}$ of the terpyridine ligand experienced a downfield shift to 8.5 ppm because of the adjacent PI-backbone. The splitting of the signal could be due to a different electronic environment resulting from 1,4- and 3,4 coupling or incomplete DPE functionalization. The degrees of polymerization were calculated by integrating the terpyridine signals, the aromatic signals of the polystyrene backbone (between 7.4 and 6.3) as well as the vinylic protons of the isoprene (between 5.2 and 4.6). Assuming complete functionalization this results in a composition of 46 units styrene and 36 units isoprene, respectively. If not all chains are functionalized with the terpyridine moiety, the molar mass of the polymer determined by integration is slightly overestimated. The protons belonging to the double bond of isoprene provide information over the content of 1,4 (at 5.1 ppm) and 3,4 (at 4.7 ppm) polymerized isoprene, respectively.[78] A high 1,4-content (94%) was found which was calculated from the relative intensities of both signals.

It can be excluded that the polyisoprenyl anion is not reactive enough to promote further functionalization since the reaction with DPE could be performed successfully. The reason for incomplete functionalization with Cl-tpy could be due to potential solvent effects. It has been reported in literature that functionalization reactions of dienes *via* anionic polymerization can be achieved with higher yields when the reaction is performed in non-polar solvents at lower temperature.[79] A potentially improved degree of polymerization might be obtained in *n*-heptane because it can be used to perform reactions down to –60 °C.

In order to prove the reactivity and livingness of the polyisoprenyl anion, a further chain extension experiment was performed. The above described synthetic approach for the preparation of the PS-*b*-PI diblock copolymer was continued to synthesize a triblock copolymer with SPS as its third block. The polymerization by sequential monomer addition as well as the functionalization with Cl-tpy is summarized schematically in Scheme 5.6.

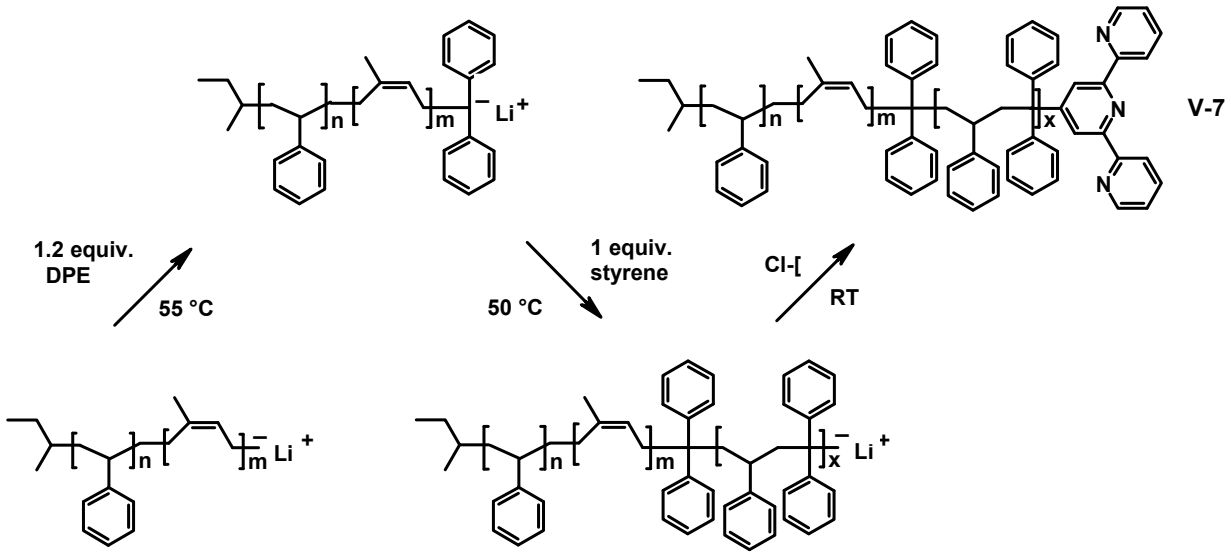

Scheme 5.6 *Schematic representation of the synthesis of the terpyridine-functionalized PS-b-PI-b-SPS-[triblock copolymer by sequential monomer addition.*

Therefore, a predetermined amount of DPE was added to the "living" PS-*b*-PI anion after complete isoprene consumption. Subsequently, the mixture was heated to 55 °C for one hour to make sure that the end-capping with DPE was complete. The reaction process could be followed by a change of the solution color from yellow to orange to red. Styrene was added to the reaction mixture which was allowed to polymerize at 50 °C for 1.5 hours. Finally, the terpyridine solution in dry toluene was added. Figure 5.17 represents the ^{1}H NMR spectrum after precipitation in methanol and the GPC traces after each polymerization step.

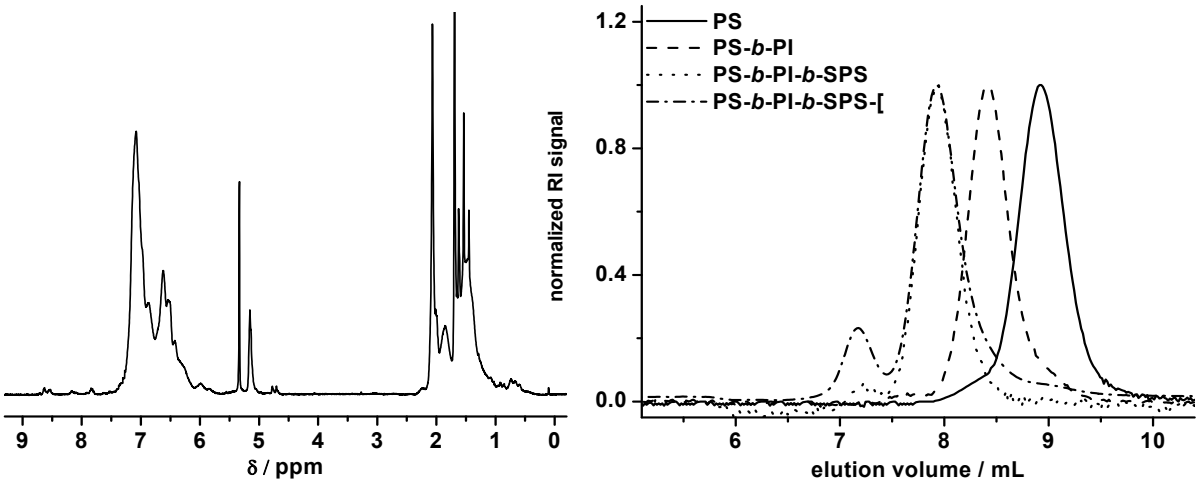

Figure 5.17 *Left: ^{1}H NMR spectrum of the terpyridine-functionalized PS-b-PI-b-SPS triblock copolymer synthesized by anionic polymerization in cyclohexane (in CD_2Cl_2). Right: Normalized GPC traces obtained upon completion of each polymerization step: the PS block (solid line), the PS-b-PI diblock copolymer (dashed line), PS-b-PI-b-SPS triblock copolymer (dotted line) and triblick copolymer after chain-end functionalization (dashed-dottet line). GPC eluent: $CHCl_3$, triethylamine, 2-propanol (94:4:2).*

The ^{1}H NMR spectrum demonstrates that the terpyridine ligand is tethered to the polymer chain end. Furthermore, it reveals the presence of the aromatic protons belonging to the styrene and DPE (region from 7.6 to 5.6 ppm), respectively. In addition, the protons related to the double bond of the PI (between 5.3 and 4.6 ppm) are present. The much larger signal at 5.2 ppm (95%) can be assigned to the CH-group resulting from 1,4-polymerized isoprene (*cis* and *trans*).[78] The smaller signal between 5.8 and 5.6 ppm arises from the CH_2-group of 3,4-polymerized isoprene. The composition of the triblock copolymer was determined by integration over the terpyridine signals revealing 42 styrene units, 33 isoprene units and 37 SPS units. The GPC chromatograms obtained after each polymerization step revealed to be unimodal. However, during functionalization a few undesired coupling reactions occurred between the "living" polymeric anions as observed in Figure 5.17. The appearance of the undesired coupling product after the functionalization on the SPS block was unexpected since it was not observed for the alternating homopolymer. It might be due to traces of impurities in the solvent or the terpyridine.

5.6 Conclusions

In the first part of this chapter the synthesis of well-defined terpyridine-functionalized poly(styrene-*alt*-diphenylethylene) (SPS) copolymers of varying chain lengths by living anionic polymerization was discussed. The materials were fully characterized by means of ^{1}H NMR

spectroscopy, GPC, UV-Vis spectroscopy, MALDI-TOF MS and elemental analysis, proving the successful incorporation of the terpyridine ligand into the copolymer. Moreover, AUC (in combination with density and viscosity measurements) was applied to obtain the absolute molar mass of the copolymers. A very good agreement was found between the molar masses obtained from different analytical techniques demonstrating quantitative functionalization. In addition, the worm-like cylinder model was applied to determine the conformational parameters from the AUC-results: the Kuhn segment length, *A*, and the hydrodynamic diameter, *d*. The obtained values were higher compared to those of linear polystyrene due to the higher stiffness of the materials. The terpyridine-functionalized copolymers were subsequently used to prepare AB diblock copolymers as well as ABA triblock copolymers in which the polymer blocks are linked together by a *bis*-terpyridine ruthenium(II) complex. Characterization methods that prove the purity of the materials include ^{1}H NMR spectroscopy and GPC with a photo-diode array detector. It was demonstrated that the elastic modulus of supramolecular materials can be changed by varying the chemical composition. The chemical composition was fine-tuned by changing the length of the soft-domain and hard-domain forming blocks, respectively. The high modulus of SPS, which is approximately 35% higher than for PS, provides a wide range for tuning the material stiffness *via* this supramolecular approach. The last part described the synthesis of block copolymers *via* sequential anionic polymerization. Here, the functionalization of the polymeric chain end with the terpyridine ligand was not as straightforward as for the SPS polymers, but the pure terpyridine-functionalized block copolymer could be obtained after purification. Therefore, an intermediate end-capping step of the highly reactive polyisoprenyl anion with 1,1-diphenylethylene (DPE) was found to be necessary for the functionalization process and to reduce undesired coupling reactions between the polymeric chains. Using this approach, a much higher degree of functionalization was achieved. Moreover, this synthetic concept was applied for the synthesis of a well-defined terpyridine-functionalized triblock copolymer.

5.7 Experimental

Reagents and Solvents. Solvents and monomers were stored under argon after the corresponding purification procedure.[21,22,80] Cyclohexane (Biosolve) was distilled from polystyryl lithium oligomers. Toluene was used from a solvent purification system (Pure-Solv). DPE (Aldrich) was dried over *sec*-butyl lithium and distilled under vacuum. *sec*-Butyl lithium (1.4 M) in cyclohexane (Aldrich) was used as received. 4'-Chloro-2,2':6',2"-terpyridine[81] was purified by repeated sublimation. Methanol (Biosolve) was degassed with argon for 15 minutes prior to use.

Characterization Techniques. GPC measurements were performed on a Shimadzu system with a SCL-10A system controller, a LC-10AD pump, a RID-6A refractive index detector and a Polymer Laboratories PLgel 5 µm Mixed-D column using *N,N*-dimethylacetamide (DMA) and LiCl as eluent at a flow rate of 1 mL/min, on a Waters system with a 1515 pump, a 2414 refractive index detector, and a Waters Styragel HT4 column utilizing a *N,N*-dimethylformamide (DMF) / 5 mM NH_4PF_6 mixture as eluent at a flow rate of 0.5 mL/min at 50 °C and on a Shimadzu system equipped with a SCL-10A system controller, a LC-10AD pump, a RID-6A refractive index detector and a PLgel 5 µm Mixed-D column with chloroform as the eluent containing 4 vol% Et_3N and 2 vol% 2-propanol as additives to reduce column interactions at a flow of 1 mL/min. Molar masses were calculated against polystyrene standards. ^{1}H-NMR spectra were recorded on a Varian Gemini 400 spectrometer using deuterated methylene chloride (Cambridge Isotopes Laboratories) at room temperature. UV/Vis spectra were recorded on a Perkin Elmer Lambda 45P spectrophotometer using quartz cuvettes (1 cm path length). For UV-vis titrations, a solution of the terpyridine-terminated polymer in chloroform was titrated with a solution of $FeCl_2$ in methanol of known concentration and followed by UV-vis spectroscopy. MALDI-TOF-MS analysis was performed on a Voyager-DE PRO Biospectrometry workstation (Applied Biosystems) in linear operation mode. Spectra were obtained in positive ion mode, and ionization was performed with a 337 nm pulsed nitrogen laser. Data were processed using the Data Explorer software package (Applied Biosystems). Elemental analyses were recorded on a Euro elemental analyzer from EuroVector. The efficiency of functionalization was determined from the nitrogen content obtained by elemental analysis measurements and UV-Vis titrations. Transmission electron microscopy measurements were performed on a FEI Tecnai 20, type Sphera TEM operating at 200 kV with a LaB_6 filament and a bottom mounted 1k x 1k Gatan CCD. Samples were prepared by blotting a dilute

solution of the respective micelle solution on a 200 mesh carbon coated grid followed by overnight drying, after which the grids were examined in the TEM. TEM grids were hydrophilized directly before use by 40 s plasma treatment. The samples for TEM measurements were not stained. Thermal transitions were determined on a NETSCH 204 F1 Phoenix DCS in a nitrogen atmosphere. Samples were two times heated from –50 °C to 225 °C at a rate of 20 K min^{-1}. The first heating run was disregarded. Polymer films were prepared for depth-sensing indentation by dropcasting the materials onto glass slides (Marienfeld, Lauda-Königshofen, Germany). The solutions contained 5 mg polymer in 50 µL chloroform (Biosolve). Several commercial polystyrenes, Styron 678 and Styron 648 (DOW Chemical) as well as N5000 (Shell), were dropcast from toluene and dried thoroughly. The elastic properties of the dried samples were studied at 11% relative humidity by depth-sensing indentation (DSI) using a Hysitron (Minneapolis, Mn) TriboIndenter equipped with a Berkovich (trigonal pyramid) probe. During the indentation experiments, the tip was loaded to maximum load in 10 s, held at maximum load for 10 s, and unloaded in 0.5 s. For each material, the experiments were repeated on at least two different dropcasted samples, and at least five maximum loads (1500, 1200, 900, 600 and 300 µN). For SPS_{11}-[Ru]-PEG_{70}, lower loads were chosen: 300, 250, 200, 150, 100, 50 µN. SPS_x-[and the polystyrenes were measured with higher loads: 2700, 2400, 2100, 1800, 1500, 1200 µN. The first two indentation responses were left out to minimize the effect of thermal drift. The load displacement responses obtained from DSI were analyzed using the method proposed by Oliver and Pharr.[68,82] Reduced moduli E_r were converted to modulus of elasticity E_i (where the subscript denotes 'indentation') using 0.35 as the poisson's ratio.[83]

Sedimentation velocity experiments. Analytical ultracentrifugation (AUC) was performed on a ProteomeLabTM XL-I (Beckman Coulter) with a rotor speed of 55 000 rpm in a double sector cell with 12 mm optical path length using interference optics. Interference scans were measured overnight in intervals of 2 to 5 min. Sedimentation coefficients s, and frictional ratios (f/f_{sph}) were otained with Sedfit.[84] Thereby, f is the translational friction coefficient of the macromolecules and f_{sph} the translational friction coefficient of a sphere with the same molar mass.[85] Linear fitting of $s^{-1} = s_0^{-1}(1 + k_s c + \ldots)$ allowed the determination of the sedimentation coefficients at infinite dilution, s_0, and the concentration-dependent Gralen coefficients, k_s. Linear fitting was also used to obtain the frictional ratio extrapolated to infinite dilution $(f/f_{sph})_0$. The number of fringes J, corresponding to the copolymer concentration in solution, was estimated from the derived curves c(s) obtained by Sedfit and used to calculate the refractive index increment:

$$\frac{\Delta n}{\Delta c} = \frac{J\lambda}{Kcl},$$

where λ is the wavelength (675 nm), K the magnifying coefficient and l the optical path. With K = 1 and l = 12 mm we obtain: $\frac{\Delta n}{\Delta c} = 5.625 \times 10^{-5} \frac{J}{c}$.[86]

Intrinsic viscosity measurements. Viscosity measurements were performed at 25.0 °C using a capillary viscometer. The relative viscosity η_r of the solutions was calculated from the equation below:

$$\eta_r = \frac{\eta}{\eta_0} = \frac{t}{\tau_0}$$

where η, and t refer to the viscosity and flow time through the capillary of the polymer solution, respectively, and η_0 and τ_0 to the viscosity and the flow time through the capillary of the pure solvent. The ratio η_r was used to determine the specific viscosities: $\eta_{sp} = \eta_r - 1$. The intrinsic viscosity, $[\eta]$, of the copolymer samples was determined both from the Huggins (1) and Kraemer (2) equations:

$$\frac{\eta_{sp}}{c} = [\eta] + k'[\eta]^2 c + \ldots \quad (1)$$

$$\ln\frac{\eta_r}{c} = [\eta] + k''[\eta]^2 c + \ldots \quad (2),$$

where k' and k'' are the Huggins' and Kraemer' parameters, correspondingly.

Density measurements. The density increment or buoyancy factor $\Delta\rho/\Delta c$ was measured with a density meter DMA 02 (Anton Paar, Graz, Austria) according to the procedure of Kratky *et al*. using the equation below:

$$\frac{\Delta\rho}{\Delta c} = (1 - \overline{\upsilon}\rho_0)$$

Where $\Delta\rho$ is the difference between the densities of the copolymer solution ρ and the pure solvent ρ_0, and $\overline{\upsilon}$ is the partial specific volume of the copolymer macromolecules.[87]
All hydrodynamic measurements were performed in dilute toluene solutions. At 20 °C the density ρ_0 of toluene has a value of 0.865 g/cm^3 and a dynamic viscosity η_0 of 0.590 cP, respectively. Dilution parameters c[η] for the sedimentation experiments were in the range of $0.01 \leq c[\eta] \leq 0.12$, and for the intrinsic viscosity measurements in the range of $0.11 \leq c[\eta] \leq 0.68$, respectively.

Terpyridine-functionalized poly(styrene-*alt*-1,1-diphenylethylene) (SPS) (V-1).
Anionic polymerizations were carried out in a 100 mL round bottom schlenk–type glass flask using inert atmosphere techniques. All utilized glassware were previously heated above 150 °C, subjected to several cycles of subsequent filling with argon and high–vacuum, and kept under argon prior to use. A general procedure for the anionic synthesis of poly(styrene-*alt*-diphenylethylene) copolymers and their functionalization with terpyridine units was performed as follows: a predetermined amount of 1,1-diphenylethylene was added into the schlenk-flask containing a predetermined amount of cyclohexane at 55 °C under argon atmosphere. After the addition of *sec*-butyl lithium, the mixture turned into a deep red solution. In the final step, styrene was added to the mixture, which was stirred for 1.5 h at a given temperature. A sample was taken from the reaction mixture for GPC characterization of the unfunctionalized copolymer. The functionalization started with the addition of a predetermined volume (1.25 molar excess in respect to *sec*-butyl lithium) of a solution of 4'-chloro-2,2':6',2"-terpyridine in toluene into the schlenk-flasks at room temperature. Instantly, after the addition of the terpyridine moieties, the solution revealed a green color. Finally, methanol was added after 8 h in order to terminate the reaction. The polymers were precipitated from chloroform into methanol, at the same time unreacted terpyridine species were removed. The obtained materials were dried at 40 °C under vacuum for 24 h and were subsequently characterized.
^{1}H-NMR (400 MHz, CD_2Cl_2) for SPS_{11}-[: δ (ppm) = 8.63 (m, 2 H; $H_{6:6"}$), 8.54 (m, 2 H; $H_{3:3"}$), 8.16 (m, 2 H; $H_{3':5'}$), 7.84 (m, 2 H; $H_{4:4"}$), 7.45-6.95 (m, 177 H; $H_{\text{aromatic DPE \& styrene}}$, $H_{5,5"}$), 2.50-0.00 (m, 66 H; $H_{\text{aliphatic polymer backbone}}$, C_4H_9 *sec*-butyl group). GPC data is summarized in Table 2, GPC eluent: DMA with LiCl (2.1 g/mL).

Terpyridine-functionalized SPS-*b*-PI using DPE as end-capper (V-6).
Anionic polymerizations were carried out in a 100 mL round bottom schlenk–type glass flask using inert atmosphere techniques. All utilized glassware were previously heated above 150 °C, subjected to several cycles of subsequent filling with argon and high–vacuum, and kept under argon prior to use. The polymerization was performed as follows: a predetermined amount of 1,1-diphenylethylene was added into the schlenk-flask containing a predetermined amount of cyclohexane at 55 °C under argon atmosphere. After the addition of *sec*-butyl lithium, the mixture turned into a deep red solution. In the final step, styrene was added to the mixture, which was stirred for 1.5 h at a given temperature. A sample was taken from the reaction mixture for GPC characterization of the unfunctionalized copolymer. After the reaction mixture was cooled to 30 °C, a predetermined amount of isoprene was added. Subsequently, a small amount of DPE was added and the reaction mixture was heated to 55 °C for one hour. Finally, the functionalization took place by adding a predetermined volume (1.25 molar excess in respect to *sec*-butyl lithium) of a solution of 4'-chloro-2,2':6',2"-terpyridine in dry toluene into the schlenk-flask at room temperature. Instantly, after the addition of the terpyridine moieties, the solution revealed a green color. The solution was stirred overnight before (degassed) methanol was added in order to terminate the reaction. The polymers were precipitated from chloroform into methanol, at the same time unreacted terpyridine species were removed. The obtained materials were dried under vacuum for 24 h and were subsequently characterized.
^{1}H-NMR (400 MHz, CD_2Cl_2) for SPS_{43}-*b*-PI_{35}-DPE-[: δ (ppm) = 8.64 (m, 4 H; $H_{6:6"}$, $H_{3:3"}$), 8.50 (m, 2 H; $H_{3':5'}$), 7.85 (m, 2 H; $H_{4:4"}$), 7.45-5.60 (m, 657 H; $H_{\text{aromatic DPE \& styrene}}$, $H_{5,5"}$), 5.30-4.60 (m, 37 H; -CH= & =CH_2) 2.50-0.50 (m, 469 H; $H_{\text{aliphatic SPS backbone}}$, $H_{\text{PI backbone}}$, C_4H_9 *sec*-butyl group). GPC (eluent $CHCl_3$, triethylamine, and 2-propanol (94:4:2): M_n = 10,300 g/mol, PDI = 1.06.

Terpyridine-functionalized PS-*b*-PI using DPE as end-capper (V-6).
Anionic polymerizations were carried out in a 100 mL round bottom schlenk–type glass flask using inert atmosphere techniques. All utilized glassware were previously heated above 150 °C, subjected to several cycles of subsequent filling with argon and high–vacuum, and kept under argon prior to use. The polymerization was performed as follows: a predetermined amount of styrene was added into the schlenk-flask containing a predetermined amount of cyclohexane at 55 °C under argon atmosphere. After the addition of *sec*-butyl lithium, the mixture turned into an orange solution and was stirred for 1.5 h at 50 °C. A sample was taken from the reaction mixture for GPC characterization of the unfunctionalized copolymer. After the reaction mixture was cooled to 30 °C, a predetermined amount of isoprene was added. Subsequently, a small amount of DPE was added and the reaction mixture was heated to 55 °C for one hour. Finally, the functionalization took place by adding a predetermined volume (1.25 molar excess in respect to *sec*-butyl lithium) of a solution of 4'-chloro-2,2':6',2"-terpyridine in dry toluene into the schlenk-flask at room temperature. Instantly, after the addition of the terpyridine moieties, the solution revealed a green color. The solution was stirred overnight before (degassed) methanol was added in order to terminate the reaction. The polymers were precipitated from chloroform into methanol, at the same time unreacted terpyridine species were removed. The obtained materials were dried under vacuum for 24 h and were subsequently characterized. ^{1}H-NMR (400 MHz, CD_2Cl_2) for PS_{46}-*b*-PI_{36}-

DPE-[: δ (ppm) = 8.65 (m, 4 H; $H_{6:6''}$, $H_{3:3''}$), 8.50 (m, 2 H; $H_{3':5'}$), 7.85 (m, 2 H; $H_{4:4''}$), 7.60-6.35 (m, 242 H; $H_{styrene}$, Ph_{DPE}, $H_{5,5''}$), 5.30-4.60 (m, 38 H; -CH= & =CH_2) 2.60-0.50 (m, 491 H; $H_{aliphatic\ PS\ backbone,}$ $H_{PI\ backbone}$, C_4H_9 *sec*-butyl group). GPC (eluent $CHCl_3$, triethylamine, and 2-propanol (94:4:2): M_n = 7,600 g/mol, PDI = 1.06.

Terpyridine-functionalized PS-*b*-PI-*b*-SPS triblock terpolymer (V-7).
Anionic polymerizations were carried out in a 100 mL round bottom schlenk–type glass flask using inert atmosphere techniques. All utilized glassware were previously heated above 150 °C, subjected to several cycles of subsequent filling with argon and high–vacuum, and kept under argon prior to use. The polymerization was performed as follows: A predetermined amount of styrene was added into the schlenk-flask containing a predetermined amount of cyclohexane at 55 °C under argon atmosphere. After the addition of *sec*-butyl lithium, the mixture turned into an orange solution and was stirred for 1.5 h at 50 °C. A sample was taken from the reaction mixture for GPC characterization of the unfunctionalized copolymer. After the reaction mixture was cooled to 30 °C, a predetermined amount of isoprene was added. Subsequently, a predetermined amount of DPE was added and the reaction mixture was heated to 55 °C for one hour before the comonomer (styrene) was added. Finally, the functionalization took place by adding a predetermined volume (1.25 molar excess in respect to *sec*-butyl lithium) of a solution of 4'-chloro-2,2':6',2"-terpyridine in dry toluene into the schlenk-flask at room temperature. Instantly, after the addition of the terpyridine moieties, the solution revealed a green color. The solution was stirred overnight before (degassed) methanol was added in order to terminate the reaction. The polymers were precipitated from chloroform into methanol, at the same time unreacted terpyridine species were removed. The obtained materials were dried under vacuum for 24 h and were subsequently characterized. ^{1}H-NMR (400 MHz, CD_2Cl_2) for PS_{42}-*b*-PI_{33}-DPE-*b*-SPS_{37}-[: δ (ppm) = 8.65 (m, 4 H; $H_{6:6''}$, $H_{3:3''}$), 8.13 (m, 2 H; $H_{3':5'}$), 7.83 (m, 2 H; $H_{4:4''}$), 7.60-5.60 (m, 777 H; $H_{PS\ \&\ SPS\ backbone}$, Ph_{DPE}, $H_{5,5''}$), 5.30-4.60 (m, 33 H; -CH= & =CH_2) 2.40-0.40 (m, 551 H; $H_{aliphatic\ PS\ \&\ SPS\ backbone,}$ $H_{PI\ backbone}$, C_4H_9 *sec*-butyl group). GPC (eluent $CHCl_3$, triethylamine, and 2-propanol (94:4:2): M_n = 12,500 g/mol, PDI = 1.05.

Synthesis of the SPS_n-[Ru]-PEG_{70} block copolymers (V-2).
The terpyridine-functionalized alternating P(S-*alt*-DPE)$_{11}$ copolymer (90 mg, M_n = 2200 g/mol, PDI = 1.17) and the $RuCl_3$ poly(ethylene oxide) *mono*complex (157 mg, M_n = 3200 g/mol, PDI = 1.07) were reacted in a 1:1.2 molar ratio in a 3:1 (1.5 mL/0.5 mL) solvent mixture of degassed chloroform and methanol for 6 hours at 80 °C in a sealed vial. Subsequently, the reaction mixture was stirred for 10 minutes at room temperature after a 10-fold excess of NH_4PF_6 was added. The solution was poured into water, and the aqueous layer was extracted twice with chloroform. The combined organic layers were dried over Na_2SO_4, filtered, and the solvent was removed *in vacuo*. The crude product was purified by preparative size exclusion chromatography (Biobeads SX1) and column chromatography (AlOx).
The following metallo-supramolecular block copolymers have been synthesized using the previous described procedure: SPS_{11}-[Ru]-PEG_{70}, SPS_{22}-[Ru]-PEG_{70}, SPS_{39}-[Ru]-PEG_{70} and SPS_{66}-[Ru]-PEG_{70}. Yield: 25-40%. ^{1}H-NMR (SPS_6-[Ru]-PEG_{70}, 400 MHz, CD_2Cl_2): δ (ppm) = 8.45-8.26 (m, 8 H; $H_{3':5''}$,$H_{3:3''}$), 8.16-7.94 (m, 4 H; $H_{4:4''}$), 7.93-7.77 (m, 4 H; $H_{6:6''}$), 7.70-5.95 (m, 104 H; $H_{PS,DPE\ backbone\ aromatic}$; $H_{aromatic}$, $H_{5,5''}$), 4.09 (m, 2 H; tpyOCH_2), 3.88-3.36 (m, 280 H; $H_{PEG\ backbone}$), 2.40-0.10 (m, 41 H; $H_{PS\ \&\ DPE\ backbone\ aliphatic,}$ *sec*-butyl group). GPC data is summarized in Table 4, GPC eluent: DMA with LiCl (2.1 g/mL).

Synthesis of $RuCl_3$ SPS *mono*-complexes (V-3).
A three fold excess of anhydrous $RuCl_3$ (85 mg, M_n = 207 g/mol) with respect to the terpyridine end functionalized polymer was heated in dry degassed DMA (3 mL) to 130 °C. After the color of the suspension turned brown, a solution of the terpyridine-functionalized SPS (300 mg, M_n = 2200 g/mol) in dry degassed DMA (2 mL) was added dropwise. Stirring continued overnight at 130 ºC at inert conditions and then the solution was allowed to cool to room temperature. The resulting mixture was partitioned between dichloromethane and water. The organic layer was separated, dried over Na_2SO_4, filtered and the solvent was removed *in vacuo*. The brown residue was taken up in a minimum amount of THF and precipitated twice into methanol.
^{1}H-NMR ($CDCl_3$): only polymer backbone protons were visible because of the paramagnetic nature of the Ru(III)-complex.

Synthesis of the SPS_n-[Ru]-PEG_{44}-[Ru]-SPS_n block copolymers (V-5).
Bis(terpyridine) end-functionalized poly(ethylene) oxide (30 mg, M_n = 2500 g/mol, PDI = 1.09) and $RuCl_3$ poly(S-*alt*-DPE) *mono*complex (63 mg, M_n = 2400 g/mol, PDI = 1.16) were reacted in a 1:2.2 molar ratio in a 3:1 (1.2 mL/0.4 mL) solvent mixture of degassed chloroform and methanol for 6 hours at 80 °C in a sealed vial. The purification was performed analog to the SPS_n-[Ru]-PEG_{70} block copolymers.
The following metallo-supramolecular block copolymers have been synthesized using the previous described procedure: SPS_6-[Ru]-PEG_{44}-[Ru]-SPS_6 and SPS_{11}-[Ru]-PEG_{44}-[Ru]-SPS_{11}.
^{1}H-NMR (SPS_6-[Ru]-PEG_{44}-[Ru]-SPS_6, 400 MHz, CD_2Cl_2): δ (ppm) = 8.45-8.26 (m, 16 H; $H_{3':5''}$,$H_{3:3''}$), 8.16-7.94 (m, 8 H; $H_{4:4''}$), 7.93-7.77 (m, 8 H; $H_{6:6''}$), 7.70-5.95 (m, 118 H; $H_{PS,DPE\ backbone\ aromatic}$; $H_{aromatic}$, $H_{5,5''}$), 4.09 (m, 4 H; tpyOCH_2), 3.88-3.36 (m, 176 H; $H_{PEG\ backbone}$), 2.40-0.10 (m, 82 H; $H_{PS\ \&\ DPE\ backbone\ aliphatic,}$ *sec*-butyl group). GPC (eluent DMF with 0.8 g/L NH_4PF_6) using PEG calibration: M_n = 8,900 g/mol, PDI = 1.15 (SPS_6-[Ru]-PEG_{44}-[Ru]-SPS_6); M_n = 15,200 g/mol, PDI = 1.55 (SPS_{11}-[Ru]-PEG_{44}-[Ru]-SPS_{11}).

5.8 References and notes

1 M. Szwarc, *Nature* **1956**, *78*, 1168.
2 M. Szwarc, M. Levy, R. Milkovich, *J. Am. Chem. Soc.* **1956**, *78*, 2656.
3 C. Lambert, P. von Rague Schleyer, *Angew. Chem. Int. Ed.* **1994**, *33*, 1129.
4 C. Schade, P. von Rague Schleyer, *Adv. Organomet. Chem.* **1987**, *27*, 169.
5 R.E. Rundle, *J. Phys. Chem.* **1957**, *61*, 45.
6 C.M. Selman, H.L. Hsieh, *Polym. Lett.* **1971**, *9*, 219.
7 J.W. Mays, N. Hadjichristidis, *Polym. Bull.* **1989**, *22*, 471.
8 D.A. Conlon, J.V. Crivello, J.L. Lee, M.J. O'Brien, *Macromolecules* **1989**, *22*, 509.
9 I. Konigsberg, J. Jagur-Grodzinski, *J. Polym. Sci.; Part A: Polym. Chem.* **1983**, *21*, 2535.
10 R.N. Young, R.P. Quirk, L.J. Fetters, *Adv. Polym. Sci.* **1984**, *56*, 1.
11 X. Zhongde, J.W. Mays, N. Xuexin, N. Hadjichristidis, F.C. Schilling, H.E. Bair, D.S. Pearson, L.J. Fetters, *Macromolecules* **1985**, *18*, 2560.
12 H. Ozaki, A. Hirao, S. Nakahama, *Macromolecules* **1992**, *25*, 1391.
13 S.K. Varshney, C. Jacobs, J.P. Hautekeer, P. Bayard, R. Jerome, R. Fayt, P. Teyssie, *Macromolecules* **1991**, *24*, 4997.
14 K. Matyjaszewski, *"Advances in Controlled / Living Radical Polymerization"*, *ACS Symp. Ser., 854,* American Chemical Society, Washington D.C., **2003**.
15 J. Jagur-Grodzinski, *J. Polym. Sci.; Part A: Polym. Chem.* **2002**, *40*, 2116.
16 R.P. Quirk, T. Yoo, Y. Lee, J. Kim, B. Lee, *Adv. Polym. Sci.* **2000**, *153*, 67.
17 M. Pitsikalis, S. Pispas, J.W. Mays, N. Hadjichristidis, *Adv. Polym. Sci.* **1998**, *135*, 1.
18 R.R. Schrock, *"Ring Opening Polymerization",* Hansa Verlag, München, **1993**.
19 H.L. Hsieh, R.P. Quirk, *"Anionic Polymerization: Principles and Practical Applications",* Dekker, New York, **1996**.
20 M. Morton, L.J. Fetters, *Rubber Chem. Technol.* **1975**, *48*, 359.
21 N. Hadjichristidis, H. Iatrou, S. Pispas, M. Pitsikalis, *J. Polym. Sci., Part A: Polym. Chem.* **2000**, *38*, 3211.
22 S. Ndoni, C.M. Papadakis, F.S. Bates, K. Almdal, *Rev. Sci. Instrum.* **1995**, *66*, 1090.
23 D. Uhrig, J.W. Mays, *J. Polym. Sci.; Part A: Polym. Chem.* **2005**, *43*, 6179.
24 J.J. Xu, F.S. Bates, *Macromolecules* **2003**, *36*, 5432.
25 J. Scheirs, D. Priddy, *Modern Styrenic Polymers*, Wiley, West Sussex, **2003**.
26 W.J. Trepka, *Polym. Lett.* **1970**, *8*, 499.
27 H. Gausepohl, S. Oepen, K. Knoll, M. Schneider, G. McKee, W. Loth, *Design. Monomer Polym.* **2000**, *3*, 299.
28 C. Guerrero-Sanchez, B.G.G. Lohmeijer, M.A.R. Meier, U.S. Schubert, *Macromolecules* **2005**, *38*, 10388.
29 B.G.G. Lohmeijer*, "Playing LEGO with Macromolecules: Connecting Polymer Chains Using Terpyridine Metal Complexes",* Dissertation thesis, Technische Universiteit Eindhoven, Eindhoven, **2004**.
30 M.W.F. Nielen, *Mass Spectrom. Rev.* **1999**, *18*, 309.
31 H. Pasch, W. Schrepp, *MALDI-TOF Mass Spectrometry of Synthetic Polymers*. Springer, Berlin, **2003**.
32 D.D. Hanton, *Chem. Rev.* **2001**, *28*, 4562.
33 S. Weidner, G. Kühn, J. Friedrich, *Rapid Commun. Mass Spectrom.* **1998**, *12*, 1373.
34 For linear polystyrene in toluene $\overline{\upsilon}$ = (0.920 ± 0.006) cm^3/g; $\Delta n/\Delta c$ = 0.11 cm^3/g at 633 nm: *Polymer Handbook*, J. Brandrup, E.H. Immergut, E.A. Grulke, Wiley, New York, **1999**.
35 V.N. Tsvetkov, *Rigid-chain Polymers.* Consultants Bureau, New York, **1989**.
36 T. Svedberg, K.O. Pedersen, *The Ultracentrifuge*, Oxford University Press, Oxford, **1940**.
37 C.R. Cantor, P.R. Schimmel, *Biophysical Chemistry*, Freeman, San Francisco, **1980**.
38 V.N. Tsvetkov, V.E. Eskin, S. Ya. Frenkel, *Structure of Macromolecules in Solutions*, Butterworths, London, **1970**.
39 H. Fujita, *Polymer Solutions*, Elsevier, Amsterdam, **1990**.
40 S. Broersma, *J. Chem. Phys.* **1969**, *51*, 233.

41 H. Yamakawa, *Modern Theory of Polymer Solutions*. Harper & Row, New York, **1971**.
42 H. Fujita, *Macromolecules* **1988**, *21*, 179.
43 (a) H. Yamakawa, M. Fujii, *Macromolecules* **1973**, *6*, 407. (b) H. Yamakawa, M. Fujii, *Macromolecules* **1974**, *7*, 128.
44 S.V. Bushin, V.N. Tsvetkov, Ye.B. Lysenko, V.N. Yemel'yanov, *Polym. Sci. U.S.S.R.* **1981**, *23*, 2705.
45 G.M. Pavlov, A.N. Kozlov, G.N. Martchenko, V.N. Tsvetkov, *Vysokomol. Soedin*. **1982**, *24B*, 284.
46 M. Bohdanecky, *Macromolecules* **1983**, *16*, 1483.
47 B. Zimm, *Macromolecules* **1980**, *13*, 592.
48 J. Garcia de la Torre, M.C.L. Martinez, M.M. Tirado, J.J. Freire, *Macromolecules* **1984**, *17*, 2715.
49 Y. Oono, M. Kohmoto, *J. Chem. Phys.* **1983**, *78*, 520.
50 G.E. McKee, F. Ramsteiner, W. Heckmann, H. Gausepohl, *Modern Styrenic Polymers: Polystyrenes and Styrenic Copolymers*, John Wiley & Sons, New York, **2003**.
51 Y. Einaga, H. Koyama, T. Konishi, H. Yamakawa, *Macromolecules* **1989**, *22*, 3419.
52 T. Arai, F. Abe, T. Yoshizaki, Y. Einaga, H. Yamakawa, *Macromolecules* **1995**, *28*, 3609.
53 G.M. Pavlov, *Eur. Phys. J. E* **2007**, *22*, 171.
54 P. Munk, Introduction to Macromolecular Science. Wiley, New York, **1989**.
55 J. Brandrup, E.H. Immergut, E.A. Grulke, *Polymer Handbook*, John Wiley & Sons, New York, 4th edn., **1999**.
56 B.P. Sullivan, J.M. Calvert, T.J. Meyer, *Inorg. Chem.* **1980**, *19*, 1404.
57 W.M. Reiff, W.A. Baker Jr., N.E. Erickson, *J. Am. Chem. Soc.* **1968**, *90*, 4794.
58 M.A.R. Meier, B.G.G. Lohmeijer, U.S. Schubert, *Macromol. Rapid Commun.* **2003**, *24*, 852.
59 U.S. Schubert, O. Hien, C. Eschbaumer, *Macromol. Rapid Commun.* **2000**, *21*, 1156.
60 U.S. Schubert, C. Eschbaumer, *Macromol. Symp.* **2001**, *163*, 177.
61 P. Guillet, C.-A. Fustin. B.G.G. Lohmeijer, U.S. Schubert, J.-F. Gohy, *Macromolecules* **2006**, *39*, 5484.
62 F.S. Bates, G.H. Fredrickson, *Phys. Today* **1999**, *52*, 32.
63 R.J. Young, P.A. Lovell, *Introduction to Polymers*, Chapman & Hall, London, 2nd edn., **1991**.
64 P. Claudy, J.M. Létoffé, Y. Camberlain, J.P. Pascault, *Polym. Bull.* **1983**, *9*, 208.
65 It is noted that apart from the crystalline fraction, a part of the PEG is expected to be amorphous and above its glass transition. Furthermore, the crystallinity observed with DSC is higher than the crystallinity of the samples subjected to indentation. During the DSC experiment (prior to the analyzed traces), the samples were dried at high temperature and subsequently cooled to lower temperatures compared to the indentation samples. Crystallization of PEG proceeds at a lower temperature than melting [ref. 58] and is enhanced by thorough drying.
66 W.C. Oliver, G.M. Pharr, *J. Mater. Res.* **1992**, *7*, 1564.
67 B.J. Briscoe, L. Fiori, E. Pelillo, *J. Phys., Part D: Appl. Phys*. **1998**, *31*, 2395.
68 J.M. Kranenburg, C.A. Tweedie, R. Hoogenboom, F. Wiesbrock, H.M.L. Thijs, C.E. Hendriks, K.J. Van Vliet, U.S. Schubert, *J. Mater Chem.* **2007**, *17*, 2713.
69 D. Tranchida, S. Piccarolo, J. Loos, A. Alexeev, *Macromolecules* **2007**, *40*, 1259.
70 H. Gausepohl, S. Oepen, K. Knoll, M. Schneider, G. McKee, W. Loth, *Design. Monomer Polym.* **2000**, 3, 299.
71 L.E. Nielsen, *Rheol. Acta* **1974**, *13*, 86.
72 M. Al-Hussein, W.H. de Jeu, B.G.G. Lohmeijer, U.S. Schubert, *Macromolecules* **2003**,*36*, 9281.
73 M. Al-Hussein, W.H. de Jeu, B.G.G. Lohmeijer, U.S. Schubert, *Macromolecules* **2005**,*38*, 2832.
74 When the moduli is plotted as a function of SPS + metal-ligand complex + counterion weight fraction, all data-points are right-shifted by the value annotated in Figure 5.13. Then, the SPS_{11}-[Ru]-PEG_{44}-[Ru]-SPS_{11} material is on the trendline constituted by the SPS-[Ru]-PEG_{70} materials, but the SPS_{11}-[Ru]-PEG_{44}-[is still located above this trendline.
75 L. Zhu, S.Z.D. Cheng, B.H. Calhoun, Q. Ge, R.P. Quirk, E.L. Thomas, B.S. Hsiao, F. Yeh, B. Lotz, *Polymer* **2001**, *42*, 5829.
76 An additional reason for the higher stiffness of SPS_{11}-[Ru]-PEG_{44}-[Ru]-SPS_{11} compared to the SPS-[Ru]-PEG_{70} could be its different architecture (ABA *vs*. AB). However, this represents probably

only a small effect as the hard phase is the continuous phase at these SPS contents [ref. 40], and then additional interactions between the hard phase regions are not as effective in raising the stiffness as for thermoplastic elastomers, where the soft phase is the continuous phase.
77 X.F. Zhong, A. Eisenberg, *Macromolecules* **1994**, *27*, 4914.
78 H. Sato, Y. Tanaka, *J. Polym. Sci.: Polym. Chem. Ed.* **1979**, *17*, 3551.
79 S. Kobatake, H.J. Harwood, R.P. Quirk, D.B. Priddy, *Macromolecules* **1999**, *32*, 10.
80 M. Morton, E.E. Bostick, R.G. Clarke, *J. Polym. Sci., Part A: Polym. Chem.* **1963**, *1*, 475.
81 U.S. Schubert, S. Schmatloch, A.A. Precup, *Des. Monomers Polym*. **2002**, *5*, 211.
82 W.C. Oliver, G.M. Pharr, *J. Mater. Res.* **1992**, *7*, 1564.
83 B.J. Briscoe, L. Fiori, E. Pelillo, *J. Phys., Part D: Appl. Phys.* **1998**, *31*, 2395.
84 P. Schuck, *Biophysical J.* **2000**, *78*, 1606.
85 C. Tanford, *Physical Chemistry of Macromolecules*. Wiley, New York, London, **1961**.
86 G. Pavlov, S. Finet, K. Tatarenko, E. Korneeva, C. Ebel, *Eur. Biophys. J*. **2003**, *32*, 437.
87 O. Kratky, H. Leopold, H. Stabinger, *Methods Enzymol*. **1973**, *27*, 98.

Advances in Supramolecular Polymer Chemistry: Well-defined Terpyridine-functionalized Materials

Summary

Controlled/"living" polymerization techniques have attracted enormous attention in the field of polymer science since they have opened an avenue to the preparation of well-defined materials with precisely designed molecular architectures like random, block, graft and comb copolymers. These techniques facilitate the creation of new materials for specialty applications as well as for elucidating the corresponding structure-property relationships. The research described in this thesis was focused on the preparation of well-defined polymers by employing controlled radical and "living" anionic polymerization processes. In addition, chelating ligands were incorporated at the end of the polymer backbone capable of connection different polymer chains together *via* non-covalent metal-ligand interactions. The introduction of directional supramolecular motifs in synthetic polymers represents a promising synthetic approach for the development of "smart" materials which combine the (reversible) binding behavior of supramolecular interactions and the processing advantages of polymers. Their remarkable properties are based on reversible self-association and, hence, they posses the capability of self-healing which makes them interesting for advanced applications in fields of nanotechnology, plastic electronics and biomedical purposes. This new methodology provides access to highly complex molecular structures that are extremely difficult or even impossible to synthesize with current covalent techniques.

The terpyridine moiety forms octahedral *bis*-terpyridine complexes with a variety of transition metal ions, such as iron, cobalt, nickel and ruthenium. Special focus in this thesis was on the synthesis of *bis*-terpyridine ruthenium(II) complexes since this transition metal ion allows the formation of homoleptic as well as heteroleptic complexes in a straightforward fashion. First, different synthetic strategies were applied to prepare *bis*-terpyridine ruthenium(II) model complexes which were subsequently characterized by means of ^{1}H NMR spectroscopy, UV-vis spectroscopy, MALDI-TOF mass spectrometry, elemental analysis, gel permeation chromatography and, in some cases, single crystal x-ray analysis. These investigations were the foundation for the construction of various polymer architectures, such as polymer *mono*-complexes, homo dimers, di-, tri- and tetrablock copolymers. For this purpose, the terpyridine ligand was inserted at the chain end(s) of a polymer. Various synthetic strategies were employed including (1) end-group modification of hydroxy end capped polymers by etherification, (2) *in situ* functionalization of polymers derived by anionic polymerization as well as (3) the utilization of a terpyridine-functionalized initiator suitable for controlled radical polymerization methods, more precisely nitroxide mediated polymerization. The latter approach was intensely explored for the preparation of terpyridine-functionalized homopolymers and block copolymers with well-defined molecular characteristics (predetermined molar mass, narrow molar mass distribution, end group control and architecture). Monomers belonging to different monomer families, e.g. styrenes, acrylates and acrylamides, were polymerized in a controlled fashion and subsequently connected to terpyridine-functionalized polyethylene glycol *via* ruthenium(II) metal ions. The resulting amphiphilic metallo-supramolecular block copolymers were primarily characterized by ^{1}H NMR spectroscopy, UV-vis spectroscopy and GPC. GPC measurements were performed using an optimized GPC system (5 mM NH_4PF_6 in DMF as eluent) that suppresses the interaction of the charged metallo-supramolecular complex. In order to prove the formation of the desired block copolymer, a photo-diode array detector was connected to the GPC. The respective 3-dimensional GPC chromatograms revealed the characteristic metal-to-ligand charge transfer band at 490 nm. A versatile post-modification reaction was applied to polymers consisting of pentafluorostyrene building blocks. Using this approach, a variety of multifunctional graft copolymers can be designed simply by reacting substituted amino-compounds carrying the

desired functionality. The scope of this approach is seemingly unlimited since it can be applied in any area that includes polymers.

Well-defined terpyridine-functionalized polymers were also obtained by employing “living” anionic polymerization. This strategy allows the access to differently composed polymers including homopolymers, alternating copolymers as well as block copolymers by sequential monomer addition. It was found that the use of 1,1-diphenylethylene as end capper is necessary to promote the functionalization with 4’-chloro-terpyridine. The alternating copolymers were fully characterized by ^{1}H NMR spectroscopy, GPC, elemental analysis, UV-vis spectroscopy and MALDI-TOF mass spectrometry revealing the successful incorporation of the terpyridine moiety at the end of the polymer chain. Moreover, analytical ultracentrifugation (in combination with density and viscosity measurements) was applied revealing an excellent agreement with respect to the molar masses obtained from analytical techniques mentioned before.

The morphologies of the amphiphilic metallo-supramolecular block copolymers were investigated in solution. The micellar aggregates formed from these copolymers in water or polar organic solvents have been studied by several analytical techniques, such as atomic force microscopy (AFM), transmission electron microscopy (TEM) and dynamic light scattering (DLS). In particular, one A-B-[Ru]-C triblock copolymer consisting of a hydrophobic (A), a fluorophilic (B) and a hydrophilic block (C), was investigated towards the influence of the solvent on the micelle formation. All basic micellar morphologies (spherical micelles, wormlike micelles and vesicles) were obtained by changing the polarity of the solvent. Moreover, the morphology of the micellar aggregates could be reversibly tuned as a function of temperature due to the upper critical solution temperature (UCST) behavior of the fluorinated middle block.

A smaller part of the thesis was dedicated to the preparation of iridium containing polymers. For this purpose, terpyridine-functionalized polymers were reacted with iridium(III) precursor complexes which form, upon bridge-splitting, polymeric mixed ligand iridium complexes. As a result of the metal-to-ligand based radiation, these materials exhibit different emission colors depending the functionality of the introduced *N,N*-chelating ligand or *N,C*-cyclometallating ligand, respectively. These luminescent polymeric materials are of special interest due to their potential application in light-emitting devices and solar cells. The optical properties of the iridium containing polymers were investigated by absorption and emission spectroscopy.

In general, it can be concluded that the combination of controlled/living polymerization methods and supramolecular chemistry represents a powerful strategy to design complex macromolecular architectures. Metallo-supramolecular polymers provide a basis for potential applications as “smart” materials due to the fact that the non-covalent bond can be reversibly broken under certain conditions. This characteristic binding behavior can be exploited for the preparation of nanoporous materials and hollow nanocages which could be of interest for applications in catalysis as well as waste water treatment. Moreover, the described triblock copolymers consisting of a hydrophilic, a hydrophobic and a fluorophilic block are promising materials with respect to the incapsulation of various guest molecules into the different core domains. This class of nanomaterials may be used in the fields of drug delivery, catalysis as well as nanotechnology.

Samenvatting

Binnen de polymeerchemie hebben gecontroleerde en/of levende polymerisatie technieken in de belangstelling gestaan omdat ze de synthese van complexe goed gedefinieerde polymeerketens met random-, blok-, graft- en kamcopolymeer architecturen mogelijk maken. Hiermee kunnen nieuwe materialen gemaakt worden die daarnaast gebruikt kunnen worden om struktuur-eigenschap relaties op te stellen. Het onderzoek in dit proefschrift beschrijft de synthese van goed gedefinieerde polymeren die met gecontroleerde radicaal- en levende anionische polymerisatie mechanismen verkregen zijn. Daarnaast, zijn aan de uiteinden van de ketens chelerende liganden geïntroduceerd waarmee verschillende ketens aan elkaar verbonden kunnen worden middels niet-covalente metaal-ligand interacties. De toevoeging van directionele supramoleculaire bindingen in synthetische polymeren vertegenwoordigd een veelbelovende route naar de synthese van “intelligente” materialen waarin de reversibele bindingen van de supramoleculaire chemie en de voordelen bij de verwerking van polymeren gecombineerd worden. De opmerkelijke eigenschappen van deze materialen zijn gebaseerd op hun omkeerbare binding waardoor ze over zelf-reparerend vermogen beschikken hetgeen ze interessant maakt voor toepassingen in bijvoorbeeld nanotechnologie, coatings en biomedische toepassingen. De combinatie van polymeer- en supramoleculaire chemie maakt de synthese van complexe polymere structuren mogelijk welke slechts zeer moeilijk, of in het geheel niet, te verkrijgen zouden zijn met conventionele covalente methoden.

Twee terpyridines vormen octaëdrische complexen door toevoeging van een groot aantal verschillende overgangsmetaal ionen zoals, ijzer, nikkel, kobalt en ruthenium. Binnen dit promotie onderzoek is speciale aandacht uitgegaan naar de synthese van *bis*-terpyridine ruthenium(II) complexen omdat dit overgangsmetaal ion de synthese mogelijk maakt van zowel complexen bestaande uit twee identieke alsook complexen bestaande uit twee verschillend gesubstitueerde liganden. Als eerste zijn op verschillende manieren *bis*-terpyridine ruthenium(II) model-complexen gemaakt welke vervolgens gekarakteriseerd zijn met behulp van ^{1}H NMR en UV-vis spectroscopie, MALDI-TOF massa spectroscopie, element analyse, gel permeatie chromatografie (GPC) en, in enkele gevallen, met kristallografie. De hierbij verkregen kennis vormt de basis voor de synthese van diverse polymeer architecturen, zoals polymere mono-complexen, homo-dimeren en di-, tri- en tetrablok copolymeren. Hiervoor zijn terpyridine liganden gekoppelt aan de keten einden van diverse polymeren. Daarvoor zijn verschillende synthetische strategieën gebruikt waaronder (1) etherificatie van hydroxy getermineerde ketens, (2) *in situ* functionalisatie van polymeren verkregen met anionische polymerisatie technieken en (3) de synthese van terpyridine gefunctionaliseerde initiatoren voor gebruik bij gecontroleerde radicaal polymerisaties. Deze laatste strategie was uitvoerig bestudeerd voor de bereiding van terpyridine gefunctionaliseerde homo- en blok copolymeren met goed gedefinieerde eigenschappen, zoals molecuul gewicht, ketenlengteverdeling, controle over eindgroepen en ketenstructuur. Verschillende klassen monomeren, bijvoorbeeld styrenen, acrylaten en acrylamiden zijn op gecontroleerde wijze gepolymeriseerd en vervolgens aan terpyridine gefunctionaliseerd polyethyleen glycol door middel van ruthenium(II) ionen. De resulterende amfifiele blok copolymeren zijn gekarakteriseerd met behulp van ^{1}H NMR, UV-vis spectroscopie en GPC. Om de vorming van de gewenste blok copolymeer te bevestigen is gebruik gemaakt van een GPC met “photo-diode array” detector. Hierbij zijn drie dimensionale GPC chromatogrammen verkregen waarin de aanwezigheid van een piek bij 490 nm karakteristieke is voor de vorming van een metaal-ligand complex. Om de interactie tussen metaal-ligand complex en GPC kolom weg te nemen is gebruik gemaakt van een 5mM oplossing van NH_4PF_6 in DMF als eluent. Voor de polymeren welke pentafluorostyreen blokken bevatten is een veelzijdige substitutie reactie met amino-verbindingen toegepast waarmee diverse multifunctionele kamcopolymeren verkregen zijn. Hiermee is een, binnen de polymeerchemie, algemeen toepasbare methode ontwikkeld.

Goed gedefinieerde terpyridine gefunctionaliseerde polymeren zijn ook verkregen middels anionische polymerisatie mechanismen. Deze strategie maakt de synthese van polymeren met verschillende structuren mogelijk waaronder, homopolymeren, copolymeren met alternerende monomeren in de keten en ook blokcopolymeren door verschillende monomeren achtereenvolgens toe te voegen. Daarbij is gevonden dat het gebruik van 1,1-diphenylethyleen als ketenstopper noodzakelijk is om de polymeerketen met terpyridine te functionaliseren. De alternerende copolymeren zijn gekarakteriseerd middels ^{1}H NMR spectroscopie, GPC, UV-vis spectroscopie, MALDI-TOF massa spectroscopie en element analyse waarbij de aanwezigheid van terpyridine aan de keteneinden aangetoond is. De materialen zijn daarnaast met analytische ultacentrigugatie bestudeerd (in combinatie met dichtheid en viscositeitmetingen) waarbij de verkregen molecuulgewichten in goede overeenstemming waren met waarden verkregen uit eerder vernoemde techieken.

In oplossing vormen de amfifiele blokcopolymeren micellen waarin de onoplosbare delen van de ketens omgeven worden door een schil van de oplosbare delen. Deze micellaire aggregaten in water en andere polaire organische oplosmiddelen zijn bestudeerd met technieken, zoals “atomic force microscopy”, transmissie elektronen microscopie en “dynamic light scattering”. Bijzondere aandacht is besteed aan het aggregatiegedrag van een specifiek ABC triblokcopolymeer in oplosmiddelen met verschillende polariteit. Voor dit polymeer bestaande uit een hydrofoob A-blok, een fluorofiel B-blok en een hydrofiel C-blok zijn alle elementele aggregatie toestanden van micellen (sferische micellen, langgerekte cilindervormige micellen, vesikel). Aangezien de oplosbaarheid van het middelste, gefluorineerde blok temperatuursafhankelijk kon door de temperatuur te wijzigen kon de morfologie van de micellen naar believen gewisseld worden door de temperatuur te variëren.

Een kleiner deel van het onderzoek is gewijd aan de bereiding van iridium bevattende polymeren. Daartoe zijn gebrugde-iridium(III) precursor complexen gebruikt welke bij complexering met terpyridine-gemodificeerde polymeerketens splitsen en leiden tot de vorming gemenge metallo-supramoleculaire polymeren. Omdat iridium complexen bekend staan om hun optische eigenschappen is toepassing van iridium in de metallo-supramoleculaire systemen interessant vanwege mogelijke toepassing in, onder andere, zonnecellen. Aangezien de emissie-eigenschappen van iridium complexen afhangen van metaal-ligand interacties kon de golflengte van het geëmitteerde licht aangepast worden door gebruik te maken van *N,N*- of *N,C* chelerende liganden. De optische eigenschappen van de diverse resulteerden metaal complexen zijn bestuurdeerd met adsorptie- en emissie spectroscopie.

Concluderend kan gesteld worden dat de combinatie van gecontroleerde polymerisatie technieken en concepten uit de supramoleculaire chemie een krachtige en veelbelovende methode is om complexe macromoleculaire structuren te bereiden. Metallo-supramoleculaire polymeren vormen een basis voor mogelijke toepassing in ‘slimme’ materialen dankzij de aanwezigheid van omkeerbare niet-covalente bindingen. Hun karakteristieke bindingsgedrag kan gebruikt worden om poreuze of holle materialen te maken met poriën met nanometer dimensies. Deze zouden gebruikt kunnen worden in de catalyes en / of bij de waterzuivering. Daarnaast zijn de aggregaten van de beschreven triblok copolymeren bestaande uit een hydrofiel, een hydrofoob en een fluorofiel blok interessant vanwege de mogelijkheid ze te gebruiken om diverse gast-moleculen op te nemen in de respectievelijk verschillende compartimenten. Dit bijvoorbeeld interessant kunnen zijn voor toepassingen binnen de katalyse, nantechnologie en als dragers voor medicijnen.

Curriculum vitae

Christina Ott was born on the 14th of March 1981 in Gera (Germany). After finishing the secondary education (Abitur) in 1999, she started her study at the Friedrich-Schiller-University in Jena, Germany. In 2001/2002 she took part in an exchange program at the Dublin City University (DCU) in Ireland. In 2004, she obtained her diploma degree at the Macromolecular and Organic Chemistry group under the supervision of Professor Elisabeth Klemm. Her graduation project was related to the development of π-conjugated polymer systems using metal-catalyzed coupling reactions. In October 2004, she moved to the Netherlands to start a Ph.D. program in polymer science in the group of Professor Ulrich S. Schubert at the Eindhoven University of Technology. The most important results of this research are described in this thesis.

List of publications

Refereed publications:

M.A.R. Meier, D. Wouters, C. Ott, P. Guillet, C.-A. Fustin, J.-F. Gohy, U.S. Schubert
Supramolecular ABA Triblock Copolymers via a Polycondensation Approach: Synthesis, Characterization, and Micelle Formation
Macromolecules **2006**, *39*, 1569-1576.

C. Ott, B.G.G. Lohmeijer, D. Wouters, U.S. Schubert
Terpyridine-terminated Homo and Diblock Copolymer LEGO Units by Nitroxide-mediated Radical Polymerization
Macromol. Chem. Phys. **2006**, *207*, 1439-1449.

C. Ott, D. Wouters, H.M.L. Thijs, U.S. Schubert
New Preparation and Purification Methods for Metallo-supramolecular Block Copolymers
J. Inorg. Organometal. Polym. Mater. **2007**, *17*, 241-249.

C. Ott, R. Hoogenboom, U.S. Schubert
Post-modification of Polypentafluorostyrene: A Versatile "Click" Method to Create Well-defined Multifunctional Graft Copolymers
Chem. Commun. **2008**, 3516-3518.

P. Guillet, C.-A. Fustin, C. Mugemana, C. Ott, U.S. Schubert, J.-F. Gohy
Tuning Block Copolymer Micelles by Metal-ligand Interactions
Soft Matter **2008**, *4*, 2278-2282.

C. Haensch, C. Ott, S. Hoeppener, U.S. Schubert
Combination of Different Chemical Surface Reactions for the Fabrication of Chemically Versatile Building Blocks onto Silicon Surfaces
Langmuir **2008**, *24*, 10222-10227.

C. Ott, R. Hoogenboom, S. Hoeppener, D. Wouters, J.-F. Gohy, U.S. Schubert
Tuning the Morphology of Amphiphilic Metallo-supramolecular Triblock Copolymers in Solution
Soft Matter **2009**, in press.

C. Ott, G.M. Pavlov, C. Guerrero-Sanchez, U.S. Schubert
Alternating Terpyridine-endfunctionalized Copolymers of Styrene and Diphenylethylene via Anionic Polymerization Techniques: A Detailed Characterization Study
submitted.

C. Ott, J.M. Kranenburg, C. Guerrero-Sanchez, S. Hoeppener, D. Wouters, U.S. Schubert
Supramolecular Assembly via Non-covalent Metal Coordination Chemistry: Synthesis, Characterization and Elastic Properties
submitted.

C. Ott, U.S. Schubert
Synthesis of Well-defined Block Copolymers Using Concepts of Controlled Radical Polymerization and Supramolecular Chemistry
in preparation.

C. Ott, Claudia Haensch, Christoph Ulbricht, U.S. Schubert
Supramolecular Polymers Bearing Mixed-ligand Iridium(III) Complexes
in preparation.

Non-refereed publications (first author):

C. Ott, U.S. Schubert
Functionalized Homo-and Heteroleptic Terpyridine Complexes via *Cis*-[Ru(2,2':6',2''-terpyridine)(DMSO)Cl_2
Polym. Preprints **2007**, *48*, 711-712.

C. Ott, C. Guerrero-Sanchez, U.S. Schubert
Tailor-made Supramolecular Building Units Prepared by Anionic Polymerization Techniques
Polym. Preprints **2007**, *48*, 627-628.

C. Ott, H. Hofmeier, U.S. Schubert
Advanced "Self-healing" Materials by Side-chain Modified Terpyridine-containing Polymers
Polym. Preprints **2008**, *49*, 956-957.

Acknowledgement

The last words of this thesis are definitely dedicated to those people who contributed to the described research and supported me during the last four years. First of all, I want to thank my promoter, Prof. Dr. Ulrich S. Schubert, for giving me the opportunity to start as a PhD student within his group at the Eindhoven University of Technology. In addition, I want to thank him for his continuous help, support and guidance. I am truly amazed by your perpetual energy and enthusiasm and I am especially fortunate that you allowed me tremendous flexibility and freedom for my research to pursue my own initiatives.

Secondly, I would also like to thank the members of my committee, my promoter Prof. Dr. Ulrich S. Schubert, Dr. Richard Hoogenboom, Prof. Dr. Jean-François Gohy, Prof. Dr. Alex van Herk, Prof. Dr. Rachel O'Reilly and Prof. Dr. Gregory Tew for reading and approving this thesis as well as for their useful comments.

Of course, I would also like to express my gratitude to all colleagues and friends from the SMN-group who accompanied me through this long and eventful journey with their support, collaborations and encouragement. Without them and their help it would not have been possible to finish this research. I thank Dr. Bas Lohmeijer who introduced me to the fabulous world of NMP when I started in this group. Even tough, the reproduction of your initiator was rather time-consuming; it was worthwhile to invest so much time since this compound is responsible for a large amount of results. Richard, I want to thank you for your help (in particular in the last year), the fruitful discussions and suggestions. I am really happy about the grafting paper; I should have started much earlier to work on this. I wish you all the best for your scientific career and lots of success for starting your own group. Furthermore, I want to gratefully acknowledge Stephanie, Daan and Claudia, the experts for AFM and TEM. Daan and Stephanie thanks for measuring my thousand and one micelle solutions, commenting on some of my papers and for the long discussions about chemistry and life beyond chemistry. At this point, I would also like to thank J.-F. Gohy again for the great support and fruitful discussions about the morphology study. Remzi, thanks for helping me with the accelerator experiment. I hope you enjoy your time in Jena and I wish you (and Ayse) lots of success for the future. I also want to thank the people who were/are responsible for MALDI and EA measurements: Caroline, Mike (also for the nice discussions especially at the beginning of my PhD), Tina, Nicole, Anja Baumgärtel, Christoph and Rebecca. Christoph, another huge thank for the help with the COSY-measurements and for the introduction of the emission spectroscopy. I admire you for your relaxed and always polite character. You are willing to help others at any time, you think of other people before you think of yourself (not if food is involved). Also thanks for the continuous food supply: fresh fruits from the market, carrots, bread, chocolate and the unforgettable, extremely tasty banana-pancakes! You are an incredible person and I wish you good luck with finishing your thesis! I am also indebted to Carlos who introduced the anionic polymerization to me. In connection with the anionic polymerization, I am very grateful to Georgy (AUC) and Hans (nanoindentation) who did a great job in looking at the polymers from the more physical point of view. My (ex-)office mates Daan, Hans, Georgy, and Erik I want to thank for the nice atmosphere, the motivation attempts, the little holiday gifts…ect. Hans, you have always been an understanding person, you were there when I needed to talk. I wish you good luck for your defense. Certainly, I do not want to forget to acknowledge those people who are taking care that all the machines are running and that the chemicals are ordered: Antje, Caroline, Renzo, Hanneke and Martin; without you my research would not even have started. Chris, I want to thank you for the nice SEM pictures as well as for the optical microscopy images we took together of the model complexes. Special thanks goes to Emma who was always poised to arrange anything imaginable, in particular when I was a newcomer. Anja Teige, thanks for the fast fax-transfer of the corrections between Jena and Eindhoven. Guido Kickelbick, I want

to thank you for the x-ray measurements; unfortunately, the europium complexes were not good enough. Moreover, I want to acknowledge Christoph, Claudia and Andreas W. for providing me with the iridium-precursor complexes as well as terpyridine ligands and of course Christian F. for the respective quantum yield determinations of the Ir-complexes. Actually, I have to thank all members of the Schubert-group for the nice atmosphere. Everybody has its own personality and contributes in her or his way to the group and to the joined group activities. I really enjoyed spending my time with you on group trips, bowling evenings, parties in the coffee corner (especially after our monthly lab cleaning) and in the student house (where food from the different nationalities was dished up), barbeques…etc.

In addition, I want to express my gratitude to my friends with whom I spend the time outside the university making the last four years here so enjoyable and worthwhile. I had/have a great time doing various kinds of sports with you. Thanks to Tina, Nicole and Claudia for joining to the aqua aerobics & aqua jogging lessons and of course to the fitness; Christoph for accompanying me to karate. Carlos, muchas gracias for the yoga Tuesdays. Moreover, I want to thank the mexican trio (Carlos, Matias and Jorge) for the climbing sessions. I also enjoyed the time playing cards and domino, eating broodje rookwurst and drinking liters of beer with the Friday-squash & fitness community (Niels, Marie Claire, Hector, Carlos, Matias, Jorge, Olavio, Julio, Armando, Gil, Hugo, Edward, Paty, Lolis, Claudia, Tina, Nicole and Daan). Beer does not play a crucial role in my life; however, in regular intervals it is highly appreciated. Therefore, thanks to Manuela and Katharina who were joining every now and then to the irish pub, thanks to Steve, Hector, MC, Niels, Carlos, Frank, Stephanie, Daan, Claudia, Nicole, Tina, Christoph, Oana, Emma, Igor, Matias, Jorge, Julio, Antje…the Thursday afternoon FORT society. Bei Katharina will ich mich auch bedanken für die zahlreichen shopping Samstage, die meistens mit einem Kaffee und Eis bei Mc D. endeten. Ich wünsche dir viel Erfolg bei deiner Verteidigung und hoffe, dass all deine Wünsche in Erfüllung gehen.

I will also never forget the numerous “mexican” parties with lots of excellent food, music, dancing, cerveza y tequila; muchas gracias a todos los mexicanos, bolivianos, colombianos, ecuatorianos y venezolanos. I can also still remember (!) the great cocktail parties with Jürgen, the german clan (Tina, Nicole, Claudia), Steve, Martin H., Sabine, Christian, Carlos, Christoph and Daan. We also went several times together to the WOK all-you-can-eat restaurant (still wondering that they did not go bankrupt) and made trips to the Christmas market in Aachen mit den extra-langen Bratwürsten, knusprigen Schweinshaxen, belgischen Waffeln, Crepes, gebratene Mandeln und natürlich jede Menge Glühwein. Moreover, we took (inactive ☺) part at carnival, we made this fantastic trip to Germany to see Robbie the hero! Another unique experience was the sailing trip to Friesland with Emma, Martin, Erik, Jürgen, Christoph & Tobias, Stephanie, Nicole and Carlos. Together we were fighting against the forces of nature and we survived, somehow!

Natürlich möchte ich mich auch bei meinen “alten” Freunden bedanken (Nicole (2x), Tina, Friederike und Ines), die ich vor 4 Jahren in Deutschland zurücklassen musste. Es ist schade, dass wir uns in der letzten Zeit so selten gesehen haben. Ich wünsche euch das Beste für eure Zukunft. Auch bei Janko möchte ich mich bedanken, der stets ein offenes Ohr für mich hatte und mich bei allem unterstützte. Ich wünsche dir und Kerstin alles Gute.

It’s sort of weird that I had to go all the way to Eindhoven to finally meet Claudia here. I want to thank you, Claudia, for your help, trust and care. You were always standing by my side; we were sharing not only the happy moments. In fact, I think you know me better than anybody else. I’m blessed with the gift of a true friendship which is priceless and rather seldom in life. Thanks for accepting to be my “paranimph”. Following I also want to thank Daan again, who was not only a great group member but is also a really good friend. I cannot remember a single incident where he denied a request. Moreover, his charisma positively affects the mind of people dealing with him. Another great person, my second paranimph, is Hanneke. She is very open-minded, honest,

friendly and helpful at all times and I really appreciated working with her. Hanneke, stay the way you are. I wish you and Gijs good luck for the future.

Ich möchte mich vor allem bei meiner Familie bedanken, besonders bei meinen Eltern Marlis und Gerhard. Ihr habt euch all die Jahre um mich gekümmert, ihr habt dafür gesorgt, dass es mir an nichts fehlt; ihr habt verzichtet wenn es darum ging, euren Kindern einen Wunsch zu erfüllen. Ich möchte mich für eine wundervolle, behütete Kindheit bedanken, für eure Liebe, eure Geduld, euer Verständnis and eure volle Unterstützung.

The very last lines of this book are dedicated to Carlos who plays a decisive role in my life; however, words alone cannot express how much he means to me. I simply enjoy every second we are spending together. You are the person with whom I can live life to the fullest; I hope this will never change.

Thanks to all of you.
Christina